

UNIVERSITY OF SOUTH WALES

---

# Early-Detection of Diabetic Foot Ulceration using Thermal Images

---

*Author:*

Benjamin Jan Paul Kluwe

*Supervisors:*

Dr. Peter Plassmann

*Enrolment Number:*

10046887

Dr. Carl Jones

*A thesis submitted in fulfilment of the requirements  
for the degree of Doctor of Philosophy*

Faculty of Computing, Engineering and Science  
School of Computing and Mathematics

In collaboration with the National Institute for Health Research, Kings  
College Hospital London, Freeman Hospital Newcastle upon Tyne, Pennine  
Acute Hospitals Trust and the National Physical Laboratory

October 2018



Candidate's Declaration Form

Note: This form must be submitted to the University with the candidate's thesis (10.5 of the Regulations refers)

Name of Candidate: Benjamin Kluwe

Degree for which thesis is submitted: PhD

1. Statement of advanced studies undertaken in connection with the programme of research (if any) (regulation 4.1 refers) eg. Additional modules

N/A

2. Concurrent registration for two or more academic awards (regulation 4.7 refers)

either \* I declare that while registered as a candidate for a research degree at the University of South Wales, I have not been a registered candidate or enrolled student for another award of the University or other academic or professional institution.

or \* I declare while registered for the University of South Wales research degree, I was, with the University's specific permission, a \*registered candidate/\*enrolled student for the following award:

3. Material submitted for another award

either \* I declare that no material contained in the thesis has been used in any other submission for any academic award.

or \* I declare that the following material contained in the thesis formed part of a submission for the award of

(state award and awarding body and list the material below or overleaf)

Signature of candidate: ..... Date: 02/07/2018

\* delete as appropriate

UNIVERSITY OF SOUTH WALES

## *Abstract*

Faculty of Computing, Engineering and Science  
School of Computing and Mathematics

### **Early-Detection of Diabetic Foot Ulceration using Thermal Images**

by Benjamin Jan Paul Kluwe

The purpose of this document is to provide an overview of the author's research into the early detection of diabetic foot ulceration using infrared imaging. This project may contribute to better treatment and potentially help to avoid a significant amount of amputations and deaths.

An experimental infrared system was developed and successfully tested within the framework of a clinical trial on 109 healthy volunteers and 112 diabetic patients at 3 collaborating clinical centres with the aim of providing information on what differentiates a 'normal', healthy foot from a diabetic foot.

This information was then used to develop a novel methodology for acquiring and analysing thermal data with the aim of identifying suitable predictors for ulceration.

Results indicate that the proposed classifiers may be used to forecast diabetic foot ulcers provided assessment intervals are short, ideally daily.

## *Acknowledgements*

I am deeply grateful to have been allowed to work on such an important topic in such a positive and productive environment led by my first supervisor Dr. P. Plassmann. His patience and knowledge amounted to the best possible guidance I could have imagined all while being able to maintain a humorous atmosphere even if things go wrong or get tough.

I would like to thank my second supervisor Dr. C.D. Jones for his support and knowledge that he provided over the course of this project.

I would like to offer my special thanks to Dsc. E.F.J. Ring. He is one of the most loving, caring and knowledgeable people I know and helped me kick-start my way into medical thermography. It has been an absolute pleasure working with one of the great minds in thermology.

I have received generous support from the collaborating partners who provided me with the expertise in their respective fields which was of key importance to the completion of this work.

Lastly, I would like to show my greatest appreciation to my friends and family, especially Sylvie Kluwe, who has been extraordinarily patient, enduring and supporting even in the few frustrating and agonising moments during this project.

This project was partly supported by the National Institute for Health Research (NIHR) Invention for Innovation (i4i) program, grant reference II\_LA\_0813\_20007.

# Contents

<b>Abstract</b>	<b>ii</b>
<b>Acknowledgements</b>	<b>iii</b>
<b>Contents</b>	<b>iv</b>
<b>1 Introduction</b>	<b>1</b>
1.1 Background . . . . .	1
1.2 Aim . . . . .	2
1.3 Hypothesis . . . . .	2
1.4 Ojectives . . . . .	3
1.5 Project Framework . . . . .	3
<b>2 Background Research</b>	<b>5</b>
2.1 Diabetic Foot Ulceration . . . . .	5
2.1.1 Detection . . . . .	5
2.2 Physiological Factors Influencing Skin Temperature . . . . .	6
2.2.1 Mass and Surface Area . . . . .	6
2.2.2 Blood Flow . . . . .	6
2.3 The Physics of Infrared Imaging . . . . .	7
2.3.1 Radiation . . . . .	7
2.3.2 Infrared Spectrum . . . . .	7
2.3.3 Emissivity . . . . .	8
2.3.4 Detector Types and Materials . . . . .	8
2.3.5 Infrared Camera Characterisation . . . . .	9
2.3.6 Error Sources . . . . .	10
2.4 Hardware . . . . .	10
2.4.1 Infrared Cameras . . . . .	10
2.4.2 Infrared Camera Stability Tests . . . . .	11
2.4.3 Computing Platforms . . . . .	14
2.5 Software . . . . .	16
2.5.1 Warping . . . . .	17
2.5.2 Pixel Interpolation . . . . .	19
2.5.3 Splines . . . . .	20
2.5.4 Combining Cubic Splines with Barycentric Coordinates . . . . .	21

2.5.5	Validity of using Barycentric Coordinates . . . . .	24
<b>3</b>	<b>Materials and Methods</b>	<b>27</b>
3.1	Study Protocol . . . . .	27
3.2	Measuring Device . . . . .	34
3.2.1	Device Hardware . . . . .	34
3.2.2	Device Software . . . . .	35
3.3	Analysis Software . . . . .	41
<b>4</b>	<b>Results</b>	<b>45</b>
<b>5</b>	<b>Analysis and Discussion</b>	<b>59</b>
5.1	Temperature Asymmetry Threshold . . . . .	59
5.2	Combining Parameters . . . . .	64
5.3	Applying Thresholds to Individual Regions of Interest . . . . .	81
5.4	Summary . . . . .	88
<b>6</b>	<b>Next Generation Device</b>	<b>91</b>
<b>7</b>	<b>Conclusion</b>	<b>99</b>
7.1	Achievement of Objectives . . . . .	99
7.1.1	Research into the Underlying Physical Principles of Infrared Imaging . . . . .	100
7.1.2	Development of the Infrared Imaging Device . . . . .	100
7.1.3	Implementation of the Device . . . . .	101
7.1.4	Implementation of Website for Mass Manual Image Object Outlining . . . . .	101
7.1.5	Analysis of the Data Collected by the Clinical Centres . . . . .	102
7.2	Contribution to Knowledge . . . . .	102
7.2.1	Journal and conference contributions . . . . .	102
7.2.2	Hardware . . . . .	103
7.2.3	Software . . . . .	104
7.2.4	Methodologies . . . . .	104
7.2.5	Analysis . . . . .	105
7.3	Achievement of Aim . . . . .	105
7.4	Future Work . . . . .	105
<b>A</b>	<b>Appendix - Data plots</b>	<b>107</b>
<b>B</b>	<b>Appendix - Receiver Operator Curves using one Dimension</b>	<b>124</b>
<b>C</b>	<b>Appendix - Applying Thresholds to ROIs</b>	<b>142</b>
<b>D</b>	<b>Appendix - Certificates of Contribution to Paper</b>	<b>171</b>
<b>E</b>	<b>Appendix - Study Protocols</b>	<b>174</b>

<b>F Appendix - Website</b>	<b>206</b>
-----------------------------	------------

<b>Bibliography</b>	<b>209</b>
---------------------	------------

# List of Abbreviations

**AlGaAs** Aluminium Gallium Arsenide

**AUC** Area under the Curve

**BBW** Bounded Biharmonic Weights

**C** Celsius

**CSV** Comma Separated Values

**DFU** Diabetic Foot Ulcer

**DFUPS** Diabetic Foot Ulcer Prevention System

**EM** Electro Magnetic Wave

**FRH** Freeman Hospital Newcastle

**FPA** Focal Plane Array

**FPR** False Positive Rate

**GB** Gigabyte

**GPU** Graphics Processing Unit

**HgCdTe** Mercury Cadmium Telluride

**i4i** Invention for Innovation program of the National Institute for Health Research (NIHR)

**I<sup>2</sup>C** Inter-Integrated Circuit

**InSb** Indium Antimonide

**IDE** Integrated Development Environment

**IR** Infrared Radiation



**ITS-90** International Temperature Scale of 1990

**K** Kelvin

**KIN** Kings College Hospital London

**LBC** Local Barycentric Coordinates

**LWIR** Long Wavelength Infrared Radiation

**MDD** Medical Device Directive

**MHRS** Medical Health Research Agency

**MTB** Metatarsal Base

**MTH** Metatarsal Head

**MVC** Mean Value Coordinates

**MWIR** Mid Wavelength Infrared Radiation

**NETD** Noise Equivalent Temperature Difference

**NH3** Ammonia

**NHS** National Health Service

**NIHR** National Institute for Health Research

**NICE** National Institute for Health and Care Excellence

**NPL** National Physical Laboratory

**NPV** Negative Predictive Value

**NTC** Negative Temperature Coefficient

**PEN** Pennine Acute Hospitals

**PMX** Photometrix

**PPV** Positive Predictive Value

**PRT** Platinum Resistance Temperature sensor

**ROC** Receiver Operator Curve

**ROI** Region of Interest

**SITF** System Intensity Transfer Function

**SNR** Signal to Noise Ratio

**SSH** Secure Shell Protocol

**SWIR** Short Wavelength Infrared Radiation

**TIBB** Thermal Imaging BlackBody

**TNR** True Negative Rate (specificity)

**TPR** True Positive Rate (sensitivity)

**QWIP** Quantum Well Infrared Photo detector

**UI** User Interface

**USB** Universal Serial Bus

**XML** Extensible Markup Language

# Chapter 1

## Introduction

### 1.1 Background

Diabetes affects 3.6 million people in the UK (5.5 % of the population). Since 1996 diabetes prevalence has doubled to the current number and over the last 3 years it has risen by approximately 250,000 cases per year. Accordingly, the cost for diabetic care is the highest source of spending for the NHS, at 10 billion pounds per year, equating 10 % of the NHS budget [1]. Diabetic foot ulcers are a common complication in diabetic patients. It is estimated that 1 %-1.4 % of all diabetics will develop a foot ulcer each year and approximately 15 % of diabetics will develop an ulcer within their lifetime [2, 3]. A Diabetic Foot Ulcer (DFU) will often lead to infection and, if not treated rapidly, gangrene and amputation. As a consequence 15 %-27 % of DFUs lead to the surgical removal of bone[4].

Diabetic foot care has gradually improved over the years but the predominant problem remains the detection of the onset of diabetic foot ulceration at the earliest point in time - if possible well before the actual ulcer manifests itself. At the moment treatment can only be started when the ulcer is close to developing or already has developed, which is often too late and if the treatment does not work, the foot or parts of the foot need to be amputated. This will not only lead to a severe reduction in the quality of the patient's life but additionally, the likelihood of the patient deceasing within 5 years after an amputation is up to 75 % [5]. Some studies even claim a mortality rate of 35 % to 65 % within the first three years after amputation [2].

An ulcer tends to develop from pressure zones underneath the foot when a person steps unevenly due to loss of sensation in their feet (neuropathy) or restricted blood

flow (angiopathy). After a period of time, the pressure zone develops into an irritation under the skin. The irritated area then gradually extends towards the surface where it eventually breaks through the skin. This process is not only painful for non-neuropathic patients but also foreshadows the aforementioned complications. The ability to detect a developing foot ulcer is currently limited by two factors:

1. Feet are visually inspected by podiatrists for redness and abnormalities. Ulcers however develop under the skin, therefore visual inspection may not provide an accurate diagnosis.
2. Feet are inspected annually for low risk patients according to NICE guidelines [6, see section 1.3.11]. A patient is classified into low, moderate, high or very high risk of developing an ulcer after each assessment and the next visit is planned accordingly. An ulcer that develops between visits will therefore be missed. This chance is greatest in low and moderate risk patients.

This work is attempting to address the above problem by exploiting the fact that a developing foot ulcer causes a change in blood flow to the affected area of the foot as the body mounts an inflammatory response to the causal irritations. These are usually mechanical: shear, friction or foreign bodies in footwear but also prolonged weight bearing on bony prominences. Other factors include excessive heat exposure (e.g. sand on a hot beach), cold and callus formation resulting in pressure and broken skin or some sort of traumatic injury. This in turn causes skin temperature to rise [7]. An early detection of the onset of foot ulceration could therefore be possible by measurement of skin temperature using thermochromic liquid crystal sheets or infrared cameras. The latter is preferred as it is a non-contact method.

## **1.2 Aim**

The aim of this research project is to develop, implement and evaluate a method for the early detection of developing foot ulceration by using infrared imaging techniques.

## **1.3 Hypothesis**

Diabetic foot ulcers can be predicted by infrared imaging due to an increase in bloodflow under the skin caused by an inflammatory response.

## 1.4 Objectives

In order to achieve the above aim the project has to meet the following objectives:

1. Research into the underlying physical principles of infrared imaging, detector technologies and their respective spatial and thermal resolutions, and error sources associated with both technology and usage in clinical practice.
2. Development of hardware and software for a device capable of addressing the aim in a clinically feasible manner, this means technically, but not methodologically, a medical device.
3. Implementation of the device and provision to the 3 clinical centres associated with this project (see section 1.5).
4. Implementation of a website capable of mass manual image object outlining.
5. Analysis of the data collected by the clinical centres with the aim of:
  - Establishing and verifying a methodology for data extraction and grouping
  - Confirming/rejecting the currently accepted  $2.2^{\circ}\text{C}$  temperature asymmetry threshold [8]
  - Finding an improved method over the  $2.2^{\circ}\text{C}$  temperature asymmetry threshold

## 1.5 Project Framework

The work described in this dissertation was embedded in a £1.2 million National Institute for Health Research (NIHR) funded Invention for Innovation (i4i) project. The project was lead by the National Physical Laboratory (NPL). The collaborating partner organisations were 3 UK Hospitals under the clinical lead of King's College London. Further participants were Photometrix Imaging Ltd (instrument design) and the University of South Wales where the author is a PhD student. The project timeline was as follows:

1. Writing an NIHR i4i grant application (2013/14)
2. In parallel: (Mid 2014)

- 
- (a) Development of the clinical protocol
  - (b) Technical R&D into an infrared imaging capable device
3. Ethics approval of the clinical protocol (End 2014)
  4. MHRA approval to use the device as a medical device (2014/15)
  5. Trial 1 on 109 healthy volunteers (2015/16)
  6. Trial 2 on 112 diabetic patients with an ulceration history (2016/17)
  7. Development of a second generation device (2017/18)

The author contributed to parts 2 (b), 5, 6 and 7.

## Chapter 2

# Background Research

In order to meet the objectives of this work this chapter is investigating:

- the motivation and justification for this work and possible approaches (section 2.1)
- human foot physiology (section 2.2)
- the underlying physics of IR imaging (section 2.3)
- potential hardware platforms that could be employed (section 2.4)
- a number of software techniques/algorithms that are useful in the context of this work (section 2.5)

## 2.1 Diabetic Foot Ulceration

### 2.1.1 Detection

The current method of detecting foot ulcers is visual inspection. However, due to the nature of how an ulcer develops, it is very difficult to visually detect or predict its formation. The work of van Netten et al., who are key contributors in this field, suggest an alternative method using infrared thermography by measuring the difference in temperature at contralateral spots on the feet of diabetics. In their study, they confirm the 2.2°C threshold that was previously established as clinically significant by Armstrong and Lavery [9, 10] and achieved a sensitivity of 76% and

specificity of 40 % [8, 11]. The papers used patients cohorts of size 85, 173, 15 and 54, respectively.

More recently a study by Frykberg quotes a sensitivity of 90 % but a specificity of only 43 % for an at least 2-day consecutive temperature threshold of 2.75 °C and a mean lead time of 37 days. In the study data was collected from a "smart temperature mat" for home use from 132 patients where the device was used  $5.5 \pm 1.2$  times per week. False positives were identified when no ulcer occurred at most 2 months after the threshold was exceeded [12].

These studies provide the foundation of the hypothesis in 1.3 and justification for the work described in this thesis.

## 2.2 Physiological Factors Influencing Skin Temperature

### 2.2.1 Mass and Surface Area

The mass and surface area of a foot are proportional to the temperature that it can maintain. The characteristic is measured in  $m^2kg^{-1}$  and is a good indication for how much heat is being radiated by a foot at a given point in time. For an average male, the surface area to mass ratio is about 0.069 and for the average female it is about 0.084. These values are approximately three times larger than the surface area to mass ratio of the whole body. This demonstrates that feet act as radiators that can be turned on and off by regulating blood flow and their thermal properties need to be taken into account in measurements over time [13].

### 2.2.2 Blood Flow

Blood flow beneath the skin has a dramatic effect on the temperature of the foot. Blood flow is measured as the amount of blood that reaches each 100 mL of cellular tissue per minute ( $mL_{\text{blood}} 100 mL_{\text{cell tissue}}^{-1} \text{min}^{-1}$ ) of the total limb volume over time. As mean body temperature and local skin temperature rise, the blood flow increases up to  $14 mL_{\text{blood}} 100 mL_{\text{cell tissue}}^{-1} \text{min}^{-1}$ , but drops down to a minimum of about  $0.8 mL_{\text{blood}} 100 mL_{\text{cell tissue}}^{-1} \text{min}^{-1}$  when both mean and local skin temperature drop, which is the minimum amount of blood flow to sustain cellular tissue [13].

In the context of this work it is anticipated that visible foot ulceration is preceded by an inflammatory reaction of the affected tissue [9] with an associated increase in



blood flow. A thermal camera should be able to detect the onset of such ulceration by observing a hot spot on those parts of skin that are covering the damaged tissue. It may be necessary to apply a cold stimulus or provocation to the foot (e.g. fan cooling) in order to visualise such a hot spot: normal unaffected tissue will react by closing down capillaries in order to prevent heat loss and thus cool down while the inflammatory tissue will remain well perfused and thus appear hotter than its surrounding tissue [14].

## 2.3 The Physics of Infrared Imaging

The physics behind Infrared Imaging involve multiple aspects that have to be taken into account in order to produce a radiometric image of sufficient quality. It is therefore important to understand how an image is created at the physical layer to correctly interpret the temperature output at a later stage.

### 2.3.1 Radiation

Radiation is perceived in the form of electromagnetic (EM) waves traversing space. An EM wave consists of two separate parts, the electric field and the magnetic field, each oscillating in phase at 90° towards to each other. Every EM wave has a specific wavelength and amplitude. The wavelength is a measurement of the wave from peak to peak (or trough to trough) and the amplitude is the min/max values of the wave. The focus of this study is infrared radiation, which is defined as EM waves with a wavelength between 1 µm and 10 µm [15, chapter 3].

### 2.3.2 Infrared Spectrum

The infrared spectrum is split into three different sections: short-wave infrared radiation (SWIR), mid-wave infrared radiation (MWIR) and long-wave infrared radiation (LWIR), which can be defined at 1-3 µm, 3-5 µm and 5-10 µm, respectively.

The wavelength with the peak spectral radiance of a black body at a specific temperature is calculated using Wien's law. It is calculated using

$$\lambda_{max} = b/T \tag{2.1}$$

where  $T$  is the absolute temperature in Kelvin (K) and  $b$  is Wien's displacement constant. Using the human body as a reference point at about 30-35 °C (303.15-308.15 K), the peak emission wavelength is between 9.4 and 9.6  $\mu\text{m}$ , which falls into the LWIR spectrum. Even though SWIR and MWIR sensors would provide a greater contrast based on Planck's law in terms of wavelength, the significantly reduced amount of incident spectral radiation would increase the measurement error. For this reason LWIR sensors a better fit than SWIR and MWIR sensors for this project. The full spectral radiance vs. wavelength graph is given by Planck's law [15, chapter 5].

### 2.3.3 Emissivity

The emissivity of an object is a measure of how effective infrared radiation is cast out by the object. The emissivity of an object can range from 0 to 1, where 0 is an object that does not emit infrared radiation at all, for example an ideal mirror, and 1 for an object that perfectly emits radiation, a so called black body. It is measured by the difference in radiation from a blackbody reference source (calculated from Planck's law) and the experimental value [15, chapter 5]. The object of interest in this study is the human skin, which is a near-perfect blackbody source with an emissivity of 0.98 [15, chapter 2].

### 2.3.4 Detector Types and Materials

There are three types of detectors that can be used: photoconductive, photovoltaic and thermal. The three types determine how the radiation is captured and passed on to a readout chip. In photoconductive detectors, the radiation is converted into a current through electron excitation. Similarly, photovoltaic detectors induce a voltage using a diode junction when radiation of the wavelength range for which they are designed hits them. The wavelength that is captured by the detector depends on the materials that are used. Thermal detectors use a different approach; they convert the radiation into heat which then changes the electrical characteristics of resistive elements. Some of the detector materials for infrared cameras include InSb for 5  $\mu\text{m}$  wavelength for MWIR, HgCdTe for 5 and 10  $\mu\text{m}$ , AlGaAs (quantum well infrared photo detector, QWIP) for 5 and 10  $\mu\text{m}$  and uncooled bolometers for 10  $\mu\text{m}$  imaging. Each detector type, except for the bolometer, must be cooled to make the detector function and reduce error sources such as the inherent resistance of electrical components, which generate heat when current passes through them and to

reduce electronic noise [15, chapter 3]. This means that photoconductive and photovoltaic detectors produce the most accurate results but are also far more expensive to produce and maintain than bolometers. The cost aspect is also what makes the use of photoconductive and photovoltaic detectors impractical for use in an everyday hospital setting. The differences are summarised in table 2.1.

Detector Type	Captured wavelength band	Cooling	Method of data extraction
Photoconductive	Narrow	Must	Current
Photovoltaic	Narrow	Must	Voltage
Thermal	Wide	May	Resistor voltage drop

TABLE 2.1: Comparison of detector types

### 2.3.5 Infrared Camera Characterisation

An infrared camera is typically characterised by its performance in terms of thermal- and spatial-resolution. To measure the thermal resolution, the camera is subjected to a uniform, large target where the input radiation is controlled. The root mean square of the 3 dimensional noise (width, height and time, expressed in *volts*) is measured and divided by the response of the System Intensity Transfer Function (SITF in *volts/K*), giving the Noise Equivalent Temperature Difference (NETD). The NETD represents the temperature difference which would produce a signal equal to the camera's noise and is inversely proportional to the Signal-to-Noise Ratio (SNR). Current infrared cameras have a NETD in the range of 20 to 100 mK. Spatial resolution on the other hand is measured using the field of view, distance to target and the amount of pixels in both the vertical and horizontal directions [15, chapter 4]. Combining all three parts gives a measurement in *pixels mm<sup>-1</sup>*, where the physical maximum resolution is given by the Rayleigh criterion:  $\sin \theta_r = \frac{\lambda}{d}$ . The amount of pixels of an imager is physically fixed to the sensor array, in the case of the Optris TIM-400 Imager (the IR camera used in this work), there are 382x288 pixels available. The newer FLIR Lepton sensor (the IR camera used in the 2nd generation device outlined in chapter 6) comes in two versions which has either 80x60 or 160x120 pixels. Although both the NETD and spatial resolution might seem to be adequate indicators of quality for an infrared camera, the accuracy of infrared sensors is also influenced by an initial offset after being turned on and a lasting bias which both need to be corrected. According to manufacturers' marketing material for uncooled bolometer sensors this is typically  $\pm 2^\circ\text{C}$  or  $\pm 2\%$ , whichever is greater. It is often unclear in the manufacturers' datasheets against what reference the  $\pm 2\%$  is measured against, e.g. 2% of the temperature in K or temperature in Celsius (C).

### 2.3.6 Error Sources

The main error sources of infrared radiation measurement are the detector's own temperature and background radiation. Depending on the detector material and type, the methods to reduce the sources of error are different. Some infrared cameras are cooled to below temperatures of 80K to reduce the amount of infrared radiation emitted from the detector itself [15, chapter 3]. Whether the camera is cooled or uncooled, the background radiation is corrected with error correction formulas.

An infrared camera is characterised by its horizontal, vertical and temporal noise attributes. These three attributes are used in the calibration step (error correction) of the camera, which occurs in a pre-defined interval but can usually also be defined by the user. This ensures that the image corresponds to the real world object being imaged [15, chapters 4 and 5].

The choice of IR camera for this project was based on understanding their respective limitations and inaccuracies. For this project it was important to realise that a bolometer camera is adequate enough to differentiate usual skin temperature fluctuation from skin temperature abnormality. The reasoning for this choice is provided in the following section 2.4.

## 2.4 Hardware

### 2.4.1 Infrared Cameras

Most of today's infrared cameras make use of uncooled bolometers, an array of negative temperature coefficient (NTC) resistors that reduce their resistance when heated by incoming infrared radiation. The cost of a uncooled bolometer camera has decreased dramatically over the last 20 years due to chip size reduction and smaller pixel sizes. Currently, the price range for an infrared camera is within thousands of dollars (US). From table 2.2, the price range in terms of dollar per pixel range puts most infrared cameras at around 0.05-0.2 dollars per pixel. For comparison, a Full HD webcam (1920x1080 pixels) costs about 30 dollars which corresponds to  $1.44 \times 10^{-5}$  dollars per pixel.

All of the cameras listed in table 2.2 are embedded devices and therefore include unnecessary components such as a screen, which is reflected in the cost of each device. Alternatively, it is possible to use sensors with common interfaces such as

USB or I<sup>2</sup>C such as the FLIR Lepton or Micro-Epsilons TIM infrared imagers. Table 2.3 shows a comparison between the two cameras.

Part#	Brand	Price (USD)	Resolution (Pixels)	Dollars per Pixel	Thermal Sensitivity	Accuracy
FLIRE4	FLIR	995.00	80 X 60 (4,800)	0.207	<.15C	±2%
FLIRE5	FLIR	1,495.00	120 X 90 (10,800)	0.138	<.10C	±2%
FLIRE40BX	FLIR	3,995.00	160 X 120 (19,200)	0.208	<.045C	-
FLIRE6	FLIR	2,495.00	160 X 120 (19,200)	0.130	<.06C	±2%
FLIRE40	FLIR	3,995.00	160 X 120 (19,200)	0.208	<.07C	±2%
TI20060HZ	Fluke	6,299.95	200 X 150 (30,000)	0.210	<.08C	±2%
TI30060HZ	Fluke	6,999.95	240 X 180 (43,200)	0.162	<.05C	±2%
FLIRE50	FLIR	5,995.00	240 X 180 (43,200)	0.139	<.05C	±2%
FLIRE60	FLIR	7,995.00	320 X 240 (76,800)	0.104	<.045C	±2%
TI40060HZ	Fluke	8,495.00	320 X 240 (76,800)	0.111	<.05C	±2%
FLIR440BX	FLIR	11,750.00	320 X 240 (76,800)	0.153	<.05C	±2%
FLIRT420	FLIR	8,750.00	320 X 240 (76,800)	0.114	<.05C	±2%
FLIRT440	FLIR	11,750.00	320 X 240 (76,800)	0.153	<.05C	±2%
FLIR420BX	FLIR	8,750.00	320 X 240 (76,800)	0.114	<.05C	±2%
FLIRE8	FLIR	3,995.00	320 X 240 (76,800)	0.052	<.06C	±2%
FLIRT620	FLIR	20,950.00	640 X 480 (307,200)	0.068	<.05C	±2%

TABLE 2.2: Comparison of FLIR and Fluke cameras [16] (market leaders at the time of writing)

Part#	Price (USD)	Resolution (Pixels)	Dollars per Pixel	Thermal Sensitivity	Accuracy
Micro-Epsilon TIM-400	7,573.80	382 X 288 (110,016)	0.069	<0.04/0.08C	±2%
FLIR Lepton Version 2 (with Shutter)	170.00	80 X 60 (4,800)	0.036	<0.05C	N/A
FLIR Lepton Version 3 (with Shutter)	240.00	160 X 120 (19,200)	0.013	<0.05C	N/A

TABLE 2.3: Comparison of FLIR Lepton and Micro-Epsilon TIM-400 [17, 18]

For this project the Micro-Epsilon TIM-400 camera was selected as a preliminary proof-of-concept device. It was the camera with the highest specification available within the project budget at the time of purchase. While it is in all likelihood over-specified in its performance parameters for the problem space its output can be artificially degraded using downsampling in order to simulate a lower specified device. This allows the determination of minimum parameters that have to be met by an IR imaging device in order to be used for a device to be used in clinical practice (see chapter 6).

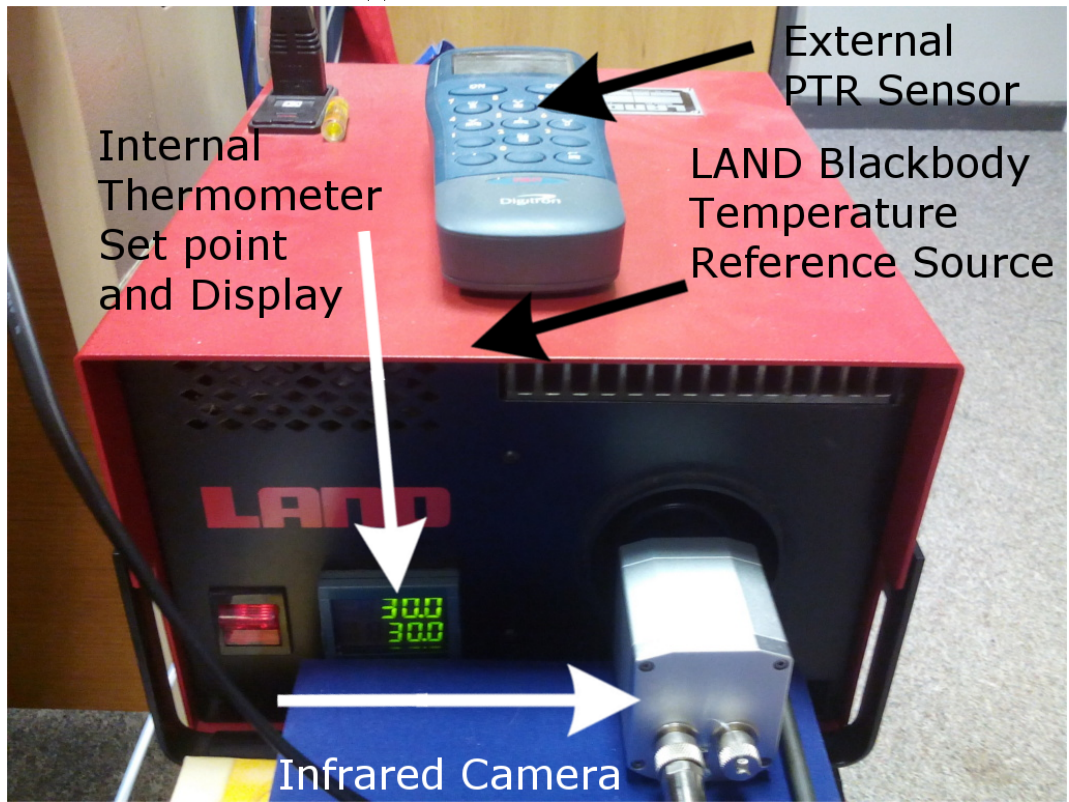
## 2.4.2 Infrared Camera Stability Tests

In the initial phases of the project, a test was carried out assessing the effect of calibration on the infra-red camera to find out how long it would take for the camera

to stabilise. The experiment was designed to record the mean temperature of the entire image for 20 minutes after turning it on. The camera was pointed at a uniform temperature reference source at  $30.0^{\circ}\text{C}$ , shown in figure 2.1a. A second independent thermometer was used to verify the temperature of  $30.0^{\circ}\text{C}$ , shown in figure 2.2 as the purple line. A calibration command was sent to the camera every minute. The blue line shown in figure 2.2 represents the mean temperature of the entire image after each calibration event and the red line shows the average temperature before the calibration event. It shows that the camera becomes adequately stable for measurements after about 10 minutes of being left on, as well as the necessity to trigger the camera's internal calibration event just before an image gets taken. The offset of about  $1.5^{\circ}\text{C}$  is notable, but was most likely caused by the camera being halfway inside the blackbody reference source and therefore the lens heating up to a higher than normal temperature. In addition, the presented camera is the projects' spare camera, i.e. that was characterised as the worst performer by the NPL among the set of five available cameras. The main outcome of this test is that the TIM-400 cameras used in this study should be sent calibration event triggers at regular intervals in order to prevent random offset fluctuations in the output IR images.



(a) TIM400 experiment setup



(b) TIM400 experiment setup

FIGURE 2.1: Experiment setup

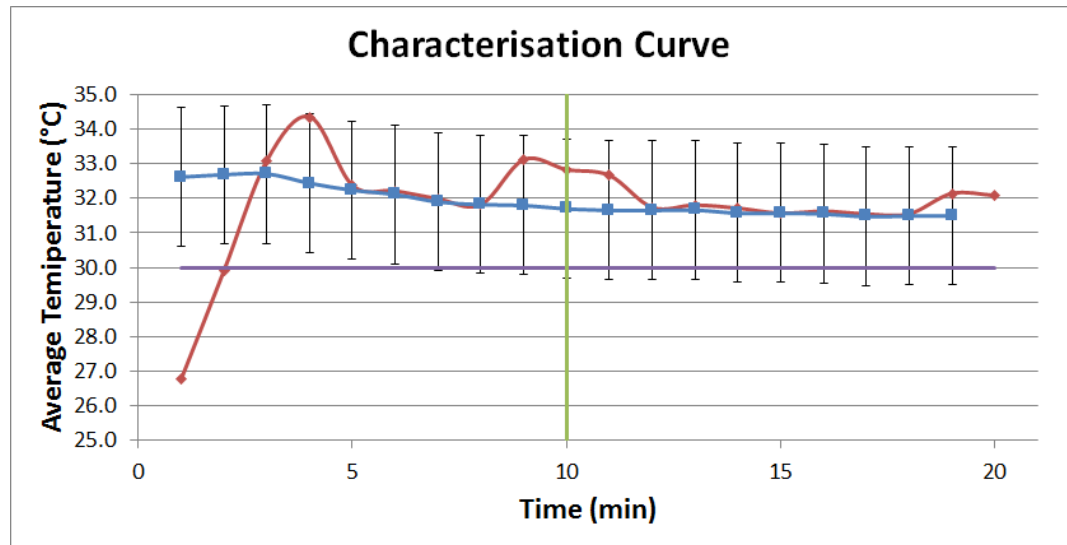


FIGURE 2.2: TIM-400 Characterisation Experiment Data  
 Purple line: LAND blackbody reference temperature as measured by PTR  
 Blue line: TIM-400 with calibration event on every 60 seconds ( $\pm 2^\circ\text{C}$  as per data sheet)  
 Red line: TIM-400 without calibration events

### 2.4.3 Computing Platforms

The platform on which the device is to be built has to fulfil specific requirements. It needs to be small and powerful enough to fit into a mobile casing, allow real-time video editing (xor rasterisation and alpha blending) in addition to fast User Interface (UI) response times and the possibility to handle two visible light cameras for 3D stereo imaging. This would allow for automatic detection and outlining of the foot as well as merging multiple individual IR images into a single 3D representation. It would also allow the correction of non-lambertian radiation power where the orientation of the foot is not orthogonal to the camera, typically at the edges of the foot. The software written for the device (see section 2.5) does not make use of a Graphical Processing Unit (GPU) and thus it is not a necessary requirement but is a nice-to-have for future developments. The following list is a summary of the individual technical minimum requirements for the computing platform:

1. Hardware
  - (a) Two webcams in order to facilitate 3D imaging
  - (b) One infrared camera
  - (c) Keyboard connection port for maintenance
  - (d) USB Stick with at least 1GB space for external IR image storage



- (e) Battery, rechargeable, 4 hours power
  - (f) At least one USB port for a USB hub or 4 USB ports for:
    - Permanently: 1a and 1b
    - Temporary: 1c and 1d
  - (g) Storage for at least 1 GB of image data
  - (h) Reasonably sized touchscreen for ease of use
2. Software
    - (a) 4 computation threads for 1a and 1b and real-time video editing
    - (b) 256 MB Memory for Linux and program overheads.
  3. Low power consumption to prevent:
    - Build-up of heat
    - Fast battery exhaustion, 1e
  4. Low EM emissions for CE marketing and medical device directive (MDD) regulatory compliance.

Some of the platforms that were available at the time were the Raspberry Pi 2, the HummingBoard and the Odroid-U3. Each of these devices is small and provides four to eight computing cores as well as a graphics processor (GPU) for fast image processing. From the comparison in table 2.4, all three mentioned computing platforms would be able to handle the requirements listed above. However, at the time of planning and construction of the device, the Banana Pi, Roseapple Pi, HummingBoard and Raspberry Pi 2/3 had not been developed yet, thus making the choice of computing device straightforward: the Odroid-U3.

Name	CPU Cores (Architecture)	GPU Cores	Memory	USB Ports	IO pins	Cost (USD)
Raspberry Pi 1 A+	1 (ARM11)	4	256MB	1	40	-
Raspberry Pi 1 B+	1 (ARM11)	4	512MB	4	40	45
Raspberry Pi 2	4 (Cortex A7)	4	1GB	4	40	45
Raspberry Pi 3	4 (Cortex A7)	4	1GB	4	40	45
Odroid-U3	4 (Cortex A9)	4	2GB	3	-	69
HummingBoard	1/2/4 (FreeScale i.MX6)	-	up to 4GB	2/4	26/36	50-102
Roseapple Pi	4 (Cortex A9)	64	2GB	3	40	-
Banana Pi	4/8	2-64	up to 2GB	0-4	40	30-50

TABLE 2.4: Comparison of various small, mobile Computing Platforms [19, 20, 21, 22]

## 2.5 Software

The software associated with this project is divided into 4 parts:

1. The device software
2. The analysis software for the users
3. The web-based analysis preparation software
4. The analysis software and scripts

The **device software** was written by the author for the purpose of visual and IR image acquisition and transferring the images to a laptop provided to the clinical users for this project. It provides facilities to enter basic patient information (trial identifier and date of birth) and semi-automatic organisation of data into folders. It was expected that the users will use the USB transfer function in the software regularly to copy the data from the device to a USB stick and further to a laptop. The details of the device software are further explained in section 3.2.2

Once the data was transferred to the laptop, a separate piece of analysis software for users, written by the authors' supervisor, was used to mark regions of interest (ROIs) on the acquired images and export the data into the well known comma separated values (CSV) format for further analysis.

The author's approach to the analysis is the usage of a standardised data set. This means that all images are processed so that they show only the feet (removing any background) and then, in a second stage, brought into a standard shape with identical size, position and orientation. A pre-processing stage is therefore needed to segment the foot or feet in each image from the background. Segmentation of the images is a non-trivial task because the infra-red band may not contain adequate contrast to the background for automated algorithms (for an example see figure 3.2a). In order to aid segmentation with 3D data, two visual cameras were originally planned for the system but could not be built in due to bandwidth limitations of the USB bus of the Odroid-U3. Instead a single visual camera was used and the IR and visual images were aligned manually. This was a labour intensive process but proved to be sufficient for the purpose of this study.

An alternative method is proposed by Vardasca et al. which allows semi-automatic data collection by warping the original images into a standardised format [23]. However, the method can become time consuming when a large amount of control points

need to be placed such as when curved outlines are involved. Instead, the author proposes the use of cubic splines to interpolate control points and thus effectively reduce the amount of control points that need to be placed.

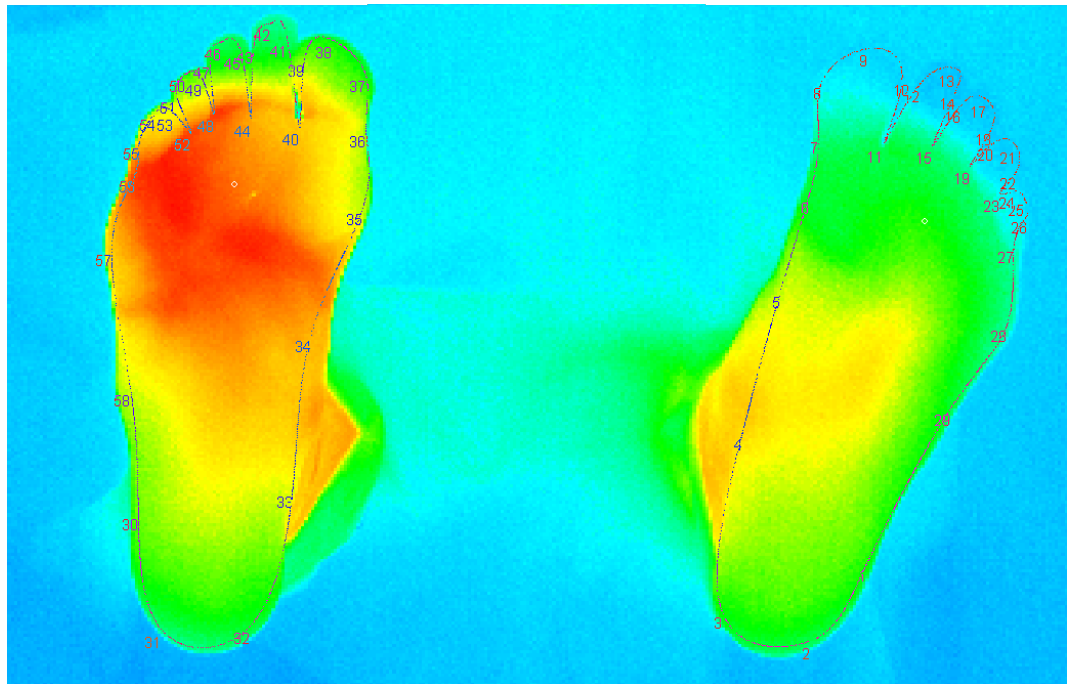
Even though the amount of control points that needed to be placed was reduced, there was still the need to place the points. For this purpose a **web-based analysis preparation software** was created by the author that allows multiple people to simultaneously place points on the data set and provides independent validation for each image. The details of this piece of software are further explored in section 3.2.2.

After the outlines had been created on the images they could be made into a standardised data set from which temperatures could be automatically extracted. The data was then able to be analysed by various classifiers. The **analysis software and scripts** are detailed in section 3.3.

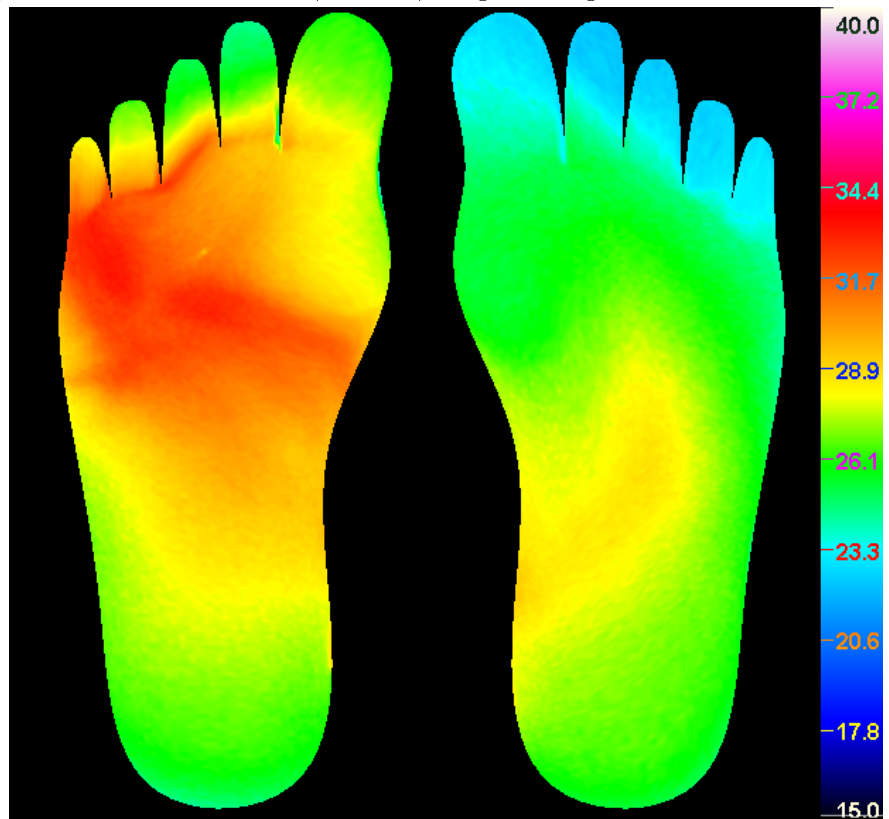
### 2.5.1 Warping

The feet of people are thermally and geometrically very different from each other and thus create technical problems when large amounts of image data are to be processed automatically. The image data therefore has to be geometrically standardised before it can be processed further. One method of doing this is called warping. Figure 2.3a shows an example of placing control points and warping using a piece of software written by the author. Figure 2.3b shows the resulting image, whose quality is lacking for three reasons:

- The information was encoded using lossy compression, where some data is permanently lost when the file is saved. This can be fixed by using the radiometric data instead.
- Post image processing was applied to the image to fill patches of unknown data created by the warping process.
- The temperature of the whole foot changes (see figure 2.3 and section 2.5.5)



(a) Control point placement (numbers), original image size 382x288, here cropped



(b) Warped image from figure 2.3a, image size 764x576

FIGURE 2.3: Example of warping process using 29 control points (interpolated to a total of 290)

As demonstrated in figure 2.3, the process of warping an image is altering parts of

it into different shape(s) and size(s). There are two possible methods of performing warping on an image; vector-based and pixel-based. Both methodologies are split further into forward-mapping and backward-mapping algorithms. Forward-mapping algorithms use the original image data and map it to new image data. Backward-mapping does the exact opposite and works out the original pixel position in the source image from the destination image position [24, 25].

Plenty of methods have been well explored in the computer animation industry due to the practical application of altering 3D objects using specified control points. Typically, an object is modelled in a rest pose and proceeds to be transformed using techniques such as bone meshes. However, in a 2D environment, the rest pose can be regarded as the original image. Most of the methods make use of barycentric coordinates, which is a method of defining a shape based on edge points.

Barycentric coordinates can be calculated in a variety of ways, but they are all defined by the reproduction property:  $\sum_{i=1}^n w_i(x)c_i = x \forall x \in \Omega$ , where  $c$  is a set of control points,  $n$  is the amount of control points and  $w$  is a function of weights for each  $x$ . There is a variety of methods available, such as mean value coordinates (MVC), bounded biharmonic weights (BBW) and local barycentric coordinates (LBC) [26, 27, 28]. In this project, BBW was used because it provided the best fit in terms of calculation speed, locality and accuracy, this is explained in more detail in the section 2.5.4.

### **2.5.2 Pixel Interpolation**

After warping is complete, the image may be missing pixels due to the possibility of enlarging parts of the image, thus creating black pixels. To compensate and allow for data analysis, the black pixels need to be filled in a manner that seems coherent to the human eye but at the same time does not alter the data by skewing the results. Several techniques for approximations are available such as nearest neighbour, bi-linear filtering and cubic interpolation.

The nearest neighbour approach uses each undefined pixel and assigns the nearest pixel's colour to it. The methodology uses a search algorithm for each pixel, making it very fast. However, the quality of the resulting image is not satisfying in the context of this work because it may override values from other neighbouring pixels, and thus it might skew the data depending on the location of the pixels before and after the transformation.

On the other hand, filtering involves calculating the intermittent values between two pixels based on the location of the resultant pixel, thus making a smooth transition between the interpolated pixels. Bi-linear filtering takes into account the four adjacent pixels and tri-linear filtering uses multiple progressively smaller, optimised, sampling images (mipmaps) together with bi-linear filtering. Due to the fact that the images being produced are in 2D, tri-linear filtering is not an option.

Bi-linear and bi-cubic filtering are very similar with regard to basing their interpolation on the four surrounding pixels but calculate the interpolated pixels differently. Where bi-linear filtering uses linear fitting, bi-cubic filtering uses cubic splines to allow for a continuous gradient across the interpolated surface but in return takes almost twice the time to compute.

Table 2.5 summarises the differences between the aforementioned pixel interpolation techniques. Although bi-cubic filtering produces visually more appealing images, bi-linear filtering is the faster and simpler-to-implement interpolation method. It was therefore chosen as the algorithm to perform pixel interpolation in the context of this work.

Name	Interpolation type	Dimensionality	skews data	speed (seconds)	suitable
Nearest neighbour	threshold	2D/3D	yes	0.0087	no
Bi-linear filtering	linear	2D	no	0.0120	yes
Tri-linear filtering	linear	3D	no	-	no
Bi-cubic filtering	cubic spline	2D	no	0.0222	yes

TABLE 2.5: Comparison of different Pixel Interpolation Techniques, speed is measured as the mean of 20 runs of up-scaling a 382x288 image to 764x576

### 2.5.3 Splines

The fundamental idea behind a spline is to create a smooth, curved boundary from control points. The shape being defined by the control points is therefore non-linear and employs curve fitting to find an optimal solution. This is particularly useful for this project due to the shape of feet and the necessity for manual segmentation arising from the lack of contrast in images. A non-linear approach to the problem requires interpolation, a concept that has been known and used since the 1950s [29]. Today, several different methods of spline interpolation exist. However in this work only methods that restrict the spline segments to pass through the control points are suitable to ease their placement. Table 2.6 shows some of the methods available and their properties. For the purposes of this work, the cubic spline method was found to be the most suitable.

Name	Passes through start and end point	Passes through all control points
Bezier Curve	Yes	No
B-spline	Yes	No
Cubic Spline	Yes	Yes

TABLE 2.6: Comparison of different Spline Interpolation techniques [30, 31, 32]

### 2.5.4 Combining Cubic Splines with Barycentric Coordinates

A necessary step before any processing can begin is solving the problem that cubic splines interpolation may create areas outside the polygon defined by the original control points. This leads to negative barycentric values (see figure 2.4) and in turn causes mapping vectors to reverse direction, effectively rendering the image warping approach useless. To counter the problem, a solution was introduced by the author to define all interpolated points from the cubic spline algorithm as control points (see section 7.2). In this approach, the polygon's area is extended to meet the cubic spline. This solution however introduces another problem; how many control points should be interpolated for each spline segment? Lastly, there was a choice between the aforementioned methods of calculating the barycentric coordinates.

Generally, the choice of how many interpolated control points to use is a trade-off between accuracy and computational complexity. As the number of interpolation points increases, the boundary becomes smoother but in turn adds a dimension for each added control point. However, the computational complexity is not a limiting factor due to possibility of backward-mapping (see 2.5.1). The coordinates therefore only need to be computed once for the destination image.

In order to assess the influence of the number of interpolation points on the process 3 different barycentric calculation methods were tested with various amounts of points. Each investigated calculation method was graphed as a map of the influence of a given selected point on the respective warping method. In figure 2.5 a higher influence is denoted by a higher coordinate value in relation to the selected point. The primary constraint for choosing an appropriate method is that the influence does not extend to a region that is not within the line of sight of the selected point as it may cause the region to move outside of the designated target polygon. Figure 2.5 shows the outcome for 2 cases: one interpolation point and 10 interpolation points, where one interpolation point signifies the original control point set. While for the latter calculations result in much smoother boundaries with each individual interpolated

point influencing a smaller area of the foot the higher amount of control points causes the calculations to become eventually unstable as demonstrated by the "did not compute" box for local barycentric coordinates.

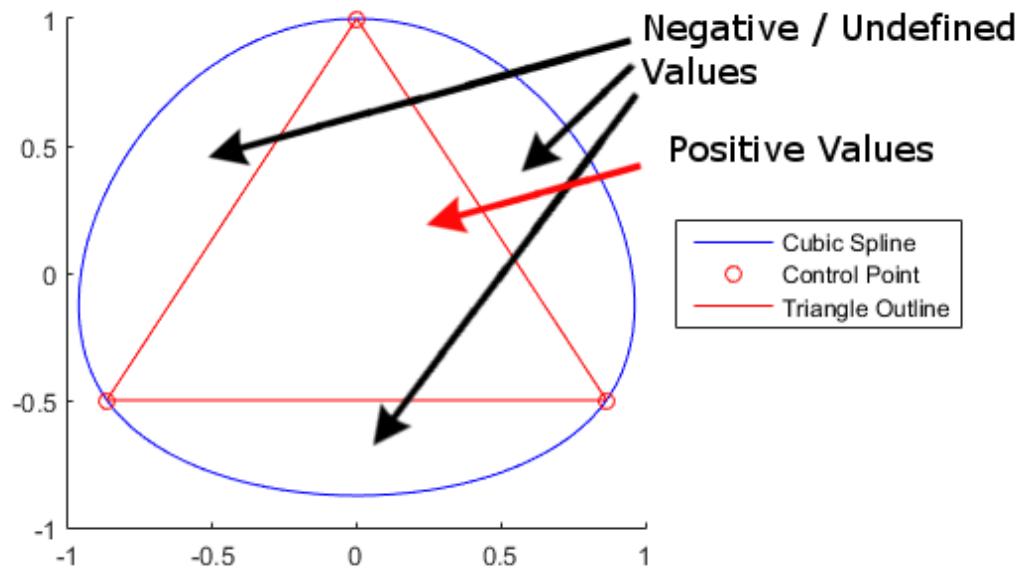
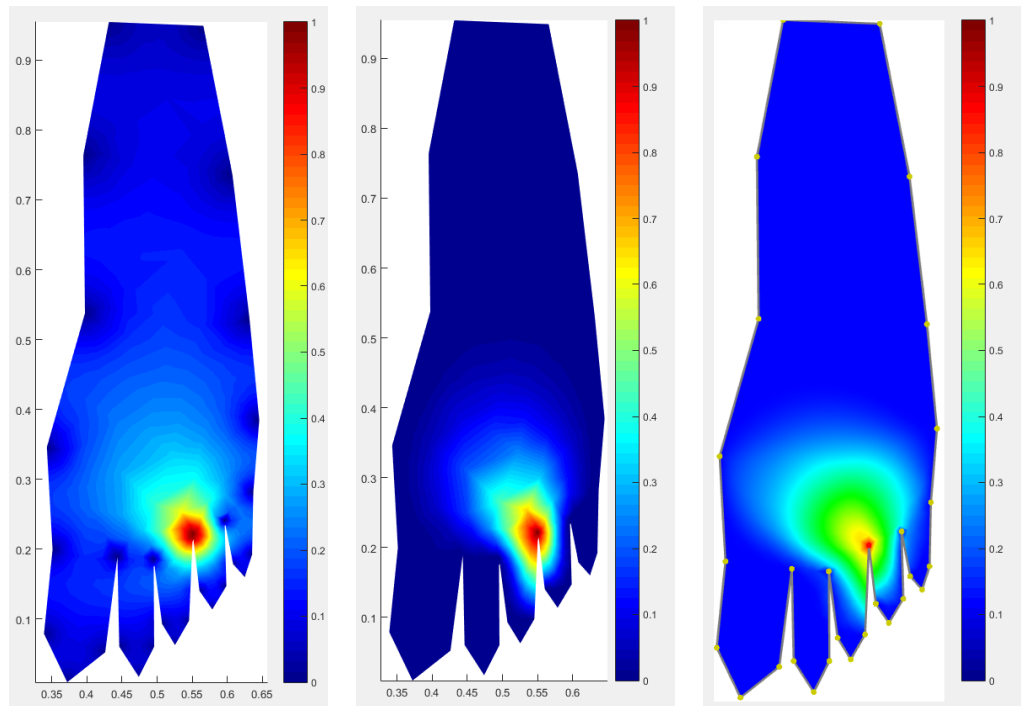
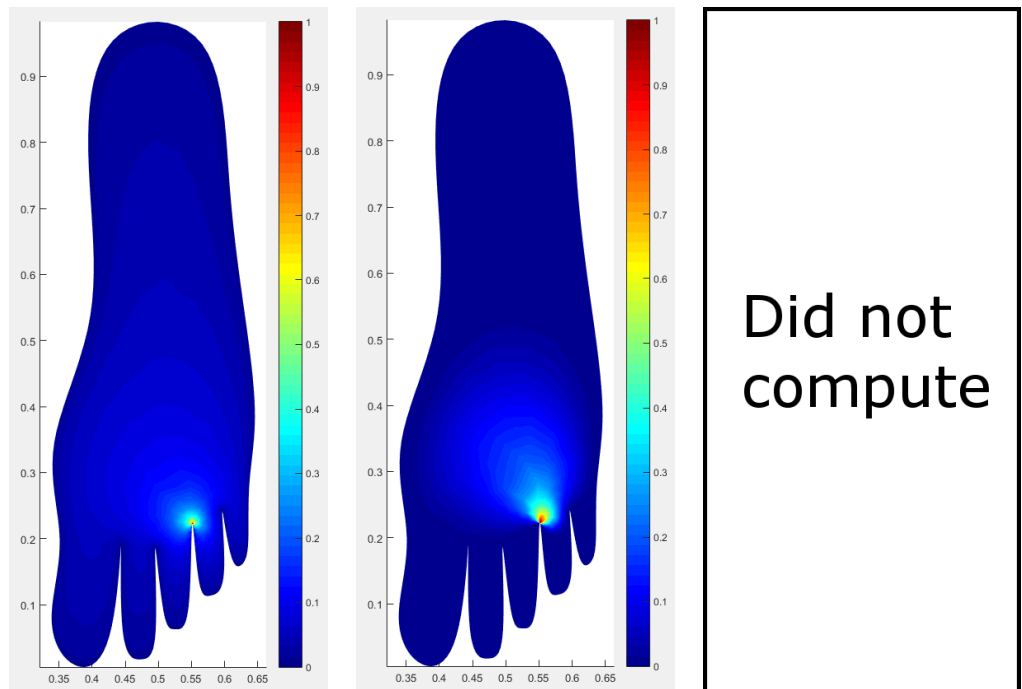


FIGURE 2.4: Diagram showing where negative points would occur





(a) Mean value coordinates with 1 interpolated point    (b) Bounded Biharmonic coordinates with 1 interpolated point    (c) Local Barycentric coordinates with 1 interpolated point



(d) Mean value coordinates with 10 interpolated points    (e) Bounded Biharmonic coordinates with 10 interpolated points    (f) Local Barycentric coordinates with 10 interpolated points

FIGURE 2.5: Comparison of different Barycentric Coordinate calculation methods  
Colours indicate the influence of the selected control point on the polygon when warping

0 indicates no effect and 1 indicates full effect

### 2.5.5 Validity of using Barycentric Coordinates

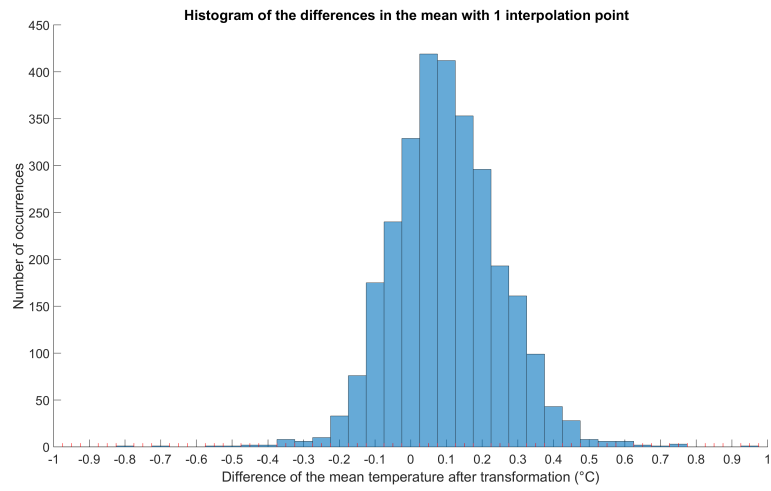
Although the method of combining barycentric coordinates with cubic splines works, it remains to be shown that the method has an insignificant effect on the temperature data once an image has gone through the warping process. This was tested by comparing the mean and standard deviation of each of the 2270 plantar foot infrared images in the second trial before and after warping. Figure 2.6 shows the histograms of the temperature differences of the mean between original and warped images. Figure 2.6a shows the difference for 0 interpolation points, figure 2.6b shows the difference for 1 interpolation point and figure 2.6c shows the difference for 10 interpolation points. Figure 2.7 shows the histograms of the temperature differences of the standard deviation between original and warped images. Figure 2.7a shows the difference for 0 interpolation points, figure 2.7b shows the difference for 1 interpolation points and figure 2.7c shows the difference for 9 interpolation points. For each of these six figures, a t-test was carried out to identify any statistically significant changes in the data.

The t-test results outlined in 2.7 show that the p-values for both the mean and standard deviation are between 0 and 0.001. These values allow the conclusion that there is strong evidence that the data before and after the transformation differ insignificantly. This is reinforced by the figures 2.6 and 2.7, which showcase the effect of the warping process. Each mean histogram in figure 2.6 has few data points that are close to -0.5 and 0.5 degrees difference but overall most of the data falls within the range of uncertainty of the infrared camera itself.

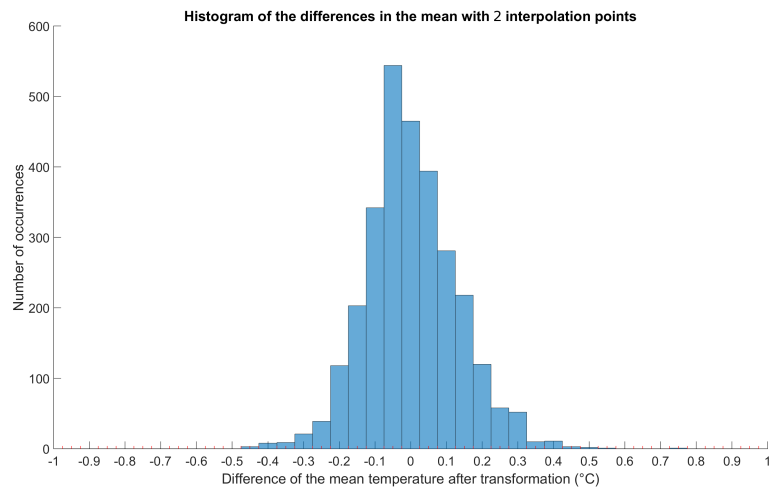
As already mentioned above, choosing the amount of interpolation points therefore becomes a trade-off between smoothness of the spline and computational complexity. The relationship between the amount of interpolation pixels and smoothness is  $\frac{1}{n}$  whereas the computational complexity for warping is  $O(p*n)$ , where n is the number of interpolation points and p the total number of points that need to be warped. The smoothness of the curve is subject to qualitative assessment and therefore the number of interpolation points that was deemed fit for this task was set to 10.

Setting	z-value (mean)	p-value (mean)	z-value (std. deviation)	p-value (std. deviation)
0 points	35.54	4e-230	-40.37	2e-283
1 point	1.03	0.0079	-8.06	1e-15
9 points	-11.7	0.0077	10.15	8e-24

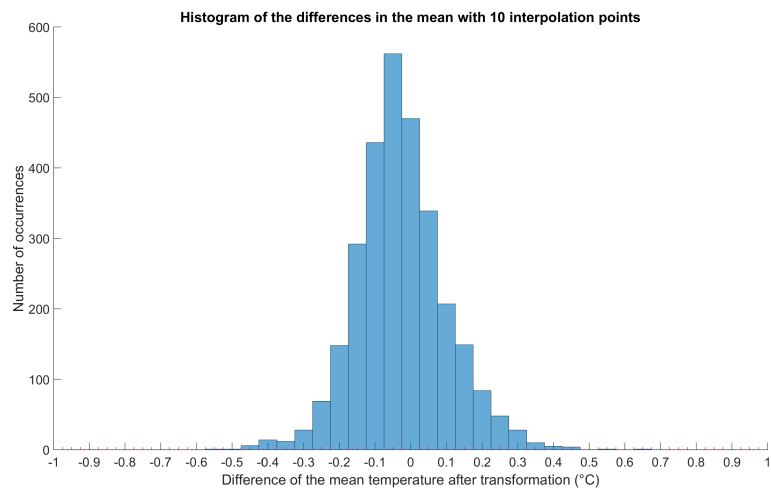
TABLE 2.7: T-test statistic values for section 2.5.5



(a)

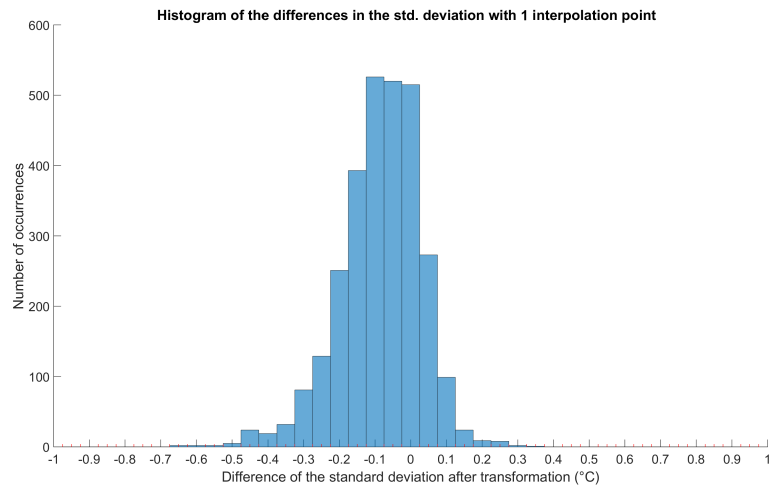


(b)

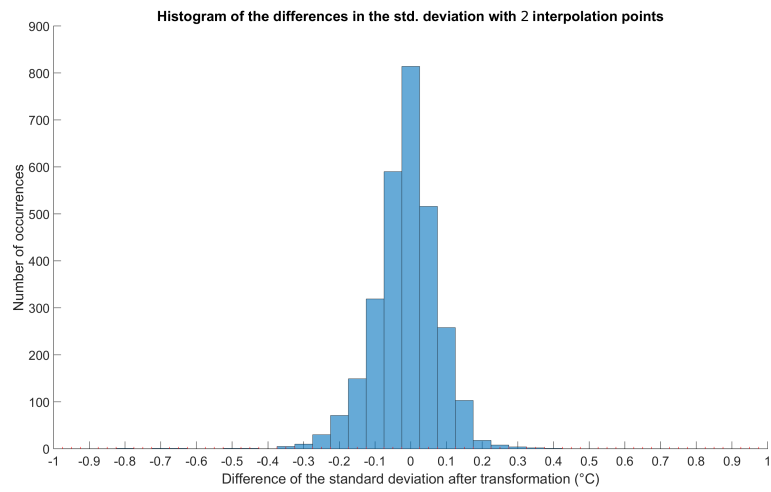


(c)

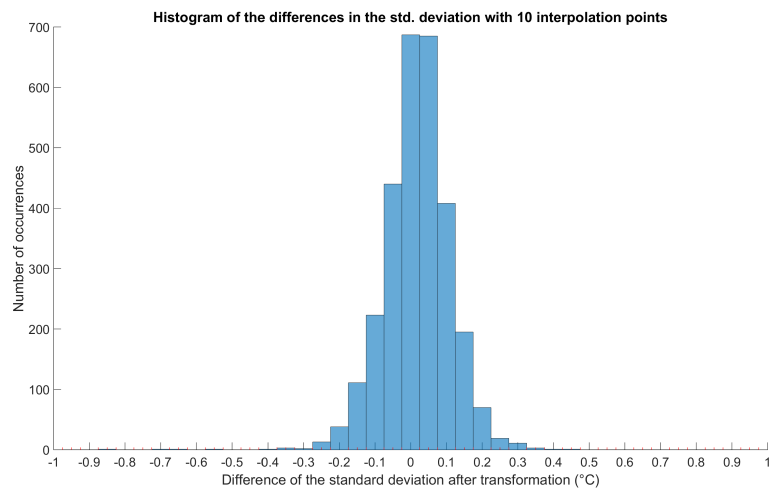
FIGURE 2.6: Histograms showing the difference in **mean** temperature between pre- and post-processing of each foot



(a)



(b)



(c)

FIGURE 2.7: Histograms showing the difference in **standard deviation** temperature between pre- and post-processing of each foot

## Chapter 3

# Materials and Methods

### 3.1 Study Protocol

The project's data collection was divided into two trials according to the project plan devised by the i4i project consortium. The first trial studied a control group with healthy volunteers, followed by the second trial with diabetics. In each trial, approximately 110 patients underwent an imaging process defined in the clinical protocol. The clinical protocol was designed with consideration to each aspect of the project:

1. Medical
2. Measurement Control
3. User Laptop Software
4. Device Software

The medical aspect of the project was assigned to the three hospitals involved in this project (Pennine Acute Hospitals, Freeman Hospital Newcastle, Kings College Hospital London), the Measurement Control aspect was directed by the National Physical Laboratory, the User Laptop Software was allocated to the authors' supervisor and the device software was assigned to the author. A copy of the protocols is provided in appendix E. The main aspects of the clinicians check-list are summarised below:

1. Check inclusion criteria:

- (a) Aged 18 or over
  - (b) Has intact feet
  - (c) Has palpable foot pulses
  - (d) Able to fluently speak and understand English and be able to provide meaningful written informed consent for the study
2. Check exclusion criteria:
    - (a) Has active foot ulceration and/or infection
    - (b) Has foot deformity which in the opinion of the Investigator, would interfere with interpreting the results of the study
    - (c) Has any uncontrolled illness that, in the opinion of the Investigator, would interfere with interpreting the results of the study
    - (d) Has an implantable electronic device
  3. Record room humidity
  4. Record room temperature (controlled as best possible to be between 22 and 24 °C).
  5. Turn on the infrared camera device (starts warm-up and self-calibration).
  6. Acclimatise the patient to room temperature for 10 minutes.

Each patient included in the study was assigned a trial identifier and a group. The identifier consisted of three numbers followed by three letters, padded by underscores. There were a total of three groups: A, B and C. Group A contained patients where clinicians were blinded with respect to the thermal data (i.e. they could not see the infrared image of the patients' feet, only the visual image), group B were not blinded (clinicians could see both infrared and visual images) and patients in group C failed the initial screening test and were thus not included in the trials.

The imaging device was programmed by the author to capture a software-defined sequence of images, divided into 6 different views, plantar (both feet), dorsal (both feet), left foot medial, right foot medial, left foot lateral and right foot lateral. Several checks were built into the software to ensure that the sequence was recorded correctly:

- A time check was implemented to enforce that the device warming-up time was observed. A further check guaranteed the correct time interval between imaging sequence repetition specified in the clinical protocol.

- After each sequence clinicians had to manually review each image and assess if it included the whole foot, that it was at the right distance (see section 3.2.1 for implementation) and did not show any unwanted items or occlusions. This process also ensured that the sequence was complete and no images were missing.
- For each image of the sequence the device was programmed to display for the clinician the name of the view to be acquired (eg. "both feet, plantar view") and an outline of this view was overlaid onto the live image to help them capture the foot image in a standard orientation so that the subsequent warping process described in chapter 2 involved as little deviations as possible.

To the best knowledge of the author this was the first time that such an enforced and controlled imaging sequence was used in a clinical trial. As a result the vast majority of image sequences complied fully to the protocol and virtually all images could be included in the analysis.

In each view, several ROIs are defined to resemble spot measurements taken with a Dermatemp 1001 spot thermometer (accepted as the "gold standard" at the time of writing) for cross-referencing. The room temperature was recorded at the beginning and the end of each patient's visit.

In the first trial, this sequence was imaged in quick succession and after each view. The sequence was then repeated and finally, three more plantar images were imaged to assess the repeatability of the infrared camera device. In the second trial the image sequence changed by removing the last three plantar images because repeatability was already established by the results from the first trial.

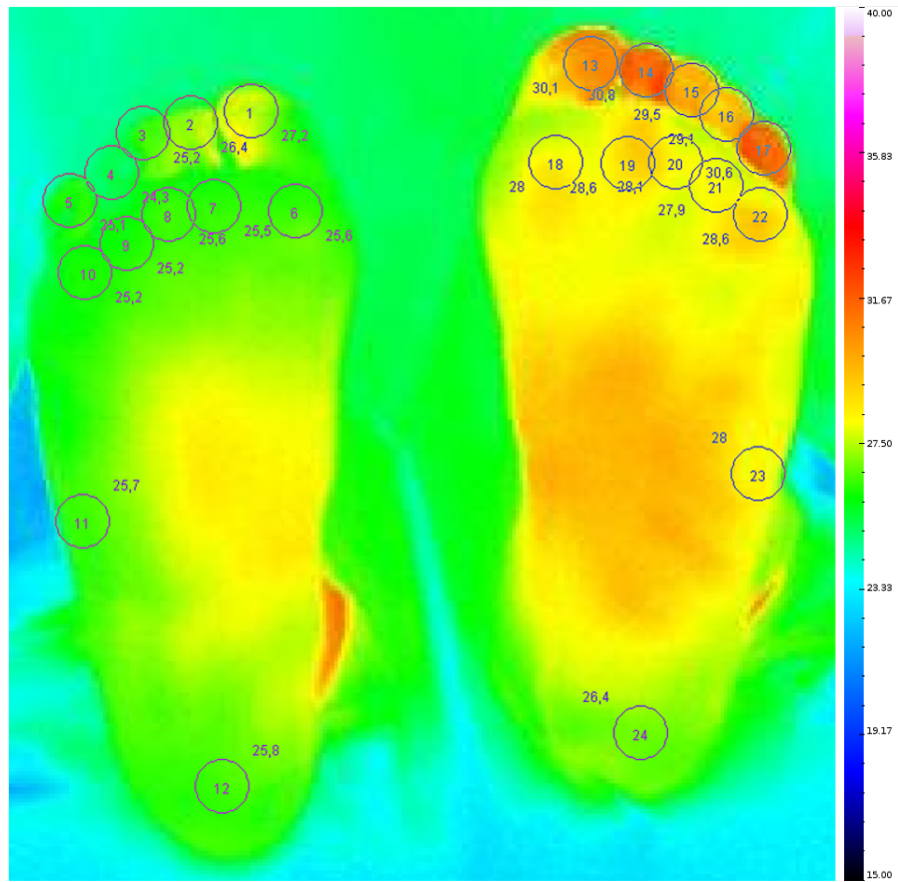
The first trial ended at the end of September/beginning of October 2015 and contributed 109 normal (control) image data sets. Figures 3.1 and 3.2 show a sample of the images that were taken. Figure 3.1 and the associated ROI data plots in figure 3.3 demonstrate that a simple comparison between left and right foot, as often indicated in literature [8, 9, 10, 11, 12], is not sufficient to confidently predict a foot ulcer. Moreover, in figure 3.2, an abrupt change in temperature can be observed between the 5<sup>th</sup> and 7<sup>th</sup> minute. It was later found that the volunteer was an active footballer, a sport that can exert high asymmetric stresses on the feet. Physiological adaptation to these stresses may explain the sudden change in observed temperature.

In their totality the results from both trials demonstrated:

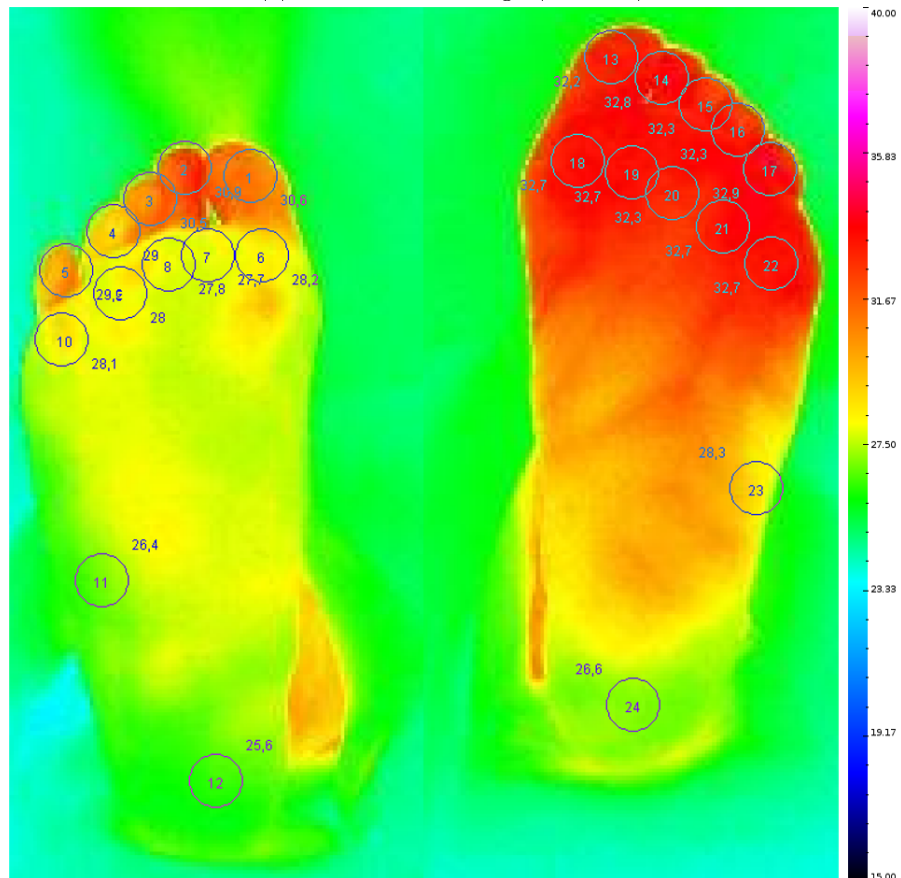
- A simple left-right temperature comparison on its own is one potential indication of a developing foot ulcer but other corroborating factors are required to achieve a reasonable specificity
- A simple hot spot definition such as a particular area of the foot being  $2.2^{\circ}\text{C}$  warmer than the average of the respective foot is also on its own not a reasonably reliable predictor
- A single thermal imaging session approximately every 4 weeks is not sufficient to capture the onset of ulceration for most patients

The data and reasoning for the above 3 statements together with a suggested improved methodology for detecting the onset of ulceration is provided in chapter 4. Before that the remaining sections of this chapter outline the hardware and especially the software produced by the author incorporated into the imaging device that helped the clinical team to arrive at the above results.



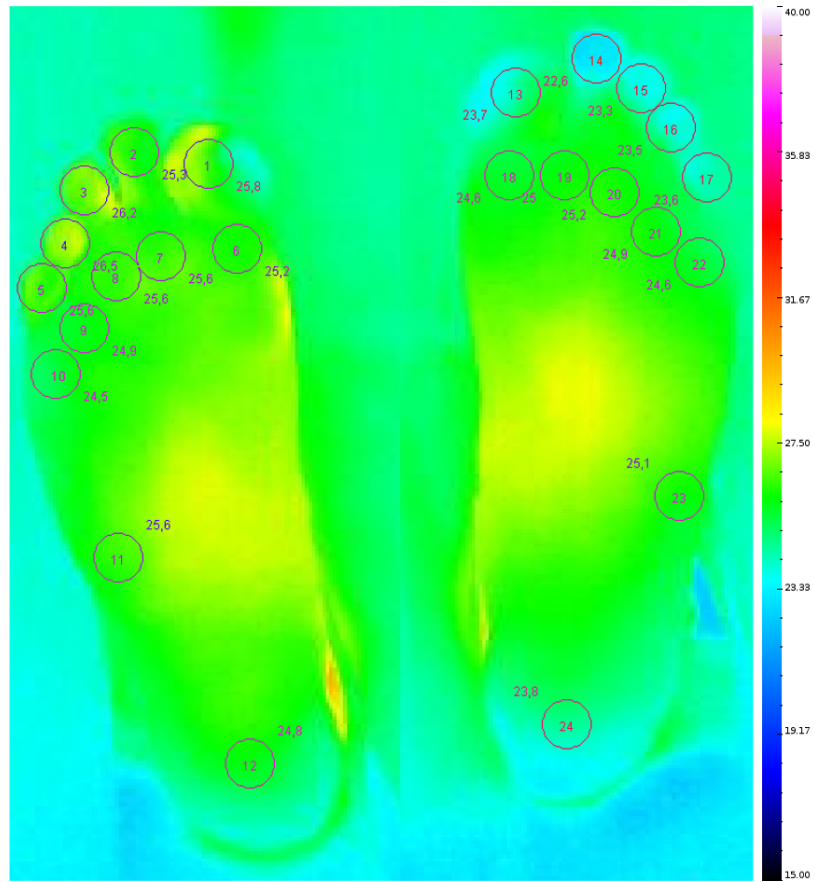


(a) First plantar image ( $t=0$  min)

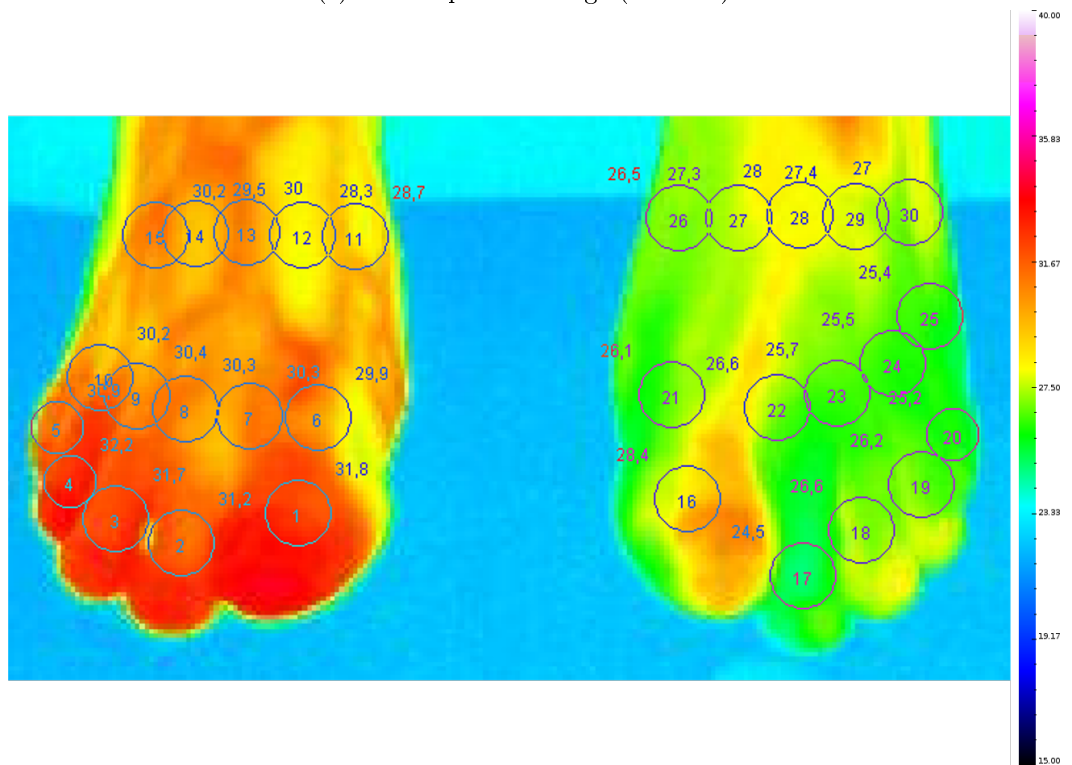


(b) Fifth plantar image ( $t=20$  min)

FIGURE 3.1: Healthy volunteer showing asymmetry between left and right plantar view at the beginning and at the end of a 20 minute examination

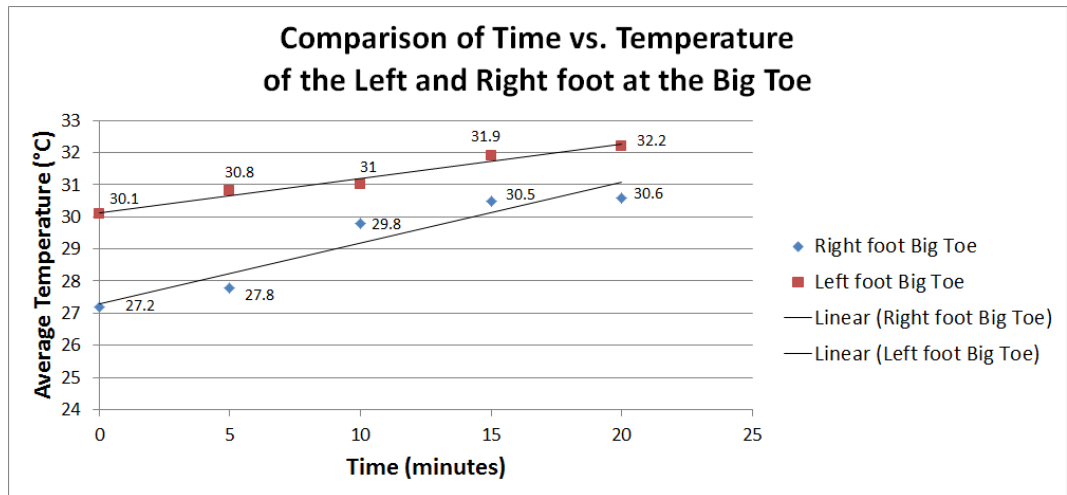


(a) Second plantar image (t=5 min)

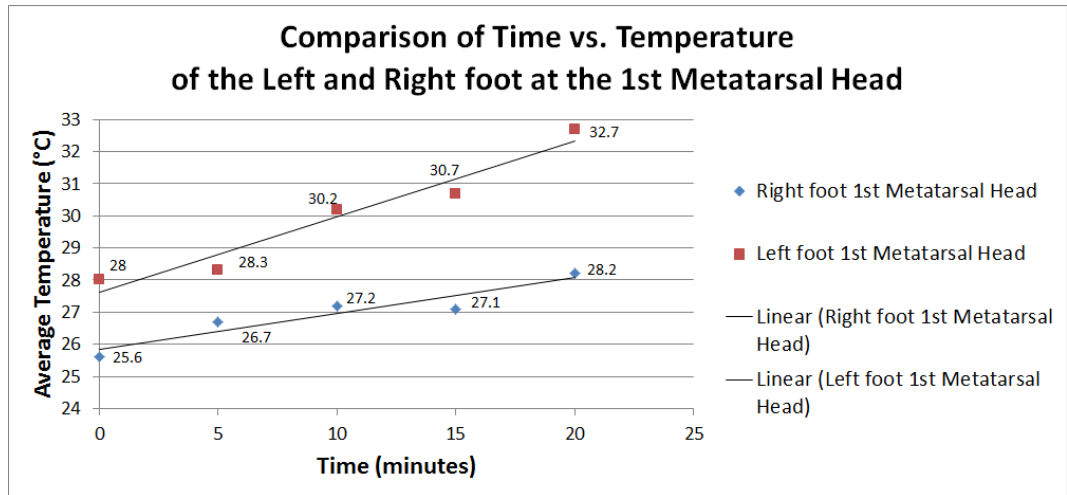


(b) Second dorsal image (t=7 min)

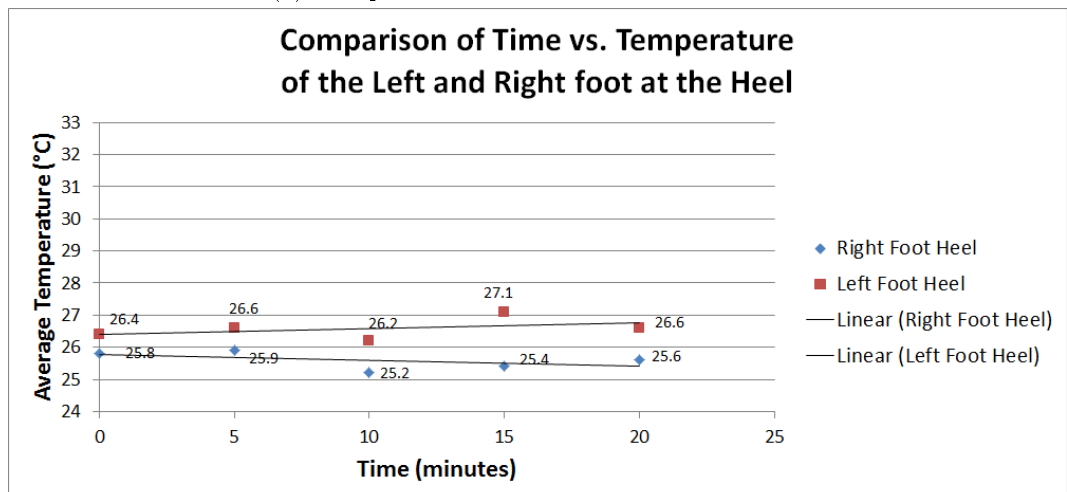
FIGURE 3.2: Healthy volunteer showing sudden temperature change within 2-3 minutes



(a) Comparison of the Big Toe



(b) Comparison of the First Metatarsal Head



(c) Comparison of the Heel

FIGURE 3.3: Data from Areas of Interest from volunteer in figure 3.1

## 3.2 Measuring Device

### 3.2.1 Device Hardware

The Diabetic Foot Ulceration Prevention System (DFUPS) device built using the specifications in table 3.1 is shown in an exploded plan of the device (figure 3.4). One of the web cameras was eventually not useable due to USB bandwidth limitations and was replaced by a speaker to provide audible feedback for the clinician when an image had been saved (artificial shutter sound). Two angled green Light Emitting Diodes (LEDs) projectors underneath the openings for the webcams allowed for a correct distance to the target by triangulation i.e. when the two projected green dots did not overlap, the distance was not correct. For the duration of the study, there were four imaging devices and three laptops available to the hospitals. Shortly after the devices were built by Photometrix Ltd. (one of the collaborating partner in this project), they were sent to the National Physics Laboratory (NPL) to characterise the infrared cameras for their drift over time, temperature difference to the ITS-90 scale and the correction thereof. The three cameras that showed the least drift in temperature over time were sent to the hospitals. The last instrument was kept as a spare in case of problems with a different device. The process of characterisation was repeated 3 times throughout the study, before trial 1, between trial 1 and 2 and at the end of trial 2. The results were stored as a linear equation per device per characterisation and later applied to the data before analysis using linear interpolation across the time scale to account for the drift effect of the cameras. This effect was in the range of -2.8% to 0%, where the percentage refers to the measured value, in addition to a static bias between 0.7°C to 2.4°C.

Component	Name
Computing Platform	Odroid-U3
Infrared Camera	Micro-Epsilon TIM-400
Webcamera #1	Odroid USB-Cam 720P
Webcamera #2	Unavailable due to USB bandwidth issues

TABLE 3.1: Current Device Components



FIGURE 3.4: DFUPS Exploded Plan - One of the web cameras was not useable due to USB bandwidth limitations and was replaced by a speaker

### 3.2.2 Device Software

The software for the imaging device was planned and developed by the author to allow the clinicians to enter details about a patient when he or she enters the trial, take images and pull images off of the device and onto a USB stick. Figure 3.5 shows the simplified flow chart outlining the control flow of the program. It shows some of the technical details for other features of the device such as automated recovery in the event that it crashes. Figure 3.6 shows screenshots of the device software and the software that runs on the laptops for the extraction of regions of interest and outlining of the feet.

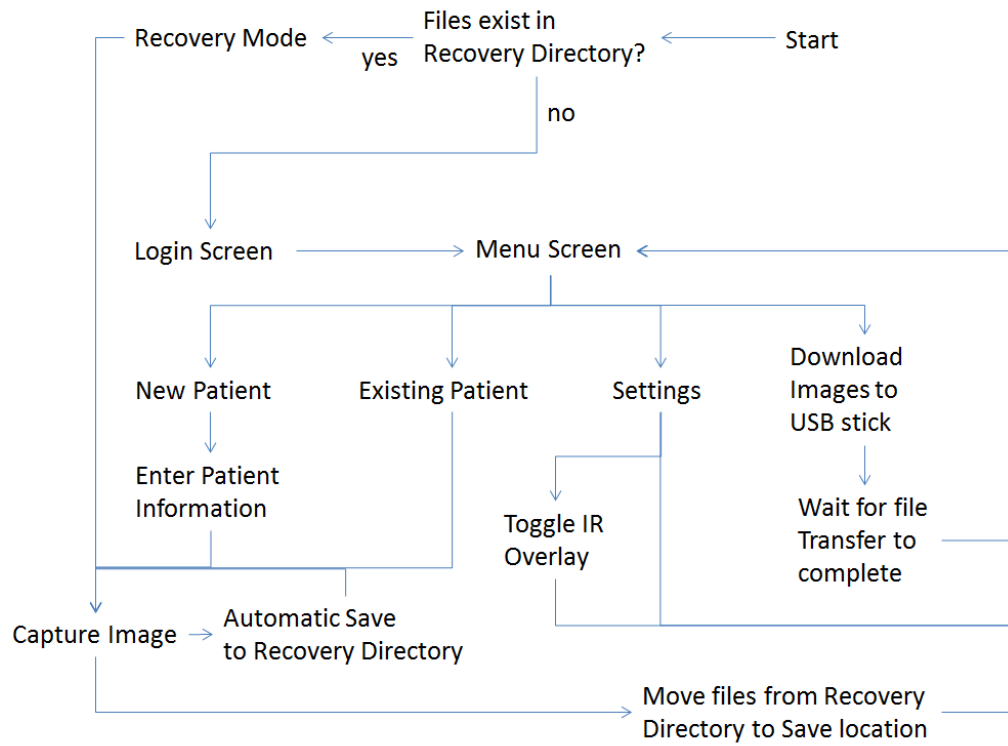
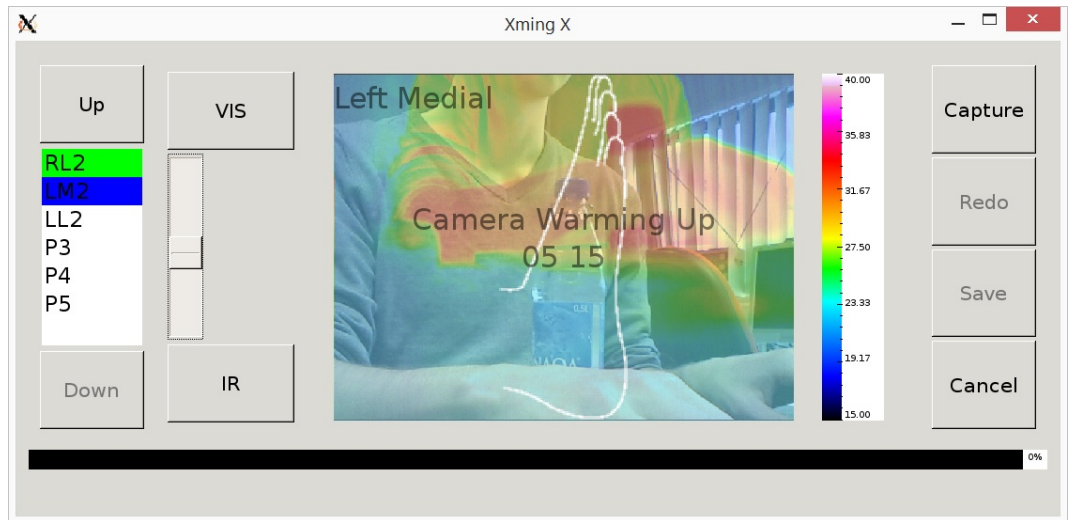


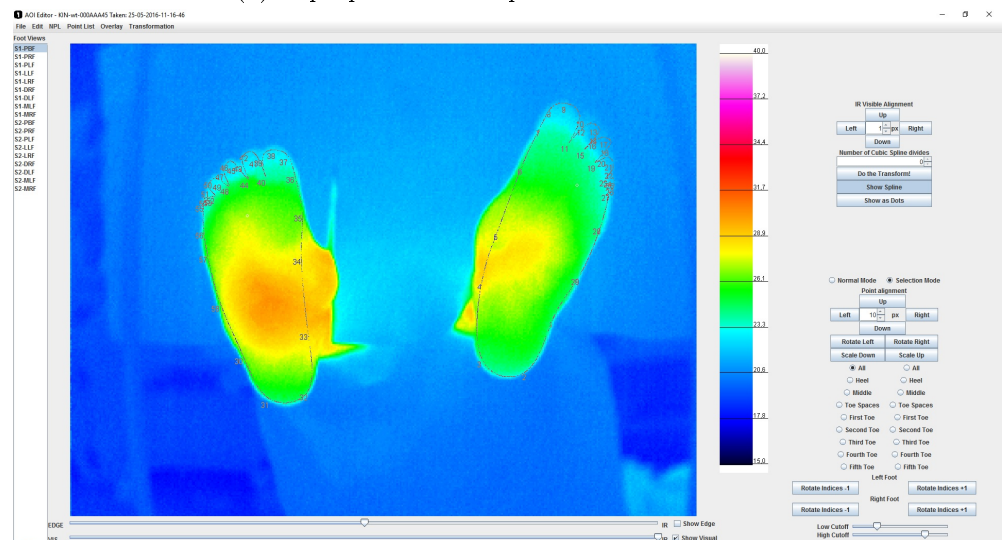
FIGURE 3.5: Flow chart of the Software running on the DFUPS device



(a) Device Software with a 50-50 mix between the infrared and visible spectra



(b) Laptop software to place Areas of Interest



(c) Laptop software to place Outline Control Points

FIGURE 3.6: Screenshots of the Device and Laptop Software

The device software makes use of various libraries to be able to function correctly. These include QT5 for the graphical display, OpenCV for the capture of images from the attached webcam and a proprietary library written by Micro-Epsilon GmbH for the infrared camera [33, 34]. The development was done using the device itself and a networking cable to communicate with the device using the secure shell protocol (SSH). The SSH protocol allows the control of a remote computer over a network and the passing of data through it. This method is called tunnelling and can be used with the default graphical interface of Linux (X server) to display and manipulate graphical programs such as QT Creator, QT's Integrated Development Environment (IDE). Within QT, there is an automation program called qmake for the generation of information on how to compile a project. The tool can be configured in a file and was used to link in the aforementioned external libraries.

To keep the development and operation of the device secure, the only method to login over the network is restricted to public-private key pairs, which is a superior method of authentication than a plain password when it comes to security. Although the network side of the device is secured, it is not secured from physical attacks, such as starting the device from a USB stick or worse, plugging in a keyboard and executing codes manually. The risk of physical entry is elevated by the fact that the user running the program has root access. However, this device does not attempt to connect to a network nor does it allow the user to input credentials to a network, so a physical attack will only result in the device being stolen. This poses a different risk altogether, as sensitive data may be stored on the devices. This is mitigated by using as little as possible identifying data in the clinical protocol. The only data related to the patients that is stored on the device are the images, the anonymised trial identifier and the patient's data of birth. Even with these measures it is still theoretically possible to correlate the data from the device with data obtained elsewhere, but the likelihood of this happening is very low and the practical difficulties of doing so are very high.

The software that runs on the device saves images in a special file format. It utilises the existing JPEG File Interchange Format (JFIF) standard [35] and adds additional information to the end of the file. This is possible due to the existence of start and end markers in the specification. Programs and Operating Systems are still able to read and display the JPEG image but have no knowledge of the appended data. The complete file structure is as follows:

1. Visual image JPEG
2. Infrared image JPEG



3. A file format version string (3 bytes in ASCII format, for example 1.6)
4. Width and height of the infrared image (expressed as `<width>x<height>px`)
5. Width and height of the visual image (expressed as `<width>x<height>px`)
6. The temperature data (array of 16-bit values, little endian format)
7. the green channel data of the visual image (in effect a monochrome image, an array of 8-bit values)
8. Extensible Markup Language (XML) format containing:
  - (a) Image identifier in the series described in the clinical protocol (for example P1, S1-PL2, D1, etc.)
  - (b) An image timestamp
  - (c) ID of the hospital (KIN, PEN or FRH)
  - (d) ID of the operator
  - (e) Anonymised ID of the patient
  - (f) Visit number (starting at 0)
  - (g) Temperature readouts of the infrared camera (shutter, housing and chip)
  - (h) Date of birth of the patient as three separate entries
  - (i) Group of the patient as described in 3.1
  - (j) Areas of interest (added manually on the laptop) as a list of:
    - i. Normalised x coordinate
    - ii. Normalised y coordinate
    - iii. Normalised radius
    - iv. Mean temperature
    - v. Flag if the ROI is an ulcer
    - vi. Flag if the ROI is tentative (to be decided if ulcer or not)
  - (k) Outline of the foot as a list of:
    - i. Normalised x coordinate
    - ii. Normalised y coordinate
    - iii. Normalised radius
  - (l) Data referring to the user interface on the laptop:
    - i. Overlay x position (visual image offset relative to the infrared program)

- ii. Overlay y position (visual image offset relative to the infrared program)
- iii. Overlay opacity
- iv. Flag to show only the visual image
- v. Number for the thresholding of the temperature data for visual effect
- vi. Beginning of the colour scale
- vii. End of the colour scale

The advantage of using a format that fits into one file is the organisation and moving of the data within an operating system but the downside is that special code is needed to read out the data. Hence another program is needed to extract the data from the file into different formats such as CSV.

Figure 3.6a shows a screenshot of the device software with the capturing screen. This software was written to be used on a touchscreen hence the buttons were made to be large to allow ease of use. The black bar at the bottom of the window is the battery charge level indicator, which was disconnected at the time, therefore showing 0% charge. Located on the left side is the ordered series of images that needed to be taken, mirrored from the clinical protocol (see section 7.2). A review policy encoded in the software enforces the clinician to look through the images before saving them (fulfilled with the "Up" and "Down" buttons). In the list of image identifiers (an abbreviated code for the foot view), green represents an image that has been saved to a temporary directory, blue the current index and white the images that have yet to be taken. To the immediate right is a slider that allowed the mixing of the infrared and visual images to be controlled. This was achieved using the XOR composition mode offered by QT's QPainter class and setting the opacity of the images to  $Visual_{opacity} = opacity$  and  $Infrared_{opacity} = 1 - opacity$ , where the opacity is a percentage expressed as a value between 0 and 1. To the right of the image is the colour scale of the thermal image, which is fixed between 15 and 40 °C; a range that was decided on by the i4i consortium early into the study to be able to compare images to each other visually, a feature that became important for the hospital's own analysis process. Lastly, on the right side of the window are the controls for taking images. When the "Capture" button is pressed, the index in the image sequence list is not immediately incremented to allow the clinician to check the image has been taken correctly and redo the capture process if necessary before moving on by pressing the "Down" button. After going through the entire sequence, the program resets the image sequence index to the start of the list and requires the clinician to look through the entire image set again before being able to save

the sequence. When it is saved, the images from the temporary directory are moved to the permanent directory structure from which the images can be downloaded. An important aspect of both directories is the usage of non-volatile memory. This enables recovery from an unexpected device state e.g. a crash or battery failure. The program is then able to read in the non-completed series and asks the clinician if it should be continued.

The images were periodically downloaded from the device on to USB storage media that were able to provide hardware encryption. These used a key that needed to be entered on the USB storage medium itself to be unlocked for use. Within the device software there is an option to download the images. This copies the data from the internal storage to the USB storage medium using an algorithm that recursively iterates through the directory structure and copies files that do not exist on the USB storage medium. This has two advantages, firstly, it minimises data transfer and therefore speeds up the operation and secondly, it is possible that the analysis program modifies the files when plugged in to the laptop, thus changes do not get overwritten. Even though this feature exists, the clinicians were instructed to copy the data from the USB storage media onto their respective laptop to have the USB storage media as a backup and the working copy on the laptop.

### **3.3 Analysis Software**

As already indicated in chapter 2 the process of analysing the images in the two trials is a 2-stage process. In the first stage images have to be brought into a geometrically standardised form by warping (see section 2.5.1). Once standardised, automated software tools can be used to efficiently gather information from individual images in the same fast and repeatable way, e.g. to answer questions such as "what is the average temperature of the left big toe in all plantar foot images of trial 1?".

The first stage of the analysis process is responsible for computing standardised images, statistical moments of each image and storing the resulting data in a format that allows consequent processing stages to recall the data in an efficient manner. To accomplish this, several steps are needed:

1. pre-compute barycentric coordinates for efficient warping for backward-mapping
2. outline the foot/feet in each image by placing control points at the appropriate anatomical positions

3. warp and store the input images as separate result images
4. further computation such as the mean and standard deviation for each warped image

The computation of barycentric coordinates was completed in Matlab using code taken from the bounded biharmonic weights website [36]. The weights were placed into CSV files to be easily readable by the analysis software. Before the weights could be applied the outline for each foot needed to be created as described in 2.5. This was done within the analysis software (shown in figure 3.6c) which was placed on a website to aid the speed of completion.

The website allows multiple people to outline points on the images simultaneously. The application presents the person with a randomly selected image from a database of as yet unprocessed images that needed to be outlined and a generic template for 29 control points per foot on the image. The person then has the choice to place the points in the correct anatomical positions or mark the image as 'unsolvable' in case the background is not distinguishable from the foreground. Once the image is fully outlined it is submitted to the website and marked as finished. After the first person has drawn the outline onto the image, it undergoes two more rounds of validation by different people in order to be sure that the people placed the outlines correctly. In addition to verification rounds, instructions were given on the website itself for proper control point placement. Screenshots of the website can be found in appendix F. For the purposes of this project, students from the University of South Wales were contracted to aid this process. After the entire process completed, the second stage of actual image analysis could commence.

The analysis software contains several individual helper programs that can be linked together as needed using standard unix file descriptors. A total of five programs were created to deal with the data, their names are:

1. DFUPS\_Analysis
2. DFUPS\_Transformer
3. DFUPS\_Interpolation\_Comparator
4. DFUPS\_Convoluter
5. DFUPS\_Tools

The **DFUPS\_Analysis** program's sole purpose is to show the images and data graphically in a format such as the one in figure 3.6c. Although options exist within the user interface to extract data points into the CSV format and revert to default ROIs, these were not used due to the command line interface being quicker and more powerful to use, especially for scripting.

The **DFUPS\_Transformer** program is responsible for transforming the images from their captured state into a standardised image. This program contains options to read in a specific configuration file for the barycentric coordinates, set the width and height of the output images, rotate all outline control points (created using the website program in stage 1) by a specified amount and flip x and y coordinates. It features the use of threading to speed up processing, as this program runs over thousands of files, it can take a day to complete when using only a single processing core. Each pixel that is not within the outline is set to a value lower than absolute zero ( $-273.16^{\circ}\text{C}$ ) to denote that it is not part of the foot.

The **DFUPS\_Interpolation\_Comparator** programs was implemented to create the graphs shown before in figures 2.6 and 2.7 as examples. It calculates the mean and standard deviation of each input image and outputs a CSV file containing the resulting statistical data.

The **DFUPS\_Convoluter** program is used for image manipulation tasks. This program uses a Parser Generator called JavaCC [37] to include an expression parser to manipulate pixels or extract data from the entire input image using a mathematical expression; for example  $\$1-\$2$  would mean subtract input image number 2 from input image number 1. The program implements a queuing system to allow operations to take place in a one-to-many relationship fashion, for example subtracting multiple input images from one mean image. This works by implementing a list of queues where every queue except the first one is circular and thus never run out when dequeued. The variable naming that is used is a dollar sign followed by the queue number. If the variable has the suffix "i", it is treated as the entire image. This is useful when calculating statistical values within an image for example using  $avg(\$1i) - \$1$  calculates the difference of each pixel to the images mean temperature.

The **DFUPS\_Tools** program is responsible for extracting and injecting information into the files. It contains options such as extract the images into known data files such as png, extract temperature data based on ROIs, inject ROIs, select a colour palette and define fixed min and max temperature for scaling.

Each piece of analysis helper software outlined above can read and write the file format mentioned in section 3.2.2. The output is however strongly dependent on the parameters passed to the program. For the analysis itself, these programs were used to transform and extract ROIs such as those shown in figure 4.1 into CSV files. The numerical data can then be read in by Matlab to analyse using a large amount of different approaches that will be detailed in the following chapter 4 to find an optimum distinction separation line between an ulceration and non-ulceration, some of which are:

1. Difference of absolute temperature between left and right foot
2. Difference of absolute temperature to the baseline data from trial 1
3. Difference of absolute temperature to intra-foot mean:
4. Difference in temperature over time

The following chapter will analyse the data using standard techniques such as Thresholding and Receiver Operator Curves. Other methods such as K-Means Clustering, Support Vector Machines and Genetic Algorithms were attempted but were found to be completely unsuitable to the task and are therefore omitted from this dissertation.

## Chapter 4

# Results

The results documented in this thesis are produced from the infrared image datasets provided by the three involved hospitals. To extract the data from these images after the pre-processing stages outlined in chapter 2 (calibration drift adjustments, segmentation and warping of images into a standard shape) two further steps are necessary; the definition of ROIs and filtering outliers based on how an ulcer occurred. The first step is shown in figure 4.1 with the definition of 12 ROIs that were taken into consideration, they were named:

1. 1<sup>st</sup>, 2<sup>nd</sup>, 3<sup>rd</sup>, 4<sup>th</sup> and 5<sup>th</sup> Toe
2. 1<sup>st</sup>, 2<sup>nd</sup>, 3<sup>rd</sup>, 4<sup>th</sup> and 5<sup>th</sup> Metatarsal Head (MTH)
3. Metatarsal Base (MTB)
4. Heel

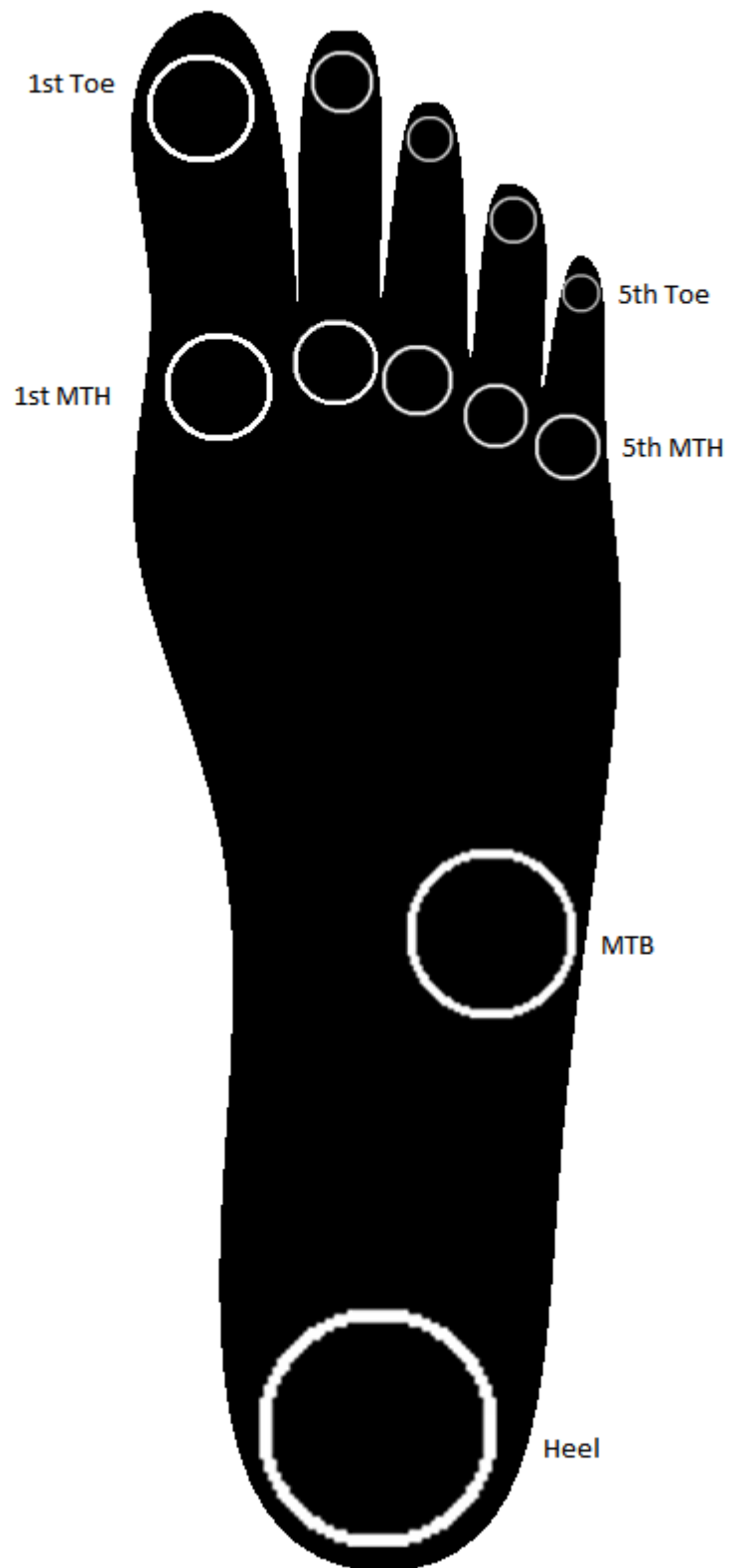


FIGURE 4.1: Definition of Regions of Interest



According to [38, 39] patients with a previous healed ulcer have a chance of 15-60% of ulcerating again the following year and, as table 4.1 shows, with 33 out of the 112 included patients (29%) this was close to the numbers seen in this trial.

The second step was accomplished by classifying each ulcer into three types of occurrence, Biological, Behavioural and Mixed. The first type describes ulcers that occurred due to underlying biological problems, the second refers to ulcers that occurred due to various interferences such as a heavy object falling onto a patients foot, walking barefoot on a hot beach and prolonged walking. The last type describes a mix between the two in cases where the patient followed the medical advice partially and the cause of the ulcer can be attributed both to underlying and behavioural causes. An example of such a case is prolonged walking in surgical shoes.

After each ulcer was classified, all ulcers that fell into the Behavioural and Mixed groups were removed from the result set since behavioural ulceration is incidental and thus impossible to predict by any technology. Of the remaining 12 ulcerations shown in table 4.2, one ulcer formed after the first visit to the clinic hence making the data unfit for time-based analysis and was therefore also left out of the dataset. The data for the remaining 11 ulcers was thereafter extracted by calculating the mean of each area of interest and written to a comma separated value file from which it could be read in and analysed using a statistical package.

-	KIN	FRH	PEN	Total
Number of Patients	63	47	21	131
Number of Group A	25	16	9	50
Number of Group B	35	18	9	62
Number of Group C (rejected)	3	13	3	19
Ratio Group A:Group B	1:0.71	1:0.89	1:1	1:0.81
Number of ulcers	20	7	6	<b>33</b>
<b>Biological cause of ulceration</b>	<b>4</b>	<b>4</b>	<b>4</b>	<b>12</b>
Behavioural cause of ulceration	9	3	2	14
Mixed cause of ulceration	7	0	0	7

TABLE 4.1: Breakdown of trial 2 Hospital Statistics

No.	Hospital	Identifier	Group	Number of Visits	Ulcer site
1	KIN	002MIR	A	18	Right 4 <sup>th</sup> MTH
2	KIN	006JAW	A	10	Right 5 <sup>th</sup> MTH
3	KIN	031MAF	B	2	Left and right 1 <sup>st</sup> Toe
4	KIN	045CAO	B	5	Left 3 <sup>rd</sup> Toe
5	FRH	013WJE	B	4	Left 4 <sup>th</sup> Toe
6	FRH	037VTH	A	5	Right Metatarsal Base
7	FRH	001DT_	A	4	Left 1 <sup>st</sup> Toe Nailbed
8	FRH	045BPH	A	9	Left 2 <sup>nd</sup> Toe Apex
9	PEN	005WT_	A	3	Left 2 <sup>nd</sup> Toe Apex
10	PEN	012JE_	B	2	Right 1 <sup>st</sup> Metatarsal Head
11	PEN	013AC_	A	2	Right 5 <sup>th</sup> Metatarsal Head
12	PEN	002MM_	A	1	Left 2 <sup>nd</sup> Toe

TABLE 4.2: Breakdown of the 12 Biological ulcer patients included in the data set for analysis, patient 12 not included in the analysis due to almost immediate ulceration after only 1 visit

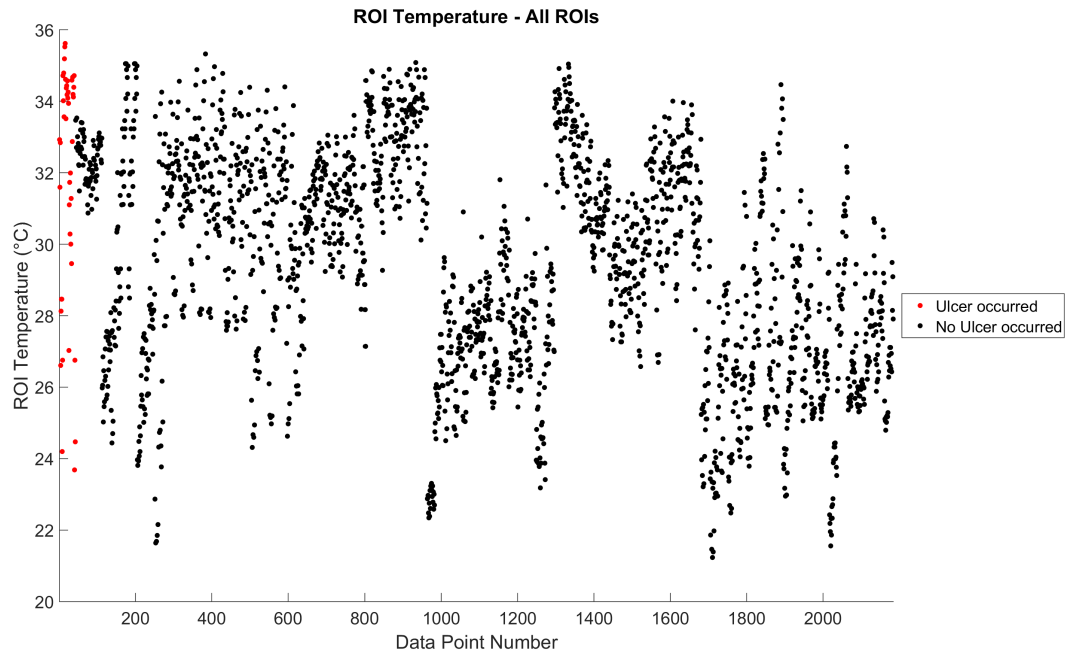
The following figures 4.2 through 4.6 show data plots of the dataset generated using the analysis helper programs described in section 3.3. Additionally a baseline image was calculated from the data from trial 1. The full set of data plots are in appendix A. To seek out which classifiers may be suitable for identifying or even predicting ulceration, the data was plotted using 5 potential classifiers:

1. ROI temperature ( $T_{ROI}$ )
2. Temperature asymmetry ( $abs(T_{left} - T_{right})$ )
3. Temperature variance ( $T_{spot} - T_{mean}$ )
4. Temperature change over time ( $T_{current\ visit} - T_{previous\ visit}$ )
5. Difference to baseline ( $T_{spot} - T_{trial\ 1\ Mean\ Image}$ )

Each of the potential classifiers is one-dimensional, meaning that in the following data plots (**Figure 4.2, 4.3, 4.4, 4.5 and 4.6**), the x coordinate is an arbitrary number given to each data point. Data points where ulceration occurred during trial two are marked in red and data points where ulceration did not occur during trial two are marked in black. Furthermore, to ease visual assessment, all data points are displayed as their absolute (difference to zero) values as well as sorted by ulceration

data i.e. the first  $n$  data points represent data where an ulcer eventually occurred and the following  $m$  data points represent data where an ulcer did not occur.

**Figure 4.2** shows the extracted data points as absolute temperatures. Each data point occurred at any given point in time during trial 2. Red data points represent patients that eventually ulcerated at a given ROI and black data points represent ROIs that did not ulcerate. Figure 4.2a shows that most of the ulcerated ROIs tend to have an elevated temperature, but not consistently so and not to such a degree that they are unambiguously distinguishable from non-ulcerated data points. Figure 4.2b shows the data points only for the 1<sup>st</sup> Toe but it also shows a similar pattern to figure 4.2a. However, most data points where ulceration occurred lie above  $T > 34^{\circ}\text{C}$ . These results point towards a detection/prevention approach that uses "high temperature" as one of its inputs.



(a) ROI temperature plot - all ROIs

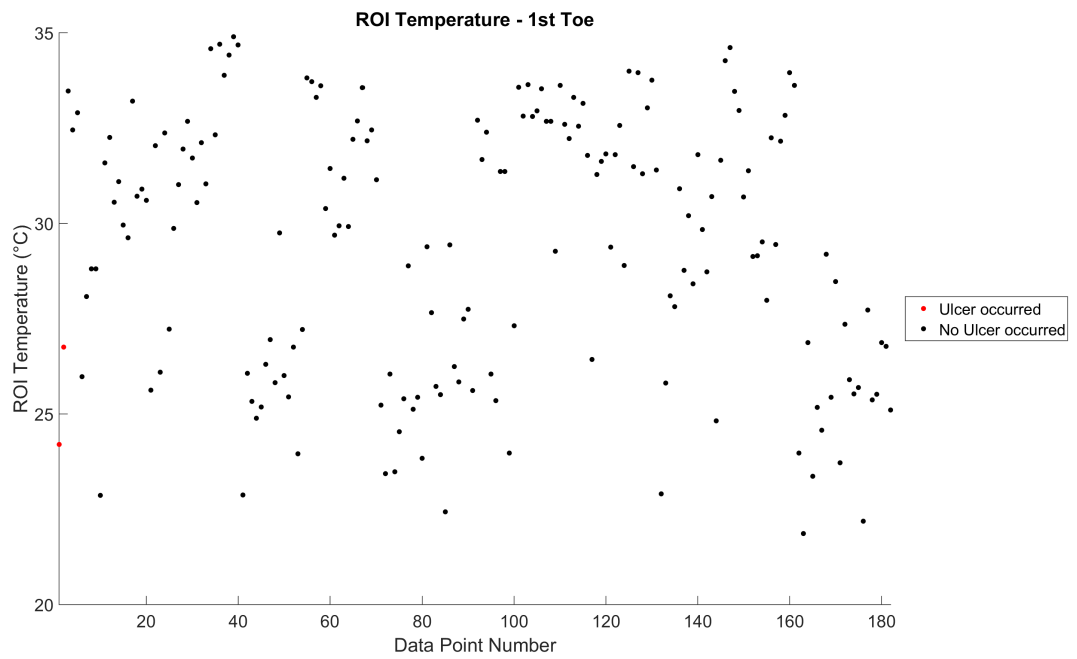
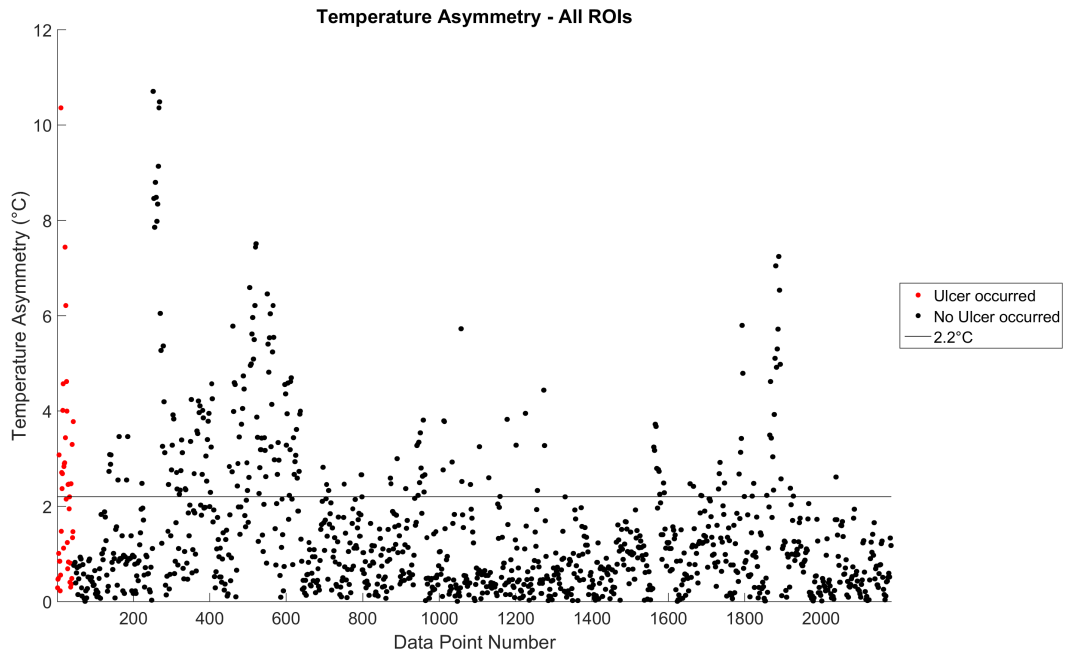
(b) ROI temperature plot - 1<sup>st</sup> Toe only

FIGURE 4.2: ROI temperature plots

**Figure 4.3** shows plots of the temperature asymmetry classifier. Each dot represents a data point calculated as the absolute value of any ROI but this time subtracted from its contralateral ROI, i.e. showing the difference in ROI temperature between left and right corresponding ROIs. The black line marks the current accepted  $2.2^{\circ}\text{C}$  gold standard threshold for ulcer prediction. The ulcerating cohort data does not show any obvious difference to the non-ulcer cohort data indicating that the  $2.2^{\circ}\text{C}$  threshold could be too simplistic.

Figure 4.3a shows in fact that there are many false positive and false negative results, displayed as black dots above the black line and red dots below the black line, respectively. Figure 4.3b shows extreme cases where simple temperature asymmetry is unsuitable for ulcer detection/prediction. In this figure, all ulcerated points are close to a  $0^{\circ}\text{C}$  difference which, according to the  $2.2^{\circ}\text{C}$  model, would falsely indicate near-perfect conditions.



(a) Temperature asymmetry plot - all ROIs

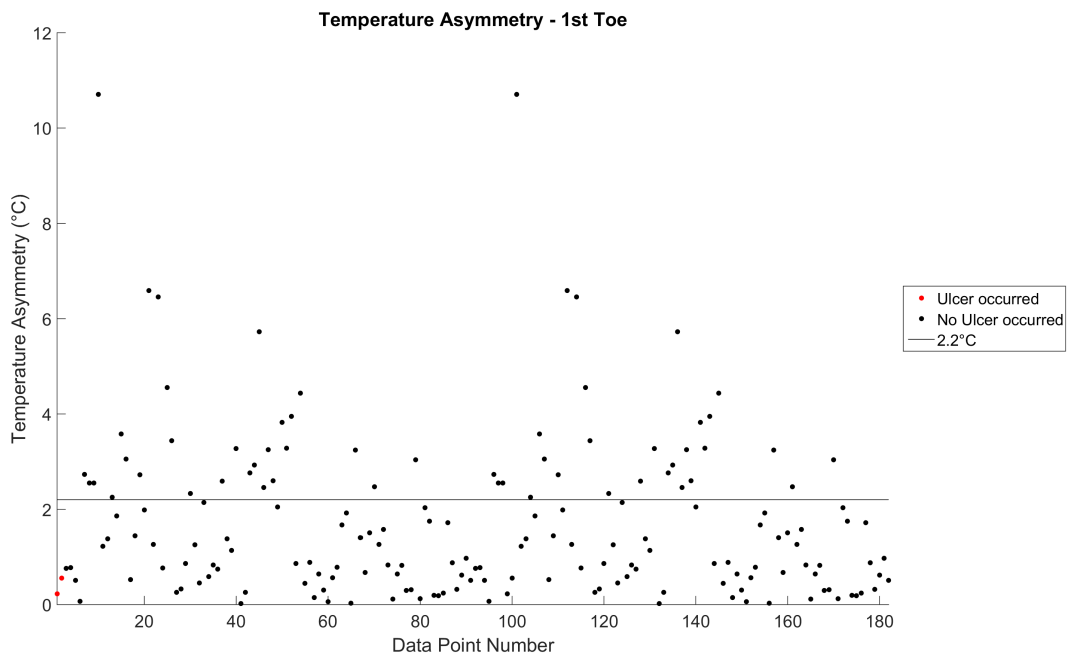
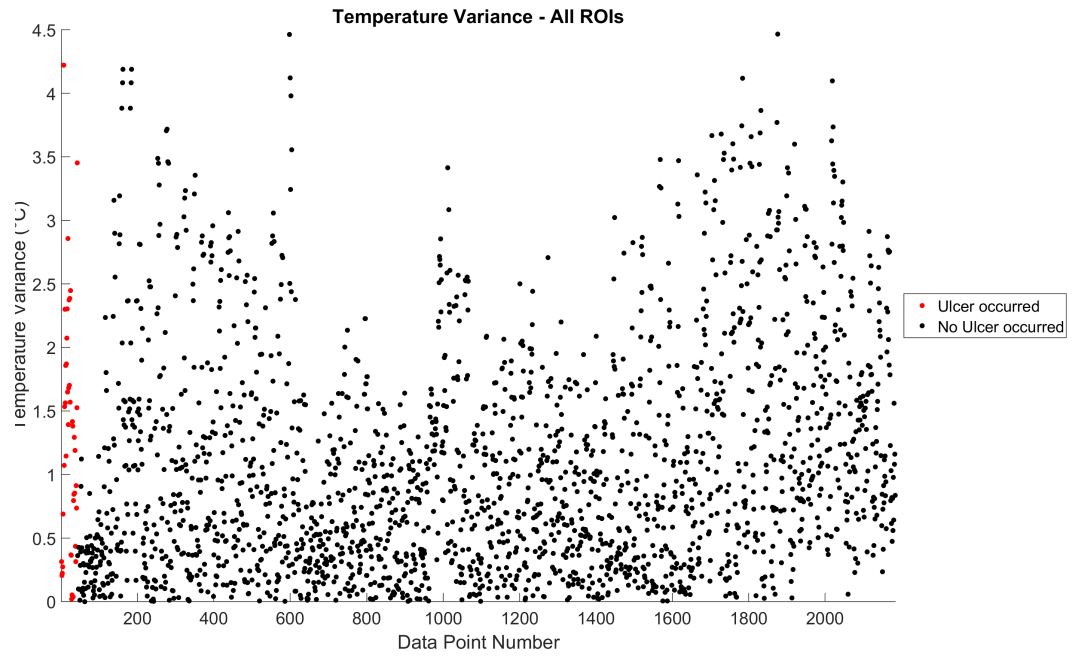
(b) Temperature asymmetry plot - 1<sup>st</sup> Toe only

FIGURE 4.3: Temperature asymmetry plots

**Figure 4.4** presents the extracted data as a plot of the ROI temperature subtracted from the foot mean temperature, which is calculated across the entire foot (not just the ROIs). The data points in figure 4.4a where ulceration occurred are spread out over the entire y axis range, with a grouping of points around the 1.5 to 2.5 °C range. However, the non-ulcerated data points are also spread out over the entire y range, with most data points being within the lower half ( $T < 2.2 - 2.3$  °C). This trend continues when the data is split into ROIs such as in figure 4.4b.



(a) Temperature variance plot - all ROIs

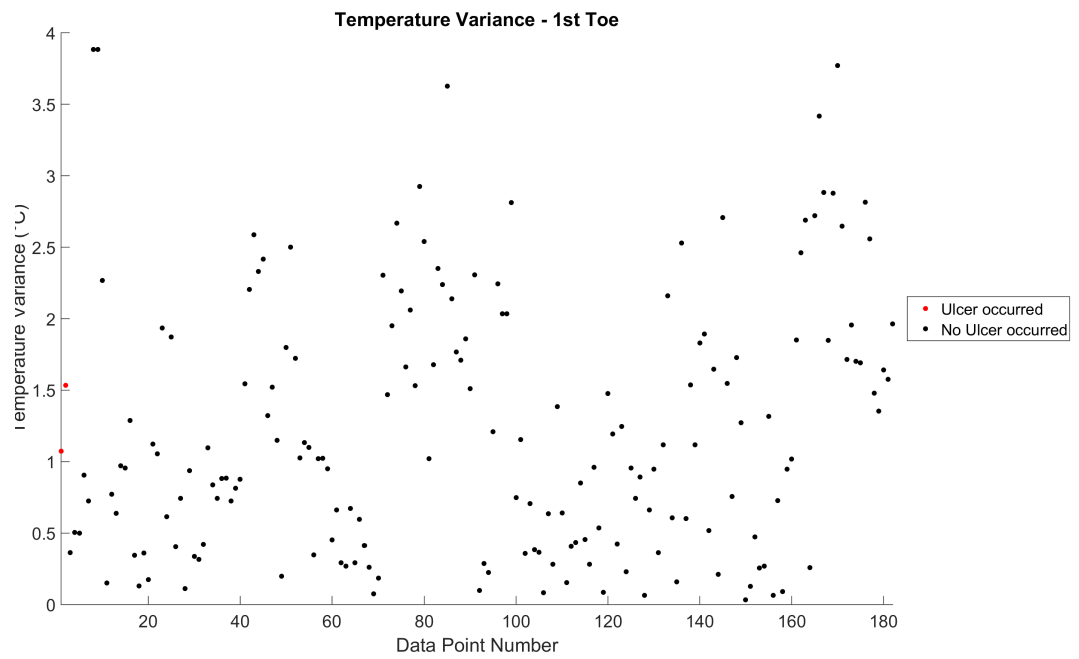
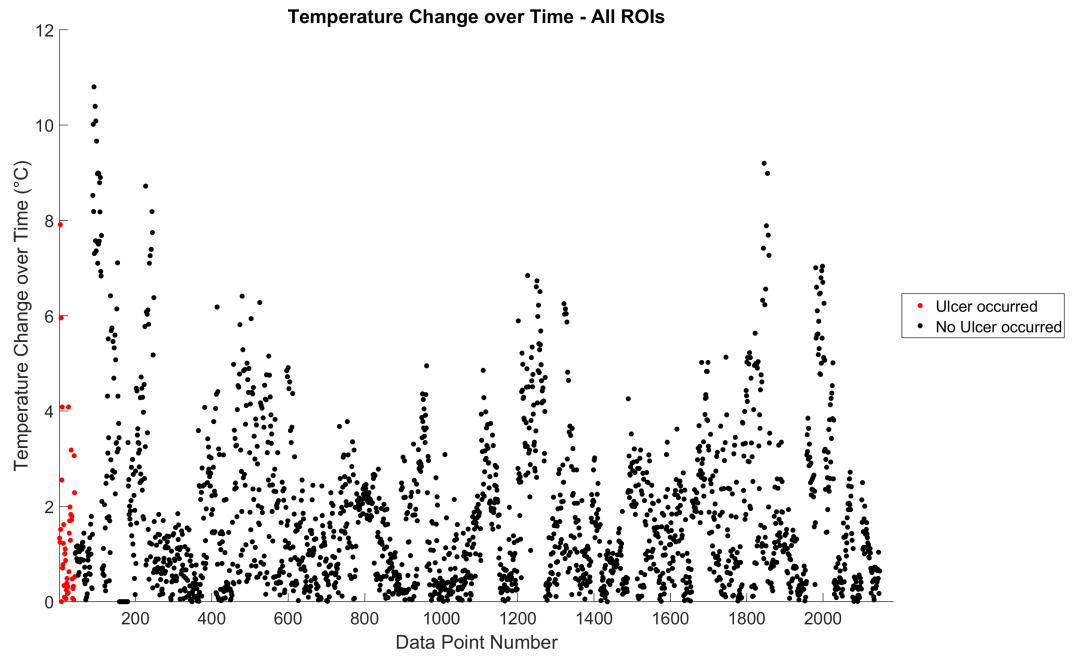
(b) Temperature variance plot - 1<sup>st</sup> Toe only

FIGURE 4.4: Temperature variance plots



**Figure 4.5** displays the data calculated as a time-based previous temperature measurement of an ROI subtracted from the current temperature measurement of the same ROI. This calculation generates a delta temperature for each ROI over time. Figure 4.5a shows that most of the ulceration cohort data is grouped below  $2^{\circ}\text{C}$ , whereas the non-ulceration cohort data covers the whole y range but most of the data points are below  $4^{\circ}\text{C}$ . Figure 4.5b shows the potential that a classifier for temperature fluctuation could have. The two ulceration cohort data points lie above most of the non-ulceration data points, but many of the non-ulceration cohort data points are within the same band ( $2.5^{\circ}\text{C} < T < 4.1^{\circ}\text{C}$ ) as the ulceration cohort data. Furthermore, there are also data points above the ulceration data points. A simple "last visit minus current visit" temperature drift measurement is therefore unlikely to contribute to a detection/prediction tool - especially if measurements are made at the rather long monthly intervals as in this study. Shorter intervals, e.g. daily, may produce a different outcome.



(a) Temperature change over time plot - all ROIs

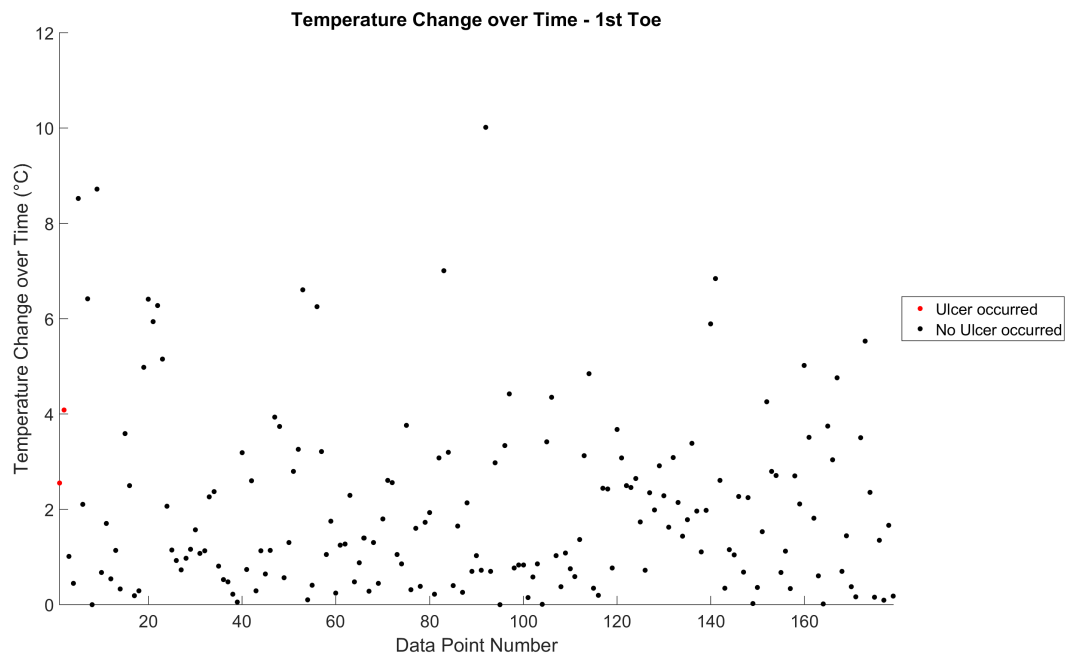
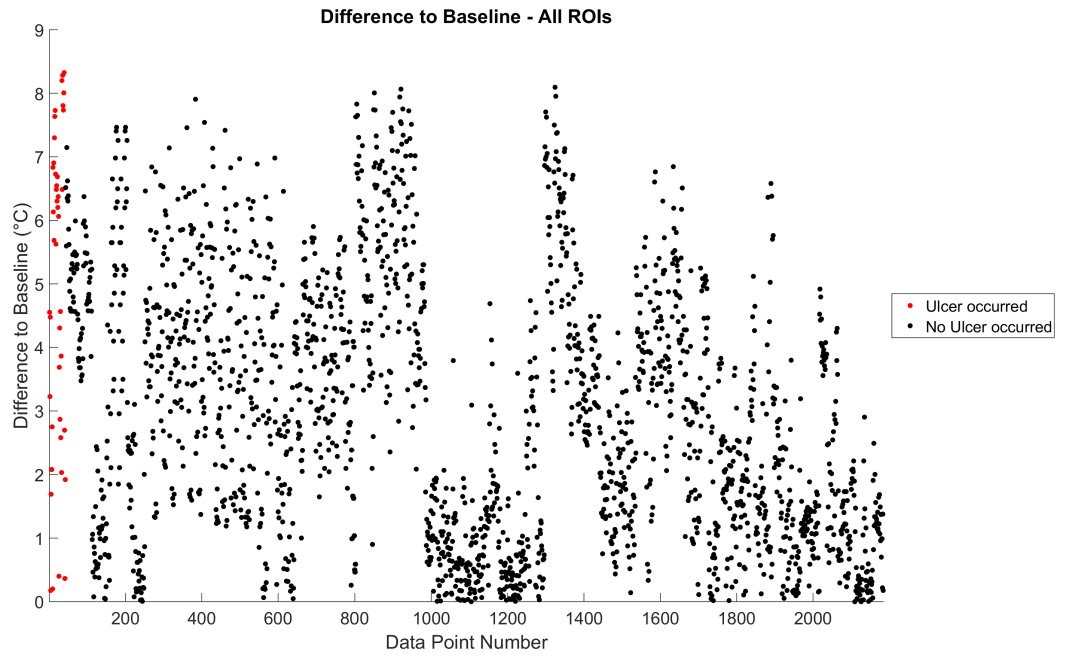
(b) Temperature change over time plot - 1<sup>st</sup> Toe only

FIGURE 4.5: Temperature change over time plots

**Figure 4.6** shows the data points calculated as the baseline image ROI subtracted from the measured ROI data point, per ROI. The underlying idea is that an increase in the the difference to a normal foot over time might indicate the onset of ulceration. However, figure 4.6a shows that the ulceration data is spread out over the whole range with some groupings at  $T > 6^\circ\text{C}$ . This is similar to what was shown before in figure 4.2 but with less precision. Figure 4.6b shows the data points for the 1<sup>st</sup> Toe ROI only. It also shows that the non-ulceration cohort data can almost entirely be mistaken for noise.

From these 10 figures is it apparent that there is no obvious simple way to use any of the 5 classifiers on its' own for reliable ulcer identification or prediction. The following chapter 5 therefore combines the information provided by the classifiers attempting to establish a particular combination that might reveal so far hidden characteristics or patterns.



(a) Difference to baseline plot - all ROIs

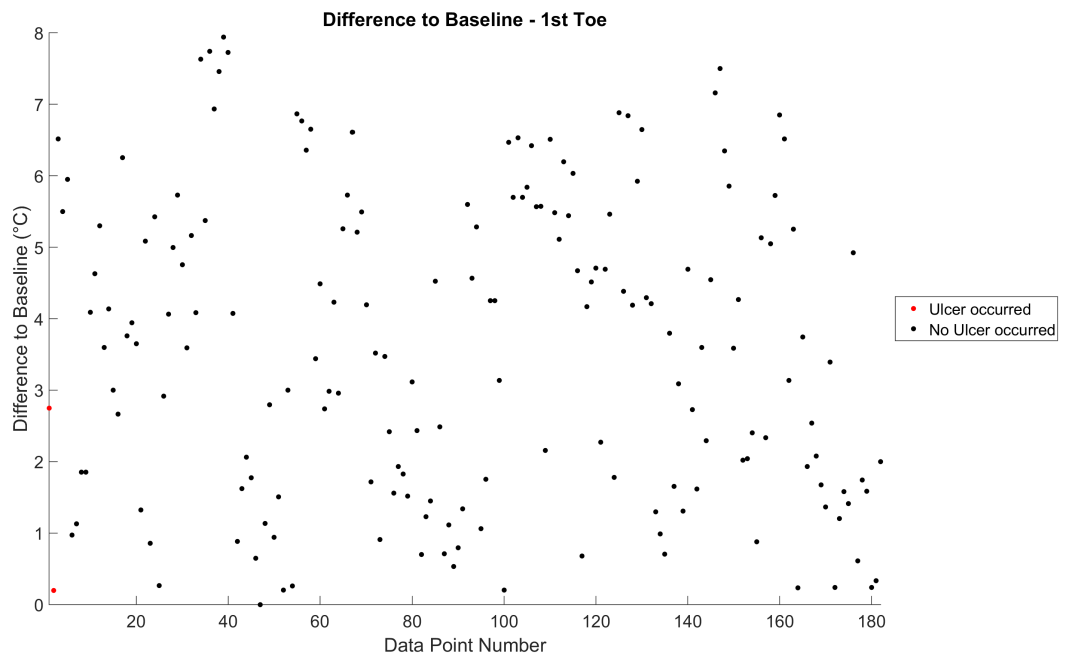
(b) Difference to baseline plot - 1<sup>st</sup> Toe only

FIGURE 4.6: Difference to baseline plots

## Chapter 5

# Analysis and Discussion

The data presented in chapter 4 is based on 5 distinct parameters to classify the data into two groups: 'Did ulcerate' and 'Did not ulcerate'. To recall, these were:

1. ROI temperature ( $T_{ROI}$ )
2. Temperature asymmetry ( $abs(T_{left} - T_{right})$ )
3. Temperature variance ( $T_{spot} - T_{mean}$ )
4. Temperature change over time ( $T_{current} - T_{previous\ visit}$ )
5. Difference to baseline ( $T_{spot} - T_{trial\ 1\ Mean\ Image}$ )

The methods that will be tested as a classifier in this chapter are:

1. Temperature asymmetry threshold (currently accepted gold standard approach)
2. Graphical assessment of all combinations using 2 parameters
3. Area under the curve of receiver operator curves

### 5.1 Temperature Asymmetry Threshold

Chapter 4 already indicated that the simple 2.2°C threshold frequently cited in literature and today's de-facto "gold standard" might not be an ideal classifier for the data obtained in this study. In order to confirm this suspicion the data was subjected to Receiver Operator Curve (ROC) analysis. The ROC space is constructed by

plotting the true positive rate (TPR or sensitivity) over the false positive rate (FPR or 1 - specificity) and results in diagram such as that shown in figure 5.1.

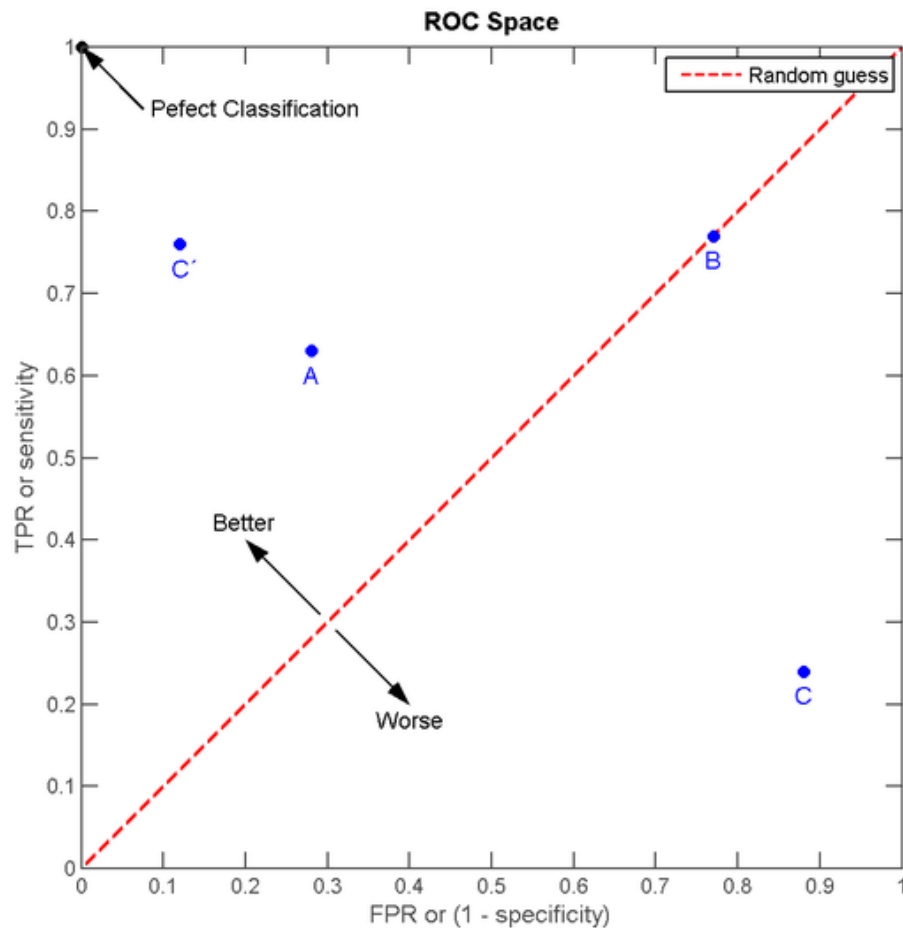


FIGURE 5.1: Receiver Operator Curve explanatory diagram, from [40]

In figure 5.1 the ROC Space is divided into two halves by the red dashed line which indicates the predictive value of a set of random guesses. A ROC located above this line represents a classifier that is better than random guessing. A perfect classifier is represented by a straight line from the origin in the lower left corner to point (0,1) in the upper left hand corner and from there to point (1,1) in the upper right corner. If the ROC is reflected over the dashed line i.e. from the origin to point (1,0) and on to point (1,1) then the classifier needs to be inverted. For example, consider an experiment to determine the relationship between the temperature and state of water (under 'normal', sea-level atmospheric pressure) and a classifier for the state of water that states  $State_{water} = liquid, \text{ if } Temperature_{water} < 0^{\circ}C$  is tested. A Receiver

Operator Curve would be below the red dotted line, indicating that the classifier is suitable to determine the state of water but that the threshold is falsely interpreted. This means that the classifier should be  $State_{water} = liquid, if Temperature_{water} > 0^{\circ}C$ . With the updated threshold, the ROC would show a near-perfect classifier.

A method to numerically determine how suitable a classifier is using a ROC is the area under its curve. By this method, a classifier that randomly guesses as shown by the red dotted line in figure 5.1 would score a value of 0.5. A perfect classifier would show a value of 1 and a falsely interpreted threshold as in the above state-of-water experiment would have an area under the curve close to 0.

Using the trial data generated in this study a ROC can be generated for a range of contra lateral difference temperatures between  $\Delta T=0^{\circ}C$  and  $\Delta T=10.7^{\circ}C$ . The resulting plot is shown in figure 5.2. The maximum distance of the curve from the random guess line i.e. the point where the predictive powers are best is in the area around  $TPR = 0.5$  and  $FPR = 0.2$ . This corresponds to a  $\Delta T$  of  $2^{\circ}C$  for the data obtained in this trial and this confirms the before mentioned  $2.2^{\circ}C$  contra lateral difference which is the current 'gold standard' for predicting the occurrence of diabetic foot ulcers.

However, as table 5.1 shows, at  $\Delta T=2.0^{\circ}C$  the sensitivity of the method is only about 45% which means that more than half of the potential ulcer developments are missed. Those 45% that are being highlighted by the threshold are then 80% likely to be correctly classified. Moreover, the positive predictive value (PPV) was only 8.9%.

This result demonstrates two things:

1. the  $2.2^{\circ}C$  threshold is close to the findings in this study and could be confirmed
2. the predictive value (sensitivity) at reasonable reliability (specificity) of the  $2.2^{\circ}C$  threshold is low

This second outcome means that other parameters should be tested if they can be combined with the  $2.2^{\circ}C$  threshold in order to improve both sensitivity and specificity. This is done in the following sections of this chapter.

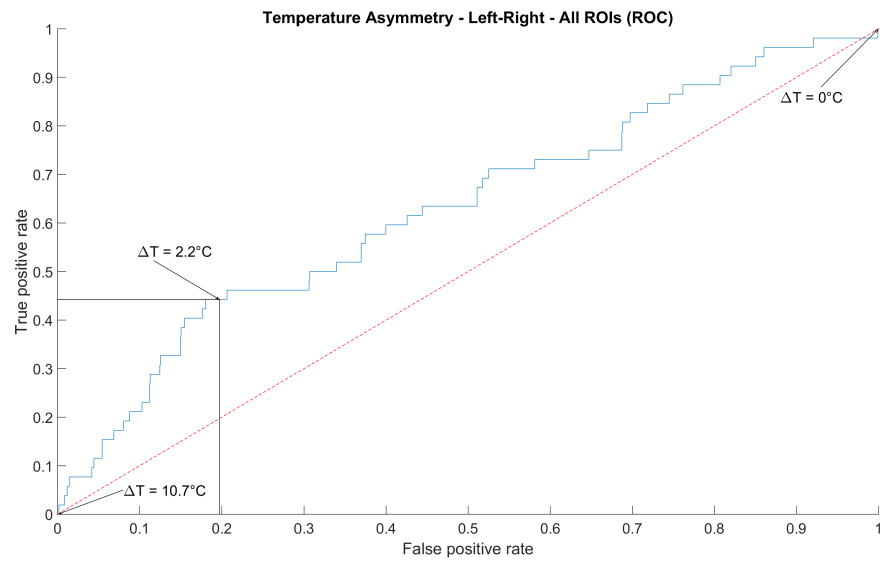


FIGURE 5.2: Analysis of the ROI temperature Difference Threshold value using a Receiver Operator Curve for differences between 0 and  $10.7^\circ\text{C}$ . The best classification on trial data is achieved in the area around  $\Delta T = 2.0^\circ\text{C}$ .



Threshold	TPR (%)	TNR (%)	PPV (%)	NPV (%)
0.1	98.1	5.9	4.3	98.6
0.2	96.2	13.3	4.6	98.8
0.3	90.4	19.0	4.6	97.8
0.4	86.5	25.4	4.8	97.7
0.5	75.0	31.8	4.6	96.7
0.6	73.1	38.0	4.9	97.0
0.7	71.2	42.0	5.1	97.1
0.8	71.2	47.0	5.5	97.4
0.9	63.5	51.2	5.3	97.0
1.0	63.5	55.2	5.8	97.2
1.1	59.6	58.4	5.9	97.1
1.2	57.7	61.9	6.2	97.1
1.3	51.9	65.2	6.1	96.9
1.4	50.0	67.9	6.3	96.9
1.5	46.2	69.7	6.2	96.8
1.6	46.2	72.3	6.8	96.9
1.7	46.2	74.4	7.3	96.9
1.8	46.2	76.3	7.8	97.0
1.9	46.2	78.3	8.5	97.1
<b>2.0</b>	<b>44.2</b>	<b>80.3</b>	<b>8.9</b>	<b>97.1</b>
2.1	44.2	81.4	9.3	97.1
<b>2.2</b>	<b>40.4</b>	<b>82.4</b>	<b>9.1</b>	<b>96.9</b>
2.3	40.4	83.7	9.7	97.0
2.4	38.5	84.7	9.9	96.9
2.5	32.7	85.6	9.0	96.7
2.6	32.7	86.4	9.4	96.7
2.7	30.8	87.5	9.6	96.7
2.8	28.8	88.5	9.8	96.6
2.9	25.0	88.8	8.8	96.5
3.0	23.1	89.4	8.6	96.4

TABLE 5.1: Statistical measures for Various ROI temperature Difference Thresholds - Simple Method (in bold: optimum  $\Delta T$  values according to literature ( $\Delta T=2.2^\circ\text{C}$  as per [12]) and as found in this study ( $\Delta T=2.0^\circ\text{C}$ ))

## 5.2 Combining Parameters

Relying on single parameters to classify data was shown to be unsatisfactory in chapter 4. Nonetheless for each of the parameters there is a corresponding ROC that may be evaluated before moving on to attempting to combine the parameters. The evaluation data is located in tables 5.3 and 5.4, the graphical representation for all data is in figures 5.3 to 5.5 and the ROCs for each ROI are in appendix B. In each graphical representation, the minimum, maximum and farthest-from-random-guess threshold values are highlighted. The aforementioned measure of classifier strength, Area under the Curve (AUC), is used to compare the the classifiers. The results in tables 5.3 and 5.4 show that the most suitable candidates according to the AUC are the ROI temperature and the difference to baseline with values of 0.72 and 0.73. This is still far from an ideal classifier also shows that there is some potential. The other classifier AUCs are in the range of 0.42 to 0.67. Splitting up the data into the respective Regions of Interest (Figure 4.1) increases the classifier strength at almost all ROIs. This suggests that each region of interest needs to be treated separately. Furthermore, in some cases, the AUC value is lower than 0.5, suggesting that at specific ROIs, the classifiers need to be inverted. This is counter-intuitive for example with temperature asymmetry in the 1<sup>st</sup> or 2<sup>nd</sup> Toe but may be explained in this particular case by the small sample size. However, the cost of splitting up the data decreases the positive sample size. In some cases, the ulceration cohort data sample size drops as low as two data points.

Prior to combining the parameters, each parameter was tested for a range of threshold values to establish a baseline. The resulting values for sensitivity and specificity are outlined in table 5.2. Some abbreviations were used in the threshold values due to limited page space; these were:

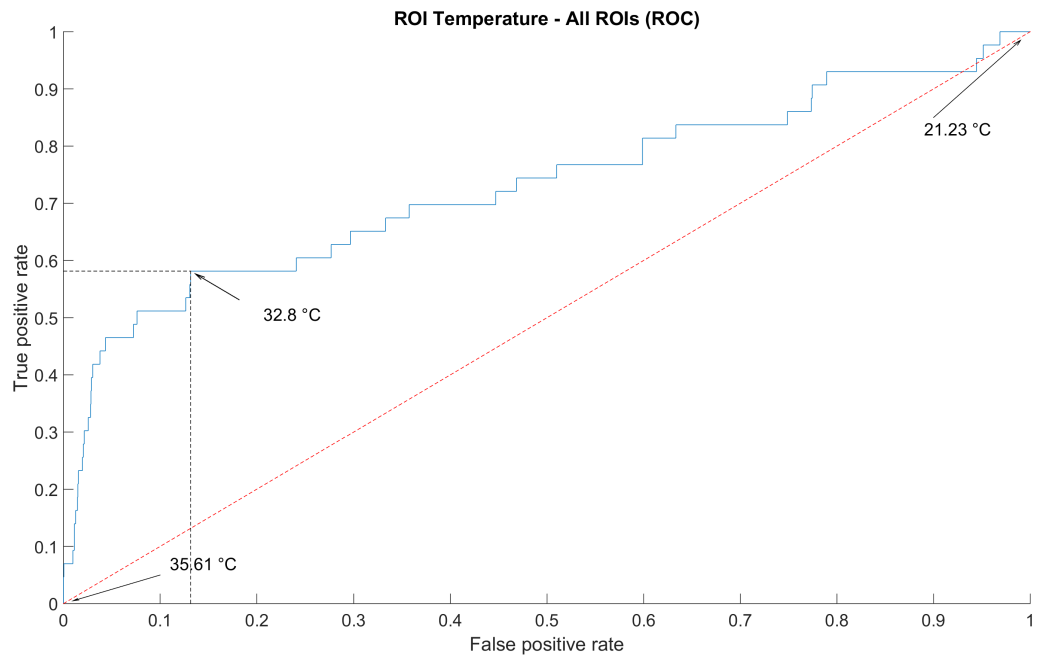
Threshold	Abbreviation
ROI temperature	$T_{ROI}$
Temperature asymmetry	$T_{asymmetry}$
Temperature variance	$T_{variance}$
Temperature change over time	$T_{change}$
Difference to baseline	$\Delta T_{baseline}$

The highest sensitivity values that also keep the specificity above 90% were 51.2% with  $33.5 < T_{ROI}$ , 48.8% using  $6.0 < abs(\Delta T_{baseline})$ , 44.2% using  $1.0 < abs(T_{variance})$  and 39.5% using  $2.0 < abs(T_{asymmetry})$ . These values can be further optimised by

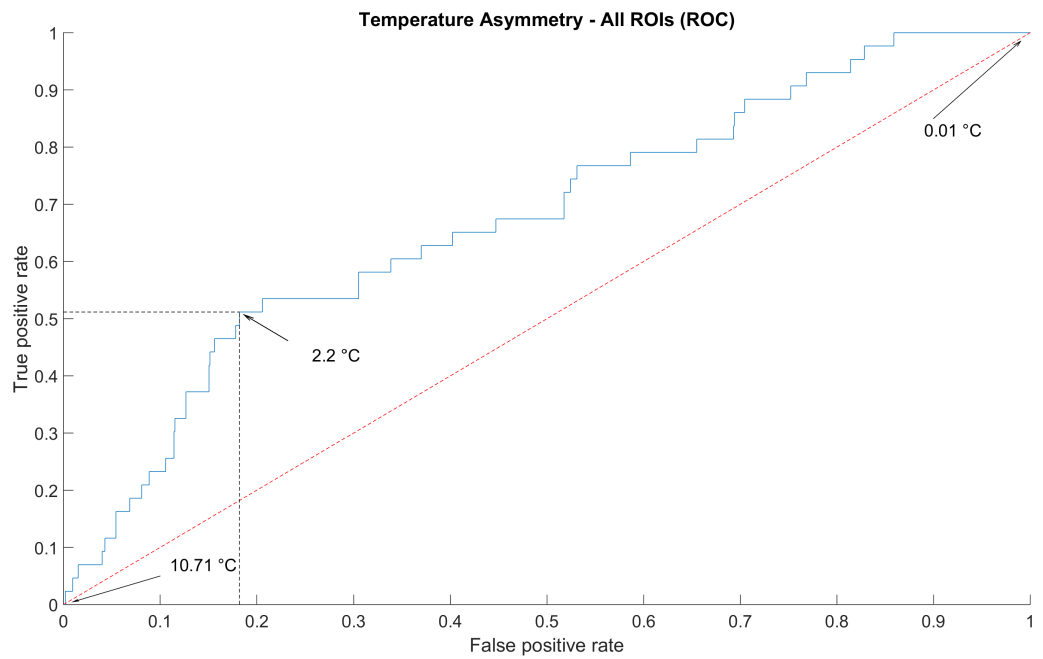
tweaking the threshold values but they provide a baseline what to expect when combining the classifiers. In the following comparisons, the classifier  $33.5 < T_{ROI}$  is used as the 'best baseline classifier'.

Threshold	TPR (%)	TNR (%)
$33.0 < T_{ROI}$	51.2	88.4
$33.5 < T_{ROI}$	51.2	92.4
$34.0 < T_{ROI}$	44.2	96.0
$34.5 < T_{ROI}$	23.3	98.3
$0.5 < abs(T_{asymmetry})$	55.8	65.8
$1.0 < abs(T_{asymmetry})$	53.5	77.6
$1.5 < abs(T_{asymmetry})$	39.5	84.9
$2.0 < abs(T_{asymmetry})$	39.5	90.1
$2.5 < abs(T_{asymmetry})$	32.6	92.8
$3.0 < abs(T_{asymmetry})$	20.9	94.6
$3.5 < abs(T_{asymmetry})$	14.0	96.2
$4.0 < abs(T_{asymmetry})$	14.0	97.3
$0.5 < abs(T_{variance})$	53.5	79.3
$1.0 < abs(T_{variance})$	44.2	90.1
$1.5 < abs(T_{variance})$	32.6	95.7
$2.0 < abs(T_{variance})$	16.3	98.7
$2.5 < abs(T_{variance})$	2.3	99.4
$abs(T_{change} < 0.5)$	34.9	75.9
$abs(T_{change} < 1.0)$	46.5	59.0
$abs(T_{change} < 1.5)$	62.8	46.0
$abs(T_{change} < 2.0)$	79.1	35.8
$abs(T_{change} < 2.5)$	81.4	26.0
$6.0 < abs(\Delta T_{baseline})$	48.8	91.8
$6.5 < abs(\Delta T_{baseline})$	32.6	94.7
$7.0 < abs(\Delta T_{baseline})$	20.9	97.4
$7.5 < abs(\Delta T_{baseline})$	18.6	99.1
$8.0 < abs(\Delta T_{baseline})$	9.3	99.9

TABLE 5.2: Sensitivity and specificity for various classifiers

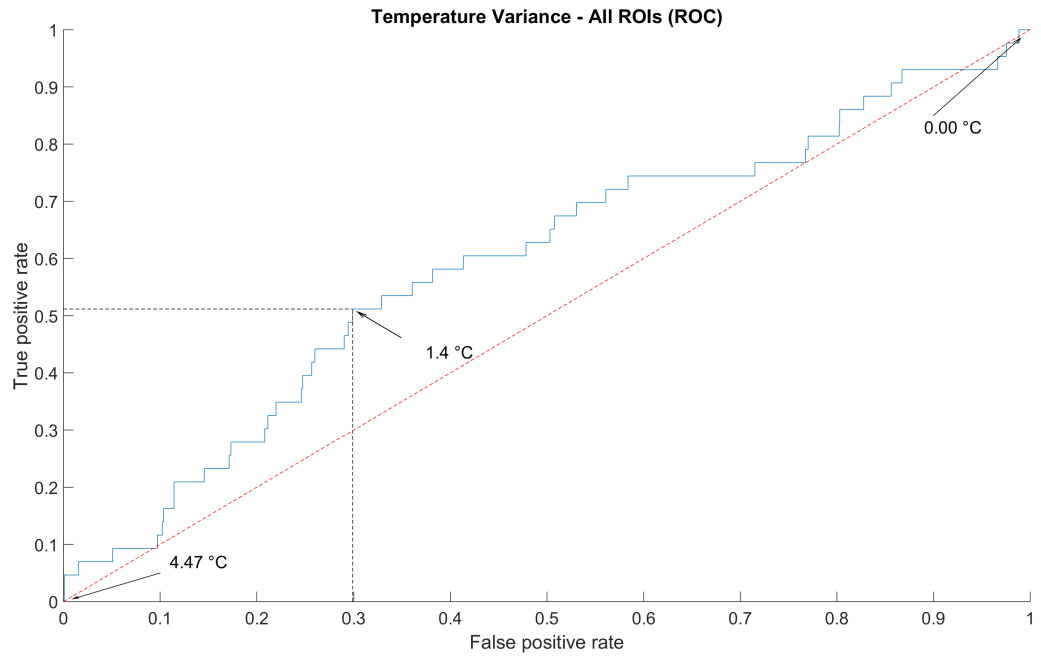


(a) ROC for the ROI temperature data in figure 4.2a

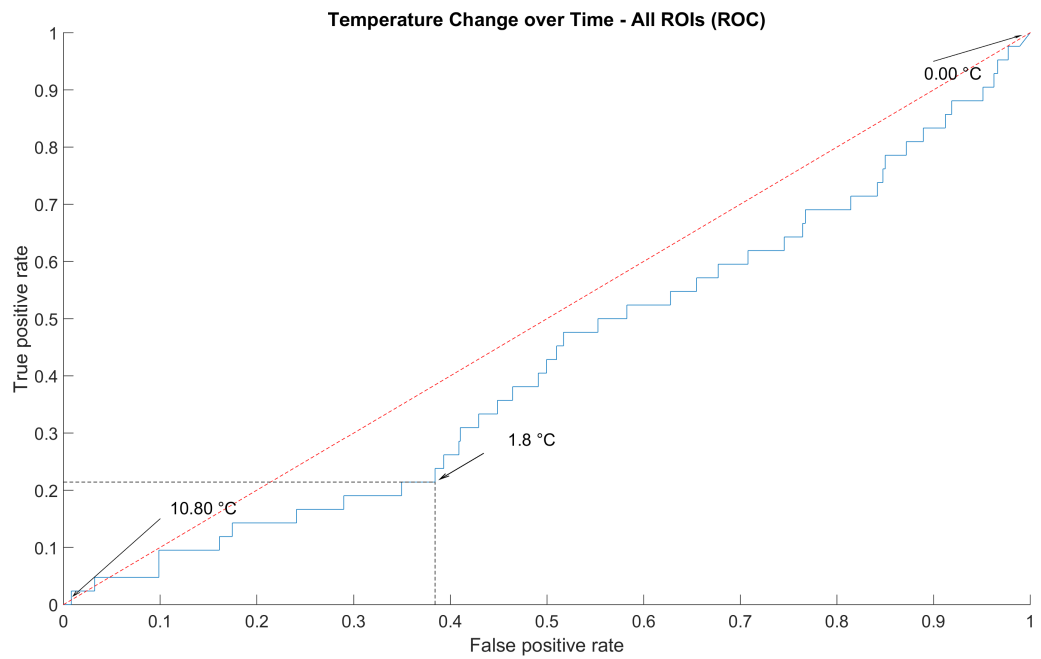


(b) ROC for the temperature asymmetry data in figure 4.3a

FIGURE 5.3: Receiver operator curves for figures 4.2 and 4.3

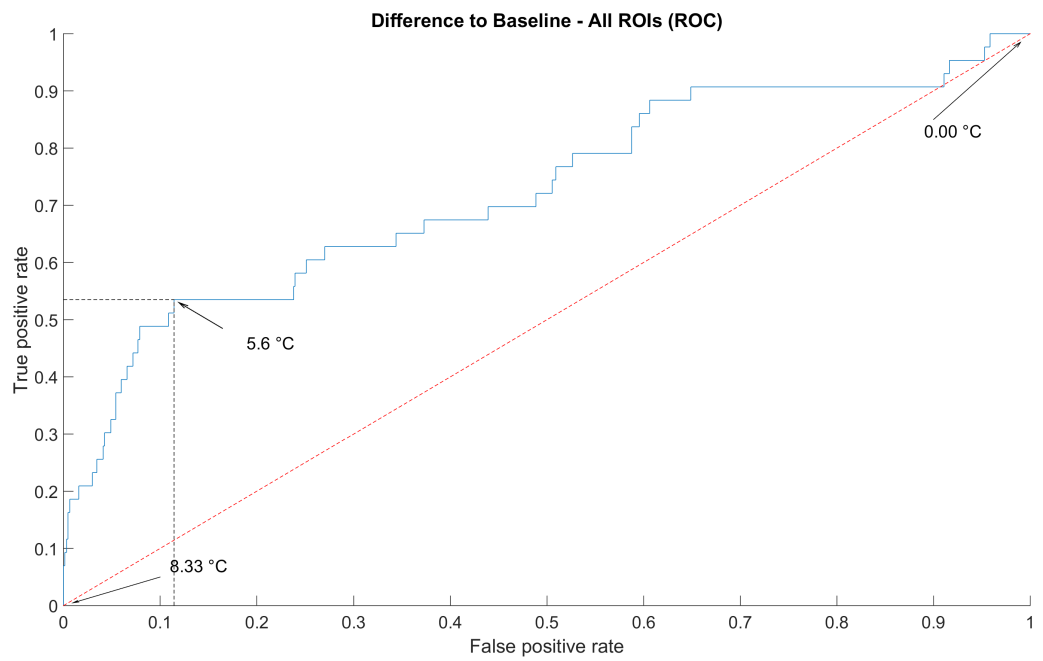


(a) ROC for the temperature variance data in figure 4.4a



(b) ROC for the temperature change over time data in figure 4.5a

FIGURE 5.4: Receiver operator curves for figures 4.4 and 4.5



(a) ROC for the difference to baseline data in figure 4.6a

FIGURE 5.5: Receiver operator curves for figures 4.4

Parameter Description	ROI	Data Size	AUC
ROI temperature	All ROIs	43	0.73
Temperature asymmetry	All ROIs	86	0.68
Temperature variance	All ROIs	43	0.59
Temperature change over time	All ROIs	42	0.42
Difference to baseline	All ROIs	43	0.72
ROI temperature	1st Toe	2	0.18
ROI temperature	2nd Toe	9	0.88
ROI temperature	3rd Toe	3	0.16
ROI temperature	4th Toe	2	0.41
ROI temperature	4th MTH	16	0.95
ROI temperature	5th MTH	8	0.54
ROI temperature	5th MTH Base	3	0.86
Temperature asymmetry	1st Toe	2	0.17
Temperature asymmetry	2nd Toe	9	0.39
Temperature asymmetry	3rd Toe	3	0.70
Temperature asymmetry	4th Toe	2	0.66
Temperature asymmetry	4th MTH	16	0.93
Temperature asymmetry	5th MTH	8	0.70
Temperature asymmetry	5th MTH Base	3	0.28

TABLE 5.3: Statistical values for the ROCs presented in appendix B

Temperature variance	1st Toe	2	0.59
Temperature variance	2nd Toe	9	0.42
Temperature variance	3rd Toe	3	0.55
Temperature variance	4th Toe	2	0.16
Temperature variance	4th MTH	16	0.94
Temperature variance	5th MTH	8	0.28
Temperature variance	5th MTH Base	3	0.25
Temperature chance over time	1st Toe	2	0.79
Temperature chance over time	2nd Toe	8	0.19
Temperature chance over time	3rd Toe	3	0.59
Temperature chance over time	4th Toe	2	0.75
Temperature chance over time	4th MTH	16	0.25
Temperature chance over time	5th MTH	8	0.61
Temperature chance over time	5th MTH Base	3	0.71
Difference to baseline	1st Toe	2	0.21
Difference to baseline	2nd Toe	9	0.86
Difference to baseline	3rd Toe	3	0.32
Difference to baseline	4th Toe	2	0.21
Difference to baseline	4th MTH	16	0.95
Difference to baseline	5th MTH	8	0.50
Difference to baseline	5th MTH Base	3	0.85

TABLE 5.4: Statistical values for the ROCs presented in appendix B continued

To combine the parameters, it is first necessary to visually compare the data by graphing the parameters against each other. Figures 5.6 to 5.15 show the graphs that put each parameter against each other parameter. The second step is to manually define thresholds or threshold ranges that look like they could separate the data in a meaningful way. These thresholds are then tested for their respective sensitivity and specificity. The statistical data is given in the format "TPR, TNR" in each of the tables 5.5 through 5.13. From there, it may be possible to combine three or more threshold values to improve the sensitivity and specificity even further.

**Figure 5.6** shows the ROI temperature data graphed against the temperature asymmetry. The temperature asymmetry is calculated as the difference between contra lateral ROIs, where the ulceration cohort data is separate for left and right. This means that for each data point on a foot that ulcerated there is also a temperature



asymmetry value on the non-ulcerated, other foot that is equal but with the opposite sign. The same principle applies when an ROI on the right foot ulcerated. The data points then results in symmetry across the y axis, but shifted by the x axis. In this graph, most of the ulceration cohort data is above  $33^{\circ}\text{C}$  but does not show a clear separation along the y axis. However, it is noticeable that every ulceration cohort point above  $33^{\circ}\text{C}$  has a temperature asymmetry that is above  $0^{\circ}\text{C}$ . Using a variable threshold for the ROI temperature between 33 and 34.5 in 0.5 steps together with the two temperature asymmetry definitions  $0 < T_{asymmetry}$  and  $0 < T_{asymmetry} < 5$  yields the data in table 5.5. The best result is achieved by a ROI threshold of  $33.5^{\circ}\text{C}$  and a positive temperature asymmetry, with a sensitivity and specificity of 51.2% and 94.3%, respectively. This value is higher than the best baseline classifier ( $33.5 < T_{ROI}$ ) in that it increased the specificity value by 1%.

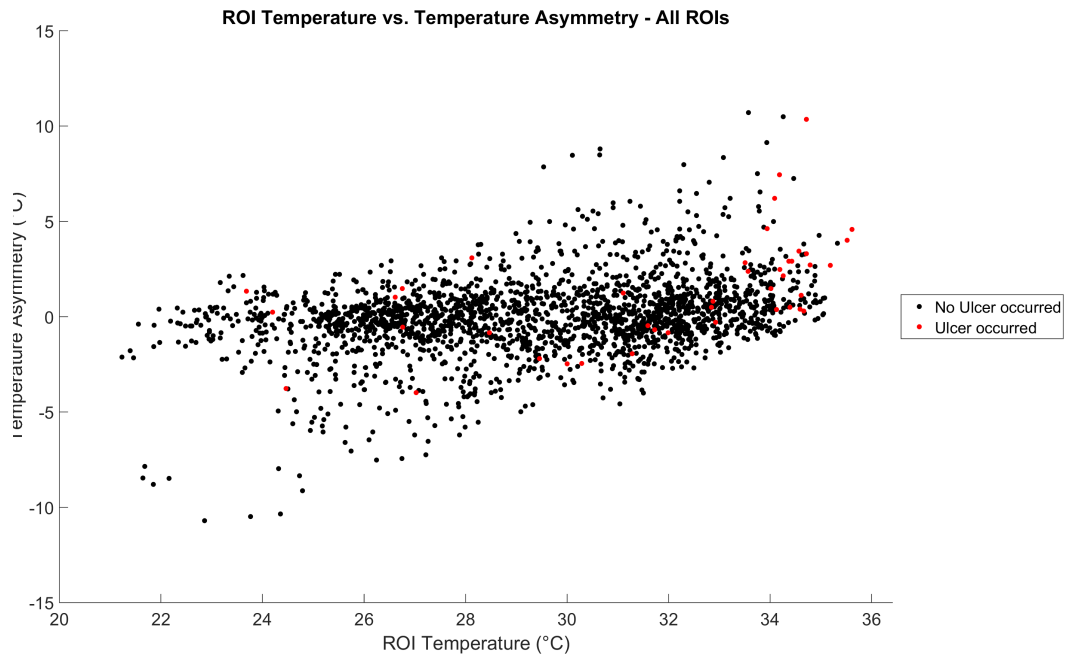


FIGURE 5.6: ROI temperature vs. temperature asymmetry plot

$y < T_{ROI}$ threshold	$0 < T_{asymmetry}$	$0 < T_{asymmetry} < 5$
33.0	51.2, 91.6	44.2, 92.2
33.5	51.2, 94.3	44.2, 94.6
34.0	44.2, 96.7	37.2, 96.8
34.5	23.3, 98.4	20.9, 98.4

TABLE 5.5: ROI temperature vs temperature asymmetry threshold assessment

**Figure 5.7** graphs the ROI temperature against the temperature variance. The data appears to be striped because the temperature variance is calculated using the ROI temperature and thus directly dependent on the ROI temperature. In this graph a grouping of points near the top right hand corner is visible. Most of the ulceration cohort data points are located above  $0^{\circ}\text{C}$  to  $1^{\circ}\text{C}$  temperature variance and above  $33^{\circ}\text{C}$ . The sensitivity and specificity data when using thresholds of  $0^{\circ}\text{C}$  to  $2^{\circ}\text{C}$  in  $0.5$  steps for the temperature variance and  $33^{\circ}\text{C}$  to  $34.5^{\circ}\text{C}$  for the ROI temperature is shown in table 5.6. The table shows the threshold with the highest sensitivity and specificity is between  $T_{ROI} > 33.5$  in combination with  $T_{variance} > 0$  with  $51.2\%$  and  $92.9\%$ , respectively. This is a slight decrease in specificity compared to the ROI temperature and temperature asymmetry approach but almost equal to the baseline.

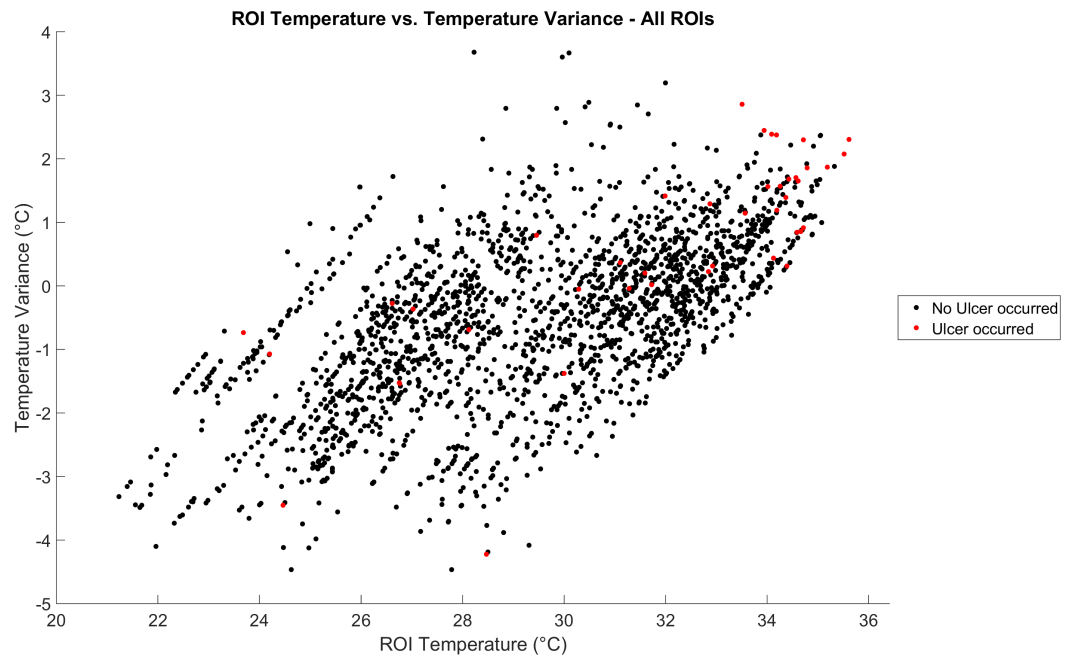


FIGURE 5.7: ROI temperature vs. temperature variance plot

$y <$ $T_{ROI}$	$x <$ $T_{variance}$	0.0	0.5	1.0	1.5	2.0
33.0		51.2, 89.8	46.5, 92.2	39.5, 95.9	32.6, 98.2	16.3, 99.6
33.5		51.2, 92.9	46.5, 94.3	39.5, 96.6	32.6, 98.5	16.3, 99.6
34.0		44.2, 96.1	39.5, 96.7	32.6, 97.6	27.9, 98.9	11.6, 99.7
34.5		23.3, 98.3	23.3, 98.3	16.3, 98.7	16.3, 99.3	7.0, 99.8

TABLE 5.6: ROI temperature vs temperature variance threshold assessment

**Figure 5.8** shows the ROI temperature graphed against its respective change over time. The graph shows a grouping of positive points with high ROI temperature and low change over time. This leads to using the same ROI temperature thresholds as previously and thresholds for the temperature change over time in the region of  $0.5^{\circ}\text{C}$  to  $2.5^{\circ}\text{C}$  in steps of  $0.5$ . The results are in table 5.7. The combination of thresholds that stands out in this data are  $33.5 < T_{ROI}$  and  $-2 < T_{change} < 2$ , which have a sensitivity of 51.2% and 94.4% specificity. These values are almost equal to the values obtained from the ROI temperature and temperature asymmetry sensitivity and specificity.

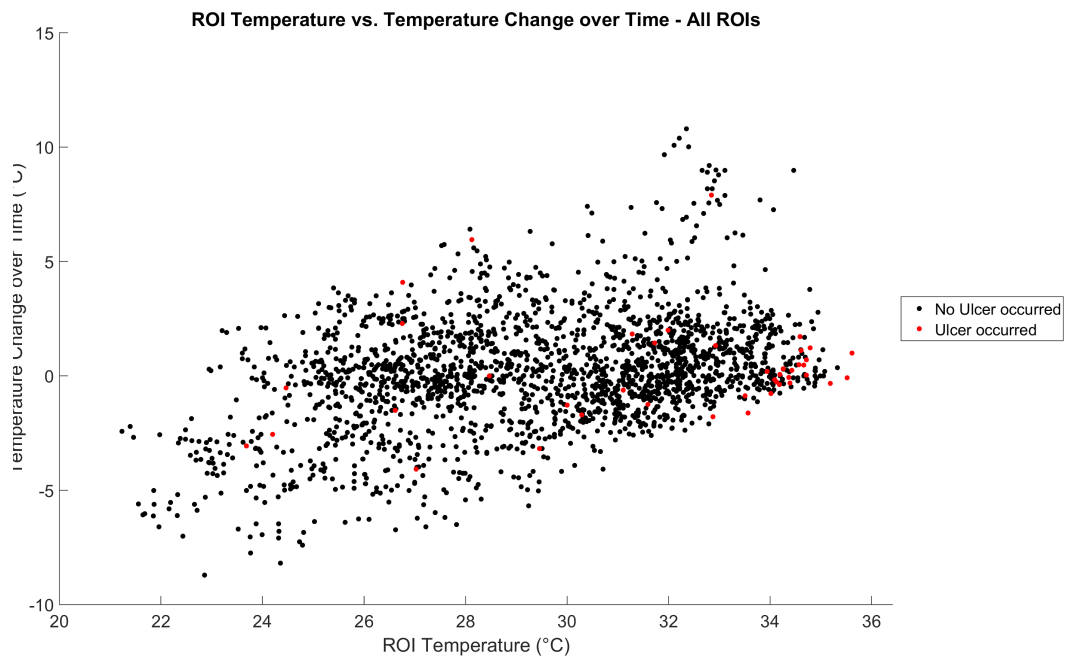


FIGURE 5.8: ROI temperature vs. temperature change over time plot

$y < T_{ROI}$	$-x < T_{change} < x$				
	0.5	1.0	1.5	2.0	2.5
33.0	32.6, 96.4	39.5, 94.3	46.5, 92.7	51.2, 91.5	51.2, 90.3
33.5	32.6, 97.2	39.5, 95.8	46.5, 95.0	51.2, 94.4	51.2, 93.5
34.0	30.2, 98.2	34.9, 97.6	41.9, 97.4	44.2, 97.1	44.2, 96.7
34.5	11.6, 99.1	14.0, 98.9	20.9, 98.8	23.3, 98.7	23.3, 98.6

TABLE 5.7: ROI temperature vs temperature change over time threshold assessment

**Figure 5.9** shows the parameters ROI temperature graphed against the difference to the baseline. This graph has a linear relationship because the two parameters depend on each other. Hence there are also no clear threshold values that can be obtained because it would be the same as a threshold for either the ROI temperature or the difference to baseline, but a combination would not.

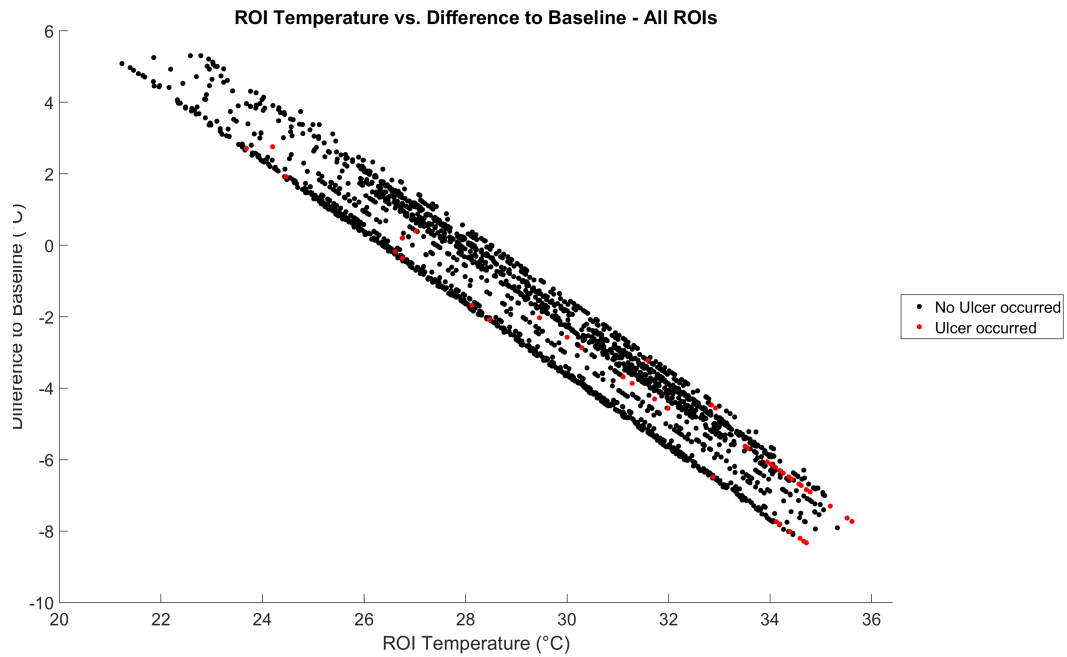


FIGURE 5.9: ROI temperature vs. difference to baseline plot

**Figure 5.10** plots the temperature asymmetry parameter against the temperature variance. There is no obvious grouping in the graph, however there are some ulceration cohort data points in the top right hand corner. The threshold intervals therefore chosen for this graph are 0.5 to 3 with a step size of 0.5 for the temperature asymmetry and 0.5 to 1 with a step size of 0.5 for the temperature variance. The calculated sensitivity and specificity values are shown in table 5.8. The thresholds that obtained the highest sensitivity are  $0.5 < T_{asymmetry}$  and  $0.5 < T_{variance}$  with 44.2% and 89.8%. Both the sensitivity and the specificity are lower than than in previous thresholds and the baseline.

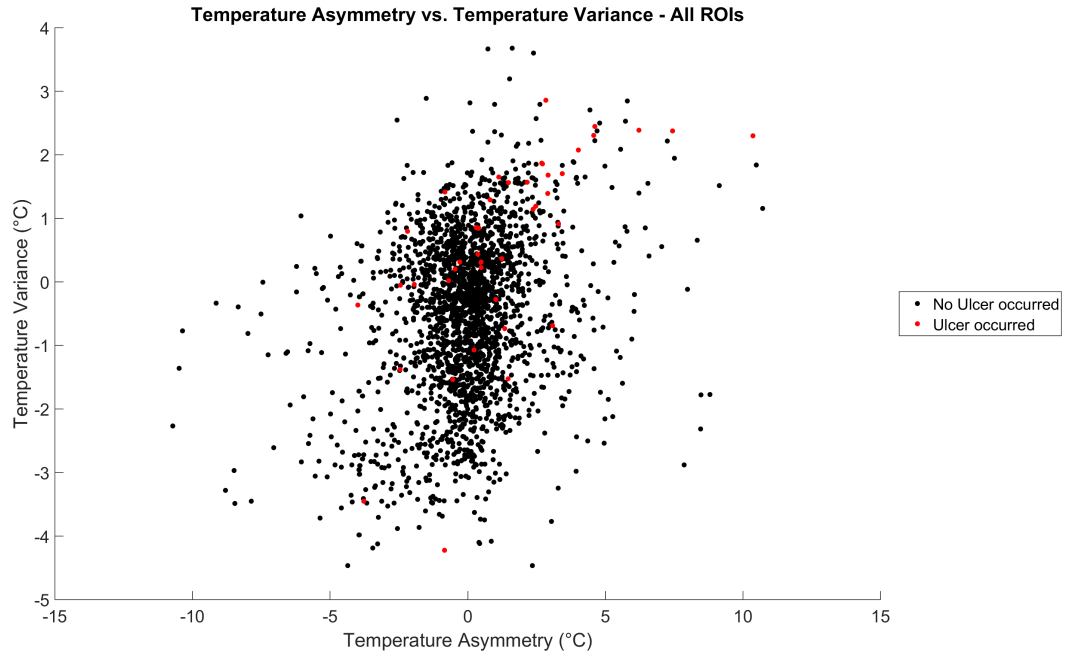


FIGURE 5.10: Temperature asymmetry vs. temperature variance plot

$y <$ $T_{asymmetry}$	$x <$ $T_{variance}$		
	0.5	1.0	1.5
0.5	44.2, 89.8	41.9, 94.0	32.6, 96.7
1.0	41.9, 92.4	39.5, 95.4	32.6, 97.3
1.5	37.2, 94.4	34.9, 96.4	27.9, 97.8
2.0	37.2, 96.2	34.9, 97.5	27.9, 98.3
2.5	30.2, 97.5	27.9, 98.3	25.6, 98.9
3.0	18.6, 98.0	16.3, 98.7	16.3, 99.0

TABLE 5.8: Temperature asymmetry vs temperature variance threshold assessment

**Figure 5.11** graphs the temperature asymmetry data against the temperature change over time data. In this graph, the 'did ulcerate' and 'did not ulcerate' data points are mixed too well to be able to establish an obvious threshold. There is a grouping of points near  $-1 < y < 1$  and  $x > 2$ , the threshold intervals chosen for this graph are therefore between 0.3 to 1.2 with a step size of 0.3 for the temperature change over time and 0 to 3 in steps of 0.5 for the temperature asymmetry threshold. The results are listed in table 5.9. In these threshold ranges, the highest sensitivity is 46.5% for  $0 < T_{asymmetry}$  and  $T_{change}$  but the specificity drops to only 74.2%. A 20% higher specificity is achieved with a higher threshold for the asymmetry ( $2 < T_{asymmetry}$ ),

where the trade-off is 10% less sensitivity. Overall, the sensitivity and specificity values are the similar to the previously explored threshold combination. However, the sensitivity is around 20% lower than in the baseline.

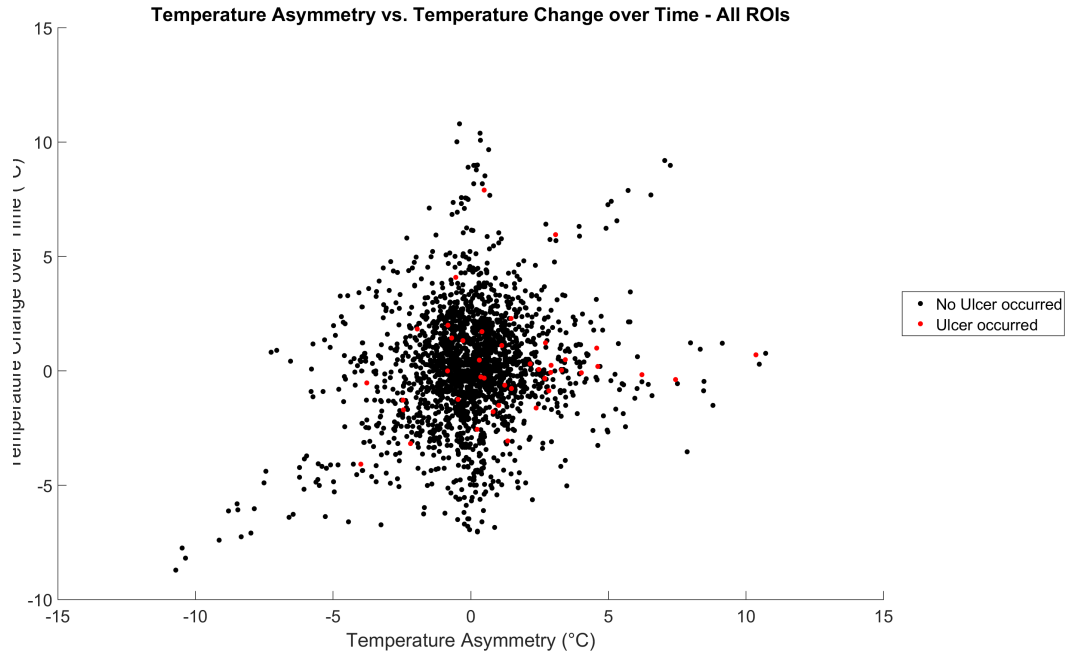


FIGURE 5.11: Temperature asymmetry vs. temperature change over time plot

$y < T_{asymmetry}$	$-x < T_{change} < x$	0.3	0.6	0.9	1.2
0.0		18.6, 91.8	32.6, 84.5	41.9, 79.1	46.5, 74.2
0.5		16.3, 94.9	25.6, 89.8	34.9, 85.5	39.5, 81.9
1.0		16.3, 97.0	25.6, 93.4	34.9, 90.3	39.5, 88.0
1.5		16.3, 98.1	25.6, 95.6	30.2, 93.5	32.6, 91.7
2.0		16.3, 98.7	25.6, 97.2	30.2, 95.9	32.6, 94.7
2.5		14.0, 99.2	20.9, 98.0	25.6, 97.1	27.9, 96.3
3.0		9.3, 99.4	14.0, 98.5	16.3, 97.8	18.6, 97.1

TABLE 5.9: Temperature asymmetry vs temperature change over time threshold assessment

**Figure 5.12** shows the temperature asymmetry data plotted against the difference to baseline data. As before when plotting the temperature asymmetry against either the temperature variance or the temperature change over time, the data does not

show any clear distinction between the two classes. The ulceration cohort data does however seem to be grouped towards the bottom left hand corner of the graph. This suggests thresholds in the region of  $-5^{\circ}\text{C}$  to  $-7^{\circ}\text{C}$  for the difference to baseline and  $0^{\circ}\text{C}$  to  $2^{\circ}\text{C}$  for the temperature asymmetry. The maximum sensitivity that can be reached is 53.5% with a specificity of 90.5%, where the thresholds are  $0 < T_{asymmetry}$  and  $\Delta T_{baseline} < -5.5$ . The sensitivity is along the lines with what the 1D classifier  $33.5 < T_{ROI}$  produced but the sensitivity is lower.

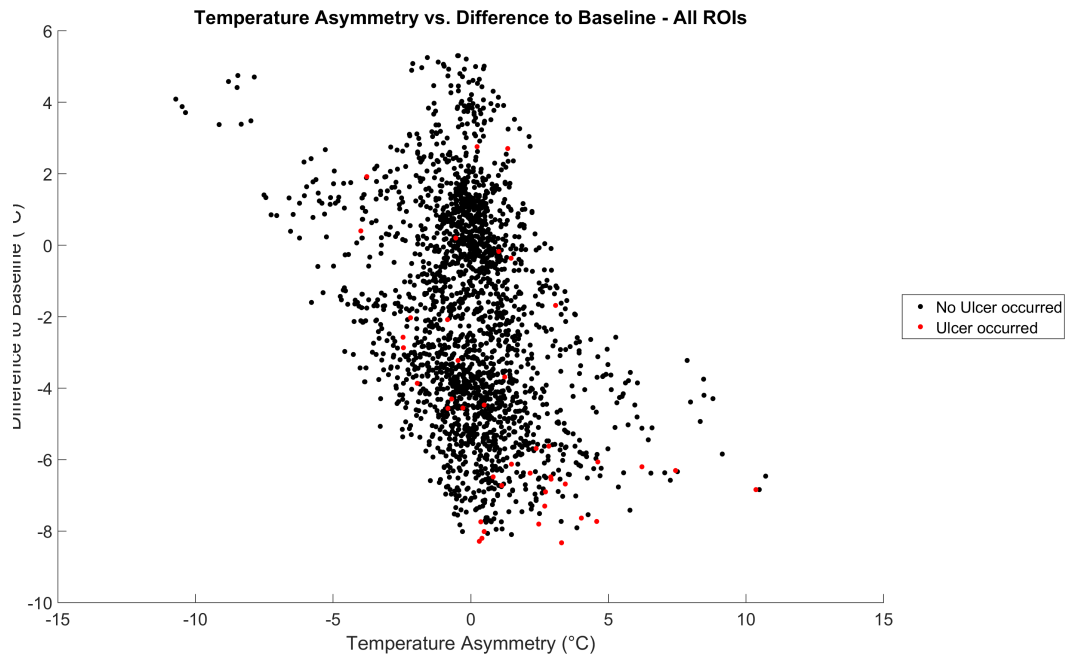


FIGURE 5.12: Temperature asymmetry vs. difference to baseline plot

$y < T_{asymmetry}$	$\Delta T_{baseline} < x$			
	-5.0	-5.5	-6.0	-6.5
0.0	53.5, 87.5	53.5, 90.5	48.8, 94.0	32.6, 96.1
0.5	44.2, 89.9	44.2, 92.1	39.5, 95.0	23.3, 96.8
1.0	41.9, 93.0	41.9, 94.6	37.2, 96.7	23.3, 98.1
1.5	37.2, 94.3	37.2, 95.6	32.6, 97.4	20.9, 98.6
2.0	37.2, 95.7	37.2, 96.6	32.6, 97.9	20.9, 98.8
2.5	30.2, 96.9	30.2, 97.4	27.9, 98.4	18.6, 99.3
3.0	18.6, 97.5	18.6, 97.9	18.6, 98.7	11.6, 99.4

TABLE 5.10: Temperature asymmetry vs difference to baseline threshold assessment

**Figure 5.13** plots the temperature variance data against the temperature change over time data. The graph presents a small grouping of the 'did ulcerate' class in the range of  $1 < T_{variance}$  and where the temperature change over time is near zero. The threshold intervals chosen for this combination of parameters is therefore between 0.3 and 1.2 for the temperature change over time and 0.5 to 2 for the temperature variance. The results are presented in table 5.11. The highest sensitivity achieved while keeping the specificity above 90% is 39.5% using thresholds of  $2.5 < T_{variance}$  and  $-0.6 < T_{change} < 0.6$ . This is lower than the previous thresholds and lower than the best baseline classifier.

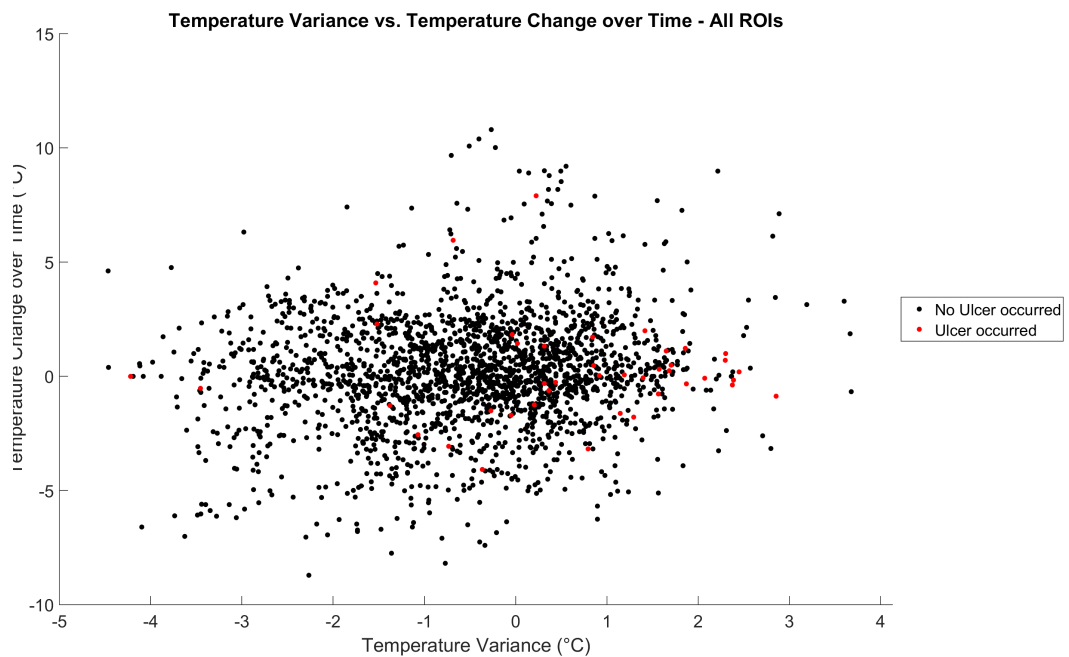


FIGURE 5.13: Temperature variance vs. temperature change over time plot

$-y < T_{change} < y$	$x < T_{variance}$	0.5	1.5	2.0	2.5
0.3		18.6, 96.2	32.6, 92.2	41.9, 89.3	46.5, 86.5
0.6		16.3, 97.3	27.9, 94.3	34.9, 92.5	39.5, 91.0
0.9		16.3, 98.4	25.6, 96.5	32.6, 95.4	37.2, 94.4
1.2		11.6, 98.9	20.9, 97.8	27.9, 97.0	32.6, 96.5

TABLE 5.11: Temperature variance vs temperature change over time threshold assessment



**Figure 5.14** shows the temperature variance plotted against the difference to the baseline. There is a grouping of ulceration cohort data points in the lower right corner of the graph. The thresholds chosen here were in the range of -7 to -5 for the difference to baseline parameter and 0 to 2 for the temperature variance. Both parameters were incremented in steps of 0.5. The results in table 5.12 show the highest sensitivity at  $\Delta T_{baseline} < -5.5$  and  $0 < T_{variance}$  with a value of 53.5%. This is higher than the baseline while maintaining a specificity of higher than 90%, even though it is lower than the baseline.

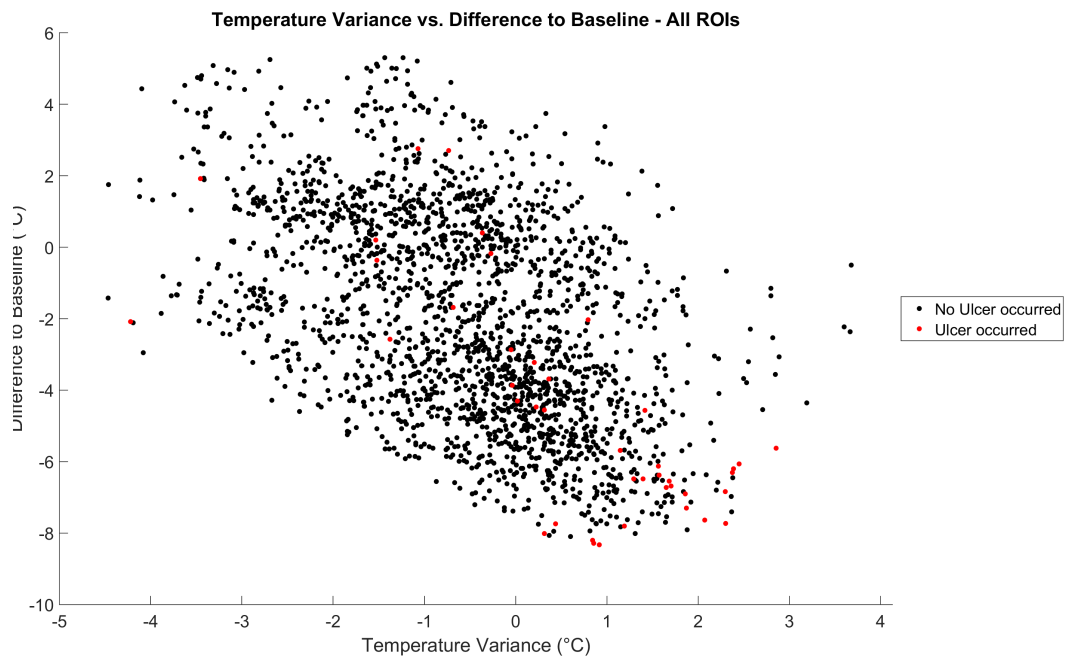


FIGURE 5.14: Temperature variance vs. difference to baseline plot

$y < T_{variance}$	$\Delta T_{baseline} < x$				
	-5.0	-5.5	-6.0	-6.5	-7.0
0.0	53.5, 87.0	53.5, 90.6	48.8, 93.3	32.6, 95.5	20.9, 97.7
0.5	48.8, 91.2	48.8, 93.2	44.2, 95.0	27.9, 96.3	16.3, 98.1
1.0	41.9, 95.5	41.9, 96.2	37.2, 96.8	20.9, 97.8	9.3, 98.9
1.5	32.6, 98.2	32.6, 98.3	30.2, 98.6	18.6, 98.9	7.0, 99.4

TABLE 5.12: Temperature variance vs difference to baseline threshold assessment

**Figure 5.15** plots the temperature change over time data against the difference to baseline data. In this graph there is a grouping of the 'did ulcerate' class data points in the lower area of the graph. This corresponds to a difference in baseline below

$-5^{\circ}\text{C}$  and a temperature change near  $0^{\circ}\text{C}$ . Therefore the threshold intervals chosen for this classifier range from  $-5^{\circ}\text{C}$  to  $-7^{\circ}\text{C}$  for the difference to baseline and  $0.5^{\circ}\text{C}$  to  $3^{\circ}\text{C}$ . Table 5.13 shows that the sensitivity can reach 53.5% while maintaining a specificity of 90.8%. This is similar to the previous temperature variance vs. difference to baseline classifier but achieves a higher specificity. However the specificity is lower than in the baseline threshold data.

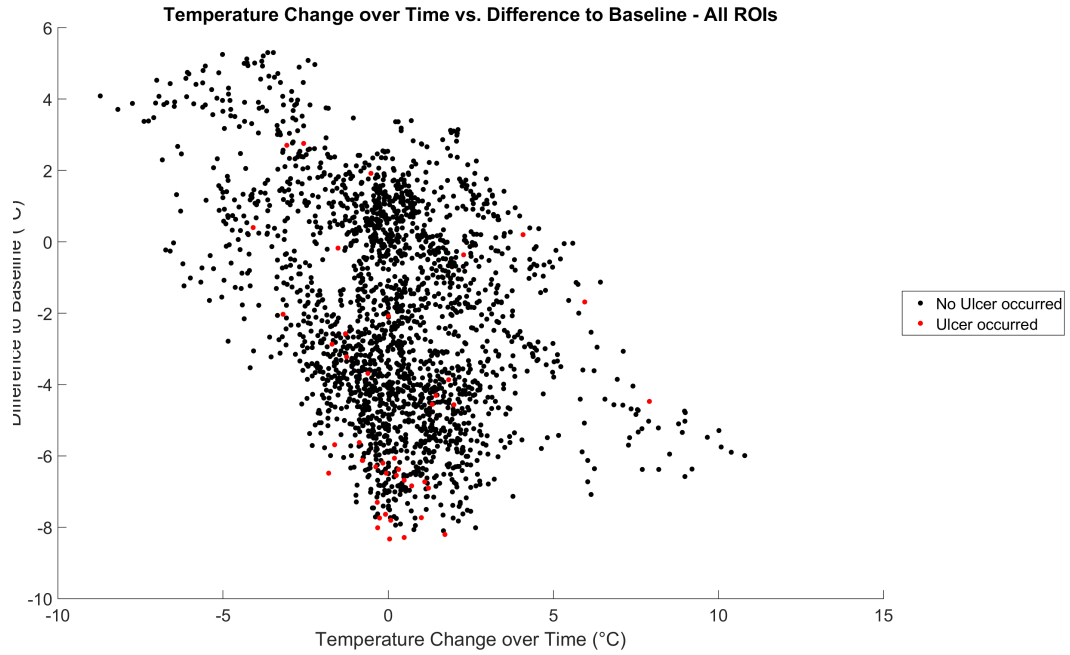


FIGURE 5.15: Temperature change over time vs. difference to baseline plot

$\Delta T_{baseline} < x$	-5.0	-5.5	-6.0	-6.5	-7.0
$-y < T_{change} < y$					
0.5	32.6, 94.9	32.6, 96.2	32.6, 97.3	20.9, 98.0	16.3, 99.0
1.0	39.5, 91.8	39.5, 93.8	37.2, 95.7	23.3, 97.1	16.3, 98.6
1.5	46.5, 89.0	46.5, 92.0	44.2, 94.8	30.2, 96.5	18.6, 98.4
2.0	53.5, 87.4	53.5, 90.8	48.8, 94.0	32.6, 96.0	20.9, 98.1
2.5	53.5, 85.1	53.5, 89.3	48.8, 93.0	32.6, 95.4	20.9, 97.7
3.0	53.5, 84.4	53.5, 88.8	48.8, 92.8	32.6, 95.2	20.9, 97.7

TABLE 5.13: Temperature variance vs difference to baseline threshold assessment

### 5.3 Applying Thresholds to Individual Regions of Interest

Using the thresholds found to be a good fit in section 5.2 the sensitivity and specificity of each was evaluated using data from each individual ROI where an ulcer occurred, similar to 5.3 and 5.4. The TPR and TNR are listed in tables 5.14 to 5.20. The results show that almost each threshold can be applied with perfect sensitivity and near-perfect specificity to the 4<sup>th</sup> MTH, with the classifier  $33.5 < T_{ROI} \& 0 < T_{asymmetry}$  scoring 100% sensitivity and 93.4% specificity. Similarly well-fit data was found in the 2<sup>nd</sup> Toe, but the highest sensitivity of 77.8% was achieved by the  $-2.0 < T_{change} < 2.0 \& -5.5 > T_{baseline}$  with a specificity of 92.5%. The other ROIs where ulceration occurred throughout the study cannot be spotted as easily by the classifiers. Here, the sensitivity is consistently 0%, meaning that the thresholds are wrongly placed.

Threshold 1	Threshold 2	Sensitivity (%)	Specificity (%)
$33.5 < T_{ROI}$	$0 < T_{asymmetry}$	0.0	91.1
$33.5 < T_{ROI}$	$0 < T_{variance}$	0.0	88.3
$33.5 < T_{ROI}$	$-2.0 < T_{change} < 2.0$	0.0	91.7
$0.5 < T_{asymmetry}$	$0.5 < T_{variance}$	0.0	83.9
$2.0 < T_{asymmetry}$	$-1.2 < T_{change} < 1.2$	0.0	100.0
$2.0 < T_{asymmetry}$	$-5 > T_{baseline}$	0.0	93.9
$2.5 < T_{variance}$	$-0.6 < T_{change} < 0.6$	0.0	100.0
$0.0 < T_{variance}$	$-5.5 > T_{baseline}$	0.0	100.0
$-2.0 < T_{change} < 2.0$	$-5.5 > T_{baseline}$	0.0	83.9

TABLE 5.14: Application of 'best' threshold values to ROIs - 1<sup>st</sup> Toe

Threshold 1	Threshold 2	Sensitivity (%)	Specificity (%)
$33.5 < T_{ROI}$	$0 < T_{asymmetry}$	66.7	97.7
$33.5 < T_{ROI}$	$0 < T_{variance}$	66.7	95.4
$33.5 < T_{ROI}$	$-2.0 < T_{change} < 2.0$	66.7	97.7
$0.5 < T_{asymmetry}$	$0.5 < T_{variance}$	33.3	97.1
$2.0 < T_{asymmetry}$	$-1.2 < T_{change} < 1.2$	0.0	100.0
$2.0 < T_{asymmetry}$	$-5 > T_{baseline}$	22.2	96.0
$2.5 < T_{variance}$	$-0.6 < T_{change} < 0.6$	0.0	100.0
$0.0 < T_{variance}$	$-5.5 > T_{baseline}$	0.0	100.0
$-2.0 < T_{change} < 2.0$	$-5.5 > T_{baseline}$	77.8	92.5

TABLE 5.15: Application of 'best' threshold values to ROIs - 2<sup>nd</sup> Toe

Threshold 1	Threshold 2	Sensitivity (%)	Specificity (%)
$33.5 < T_{ROI}$	$0 < T_{asymmetry}$	0.0	96.1
$33.5 < T_{ROI}$	$0 < T_{variance}$	0.0	96.1
$33.5 < T_{ROI}$	$-2.0 < T_{change} < 2.0$	0.0	96.1
$0.5 < T_{asymmetry}$	$0.5 < T_{variance}$	0.0	96.1
$2.0 < T_{asymmetry}$	$-1.2 < T_{change} < 1.2$	0.0	100.0
$2.0 < T_{asymmetry}$	$-5 > T_{baseline}$	0.0	92.7
$2.5 < T_{variance}$	$-0.6 < T_{change} < 0.6$	0.0	100.0
$0.0 < T_{variance}$	$-5.5 > T_{baseline}$	0.0	100.0
$-2.0 < T_{change} < 2.0$	$-5.5 > T_{baseline}$	0.0	84.9

TABLE 5.16: Application of 'best' threshold values to ROIs - 3<sup>rd</sup> Toe

Threshold 1	Threshold 2	Sensitivity (%)	Specificity (%)
$33.5 < T_{ROI}$	$0 < T_{asymmetry}$	0.0	98.9
$33.5 < T_{ROI}$	$0 < T_{variance}$	0.0	99.4
$33.5 < T_{ROI}$	$-2.0 < T_{change} < 2.0$	0.0	98.3
$0.5 < T_{asymmetry}$	$0.5 < T_{variance}$	0.0	98.3
$2.0 < T_{asymmetry}$	$-1.2 < T_{change} < 1.2$	0.0	100.0
$2.0 < T_{asymmetry}$	$-5 > T_{baseline}$	0.0	93.3
$2.5 < T_{variance}$	$-0.6 < T_{change} < 0.6$	0.0	100.0
$0.0 < T_{variance}$	$-5.5 > T_{baseline}$	0.0	100.0
$-2.0 < T_{change} < 2.0$	$-5.5 > T_{baseline}$	0.0	86.7

TABLE 5.17: Application of 'best' threshold values to ROIs - 4th Toe

Threshold 1	Threshold 2	Sensitivity (%)	Specificity (%)
$33.5 < T_{ROI}$	$0 < T_{asymmetry}$	100.0	93.4
$33.5 < T_{ROI}$	$0 < T_{variance}$	100.0	89.2
$33.5 < T_{ROI}$	$-2.0 < T_{change} < 2.0$	100.0	91.6
$0.5 < T_{asymmetry}$	$0.5 < T_{variance}$	100.0	86.1
$2.0 < T_{asymmetry}$	$-1.2 < T_{change} < 1.2$	0.0	100.0
$2.0 < T_{asymmetry}$	$-5 > T_{baseline}$	87.5	98.8
$2.5 < T_{variance}$	$-0.6 < T_{change} < 0.6$	0.0	100.0
$0.0 < T_{variance}$	$-5.5 > T_{baseline}$	6.3	100.0
$-2.0 < T_{change} < 2.0$	$-5.5 > T_{baseline}$	100.0	91.6

TABLE 5.18: Application of 'best' threshold values to ROIs - 4<sup>th</sup> MTH

Threshold 1	Threshold 2	Sensitivity (%)	Specificity (%)
$33.5 < T_{ROI}$	$0 < T_{asymmetry}$	0.0	85.6
$33.5 < T_{ROI}$	$0 < T_{variance}$	0.0	84.5
$33.5 < T_{ROI}$	$-2.0 < T_{change} < 2.0$	0.0	87.4
$0.5 < T_{asymmetry}$	$0.5 < T_{variance}$	0.0	78.2
$2.0 < T_{asymmetry}$	$-1.2 < T_{change} < 1.2$	0.0	100.0
$2.0 < T_{asymmetry}$	$-5 > T_{baseline}$	0.0	90.2
$2.5 < T_{variance}$	$-0.6 < T_{change} < 0.6$	0.0	100.0
$0.0 < T_{variance}$	$-5.5 > T_{baseline}$	0.0	100.0
$-2.0 < T_{change} < 2.0$	$-5.5 > T_{baseline}$	0.0	86.2

TABLE 5.19: Application of 'best' threshold values to ROIs - 5<sup>th</sup> MTH

Threshold 1	Threshold 2	Sensitivity (%)	Specificity (%)
$33.5 < T_{ROI}$	$0 < T_{asymmetry}$	0.0	97.2
$33.5 < T_{ROI}$	$0 < T_{variance}$	0.0	96.1
$33.5 < T_{ROI}$	$-2.0 < T_{change} < 2.0$	0.0	98.3
$0.5 < T_{asymmetry}$	$0.5 < T_{variance}$	0.0	87.7
$2.0 < T_{asymmetry}$	$-1.2 < T_{change} < 1.2$	0.0	100.0
$2.0 < T_{asymmetry}$	$-5 > T_{baseline}$	0.0	98.9
$2.5 < T_{variance}$	$-0.6 < T_{change} < 0.6$	0.0	100.0
$0.0 < T_{variance}$	$-5.5 > T_{baseline}$	0.0	100.0
$-2.0 < T_{change} < 2.0$	$-5.5 > T_{baseline}$	0.0	99.4

TABLE 5.20: Application of 'best' threshold values to ROIs - 5<sup>th</sup> MTH Base

This becomes apparent when one looks at the graphing for these parameters, a sample of which are in figures 5.16 to 5.22. The full set of graphs are shown in appendix C. In figures 5.16, 5.18, 5.19 and 5.22 the amount of ulceration cohort data is too low for analysis (2-3 data points) however they do show signs that the separation of the data points is not as easy as a simple threshold. On the other hand, figures 5.17 and 5.20 reflect the improved classifier results in table 5.15 and 5.18. Here the ulceration data can be separated from non-ulcerated points by a threshold value with few false positive and false negative results.

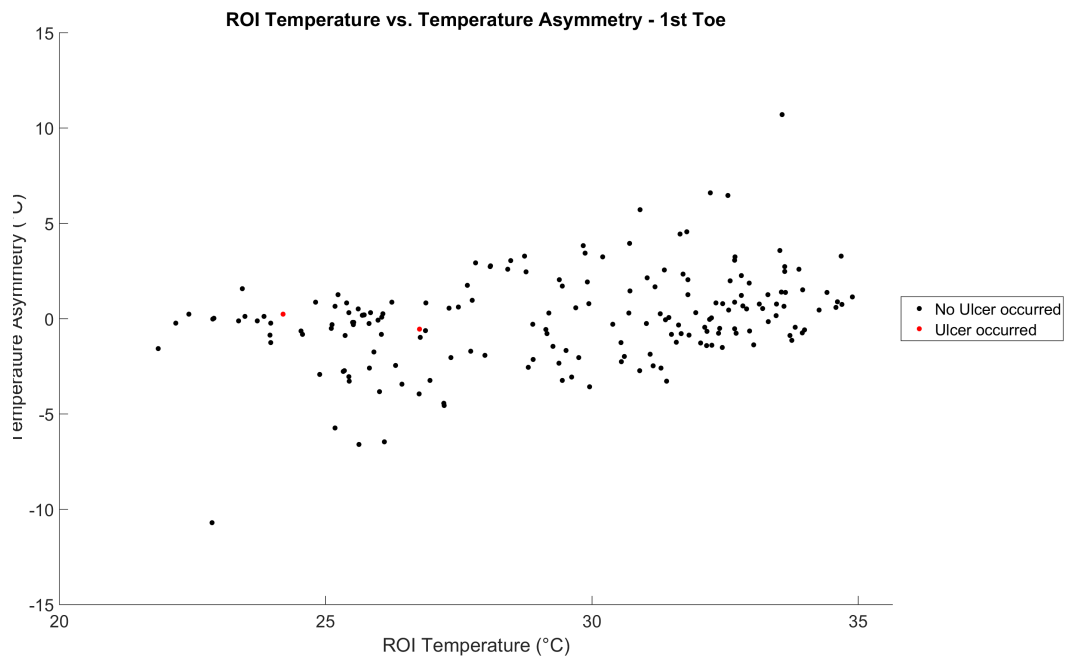


FIGURE 5.16: ROI temperature vs temperature asymmetry 1st toe plot

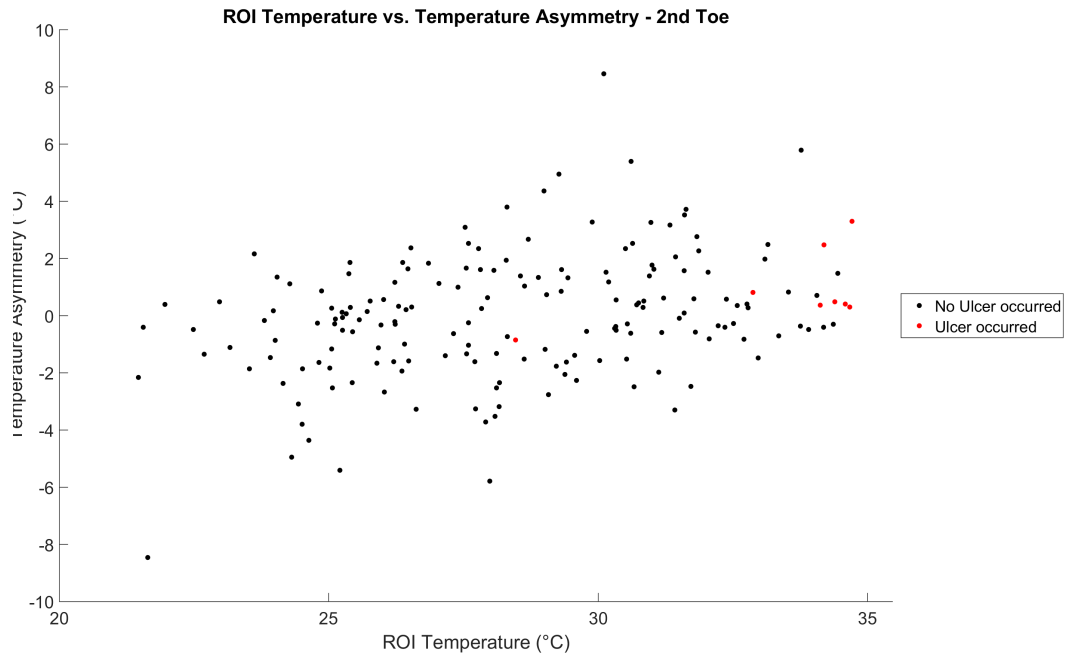


FIGURE 5.17: ROI temperature vs temperature asymmetry 2nd toe plot

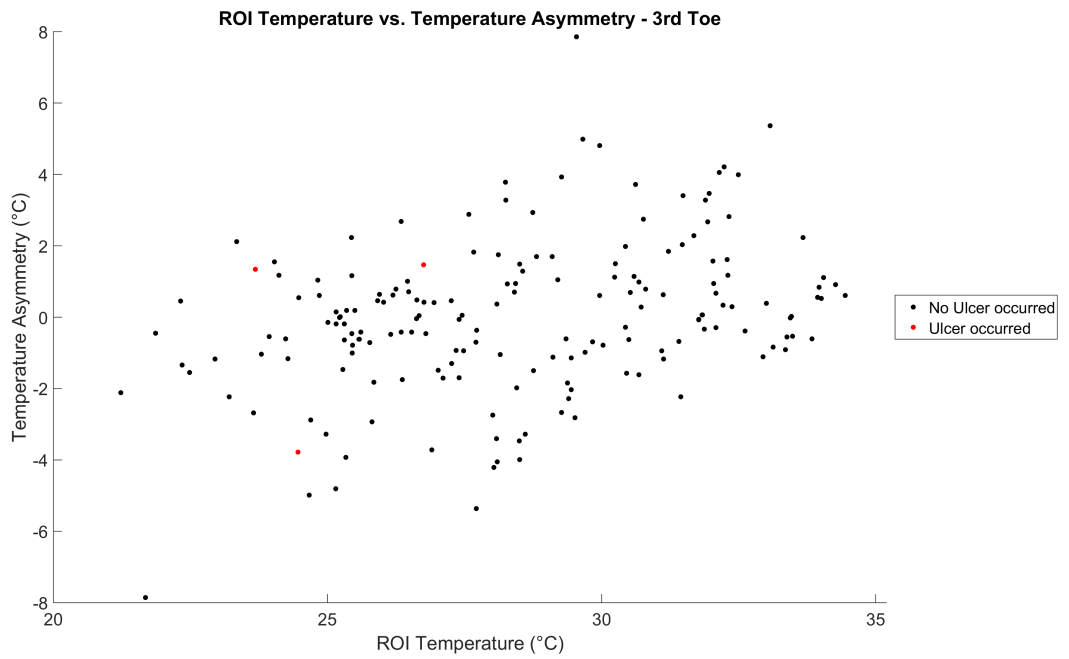


FIGURE 5.18: ROI temperature vs temperature asymmetry 3rd toe plot

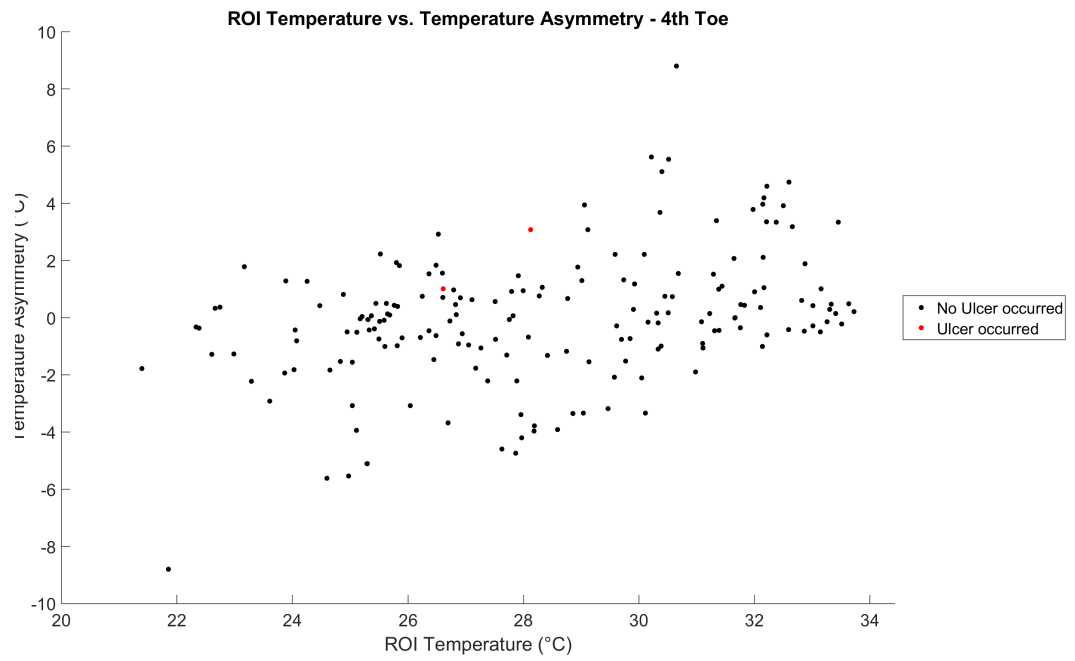


FIGURE 5.19: ROI temperature vs temperature asymmetry 4th toe plot

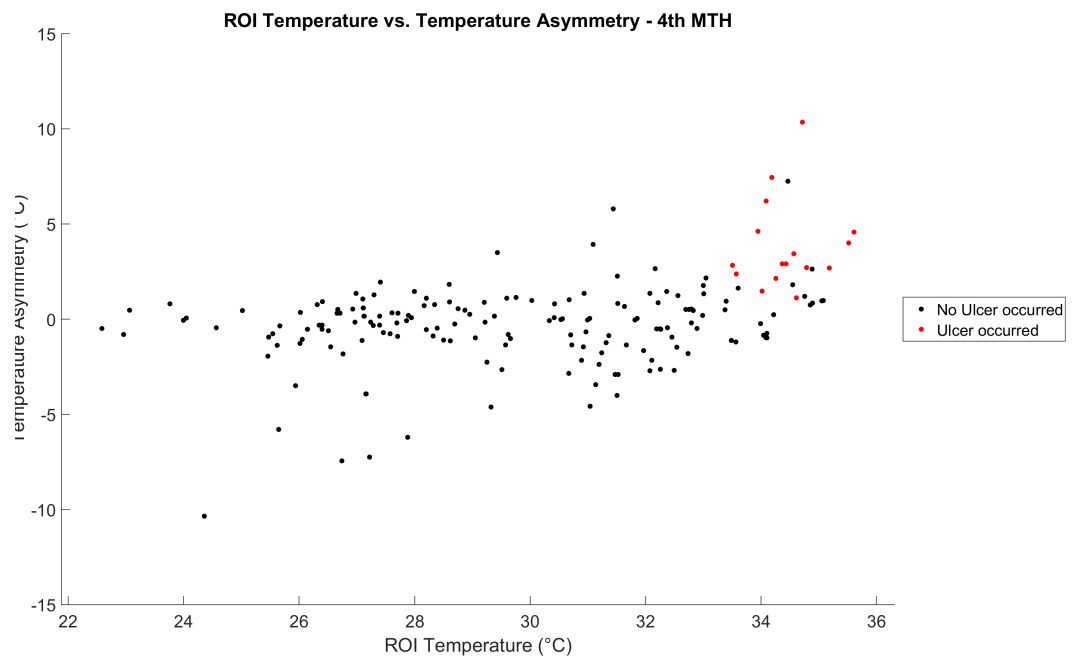


FIGURE 5.20: ROI temperature vs temperature asymmetry 4th MTH plot



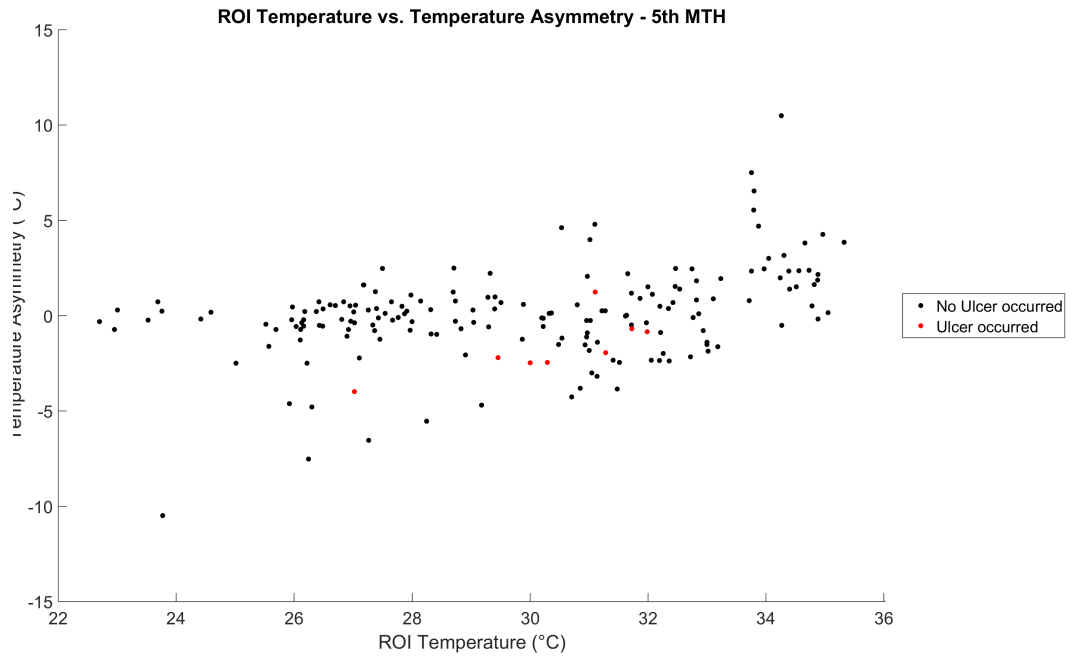


FIGURE 5.21: ROI temperature vs temperature asymmetry 5th MTH plot

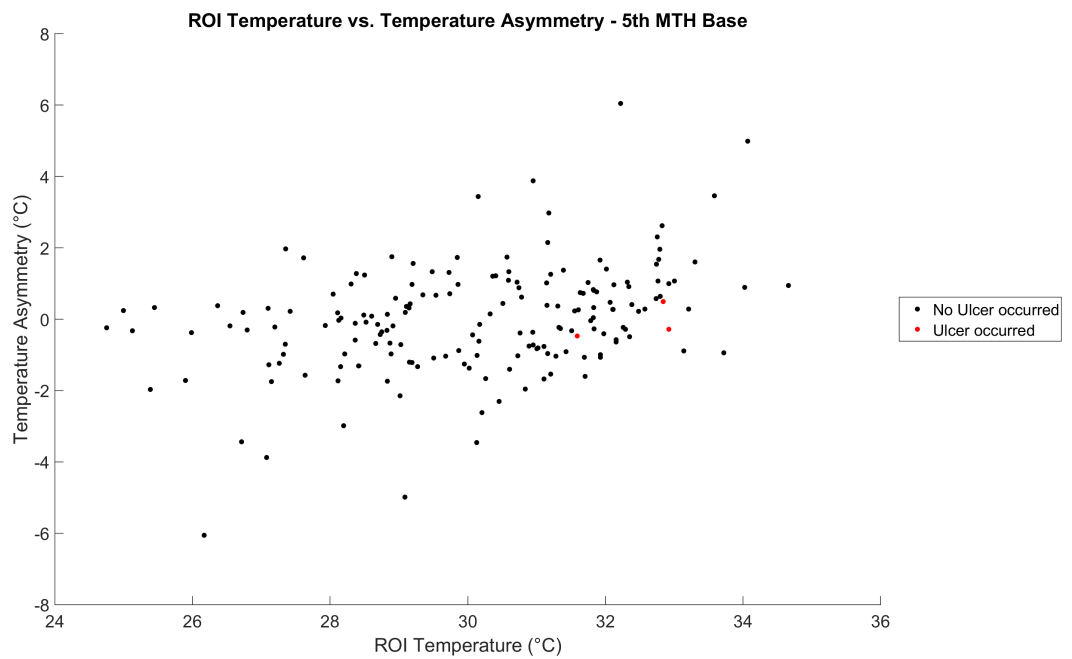


FIGURE 5.22: ROI temperature vs temperature asymmetry 5th MTH Base plot

## 5.4 Summary

In summary, three methods were used to evaluate five parameters by thresholds. In the first method the current "gold standard" classifier was evaluated with various thresholds against the data gathered in this project. The evaluation showed that this method is not very reliable and achieves sensitivity and specificity values between 40-44% and 80-82%, respectively. The second method attempted to combine two threshold methods into a classifier for all data points. These classifiers showed improved results with sensitivity and specificity values between 50-53% and 90-95%, respectively. The third method that was attempted was splitting the data into the 12 ROIs assigned in chapter 4 (Figure 4.1) and apply the most promising classifiers that were defined in the second method. This method showed to be the most effective method for the 2<sup>nd</sup> toe and 4<sup>th</sup> MTH, where the sensitivity and specificity values increased greatly. In most of the classifiers for the 4<sup>th</sup> MTH, the sensitivity is 100% and the specificity is above 90%. However, this is based on the ulceration cohort data of a single person only. Consequently, when applied to the remaining five ROIs, the sensitivity drops to 0%.

Even though it has been shown that splitting the data into ROIs before analysis can increase the sensitivity and specificity to predict an ulcer, the data set suffers from the lack of positive outcomes, the low measurement frequency and the inaccuracy of the infrared camera. The small sample size of positive outcomes in this study of 26 (excluding behavioural ulcers) is not sufficient to draw definitive conclusions about how an ulcer could be predicted using only temperature measurements. This problem is amplified by the low measurement frequency of, on average, one month. Furthermore, the inaccuracy of the camera allows for a temperature variation of  $\pm 0.2^\circ\text{C}$  (after calibration by NPL). In addition, the temperature is varied by another  $\pm 0.24^\circ\text{C}$  (two standard deviations) by the warping process (see section 2.5.5). These three factors combined reduce the believability of the threshold values but on the other hand may provide an explanation as to why the data is spread out in some of the presented graphs.

The spread of the data in graphs such as figure 5.21 may be explained by the frequency of measurements. If a shorter interval between measurements such as daily as used in [12] were used, the increase in data would allow for a complete history of the development of an ulcer and a an increase in the believability of the stated classifiers.

In comparison to what is currently the 'gold standard', this data set does not reflect an accurate classifier, with the highest sensitivity that could be achieved reaching 39.5% while maintaining a specificity of at least 90% using  $2.0 < abs(T_{asymmetry})$ . This is a similar threshold that was previously used by Frykberg [12] and Van Netten [8]. The values found for the sensitivity and specificity are similar but cannot be directly compared to Frykberg because the time element is missing. When applying a time constraint to the data the sensitivity drops below 2%, but even this is not a 100% compatible classifier (Table 5.21).

In conclusion, the likelihood of the explored classifiers being a realistic predictor of foot ulceration is low due to the combination of small ulceration cohort number, low measurement frequency and camera inaccuracy.

Threshold	TPR (%)	TNR (%)	PPV (%)	NPV (%)
0.1	0.8	70.0	16.7	8.5
0.2	0.9	81.1	16.7	15.7
0.3	0.7	84.7	13.0	21.2
0.4	0.8	87.8	13.0	27.5
0.5	0.6	89.4	9.3	33.7
0.6	0.7	90.9	9.3	39.7
0.7	0.7	91.6	9.3	43.6
0.8	0.8	92.4	9.3	48.5
0.9	0.7	92.8	7.4	52.5
1.0	0.7	93.3	7.4	56.4
1.1	0.6	93.5	5.6	59.6
1.2	0.7	93.8	5.6	62.9
1.3	0.7	94.1	5.6	66.2
1.4	0.5	94.2	3.7	68.8
1.5	0.5	94.3	3.7	70.6
1.6	0.6	94.5	3.7	73.1
1.7	0.6	94.7	3.7	75.1
1.8	0.7	94.8	3.7	77.0
1.9	0.8	94.9	3.7	78.9
2.0	0.8	95.0	3.7	80.8
2.1	0.9	95.1	3.7	81.9
2.2	0.9	95.1	3.7	82.8
2.3	1.0	95.2	3.7	84.1
2.4	1.1	95.3	3.7	85.1
2.5	1.1	95.3	3.7	86.0
2.6	1.2	95.4	3.7	86.7
2.7	1.3	95.4	3.7	87.8
2.8	1.4	95.5	3.7	88.8
2.9	1.5	95.5	3.7	89.1
3.0	1.6	95.5	3.7	89.7
3.1	1.6	95.5	3.7	90.1
3.2	1.7	95.5	3.7	90.7
3.3	1.9	95.6	3.7	91.5
3.4	1.9	95.6	3.7	91.8
3.5	2.2	95.6	3.7	92.8

TABLE 5.21: Statistical values for various ROI temperature difference thresholds  
- taking into account time

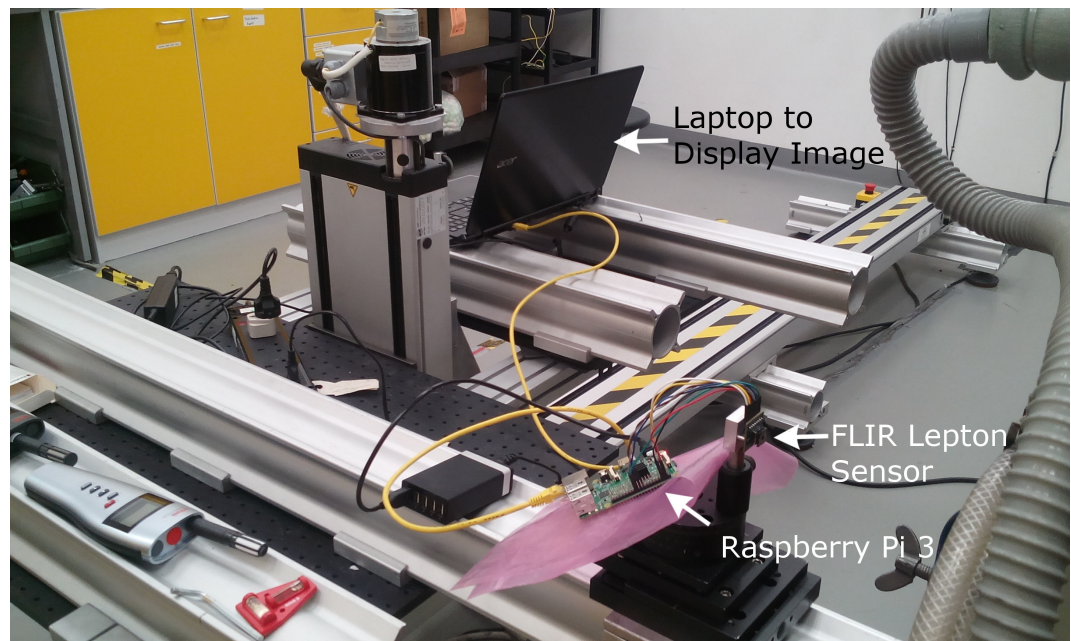
## Chapter 6

# Next Generation Device

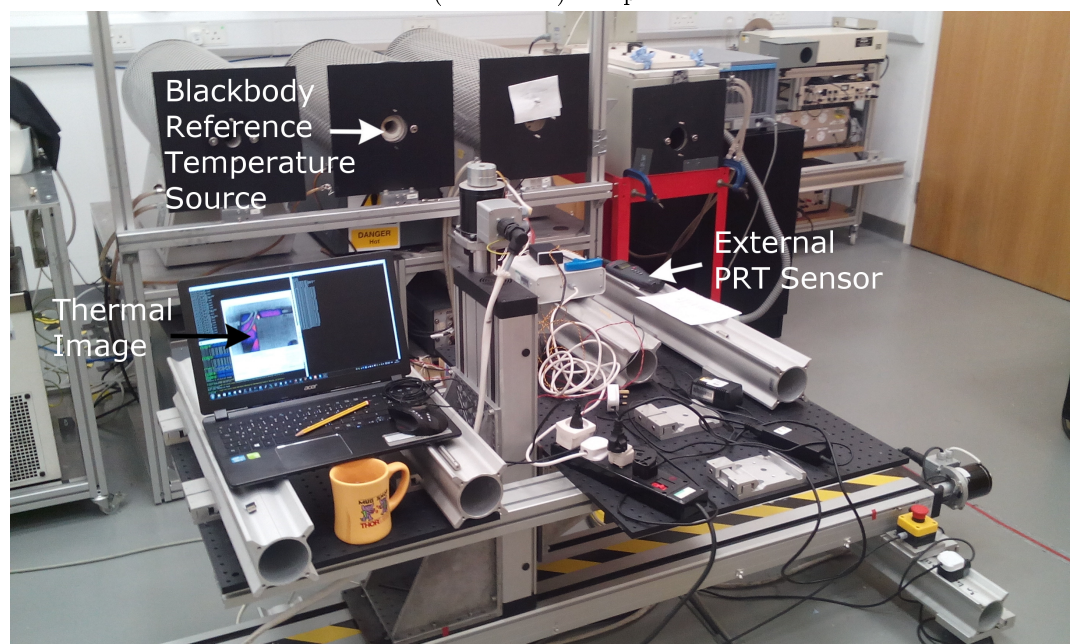
The performance of the first generation device was assessed throughout the trials by feedback from the clinical centres and updated to suit the needs of the centres. The device itself was characterised by the NPL at the start, once in between and finally again at the end of both trials. It was also compared to the current gold standard spot measurement device during the first trial [41]. The characterisation and comparison showed the device to be suitable for imaging the foot and analysis, satisfying all clinical requirements in full.

Based on the experience gained the next generation of this device is already in development and utilises the well known Raspberry Pi cameras. With new technology emerging around smaller and cheaper infrared cameras, the FLIR Lepton Version 3 (160x120 pixels) was chosen as the infrared sensor for the successor to the DFUPS device to cut cost, size and weight. The device is equipped with two Raspberry Pi computers, two cameras for stereovision, a flash mechanism consisting of four power LEDs, a speaker and fans for cooling. The device incorporates the same 'targeting' system as the DFUPS device (briefly mentioned in section 3.2.1) to take images from the correct distance with the addition of a method to adjust the height of the projected dots.

The FLIR Lepton sensor was calibrated with the help of the NPL and control software written by the author. Figures 6.1a and 6.1b show the calibration setup at the NPL. Calibration is necessary as the FLIR Lepton comes equipped only with default factory values for calibration which do not account for the variations present in each individual sensor. However it is possible to read out raw sensor data, from which an individual calibration can be created. In the background of figure 6.1b, 4 blackbody reference devices are shown against which the sensor was tested.



(a) FLIR Lepton calibration  
(back view) setup



(b) FLIR Lepton calibration  
(front view) setup

FIGURE 6.1: FLIR Lepton calibration setup

The process of calibration was carried out using several different blackbody reference devices. These included:

1. Ammonia ( $\text{NH}_3$ ) - temperature range from  $-40$  to  $40^\circ\text{C}$

## 2. Thermal Imaging BlackBody (TIBB) - temperature range from 10 to 80 °C

The first step of the calibration was to gather data from the sensor. It was carried out in multiple runs at varying temperatures from the blackbody reference device at a set distance of 30 cm. For each run, the blackbody reference device was set to the desired temperature and after reaching the set point, a further 10 minute delay was added to make sure the temperature was stable. This was cross-referenced using a PRT. The Lepton sensor was then aligned with the device at a specific distance and 12 images were taken in series to establish repeatability. A note was made of the temperature measured by the PRT for every image. A total of 11 runs were done on the NH<sub>3</sub> device and 21 on the TIBB device. The ambient temperature was kept as close as possible to 21 °C.

A second calibration was attempted by moving the Lepton along a predefined grid to attain different angles to the measurement source. This proved to be difficult to analyse in later processing.

The second step of the calibration consists of a computer vision approach to segmenting the images into black body cavity and background. This was accomplished using a series of standard computer vision techniques available in the open source OpenCV library network and a custom algorithm written by the author. An example is shown in figure 6.2. The input image (figure 6.2a) is first passed through a Gaussian filter followed by a Canny edge detector with the default OpenCV parameters. From the resultant edge image, the contours are extracted using OpenCV's findContours function. This leaves only outlines of shapes (figure 6.2b). From there, an attempt is made to find the largest area circle without touching any contour starting from the center of the image, which is assumed to be the center of blackbody reference device. This is done by defining a circle with a radius of 0 pixels at the center of the image and incrementing the radius until a boundary (white pixel) is encountered on the edge of the circle. When this happens, the centroid of all intersections to the boundary is calculated and the center of the circle is moved by 1 pixel in the opposite direction of the intersections. This corrects for non-perfect alignment between the sensor and the device, which was done visually only. The two steps of enlarging the circle and moving the center of the circle is repeated until the center of the circle returns to a position in which it has already been. The radius is then multiplied by  $\frac{2}{3}$  to ensure that the edges of the circle, which may have a slightly different temperature, are not taken into account. An example of the completed algorithm is shown in 6.2c.

The same process is shown in figure 6.3, but this time with a temperature of 15 °C set on the blackbody reference device. In figure 6.3b, some additional edges are seen that should be interpreted as noise. Most of these contours are ignored (figure 6.3c), but there is another contour within the target area which limits the detected area.

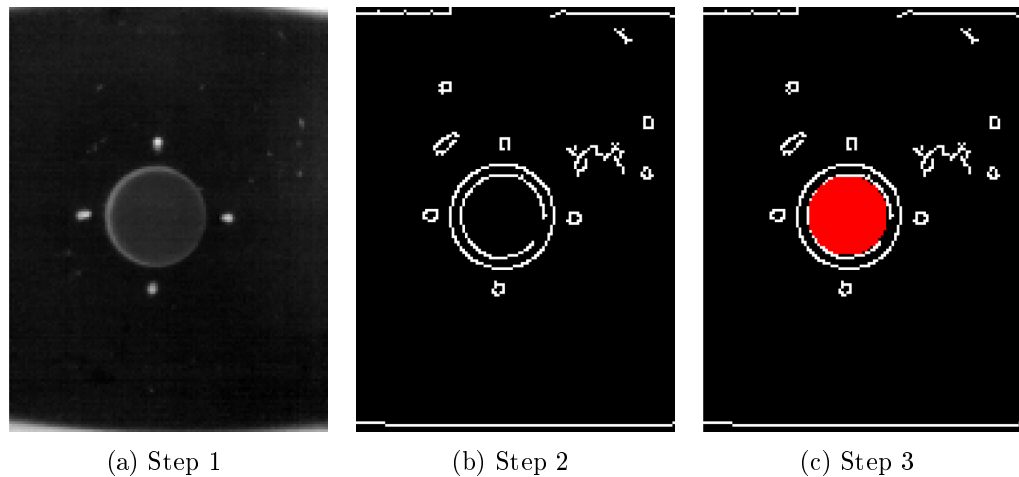


FIGURE 6.2: FLIR Lepton software extraction 15 °C example

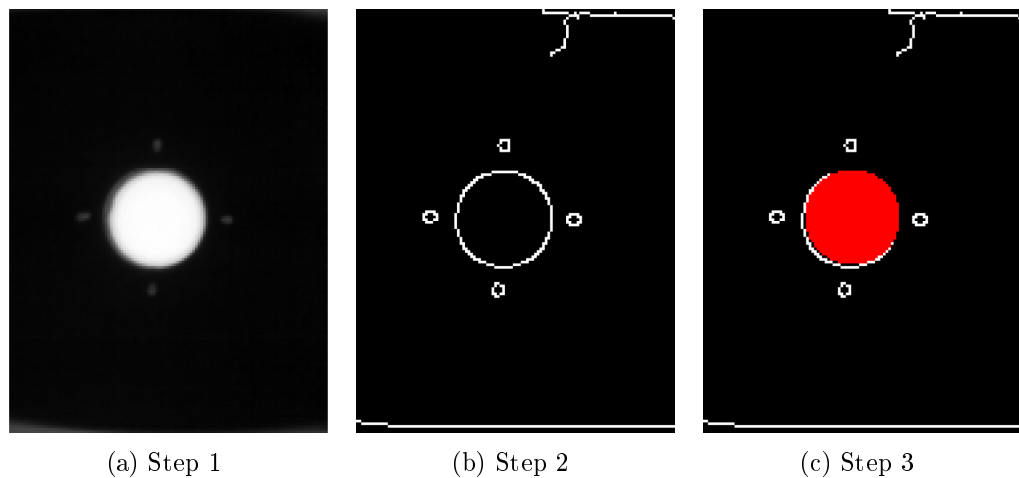
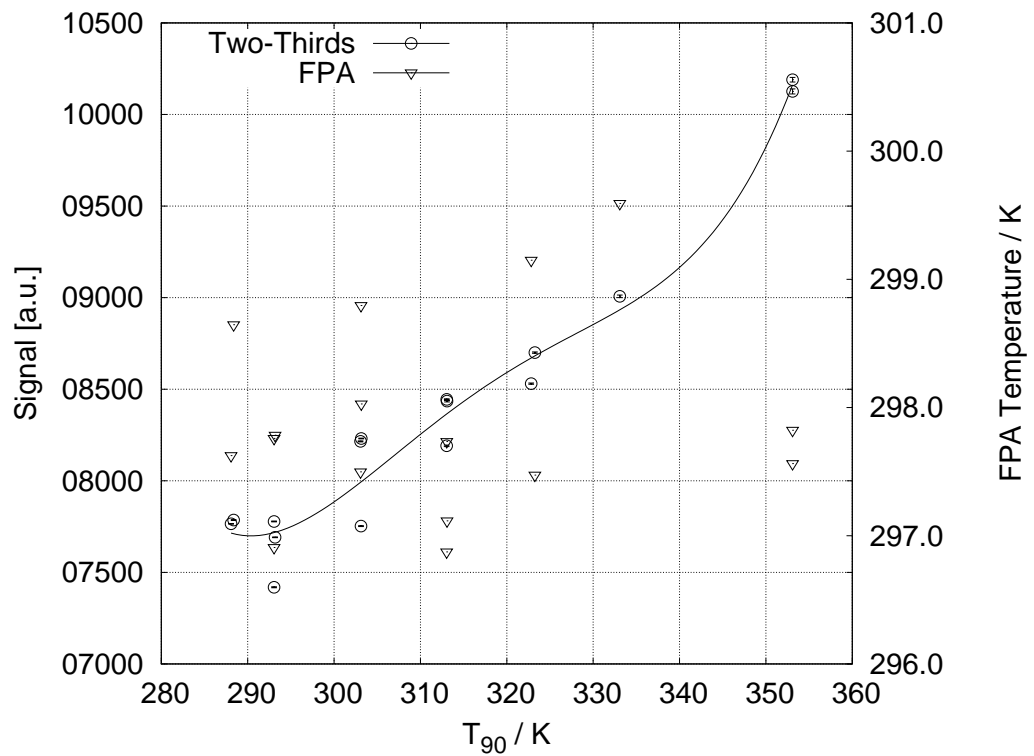


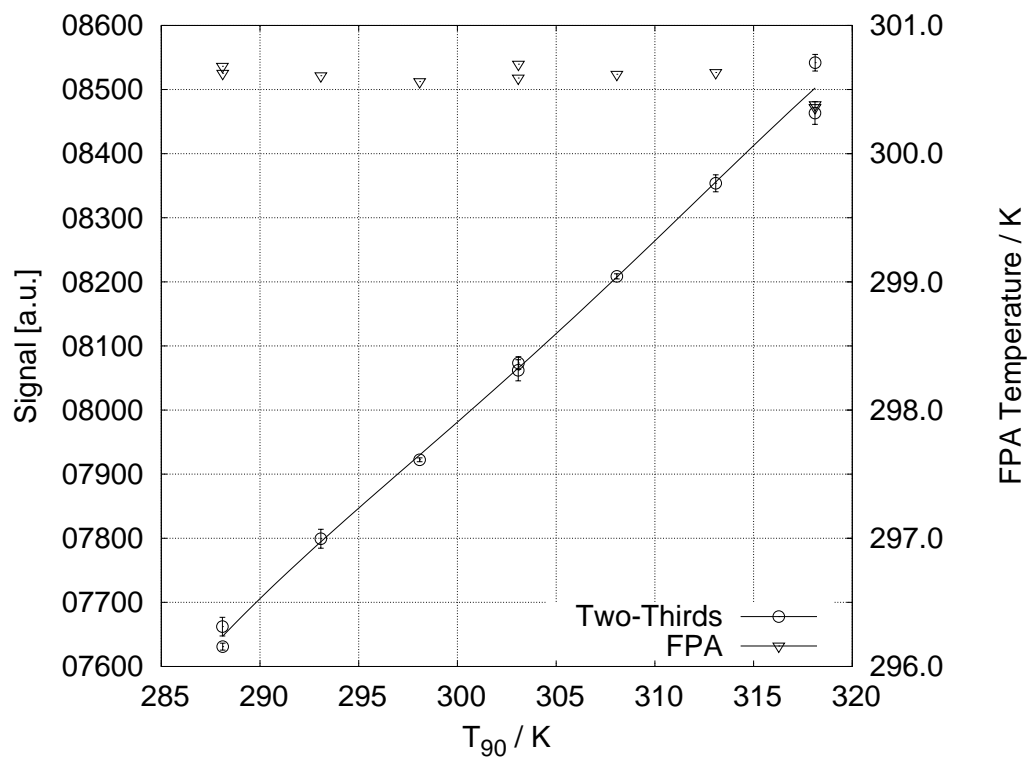
FIGURE 6.3: FLIR Lepton software extraction 45 °C example

The extracted data was then graphed and analysed by the NPL. The results show that it is advantageous to stabilise the Focal Plane Array (FPA) temperature as best as possible to ensure a consistent temperature readout. This is demonstrated by figures 6.4a and 6.4b. There was no conclusive relationship between the signal value, FPA temperature and radiant temperature.





(a) Non-stabilised FPA



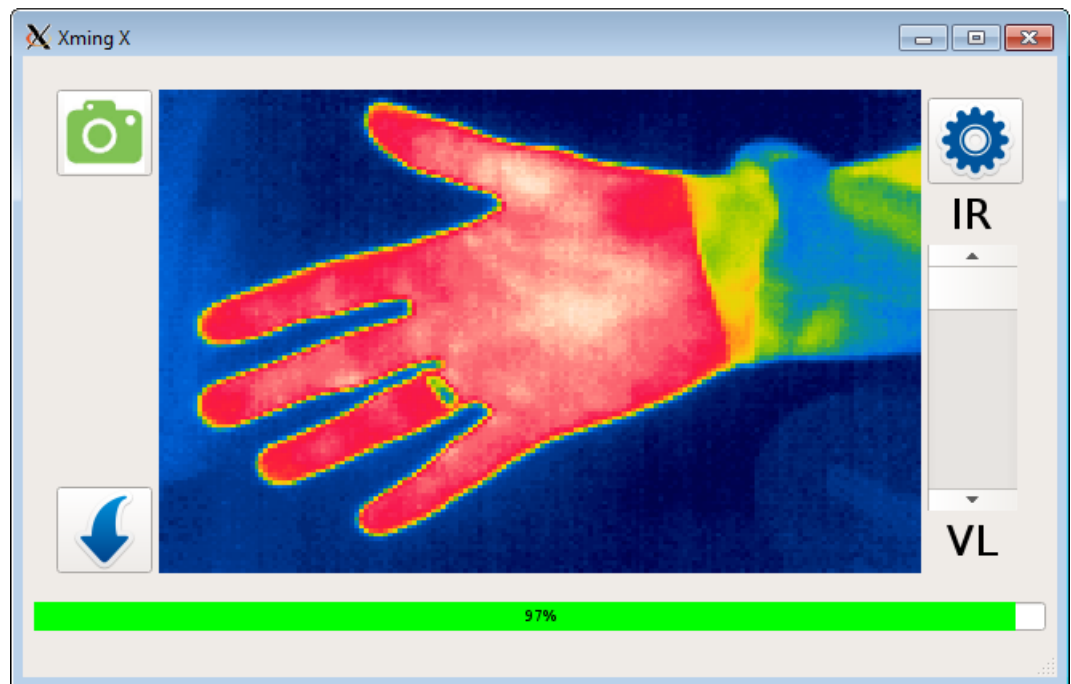
(b) Stabilised FPA

FIGURE 6.4: Lepton calibration data graphing

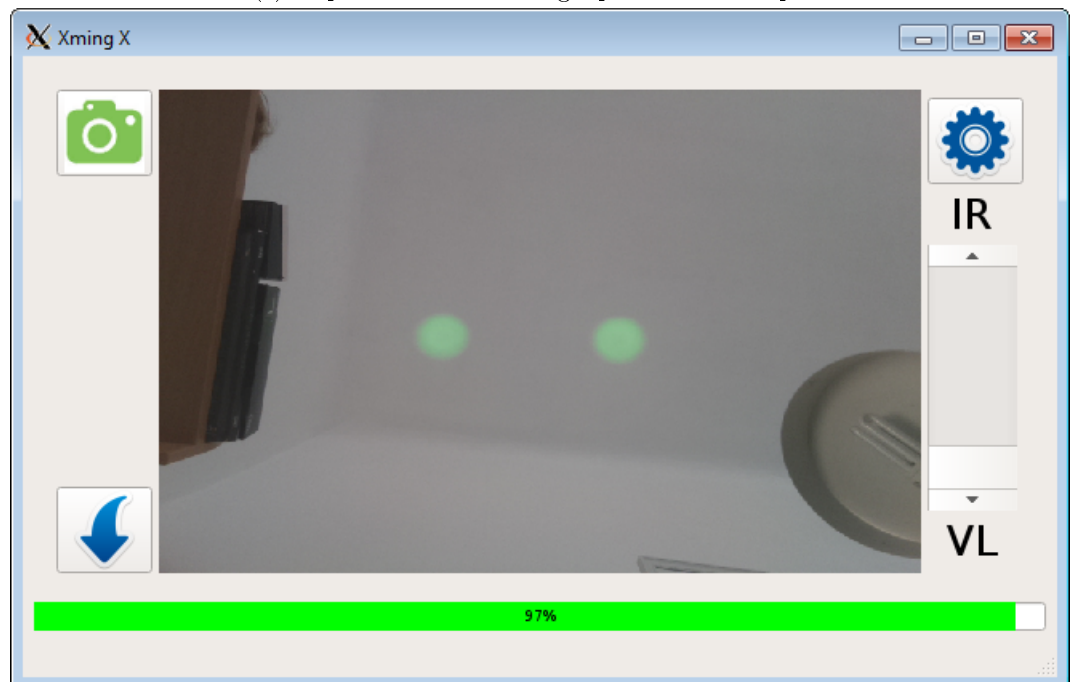
The other aspect of the next generation device is the software, written by the author. The user interface is based on the software of the DFUPS device, with minor variations. Figures 6.5 and 6.6 show screenshots of various parts of the software. These are comparable to figure 3.6a. In the second version of the software, the fixed image series restriction is lifted because the next generation device is meant to be a generic imaging device. The addition of icons serves the purpose of making the interface smaller in addition to maintaining a clear message for each button.

20 of these devices have been built and sold to the NPL in its current stage of development. Negotiations are under way for the mass production of these devices. Currently, there is a student continuing work on the user interface and a PhD candidate at the University of South Wales working on improving the 3D image generation algorithms. These improvements will hopefully allow the integration of more advanced algorithms for point cloud processing and enable automated data extraction.

Future versions will combine the electronics into one printed circuit board to enable mass manufacturing. Moreover, elements for heating and cooling need to be added to allow for the stabilisation of the thermal camera as well as software to control them. This thought can be extended to the visual camera, where an improved method of securing the cameras will result in a less noisier input image to the algorithm responsible for calculating the 3D images.

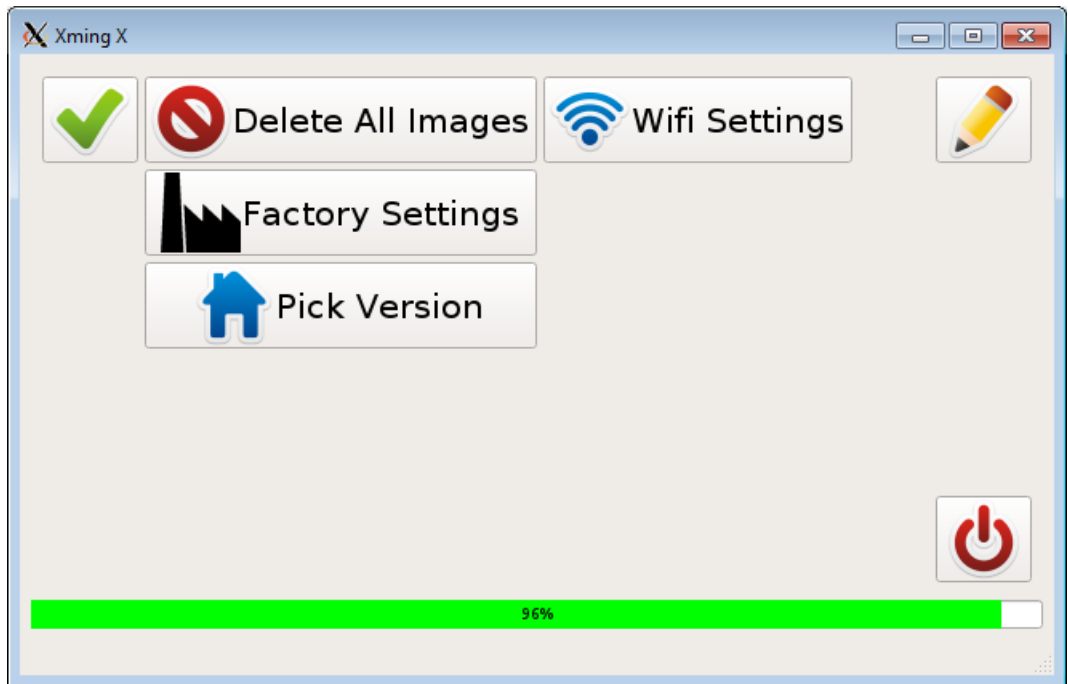


(a) Capture screen showing lepton sensor output

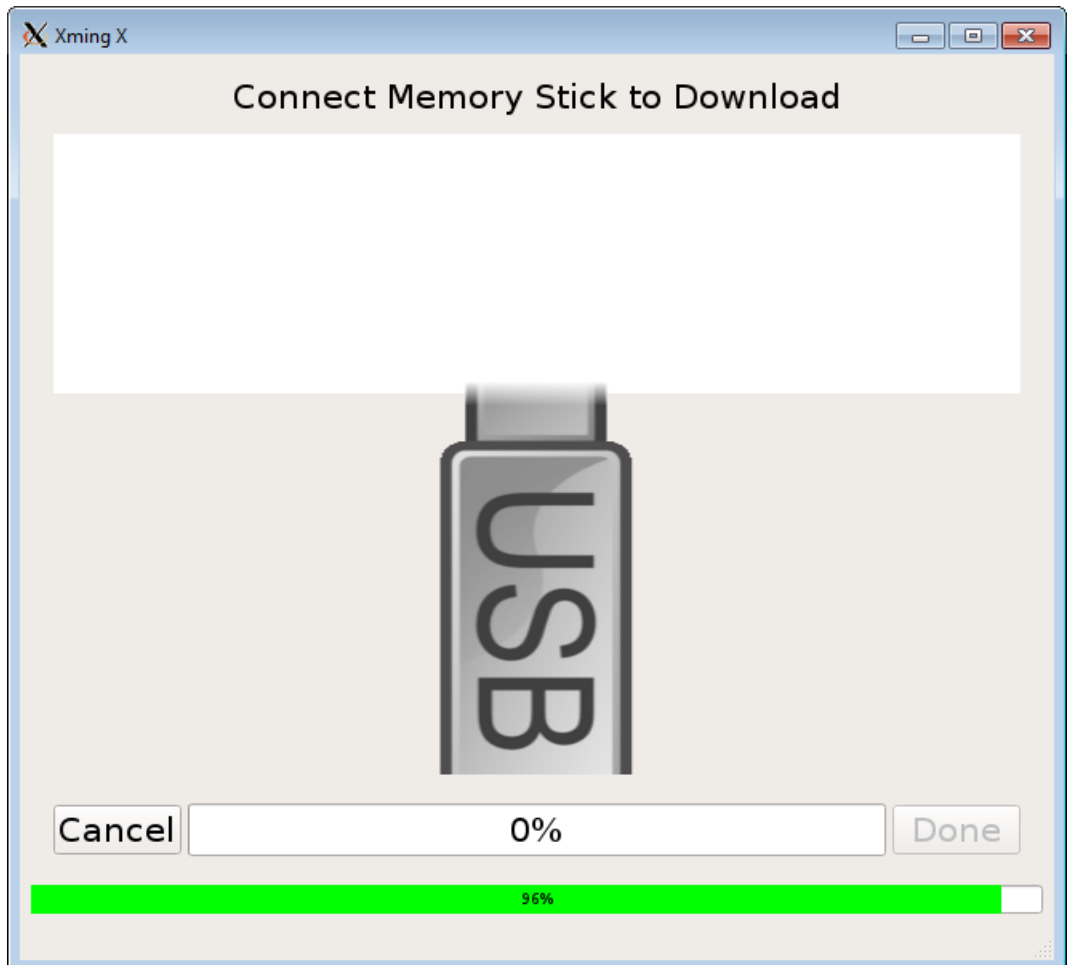


(b) Capture screen showing raspberry pi camera output

FIGURE 6.5: Software version 2 screenshots



(a) Settings screen



(b) Download screen

FIGURE 6.6: Software version 2 screenshots - continued

# Chapter 7

## Conclusion

### 7.1 Achievement of Objectives

The following section summarises the objectives of this thesis in regards to the research question and discusses how well they were achieved. The specific objectives, originally set in section 1.4, are:

1. Research into the underlying physical principles of infrared imaging, detector technologies and their respective spatial and thermal resolutions, and error sources associated with both technology and usage in clinical practice.
2. Development of hardware and software for a device capable of addressing the aim in a clinically feasible manner.
3. Implementation of the device and provision to the 3 clinical centres associated with this project.
4. Implementation of a Website capable of mass manual image object outlining.
5. Analysis of the data collected by the clinical centres with the aim of:
  - Establishing and verifying a methodology for data extraction and grouping
  - Confirming/rejecting the currently accepted 2.2°C threshold
  - Finding an improved method over the 2.2°C threshold

The extent to which these objectives were met is now discussed in the following sections 7.1.1 to 7.1.5.

### **7.1.1 Research into the Underlying Physical Principles of Infrared Imaging**

Research into the physical principles is primarily documented in the background research chapter of this thesis. Principal knowledge for infrared imaging was acquired about the different types of infrared radiation and common detector types. This knowledge allowed for the correct choice of infrared imager for the project and appropriate measures to control environmental variables. The off-the-shelf thermal camera that was used is similar to those used for thermography in biomedicine. The factory accuracy of the thermal imager is  $\pm 2\%$  of the temperature value or  $\pm 2^\circ\text{C}$ , whichever is greater. This was corrected using characterisation data provided by the NPL, thus allowing for above-average quality measurements to take place. Instead of the original  $\pm 2\%$  accuracy the author's software corrected the thermal data to within  $\pm 0.2^\circ\text{C}$ .

### **7.1.2 Development of the Infrared Imaging Device**

The development of the preliminary hard- and software for this project had to be achieved within a time span of 3 months in order to stay in the project time plan and to allow clinicians sufficient time to complete two clinical trials. Throughout the following two years of usage, several minor shortcomings were discovered in the device. None of these shortcomings jeopardised the project at any moment in time. Software issues could be dealt with swiftly but issues with the hardware were persistent. For example, the USB bus of the Odroid-U3 was not able to support two cameras as expected, which would have allowed for stereoscopic vision and thus a 3D image with which control points could have been placed automatically onto the images. This called for an extra step in the process of analysis to take place, namely the use of a website designed and implemented by the author to be able to complete the task of outlining feet on hundreds of images by 14 volunteers (see 7.1.4 below).

Similar devices have been constructed in the past but have not been used extensively in a clinical context [42, 43, 44]. Devices that are used in a clinical setting tend to be rigid and bulky such as the system used in [8]. Additionally, the device conceptualised in this project is approved as a medical device (for the purpose of this particular clinical investigation, not for general use or sale) and has been tested in multiple clinical centres with positive feedback. Its small footprint combined with the modern imaging capability proved to be a successful design.

### **7.1.3 Implementation of the Device**

The implementation of the device was fulfilled adequately for the two trials. The hardware was assembled according to the plans created in the previous objective. However, in some devices, the camera responsible for capturing the visible spectrum came loose during operation and captured images with a large offset with respect to the infrared image. This was, however, not a concern as the visual images were not used during analysis for automatic segmentation.

The software for the device was created by the author in Qt and C++ and continuously revised during the project utilising feedback from the clinical centres. It is a graphical user interface and similar to a generic imaging device but includes options dedicated to this project such as the device forcing a series of images to be taken with correct labelling according to the specification of the clinical trial protocol. To the best of the author's knowledge such a software driven protocol implementation has never been attempted before but it proved to be highly successful. Virtually all image data could be used in the analysis with no data set being invalid due to wrong timings, views, order or other typical user mistakes. Some issues surrounding the operating system and software occasionally stopped a device from working altogether. However, these incidents were small in number and could usually be resolved by turning the device off and on again.

### **7.1.4 Implementation of Website for Mass Manual Image Object Outlining**

The implementation of a website for outlining was successfully completed. The main aspect of this objective was to increase the speed which was fulfilled as it took the participating volunteers only two weeks after the launch of the website to complete 1361 plantar images (7.7% of all images, including unused and unusable) outlines. However, even though there were measures in place to stop erroneous placement of control points and correcting the order in which the points were placed, approx. 500 images needed reworking. In addition, the website required some maintenance for the database that stored the images and kept track of what was being done. The outcome was, however, very successful as it would have taken one person several weeks to outline all images, even when taking into account the reworking of images.

### 7.1.5 Analysis of the Data Collected by the Clinical Centres

The analysis of the collected data was completed using three distinct methods and five input parameters using 12 measurement spots. Although each method shows potential to spot an ulceration site, emphasis should be put into dividing the foot into regions of interest that are analysed individually. This has not been done before to the best knowledge of the author. This particularly applies to areas where lower temperatures resulted in ulceration. The author's analysis shows that it may be possible to predict the onset of foot ulceration using a variety of different methods. However, at the same time three limitations combine to drastically lower the likelihood of this being a realistic method.

The current gold standard  $2.2^{\circ}\text{C}$  temperature asymmetry threshold was assessed using the collected data and found to be not suitable for the task of predicting the onset of foot ulceration when using a measurement interval of four weeks only. Using instead the threshold of  $33.5^{\circ}\text{C} < T_{ROI}$  increased the sensitivity and specificity that the gold standard produces. This sensitivity and specificity can be further increased using a combination of  $33.5^{\circ}\text{C} < T_{ROI}$  and  $0 < T_{asymmetry}$ .

## 7.2 Contribution to Knowledge

The contributions to knowledge that arose from this project are:

1. Journal and conference contributions
2. Hardware
3. Software
4. Methodologies
5. Analysis

These are detailed in the following sections 7.2.1 to 7.2.5.

### 7.2.1 Journal and conference contributions

The author has successfully published a paper on the 'Segmentation of Infrared Images Using Stereophotogrammetry' [45] and contributed to two papers that emerged from this project (see appendix D for certificates of contribution):



1. A medical thermal imaging device for the prevention of diabetic foot ulceration - Physiological measurement (2017)
2. Thermal symmetry of healthy feet: a precursor to a thermal study of diabetic feet prior to skin breakdown - IOPScience (2016)

as well as 5 conferences in the field of thermography and medicine:

1. European Association of Thermography, Madrid, September 2015
2. Medical Infrared Thermography, London, April 2016
3. European Association of Thermography, Gdansk, July 2016
4. European Association of Thermography, Zakopane, April 2017
5. European Congress on Computational Methods in Applied Sciences and Engineering, Porto, October 2017
6. Congress on Thermology in Medicine: Clinical Thermometry and Thermal Imaging, London 2018

### **7.2.2 Hardware**

Over the course of this project a device which integrates a thermal camera, an embedded computing device and a 3D stereophotogrammetric camera system and touch screen technology in a novel and up-to then non-existing manner was developed. It enabled research into the mass adoption of thermal imaging devices in a clinical setting and the necessary steps into mass analysis of thermal images. Moreover, it allowed to assess the necessity of a thermal imaging device in the context of diabetic foot ulceration. Although this has already been done in the past it has not been done on this project's scale.

The second generation device is currently being developed on the basis of a Raspberry Pi to overcome the shortcomings of the first generation. It features two visual cameras and a FLIR Lepton sensor for data acquisition. This allows it to have a smaller footprint than the first device and enables novel integrated 3D thermal imaging.

### 7.2.3 Software

The software aspect of this project is split into two parts: The device software and algorithmic developments.

The device software is comprised of a new specialised user guidance concept with error resilience and various hardware technologies integrated into a single unit. Another innovation is the user interface for the device which was tailored to the clinical protocol's demands such as the order of taking images and saving the data into a structure that combines all images into one file. New insights into user guidance, error resilience (e.g. automated recovery, detection of improbable device states and imaging results), and the integration of the various hardware technologies into a single unit have been gained. The methodology of guiding the user through the process of entering basic patient information and identifiers and then going through a specific order of imaging was adapted from the clinical protocol.

The novel algorithmic developments that arose from this project are the use of barycentric coordinates in combination with cubic splines to allow smooth outlines to be warped into a standardised shape. This algorithm is aimed at image data in which segmentation is difficult to achieve using standard methods of computer vision. This algorithm was integrated into a tool set written by the author; capable of automatic data point extraction and processing. An error analysis was performed to assess its performance (2.5.4).

### 7.2.4 Methodologies

Several novel methods were developed for the various aspects of the project. These were:

1. Data collection protocol developed in collaboration with the project's clinical partners (section 3.1)
2. Contributions to FLIR Lepton calibration procedure in collaboration with the NPL (chapter 6)
3. Analysis methodologies (section 3.3 and chapter 5)
4. Method for simultaneous drawing of boundaries by volunteers (section 3.3)

Each of these methodologies is novel and unique to the best of the author's knowledge.

### 7.2.5 Analysis

The analysis of the data was completed using previously unexplored input parameters in an attempt to find a suitable classifier or combination of classifiers for the prediction of foot ulceration. These include the use of the temperature variance, difference over time and the difference to a baseline. Moreover, the data was separated into 12 regions of interest that were analysed individually.

It was found that the currently accepted threshold ( $abs(T_{asymmetry}) < 2.2^{\circ}\text{C}$ ) is correct but is not a good qualifier on its own. Using combinations of input parameter thresholds showed an improvement in the results. In particular the use of  $T_{ROI} > 33.5^{\circ}\text{C}$  and  $abs(T_{changeovertime}) < 2^{\circ}\text{C}$  increased the sensitivity and specificity with respect to the gold standard by 11% and 14%, respectively.

## 7.3 Achievement of Aim

The aim of predicting diabetic foot ulceration with the aid of infrared imaging has been reached partially. The analysed methods and parameters hint towards it being possible to predict ulceration. The results are, however, not conclusive due to two reasons. The first reason is the relatively long period of time between measurements of about four weeks, where other researchers have measured daily and claim a lead time of approximately 30 days when three consecutive measurements are outside the accepted tolerance [12]. The second reason is the amount of data points available for analysis. 12 ulcers were registered during the second trial period (11 usable) and a total of 52 data points could be extracted. This number is too low to allow conclusive results. The hypothesis can therefore neither be accepted nor rejected.

## 7.4 Future Work

The data presented in this project shows the potential for predicting ulceration with increased accuracy and the creation of complex devices with low-cost hardware. In light of the results from this project, a new company was founded by some of the project collaborators with the aim of developing a low-cost home monitoring system which users can use daily. The results presented in this thesis are informing the development process of this device. A second device for clinical use, complementary to the home use system and close to the one presented in this work is also under

development. Both the home use and clinical device are likely to open up the possibility for exploring the methods and techniques presented in this work in more depth than is currently possible.

# Appendix A

## Appendix - Data plots

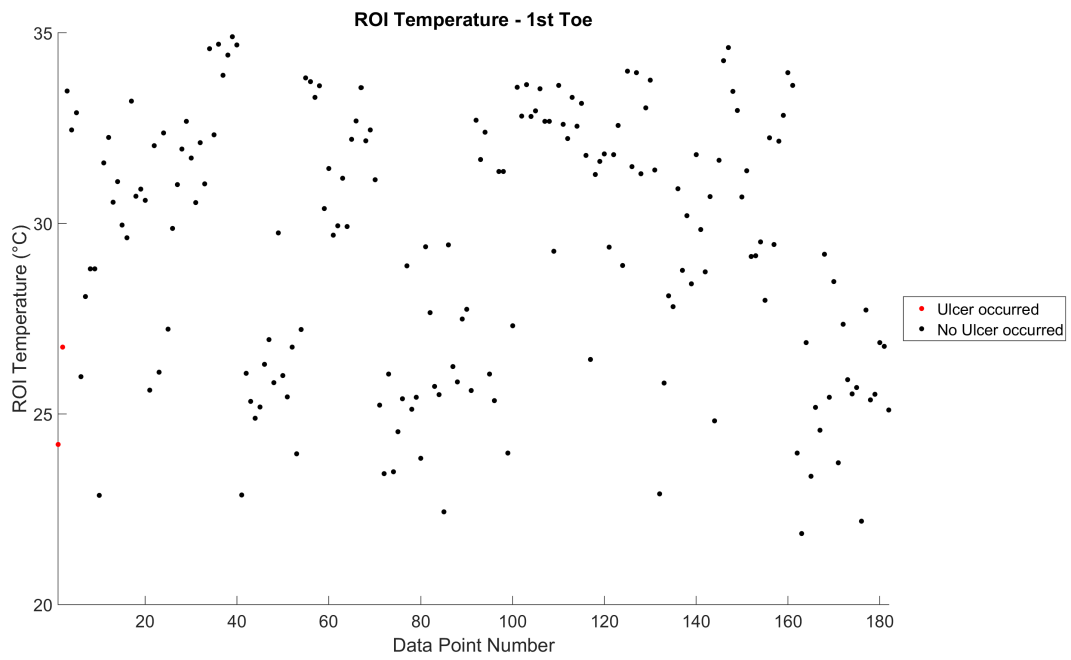
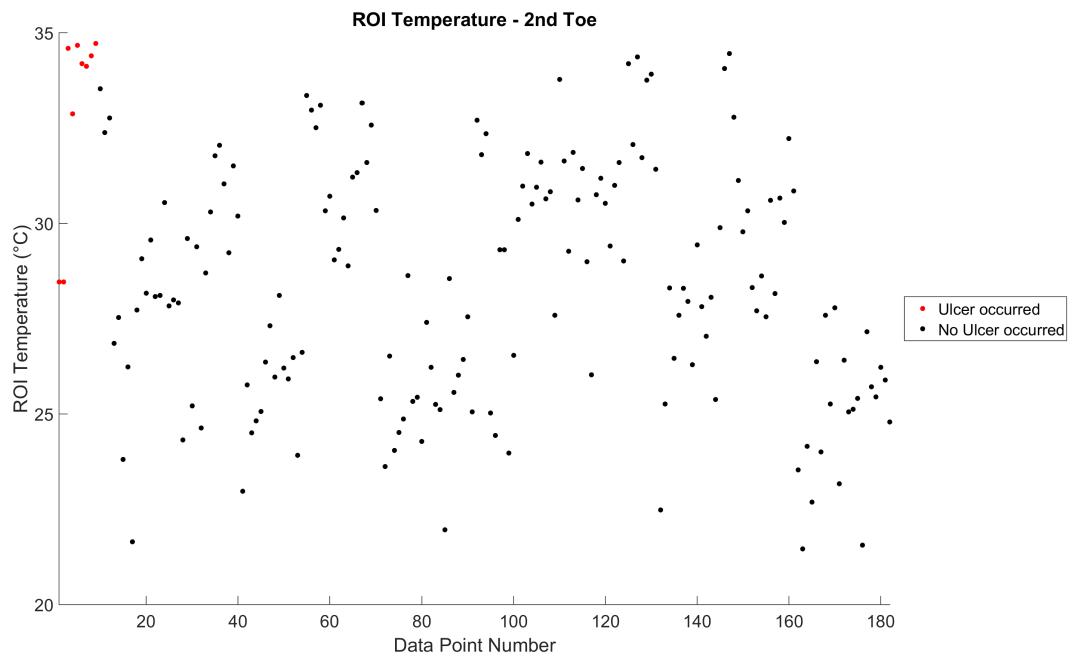
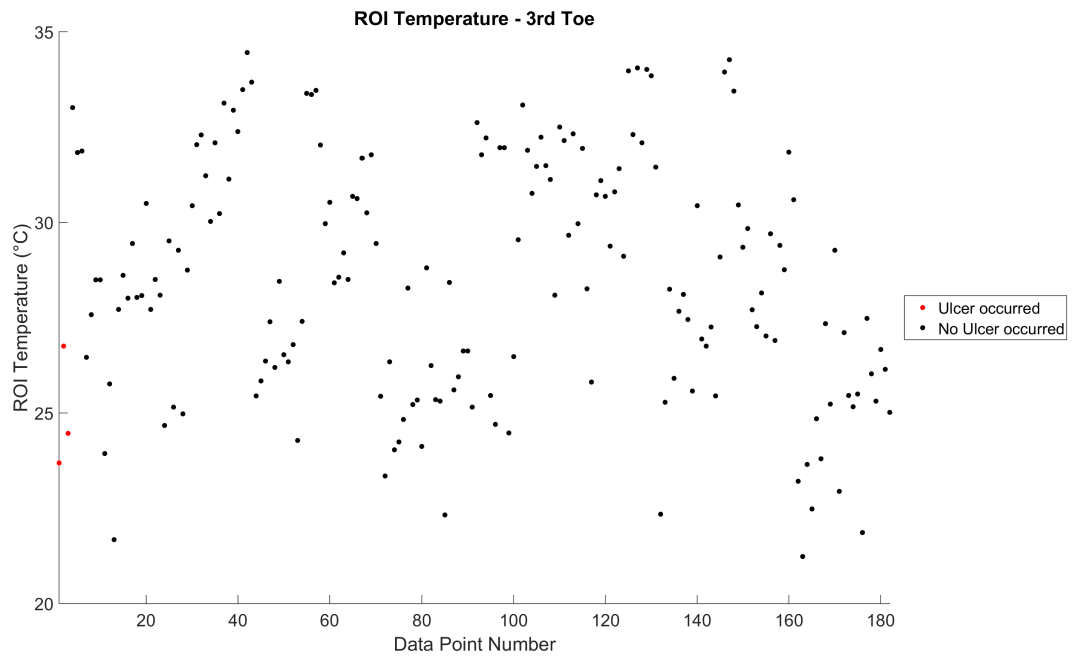
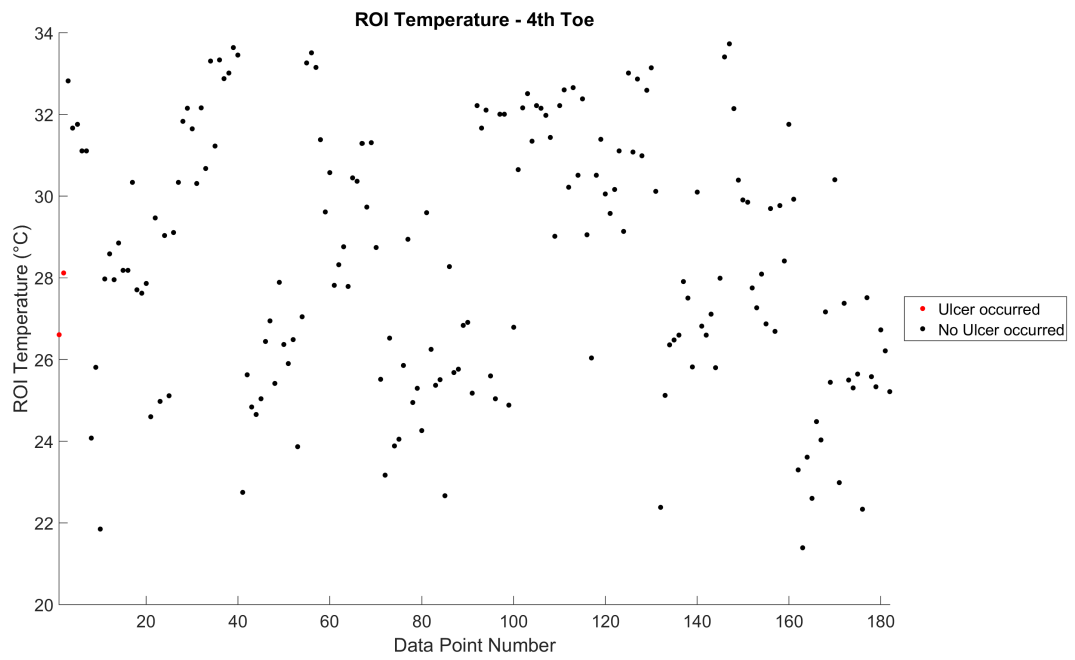
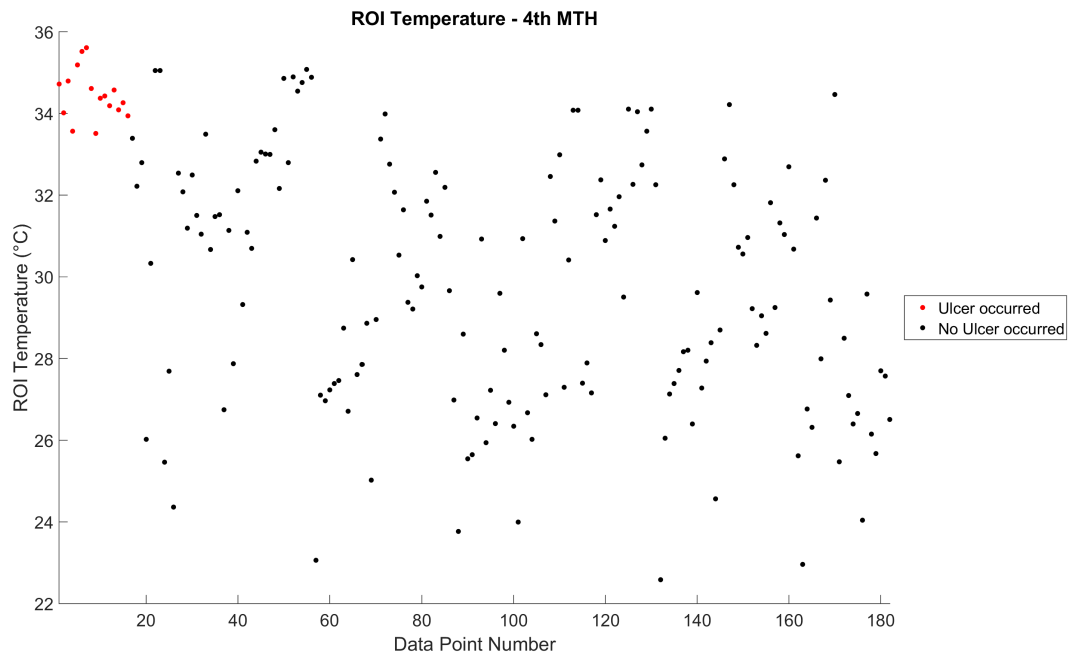
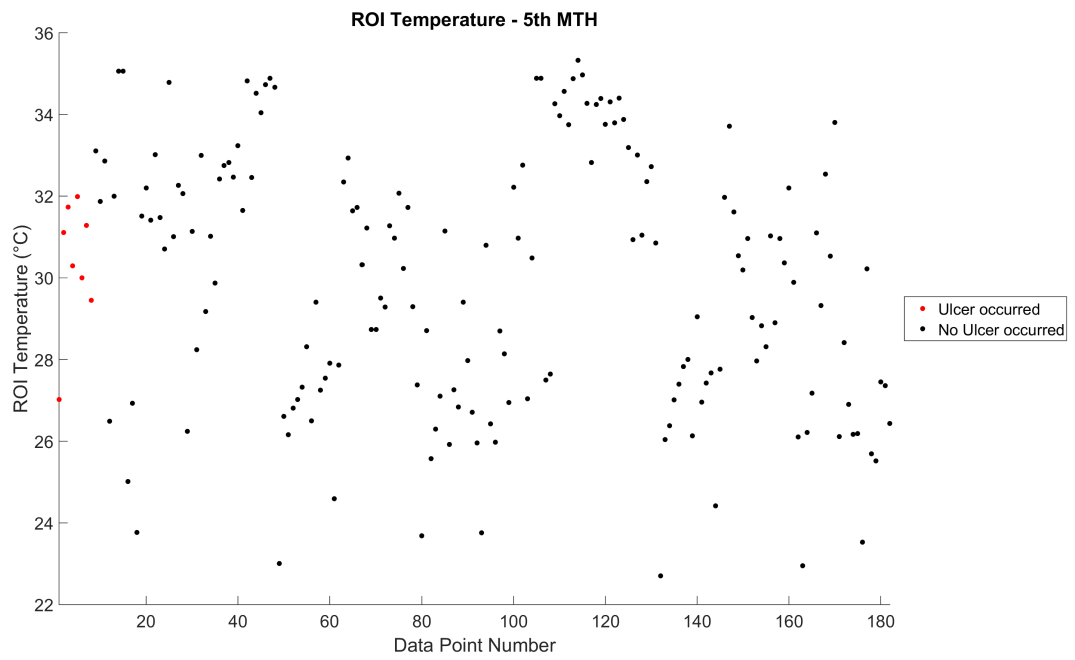
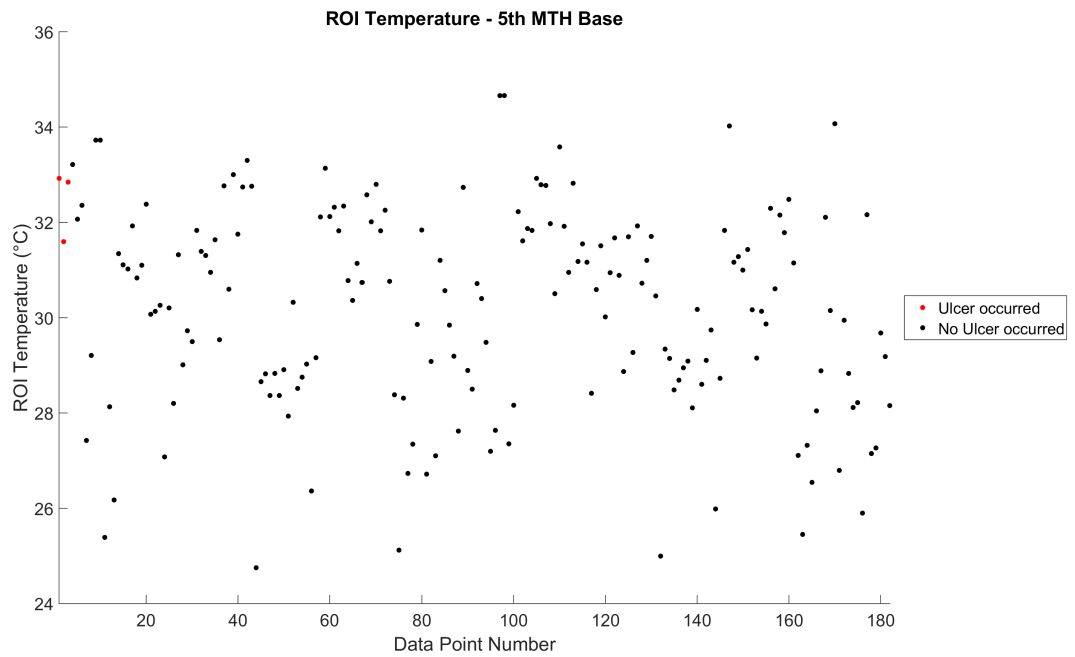


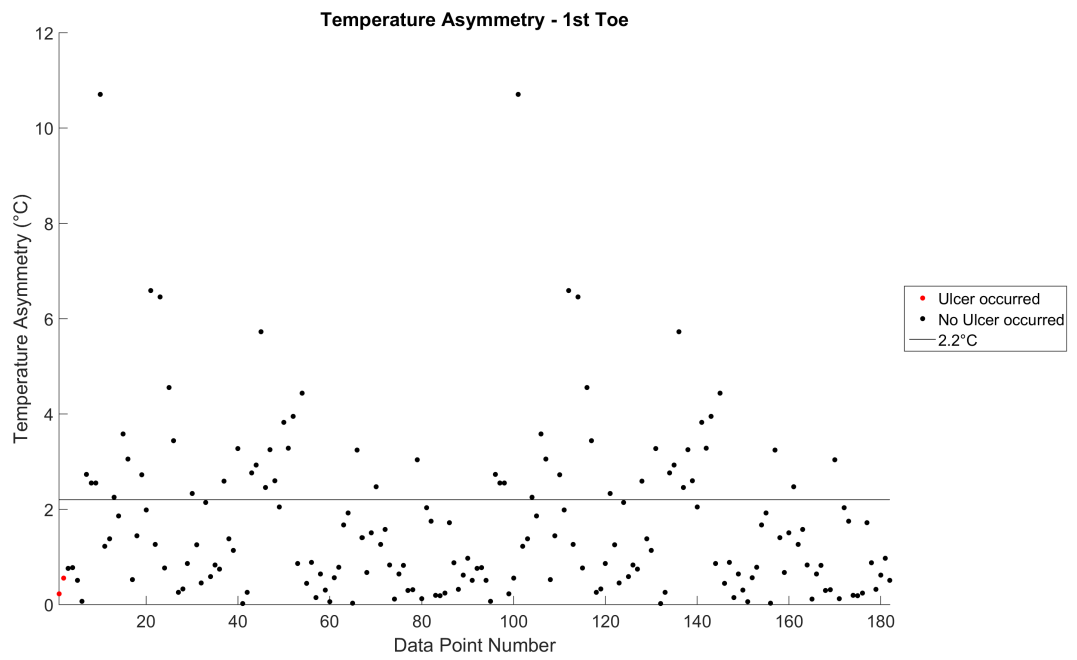
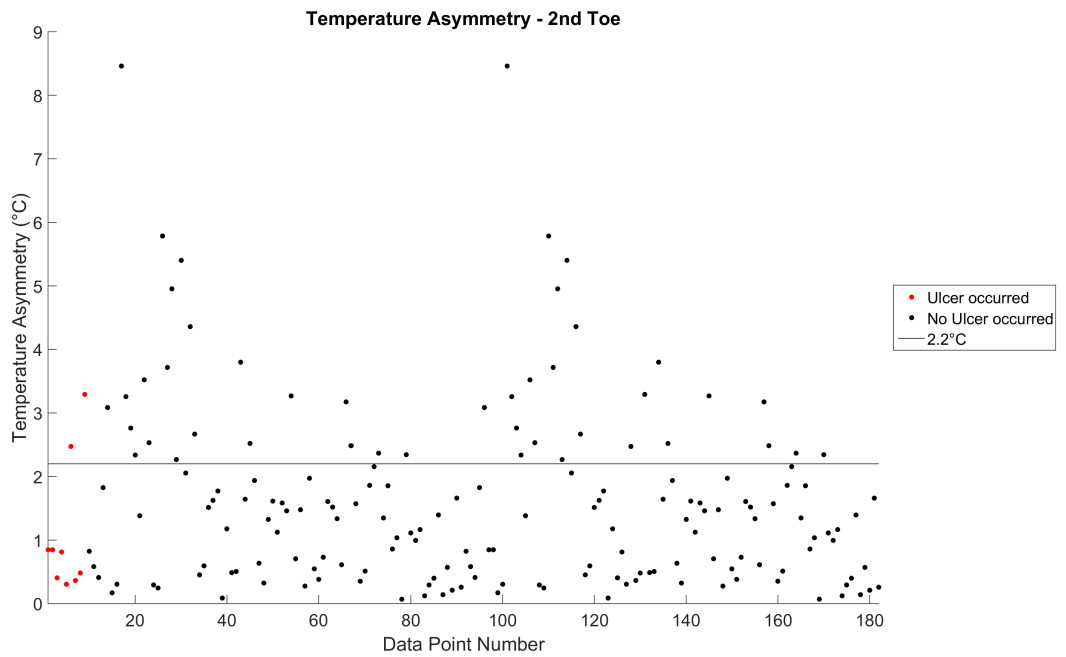
FIGURE A.1: ROI temperature plot - 1<sup>st</sup> Toe

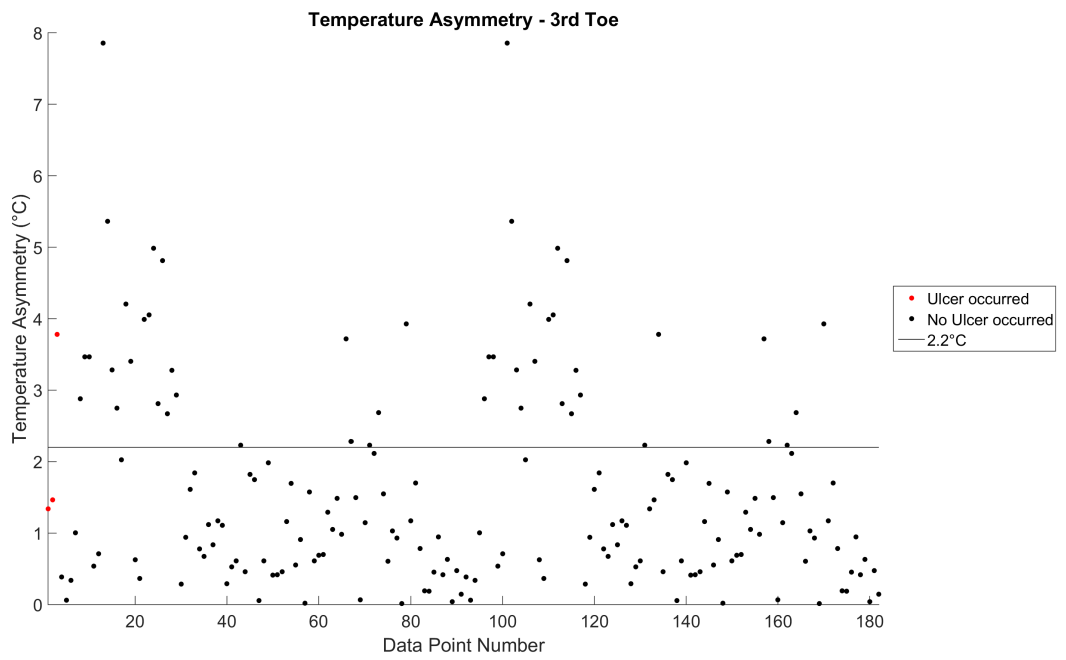
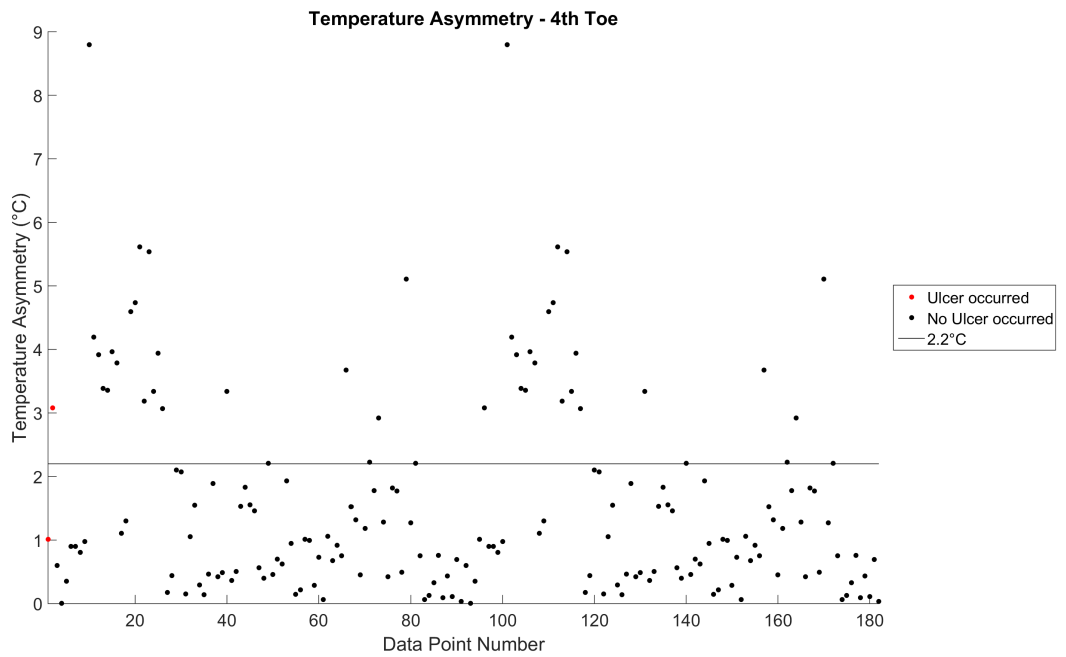
FIGURE A.2: ROI temperature plot - 2<sup>nd</sup> ToeFIGURE A.3: ROI temperature plot - 3<sup>rd</sup> Toe

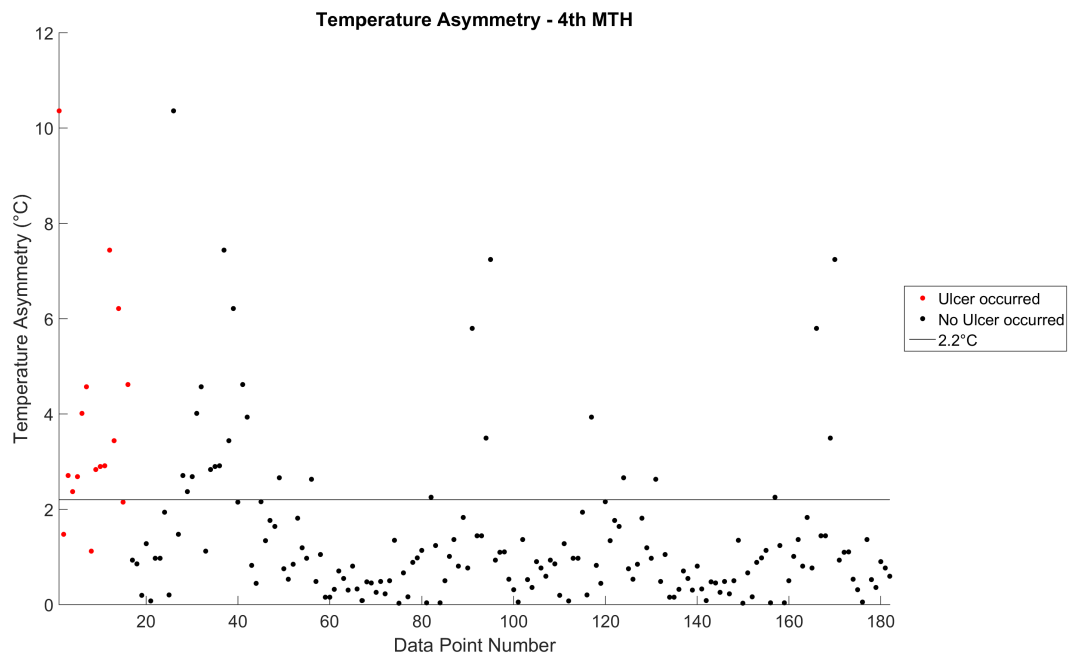
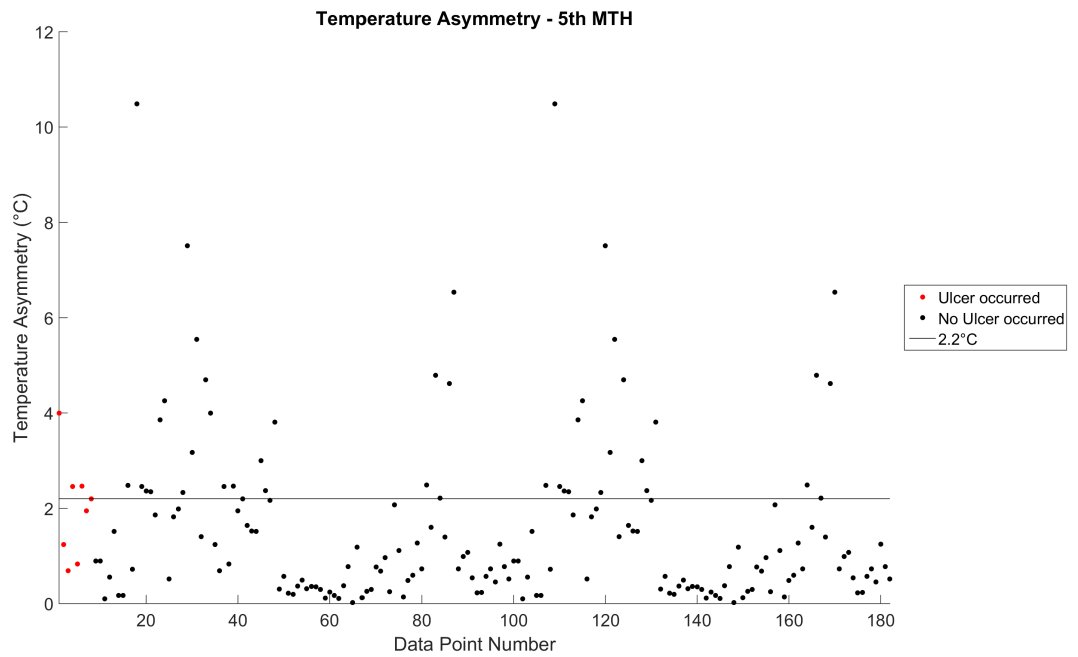
FIGURE A.4: ROI temperature plot - 4<sup>th</sup> ToeFIGURE A.5: ROI temperature plot - 4<sup>th</sup> MTH

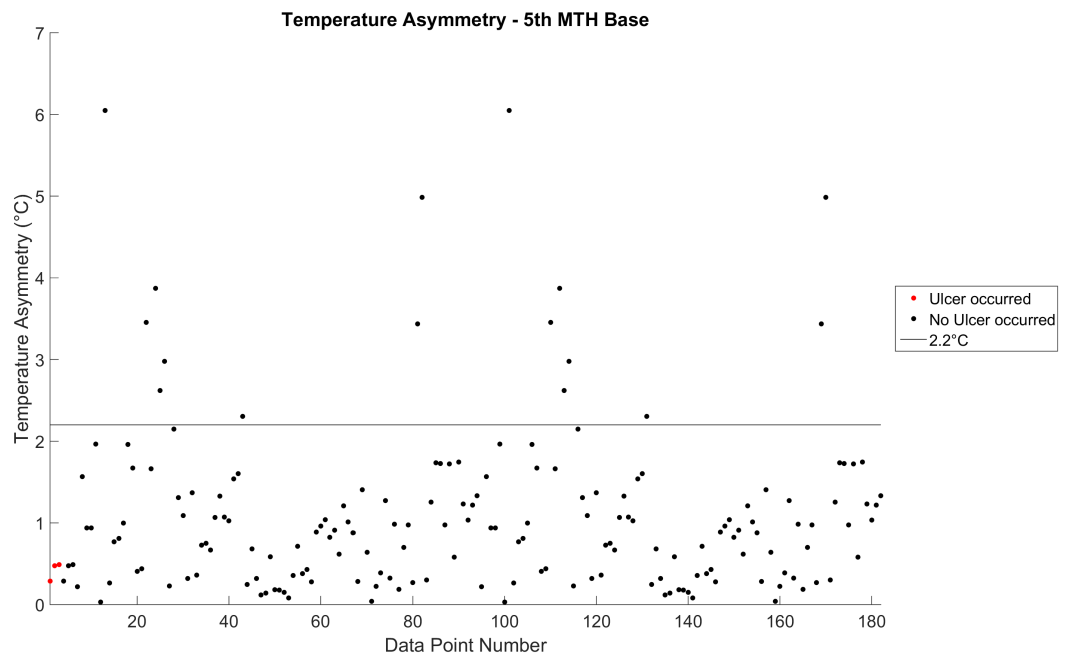
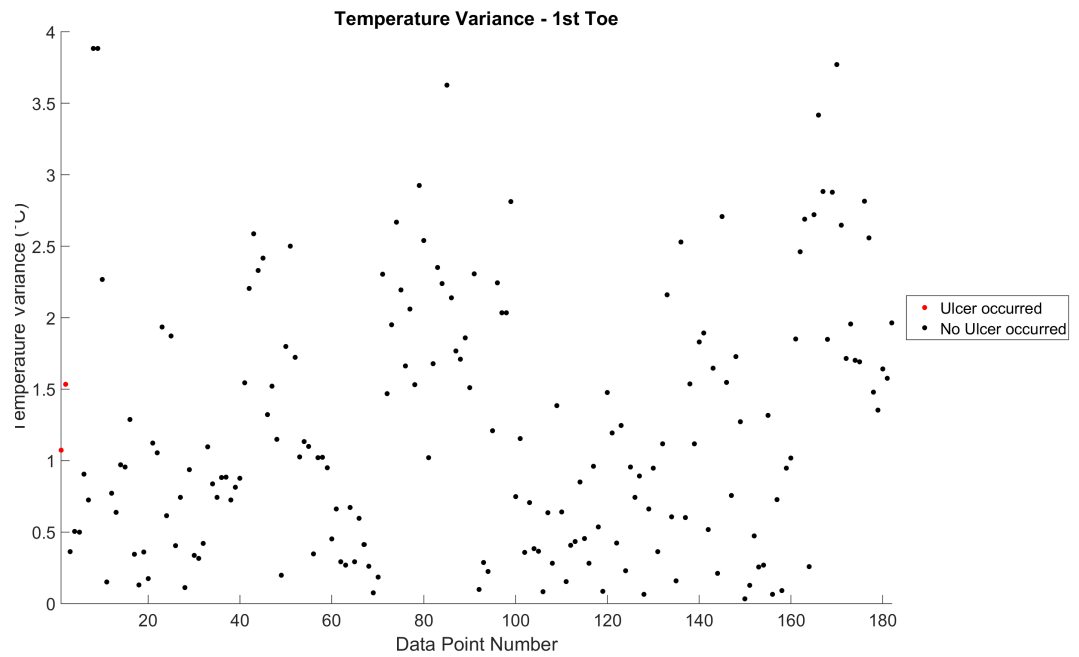
FIGURE A.6: ROI temperature plot - 5<sup>th</sup> MTHFIGURE A.7: ROI temperature plot - 5<sup>th</sup> MTH Base

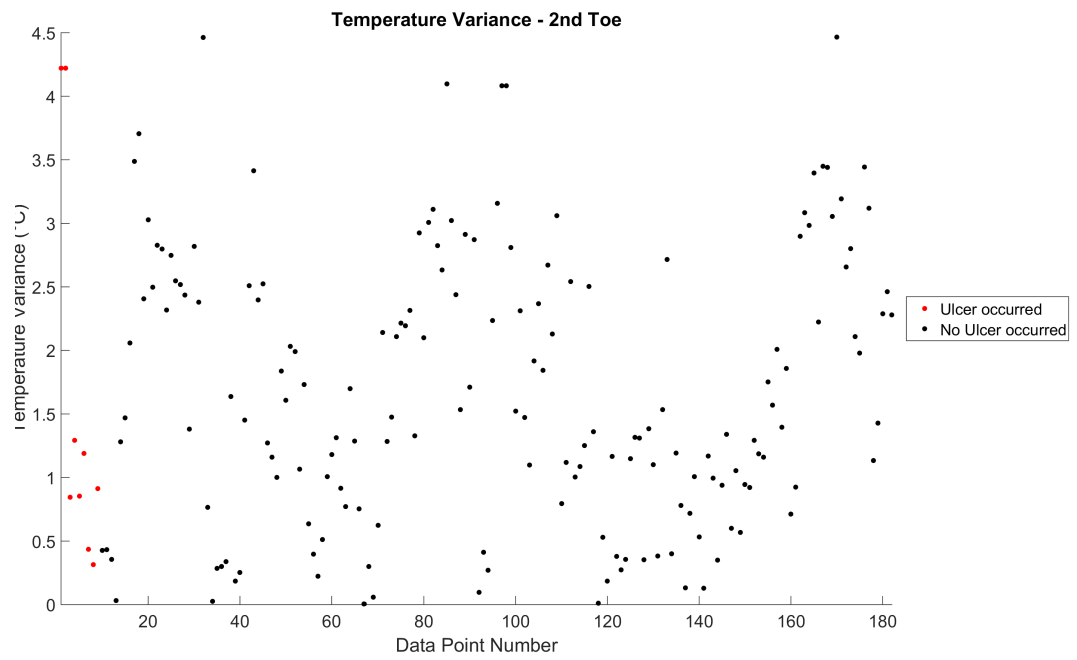
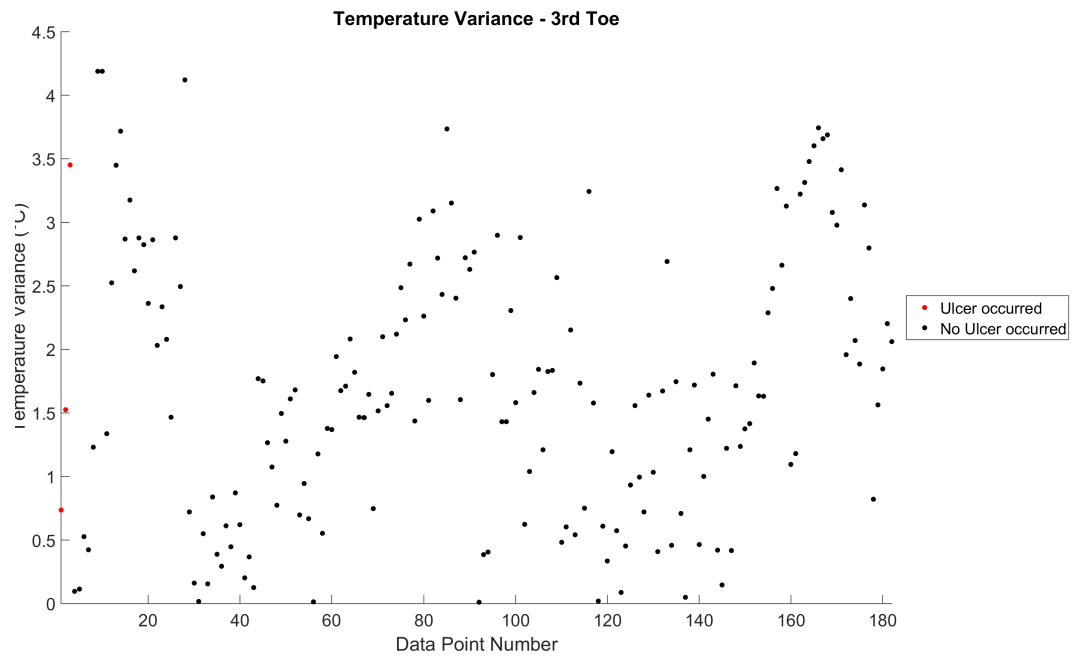


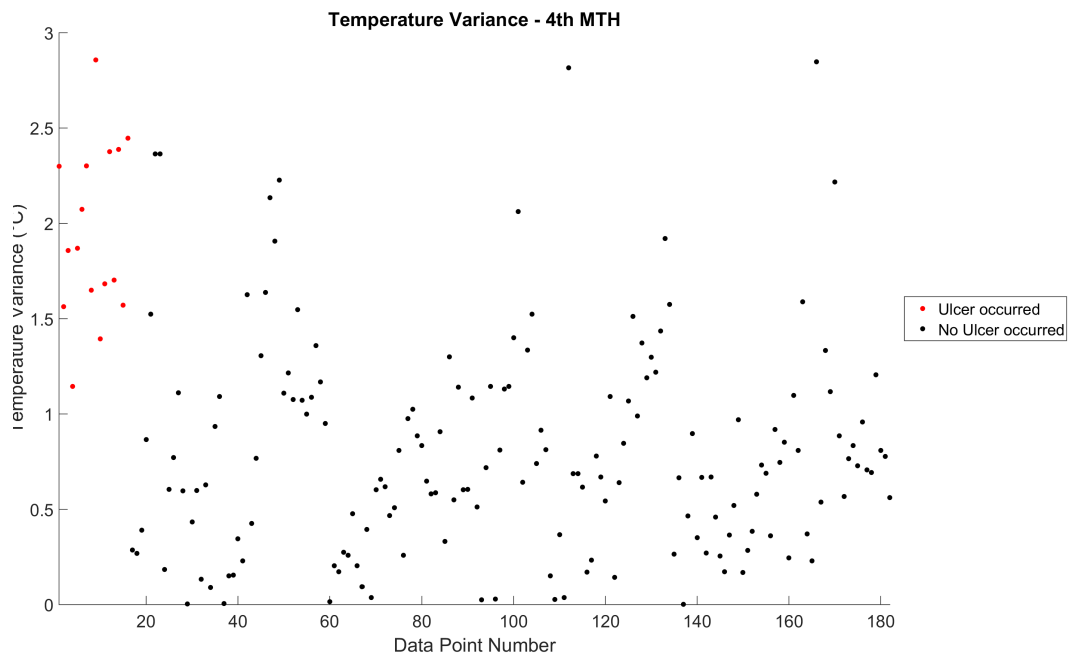
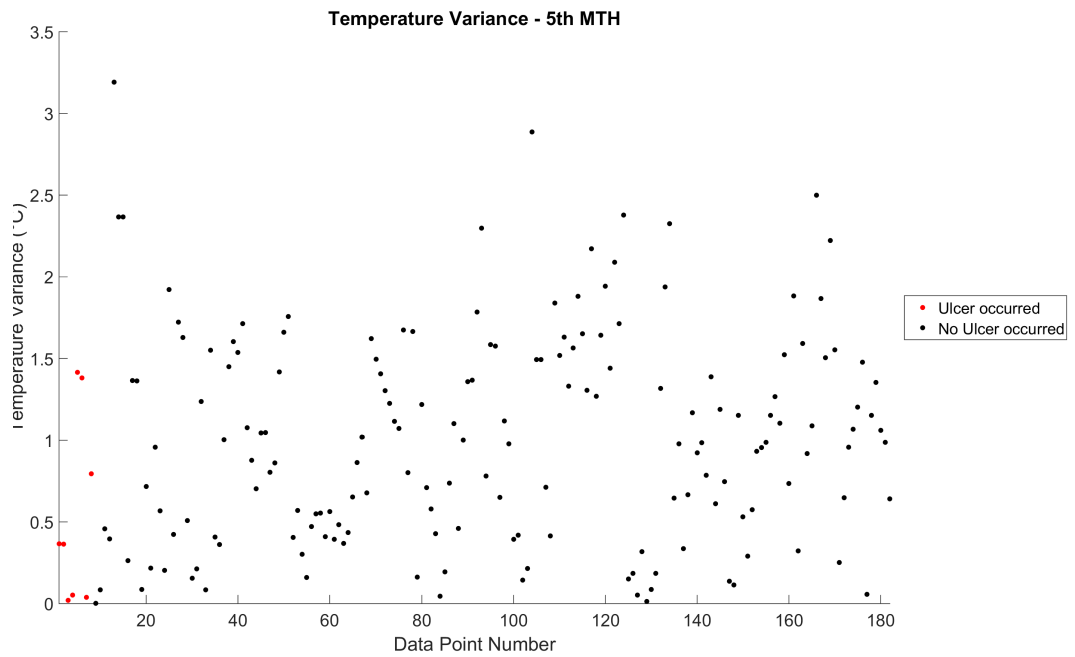
FIGURE A.8: Temperature asymmetry plot - 1<sup>st</sup> ToeFIGURE A.9: Temperature asymmetry plot - 2<sup>nd</sup> Toe

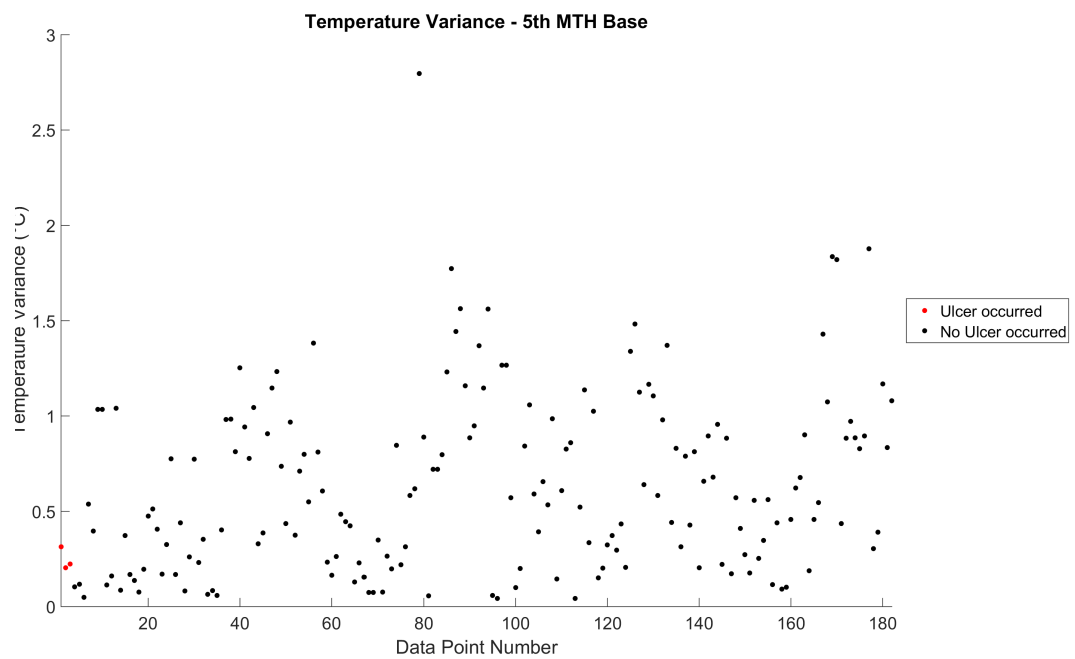
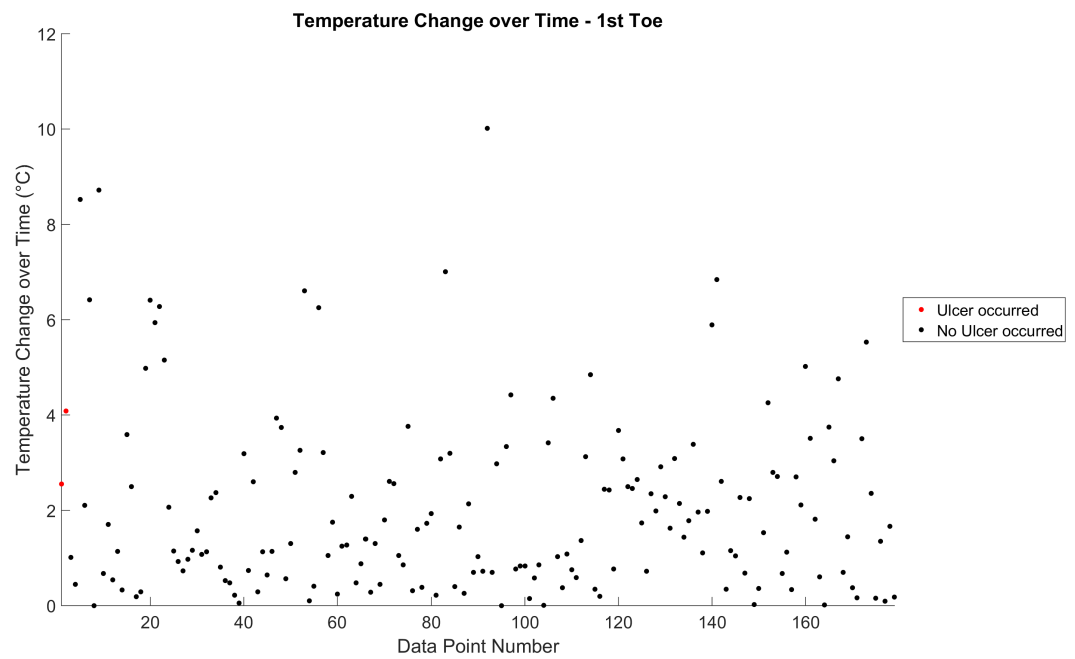
FIGURE A.10: Temperature asymmetry plot - 3<sup>rd</sup> ToeFIGURE A.11: Temperature asymmetry plot - 4<sup>th</sup> Toe

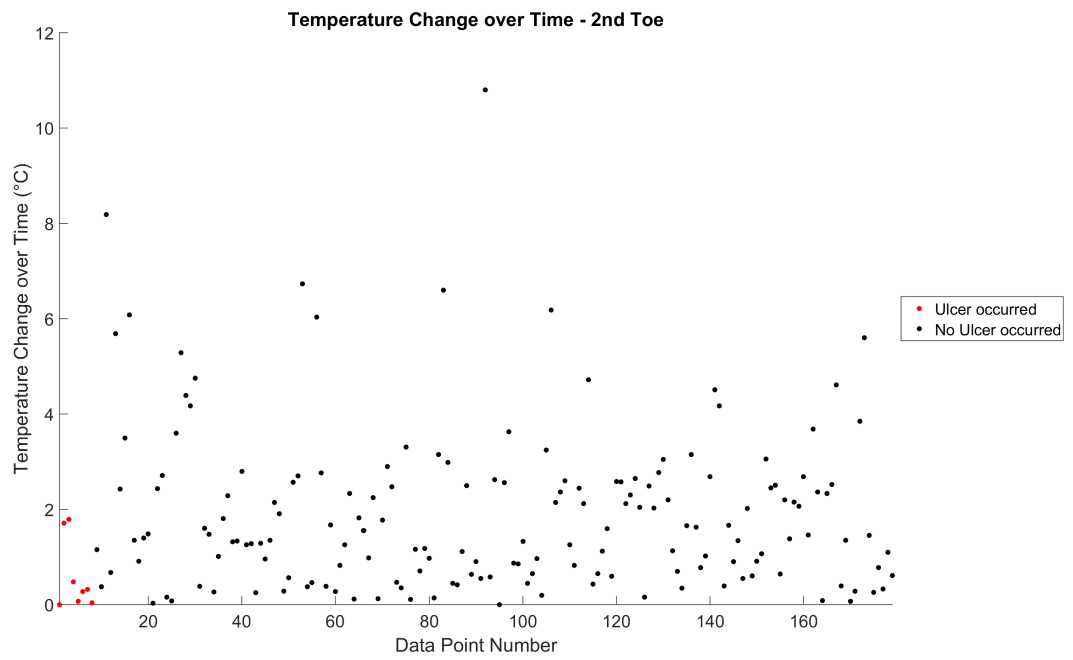
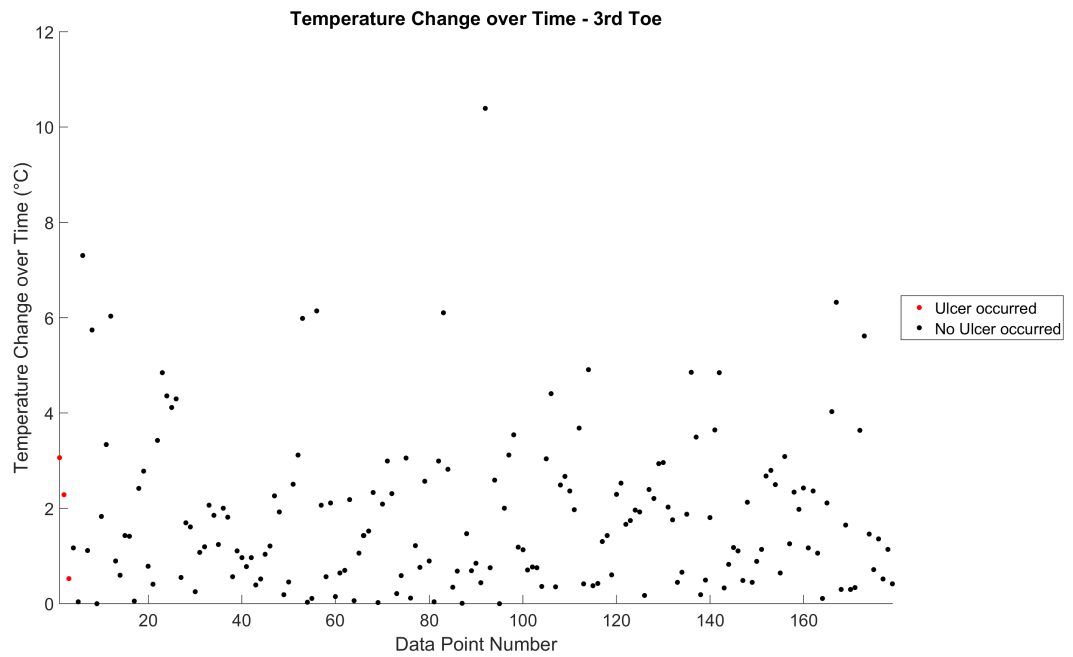
FIGURE A.12: Temperature asymmetry plot - 4<sup>th</sup> MTHFIGURE A.13: Temperature asymmetry plot - 5<sup>th</sup> MTH

FIGURE A.14: Temperature asymmetry plot - 5<sup>th</sup> MTH BaseFIGURE A.15: Temperature variance plot - 1<sup>st</sup> Toe

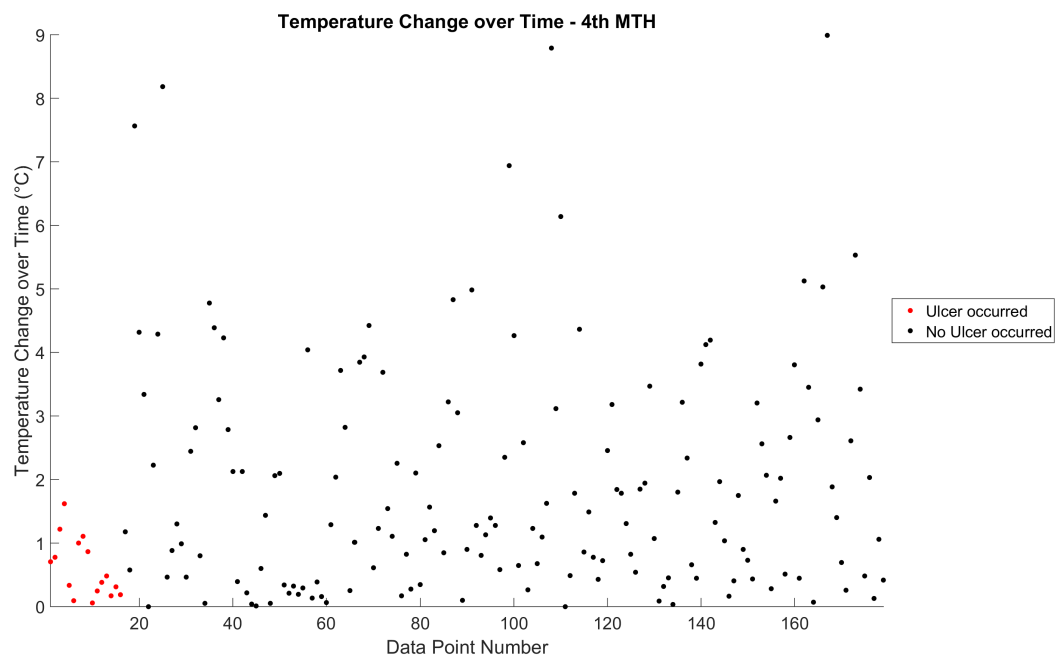
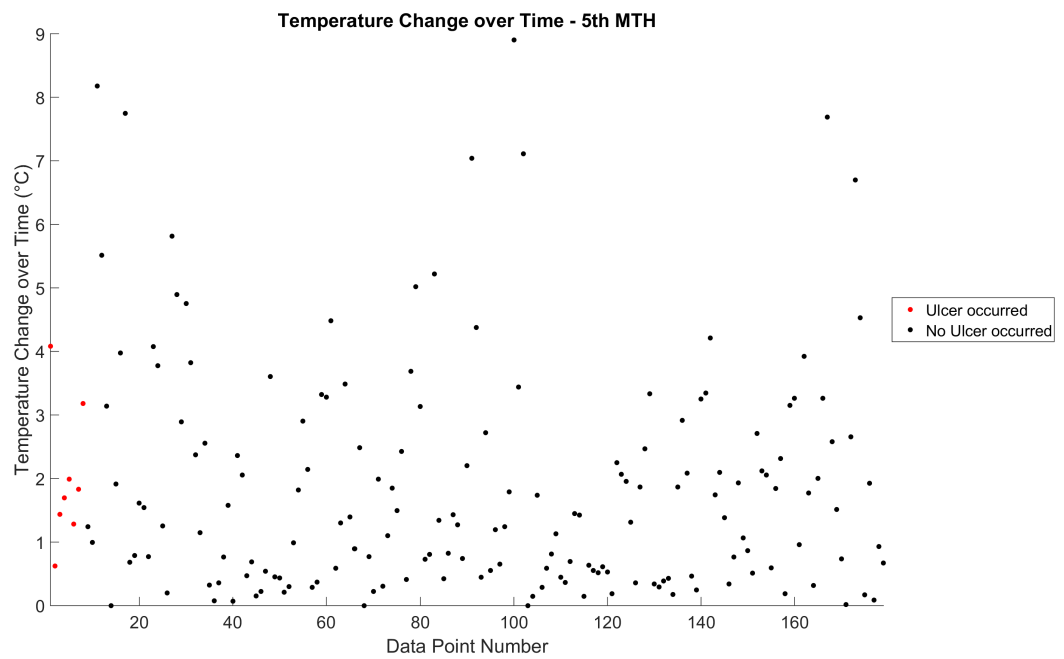
FIGURE A.16: Temperature variance plot - 2<sup>nd</sup> ToeFIGURE A.17: Temperature variance plot - 3<sup>rd</sup> Toe

FIGURE A.18: Temperature variance plot - 4<sup>th</sup> MTHFIGURE A.19: Temperature variance plot - 5<sup>th</sup> MTH

FIGURE A.20: Temperature variance plot - 5<sup>th</sup> MTH BaseFIGURE A.21: Temperature change over time - 1<sup>st</sup> Toe

FIGURE A.22: Temperature change over time - 2<sup>nd</sup> ToeFIGURE A.23: Temperature change over time - 3<sup>rd</sup> Toe



FIGURE A.24: Temperature change over time - 4<sup>th</sup> MTHFIGURE A.25: Temperature change over time - 5<sup>th</sup> MTH

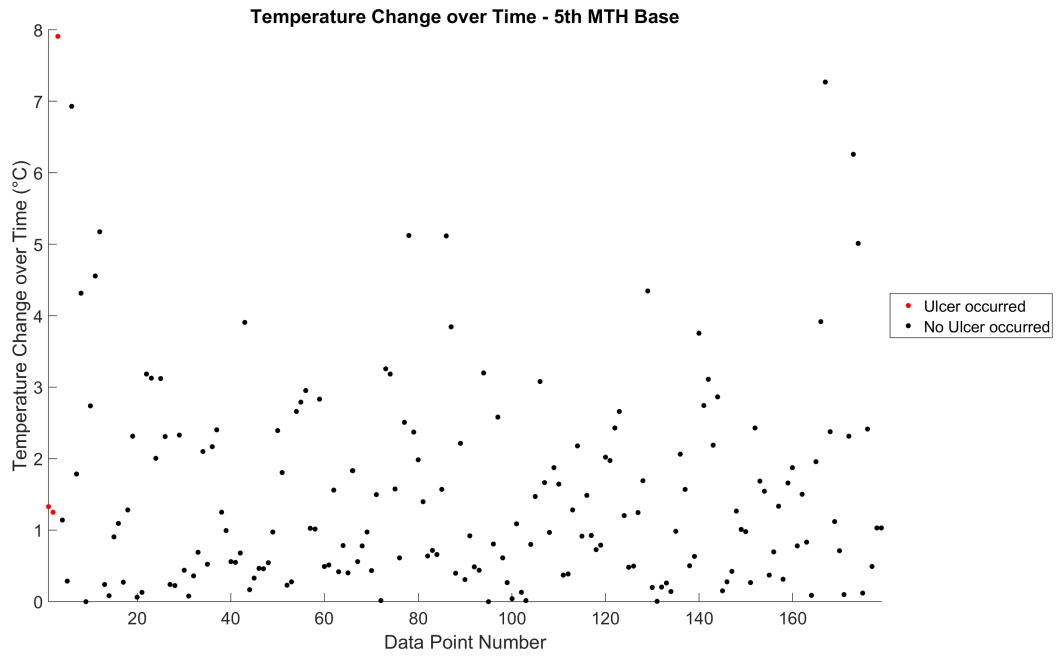


FIGURE A.26: Temperature change over time - 5<sup>th</sup> MTH Base

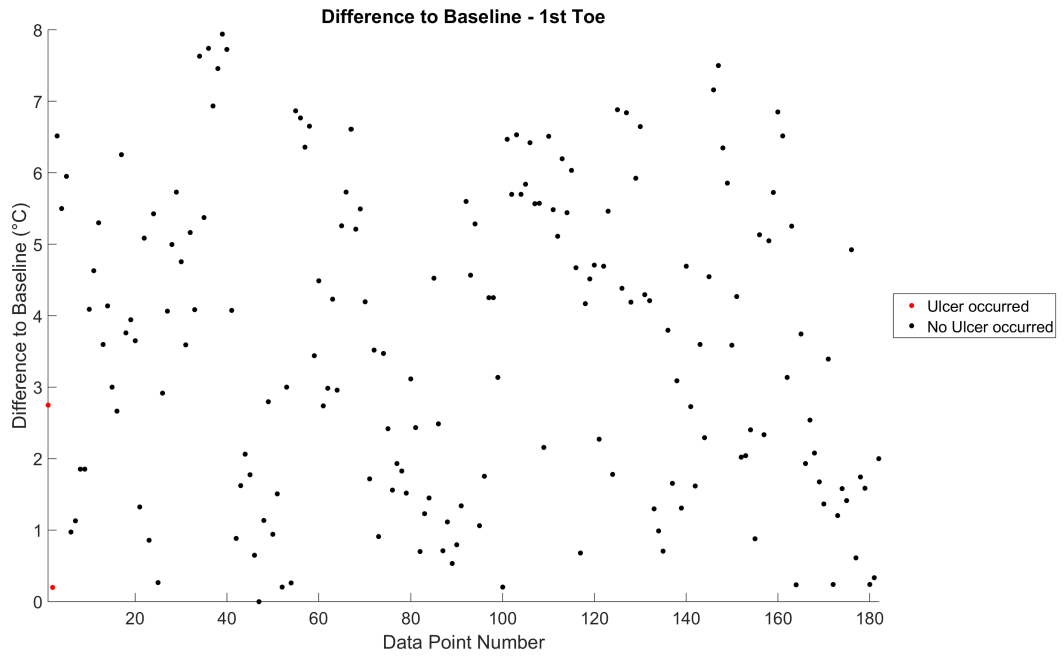
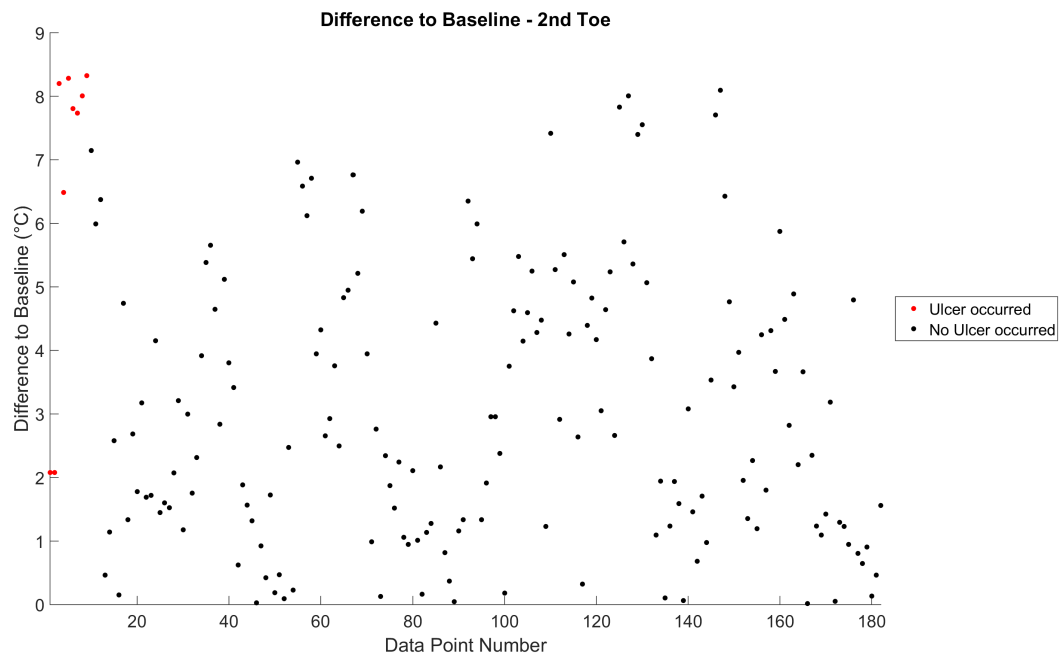
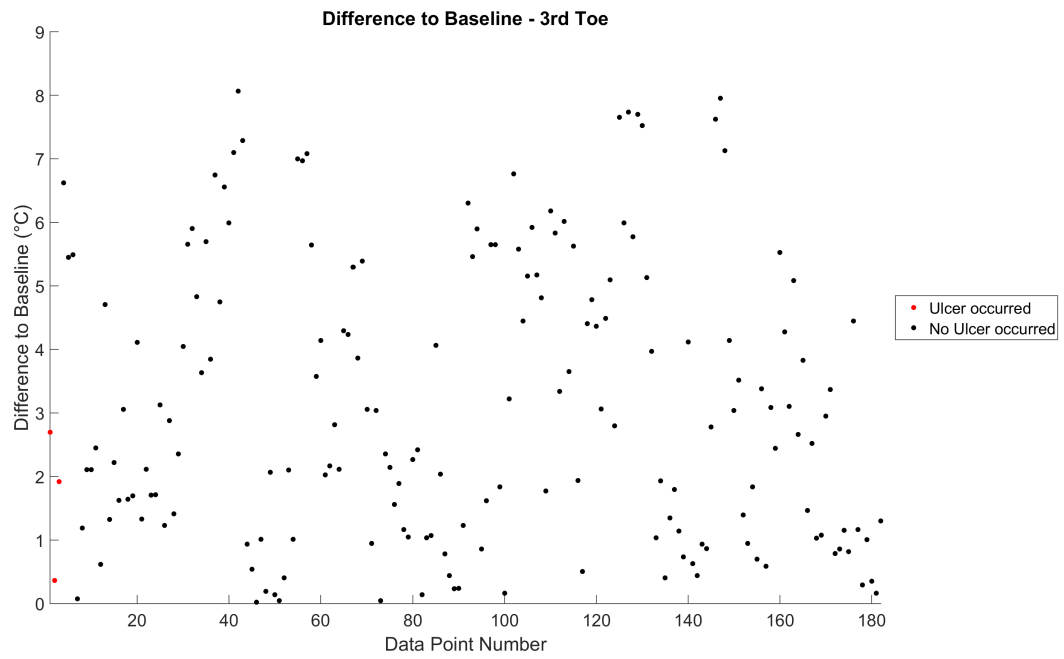
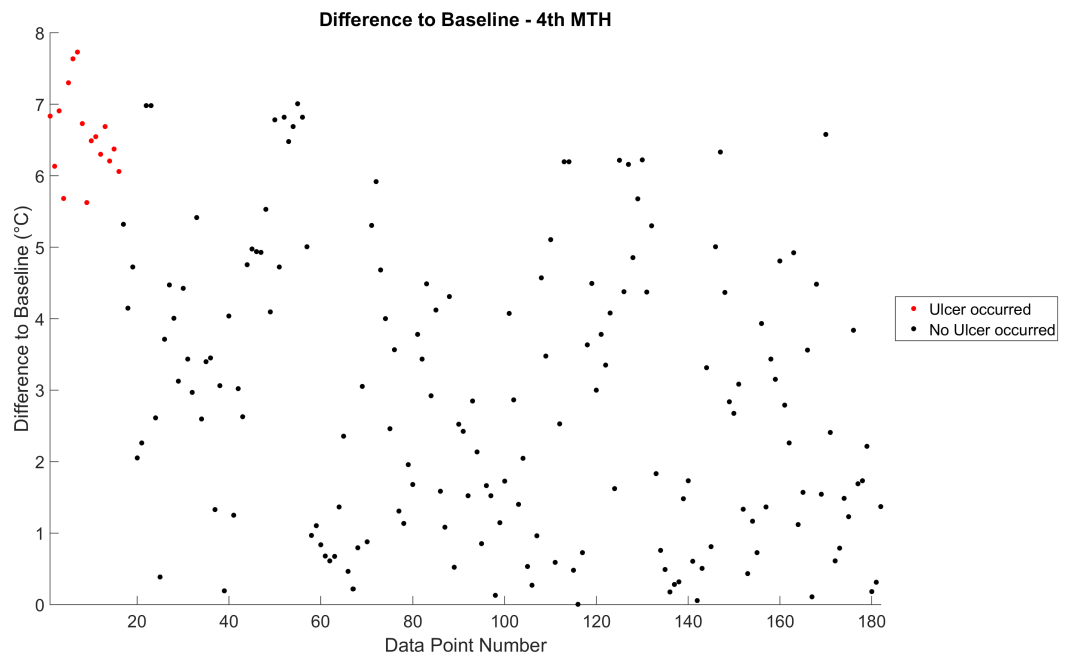
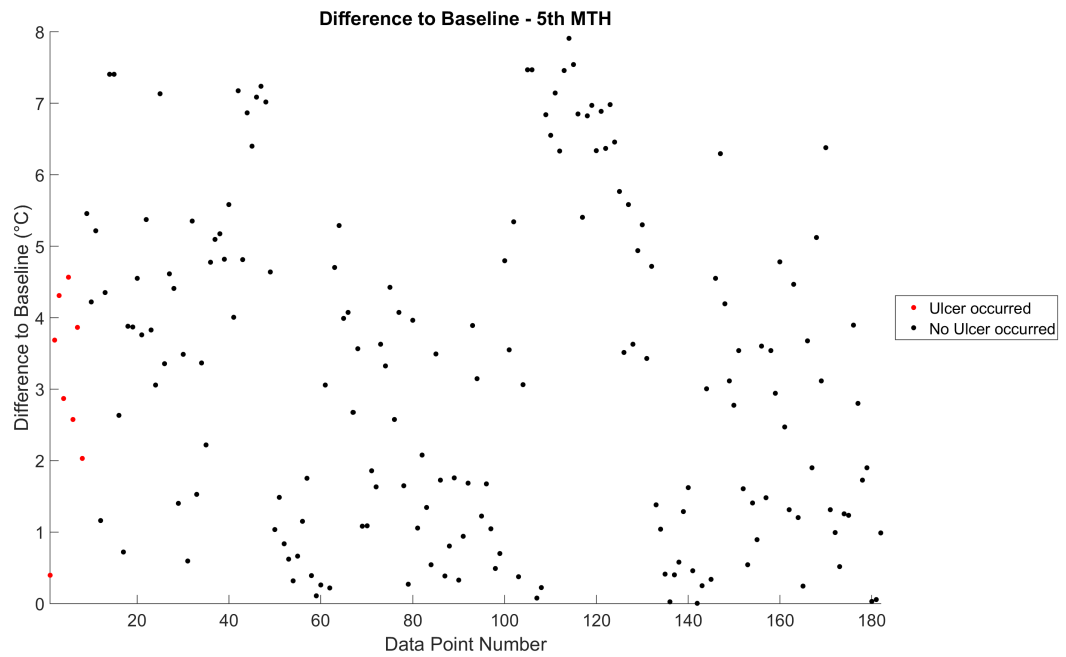
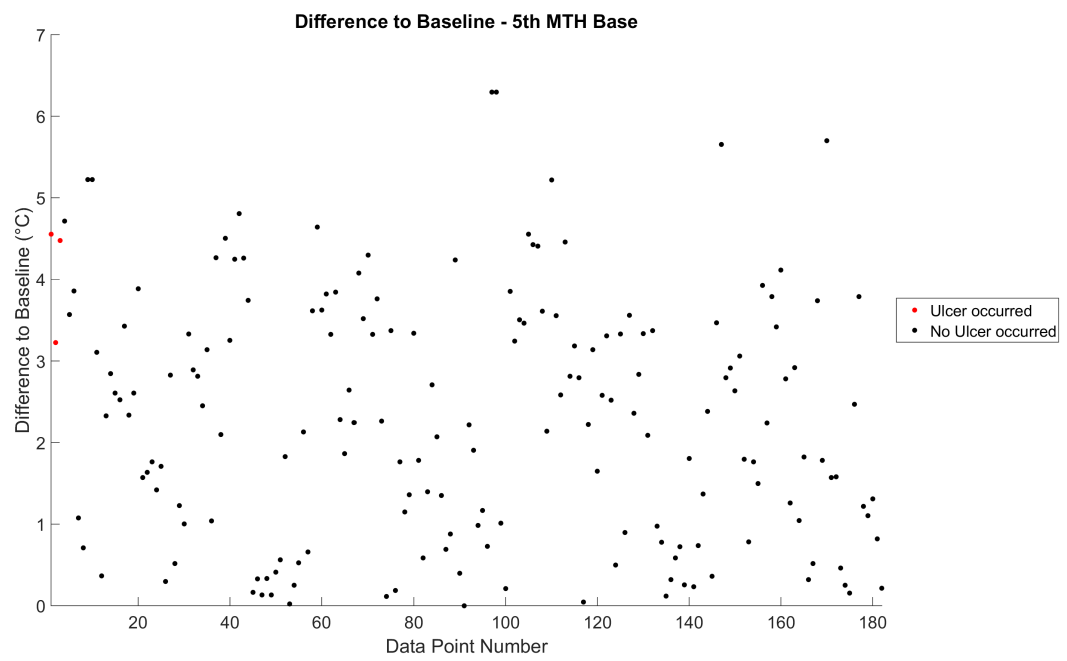


FIGURE A.27: Difference to baseline - 1<sup>st</sup> Toe

FIGURE A.28: Difference to baseline - 2<sup>nd</sup> ToeFIGURE A.29: Difference to baseline - 3<sup>rd</sup> Toe

FIGURE A.30: Difference to baseline - 4<sup>th</sup> MTHFIGURE A.31: Difference to baseline - 5<sup>th</sup> MTH

FIGURE A.32: Difference to baseline - 5<sup>th</sup> MTH Base

## Appendix B

# Appendix - Receiver Operator Curves using one Dimension

FIGURE B.1: ROI temperature ROC - 1<sup>st</sup> Toe

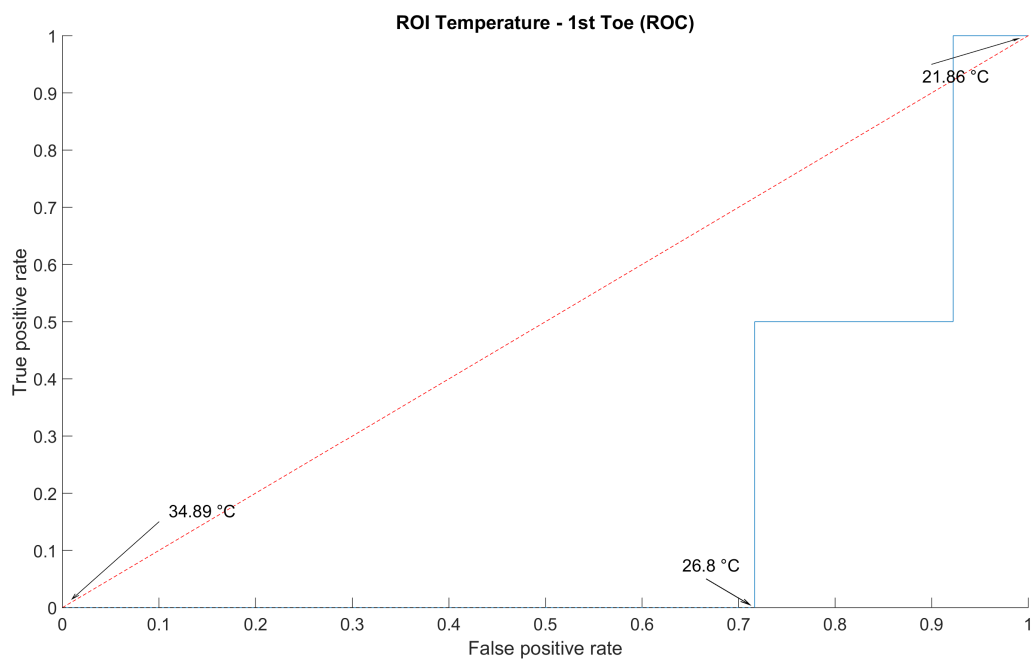


FIGURE B.2: ROI temperature ROC - 2<sup>nd</sup> Toe

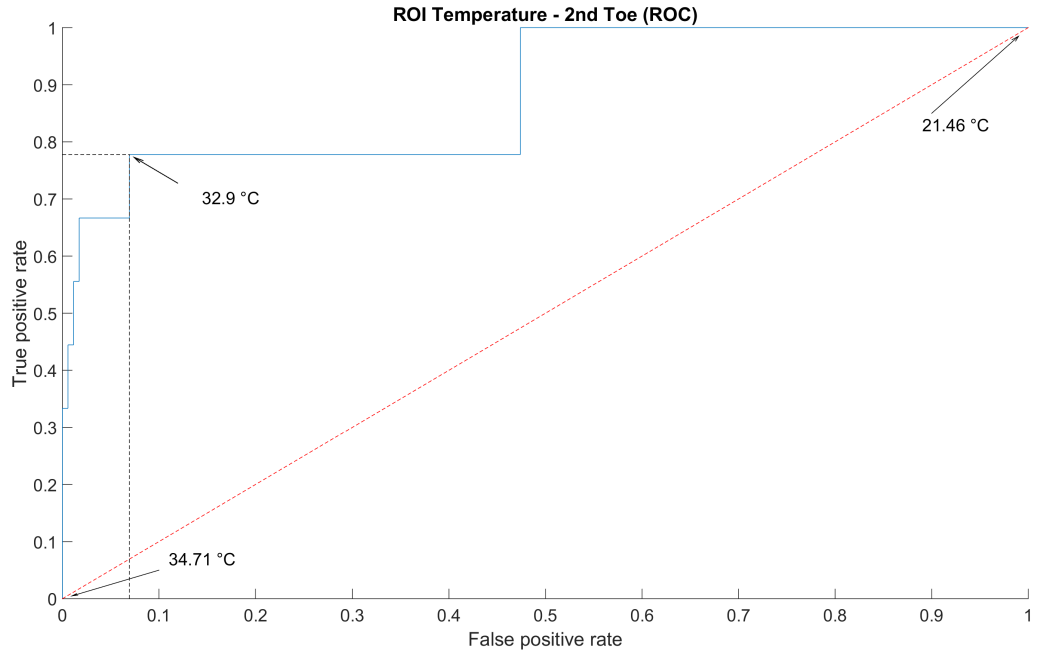


FIGURE B.3: ROI temperature ROC - 3<sup>rd</sup> Toe

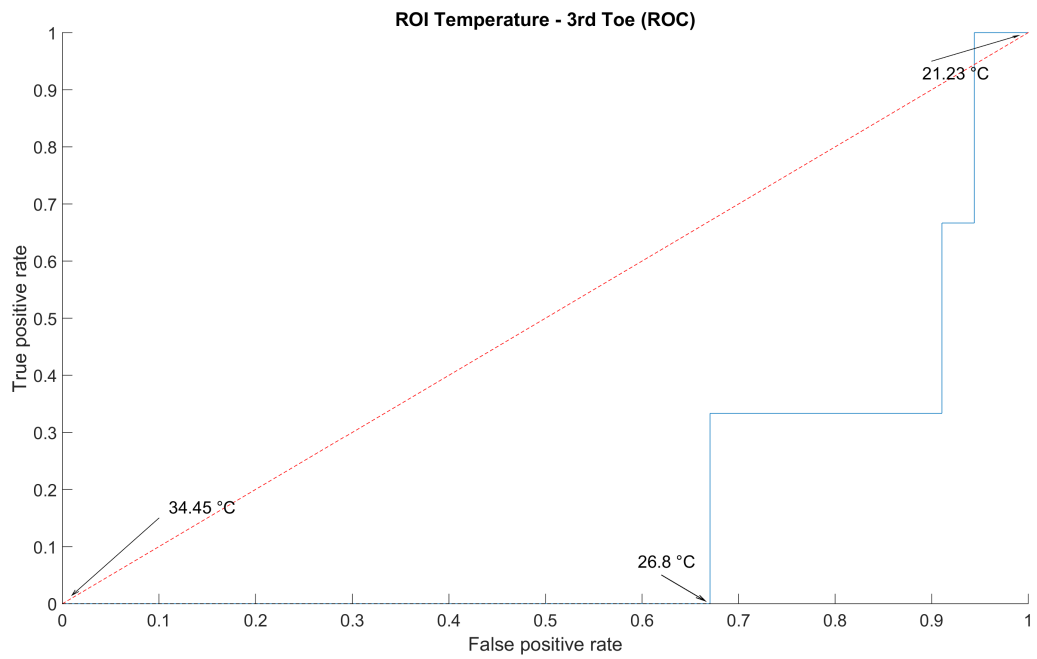


FIGURE B.4: ROI temperature ROC - 4<sup>th</sup> Toe

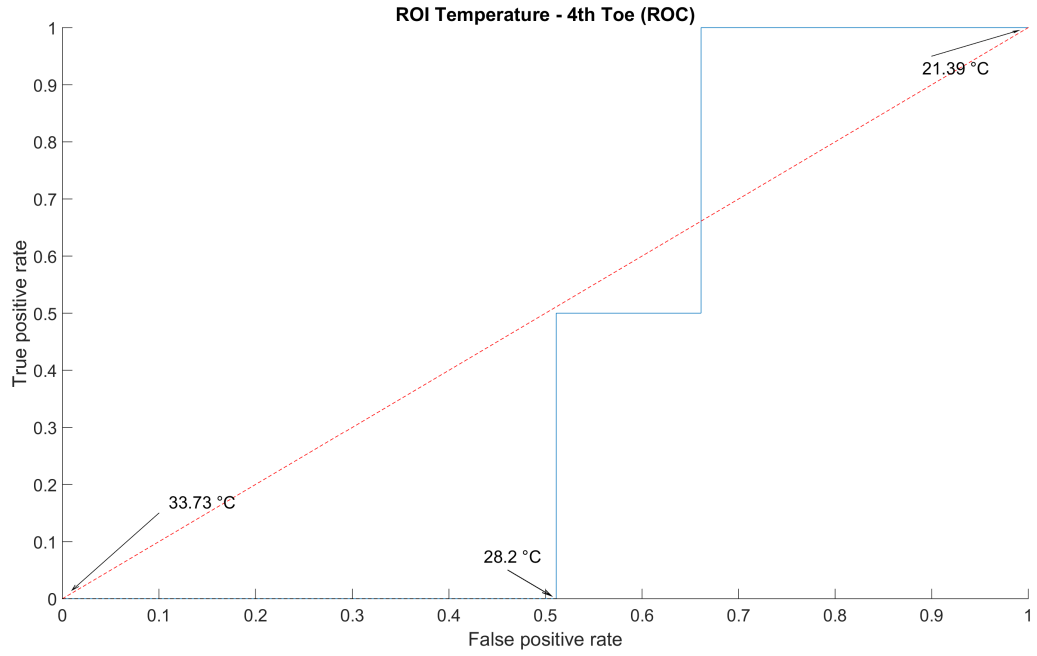


FIGURE B.5: ROI temperature ROC - 4<sup>th</sup> MTH

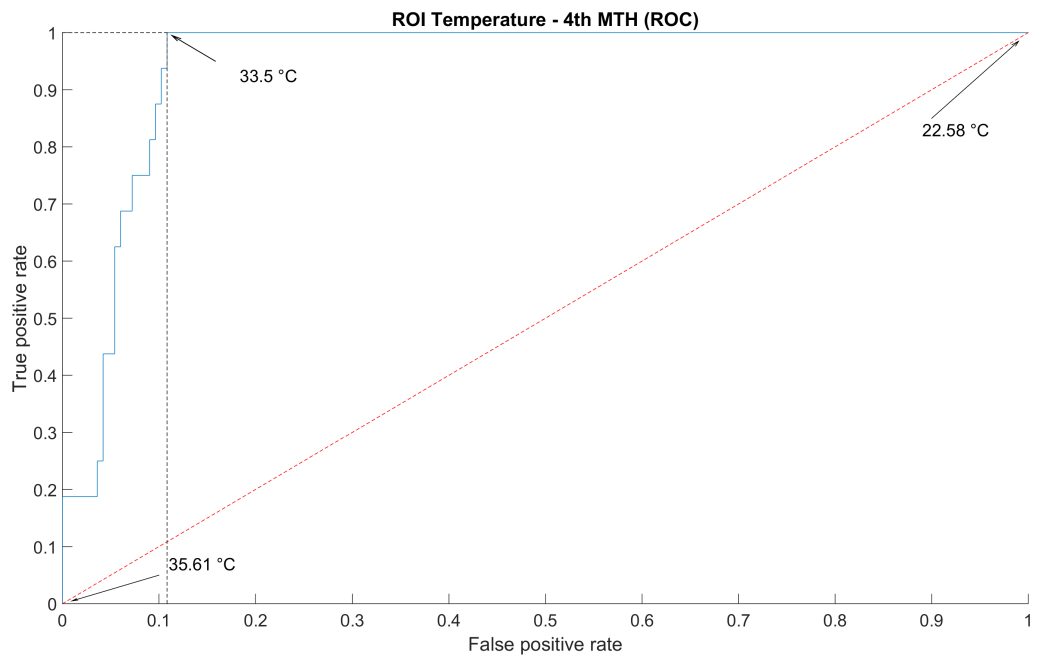




FIGURE B.6: ROI temperature ROC - 5<sup>th</sup> MTH

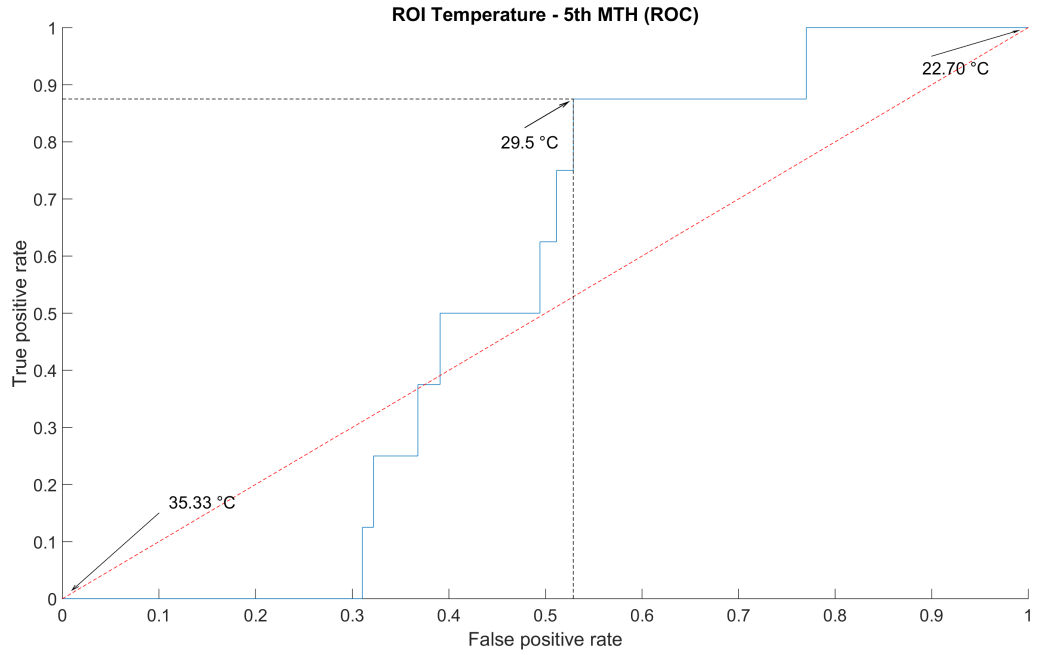


FIGURE B.7: ROI temperature ROC - 5<sup>th</sup> MTH Base

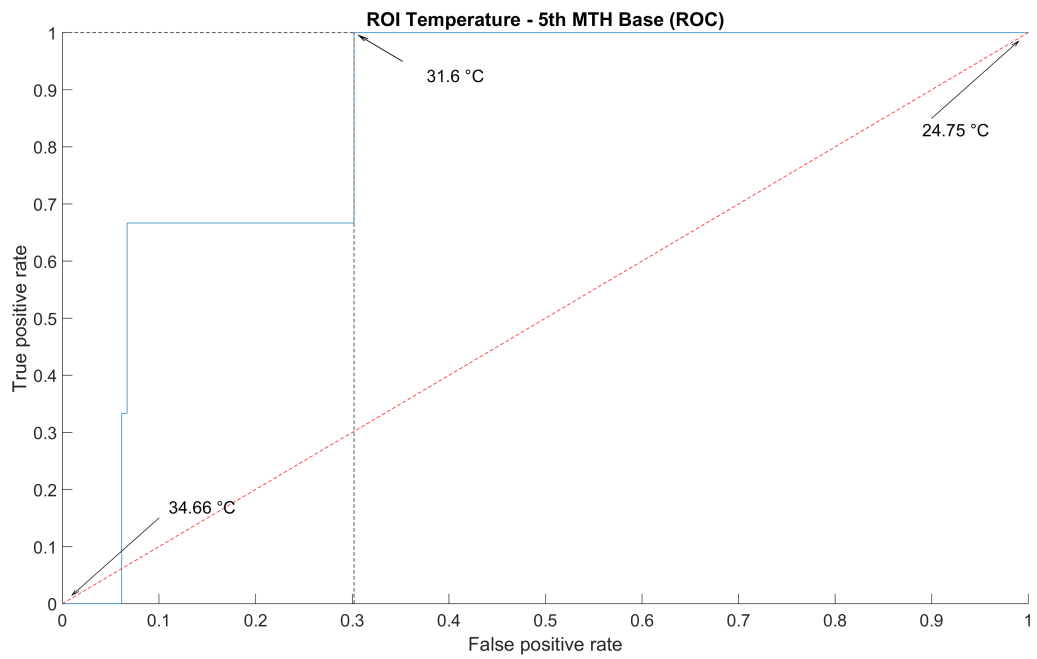


FIGURE B.8: Temperature asymmetry ROC - 1<sup>st</sup> Toe

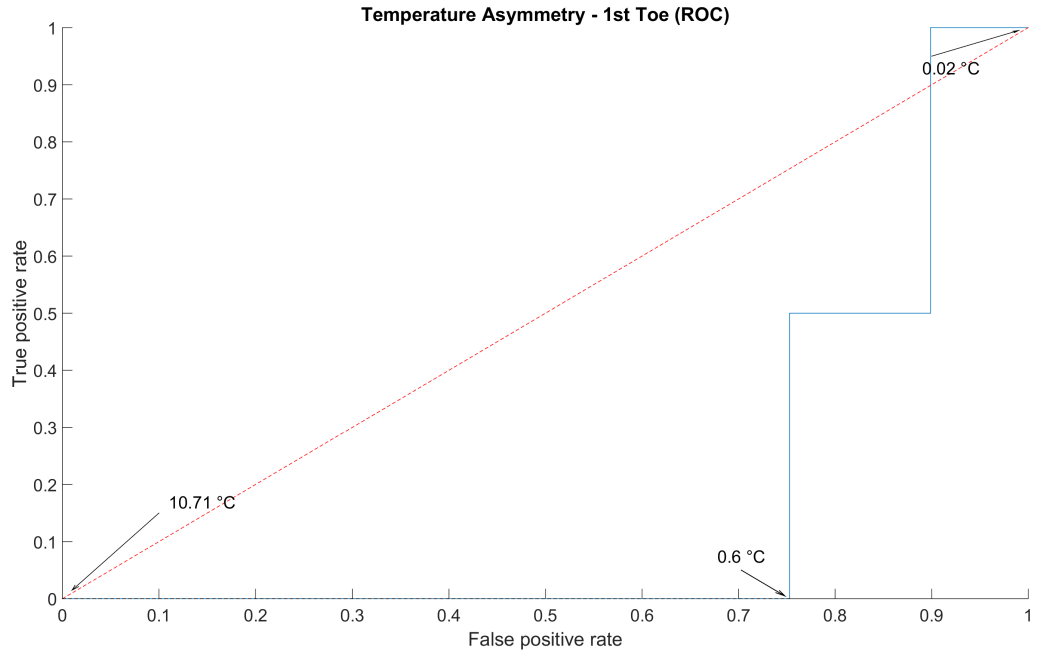


FIGURE B.9: Temperature asymmetry, ROC - 2<sup>nd</sup> Toe

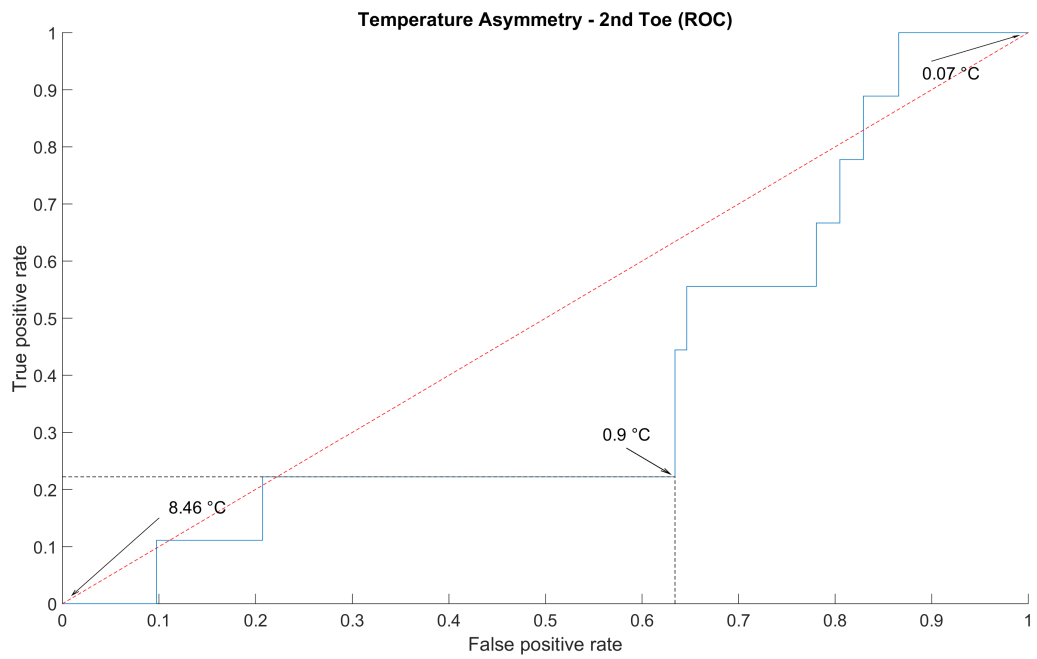


FIGURE B.10: Temperature asymmetry, ROC - 3<sup>rd</sup> Toe

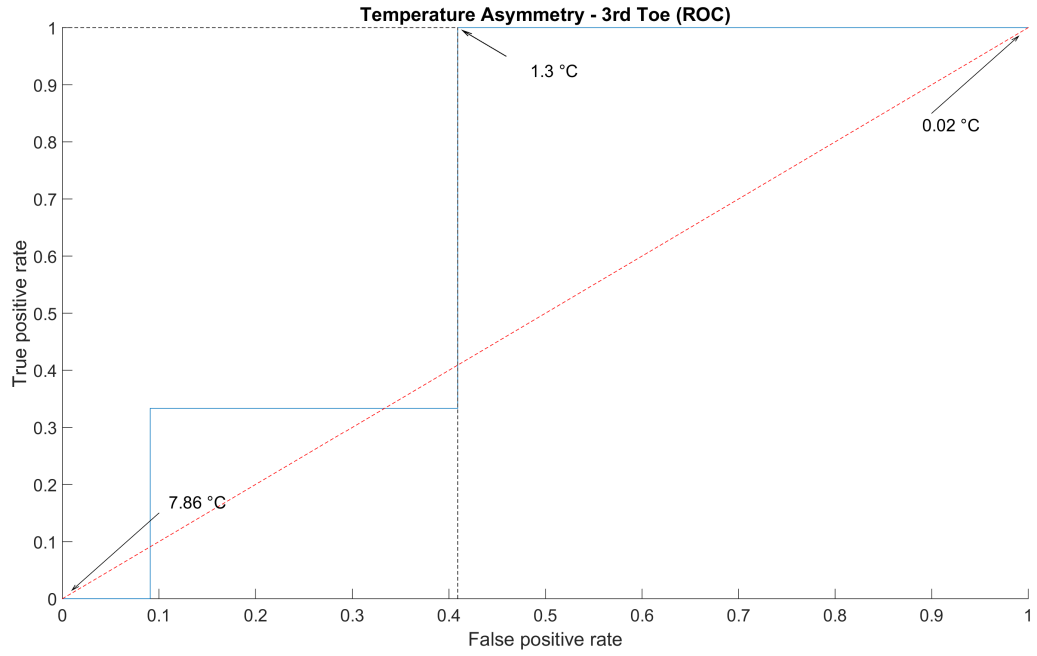


FIGURE B.11: Temperature asymmetry, ROC - 4<sup>th</sup> Toe

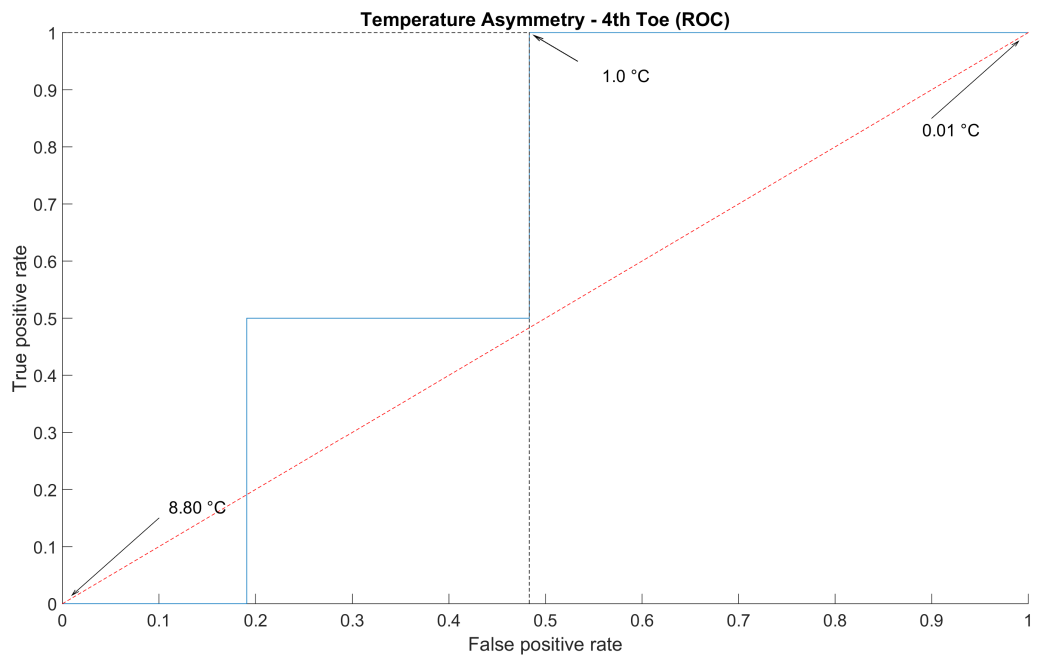


FIGURE B.12: Temperature asymmetry, ROC - 4<sup>th</sup> MTH

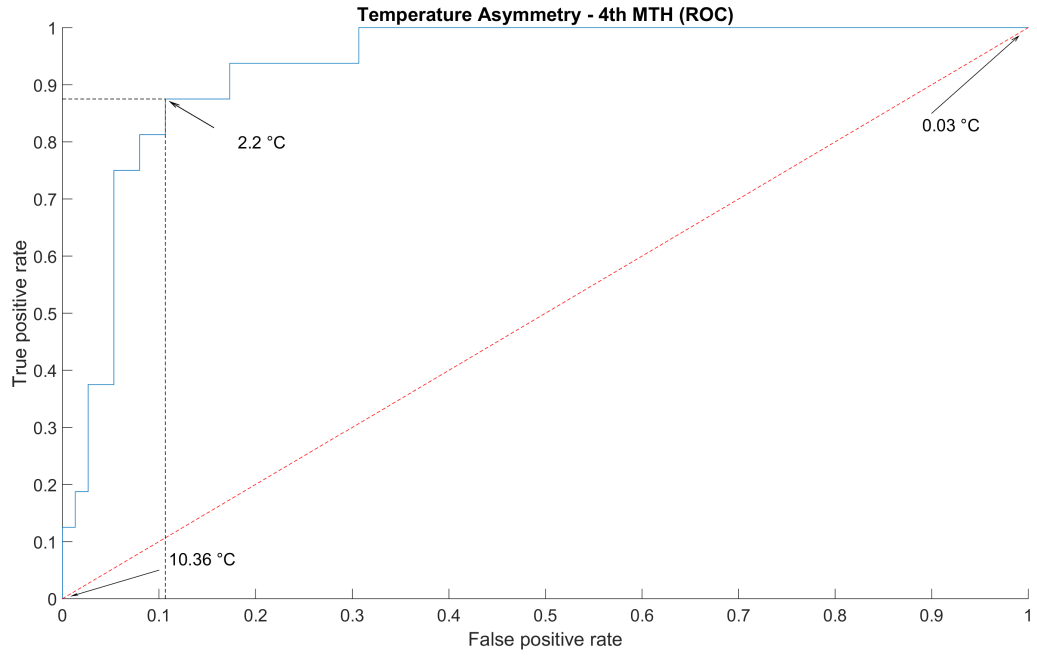


FIGURE B.13: Temperature asymmetry, ROC - 5<sup>th</sup> MTH

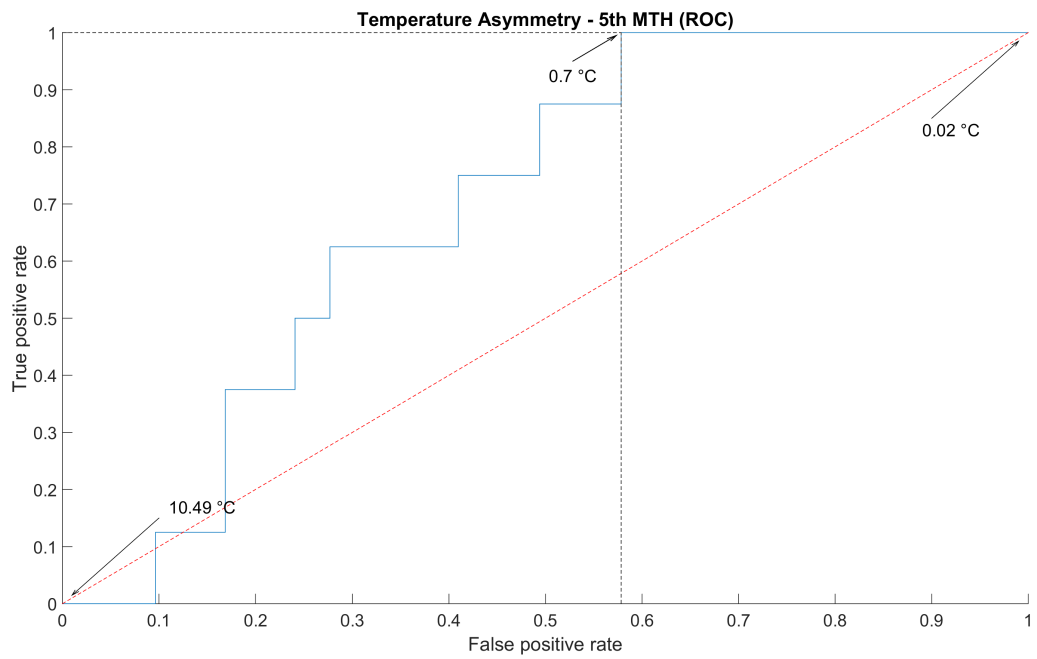


FIGURE B.14: Temperature asymmetry, ROC - 5<sup>th</sup> MTH Base

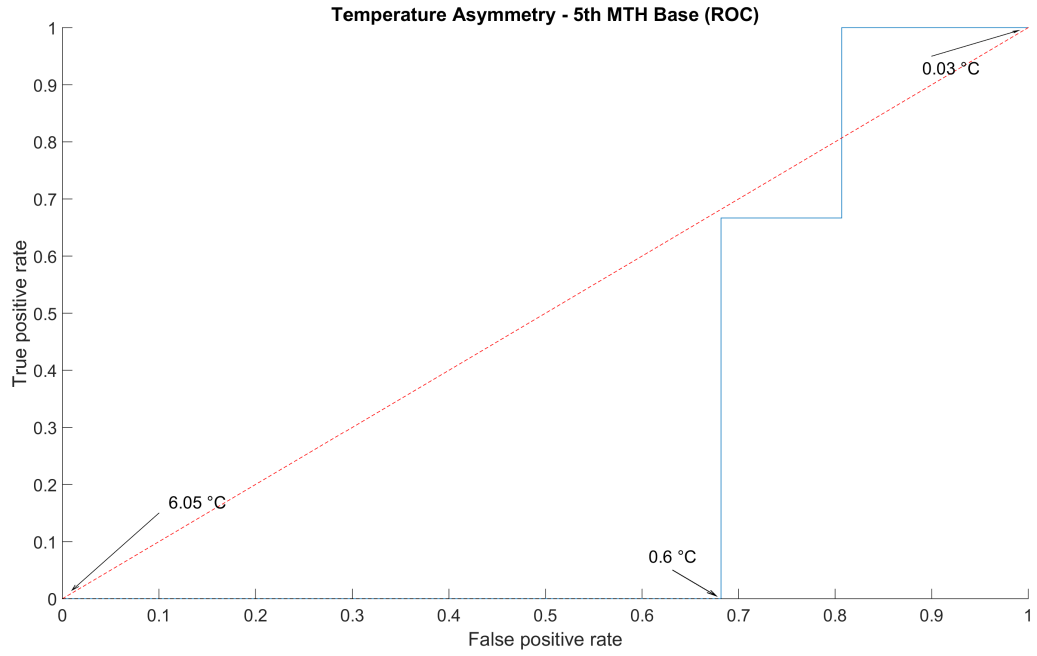


FIGURE B.15: Temperature variance ROC - 1<sup>st</sup> Toe

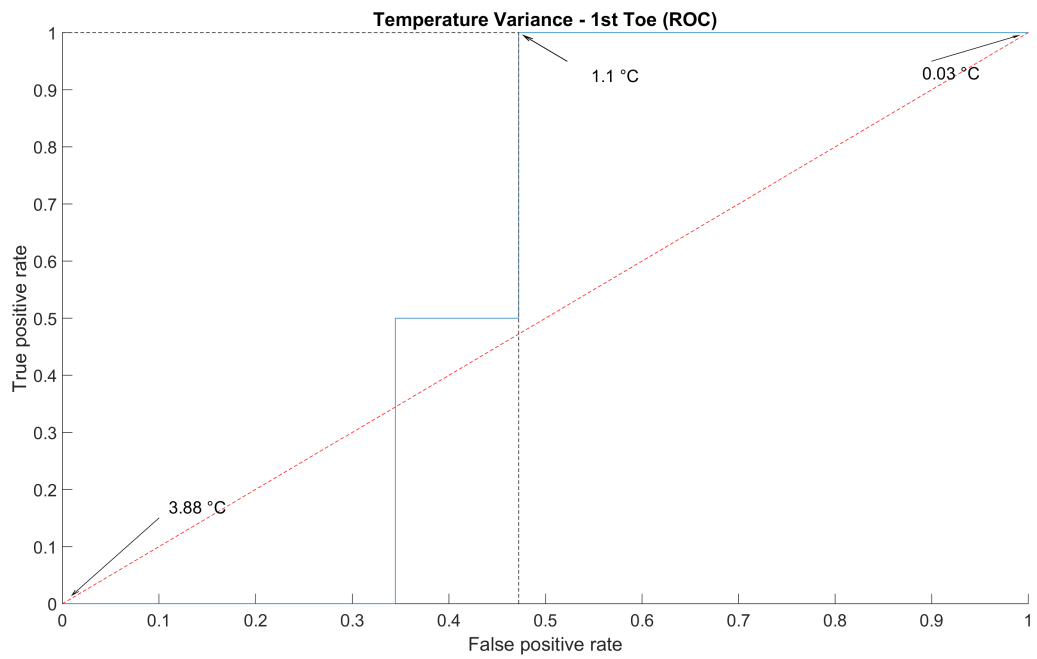


FIGURE B.16: Temperature variance ROC - 2<sup>nd</sup> Toe

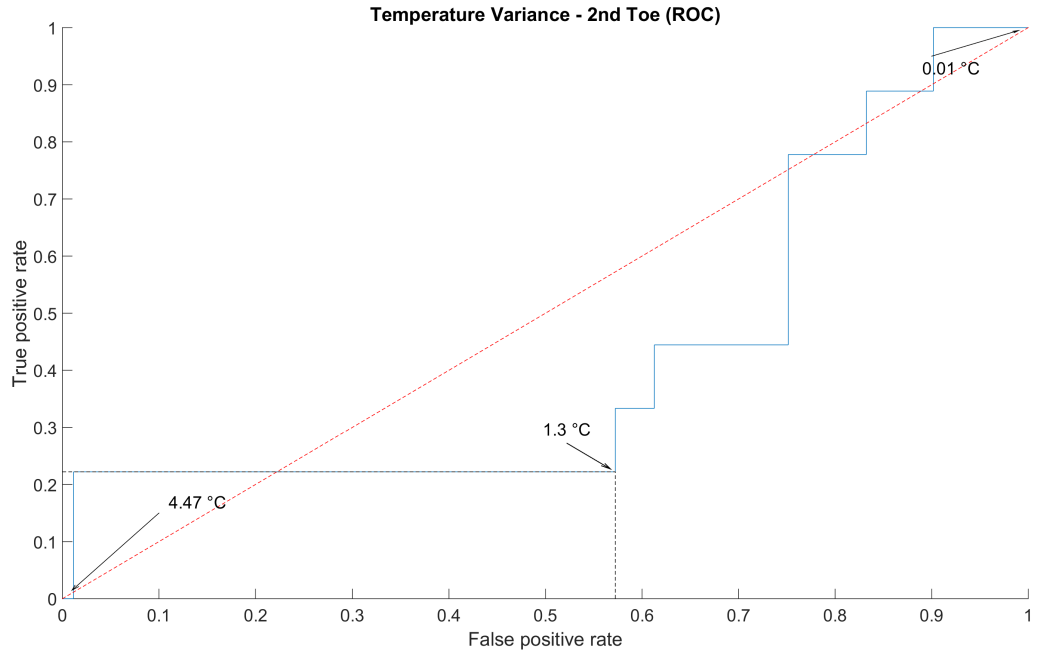


FIGURE B.17: Temperature variance ROC - 3<sup>rd</sup> Toe

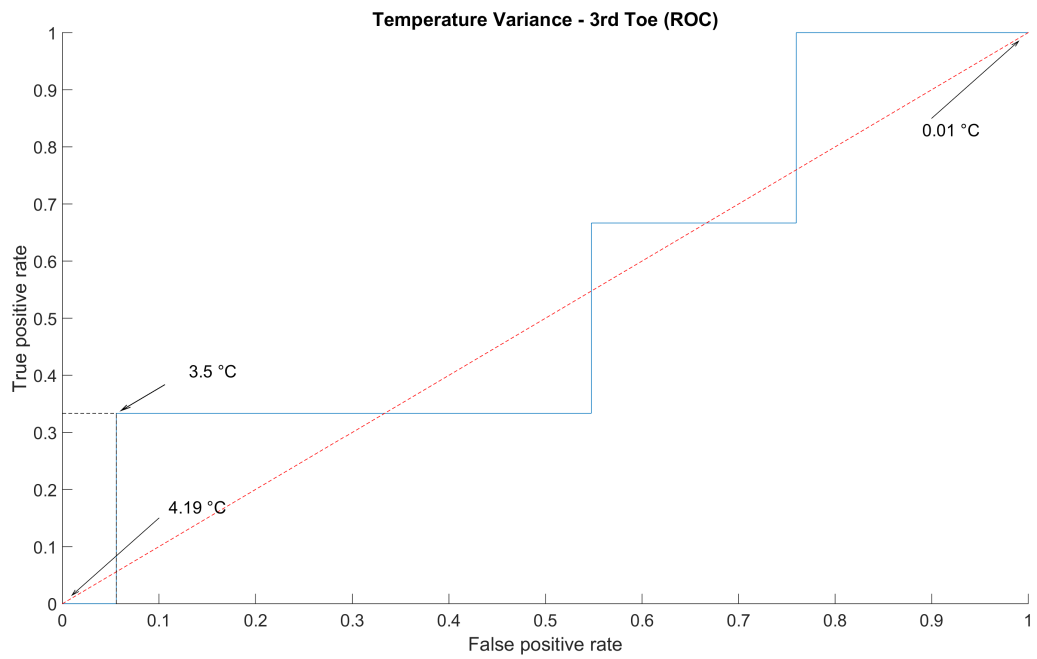


FIGURE B.18: Temperature variance ROC - 4<sup>th</sup> Toe

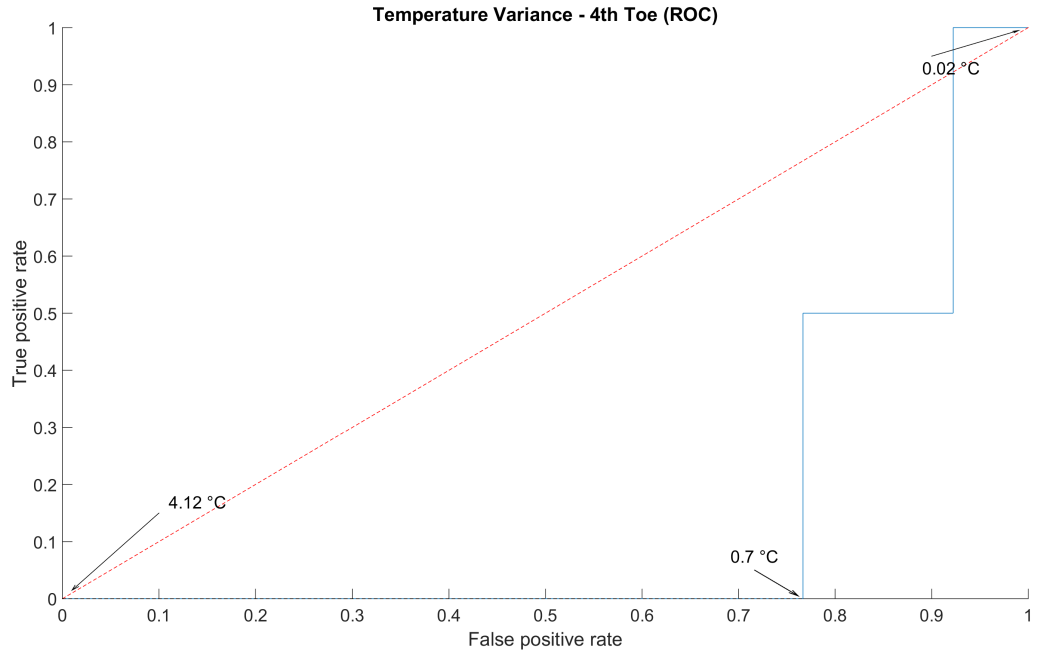


FIGURE B.19: Temperature variance ROC - 4<sup>th</sup> MTH

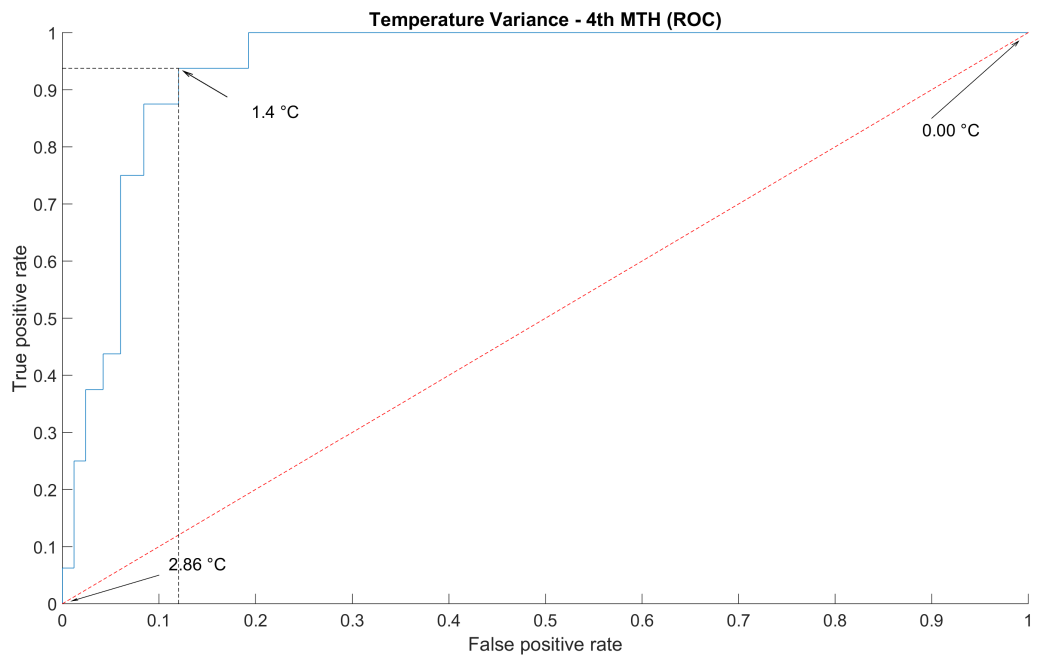


FIGURE B.20: Temperature variance ROC - 5<sup>th</sup> MTH

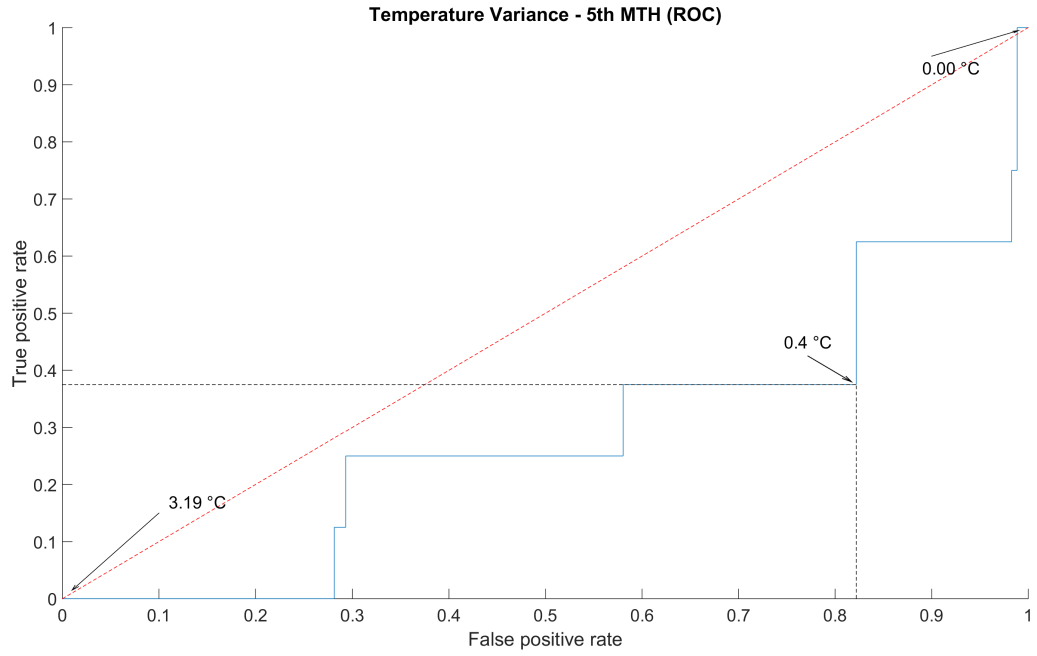


FIGURE B.21: Temperature variance ROC - 5<sup>th</sup> MTH Base

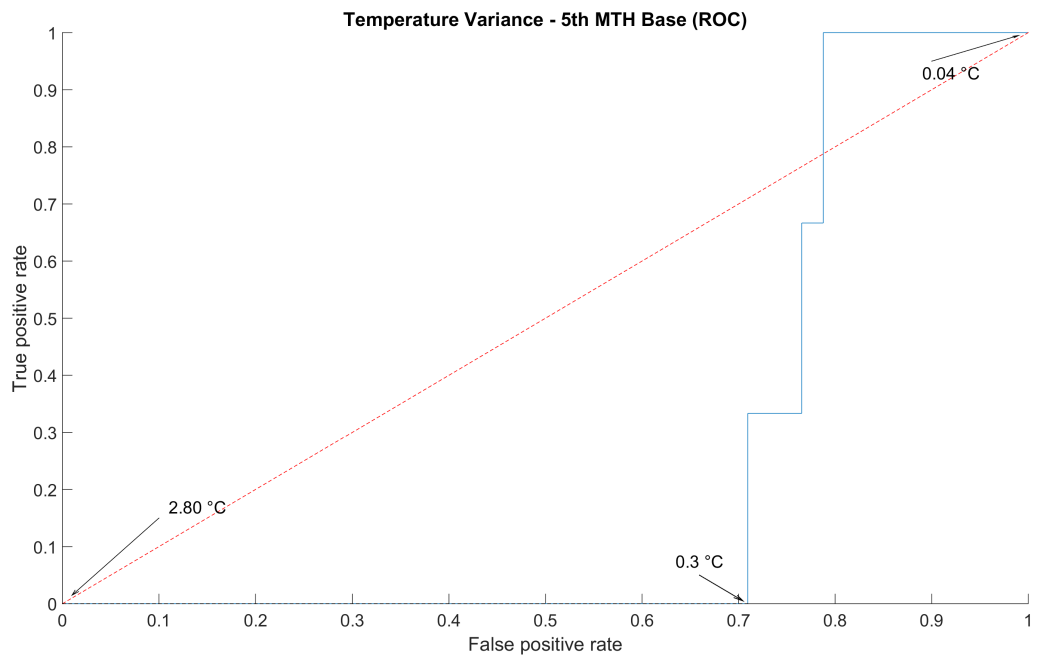




FIGURE B.22: Temperature change over time ROC - 1<sup>st</sup> Toe

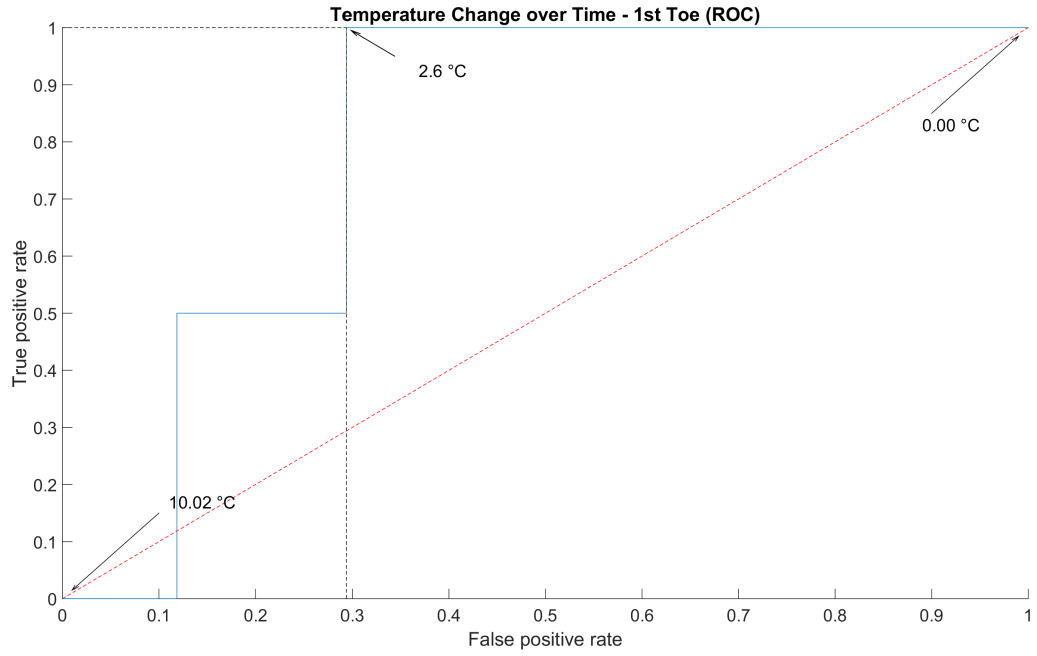


FIGURE B.23: Temperature change over time ROC - 2<sup>nd</sup> Toe

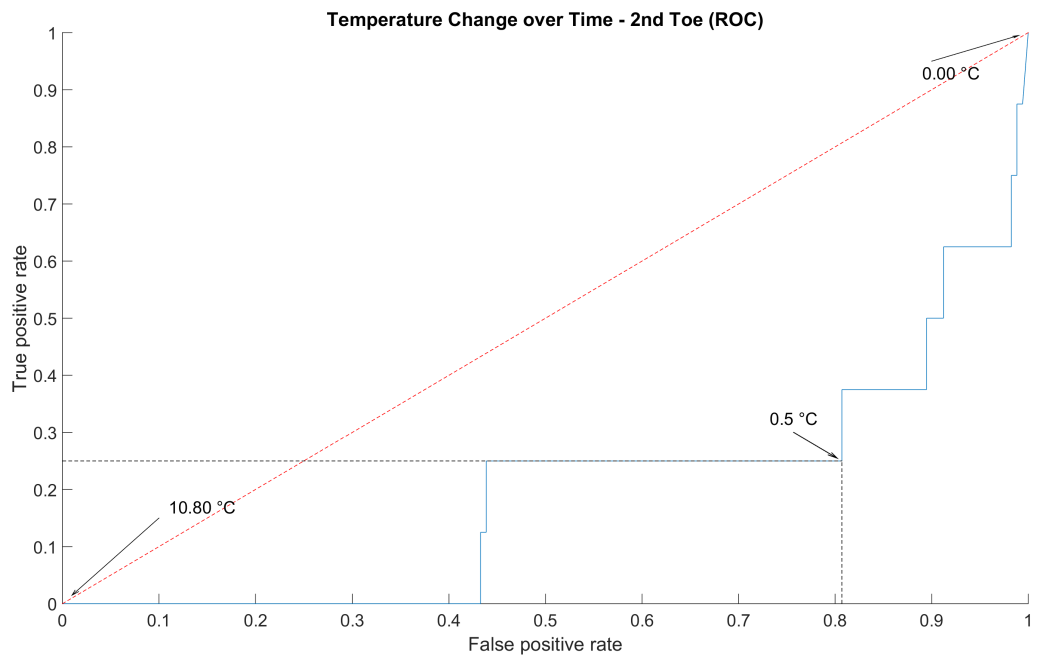


FIGURE B.24: Temperature change over time ROC - 3<sup>rd</sup> Toe

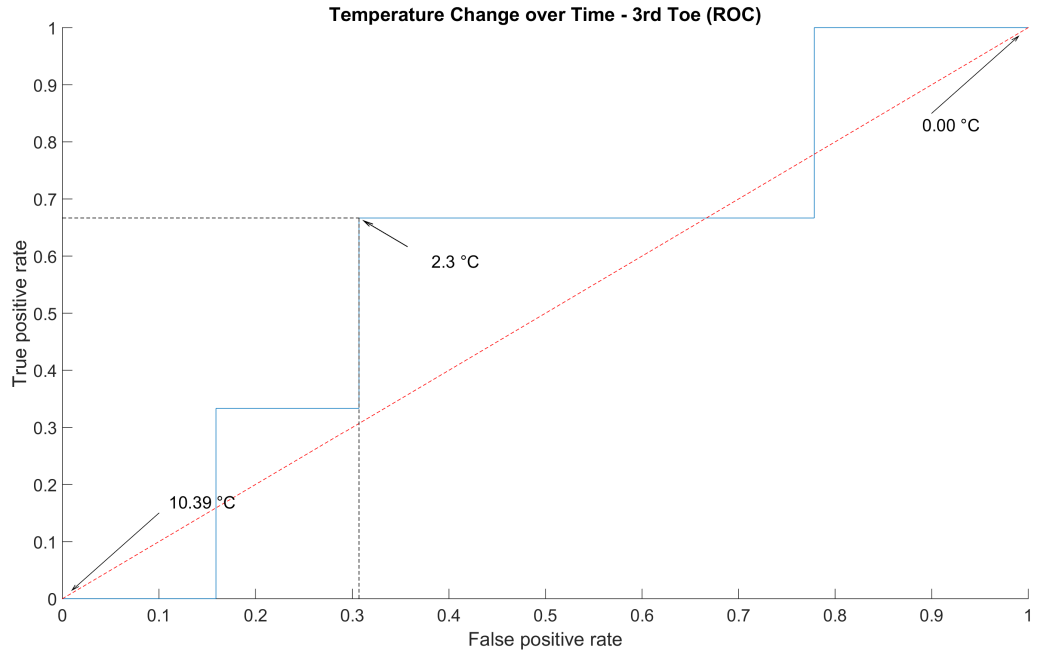


FIGURE B.25: Temperature change over time ROC - 4<sup>th</sup> Toe

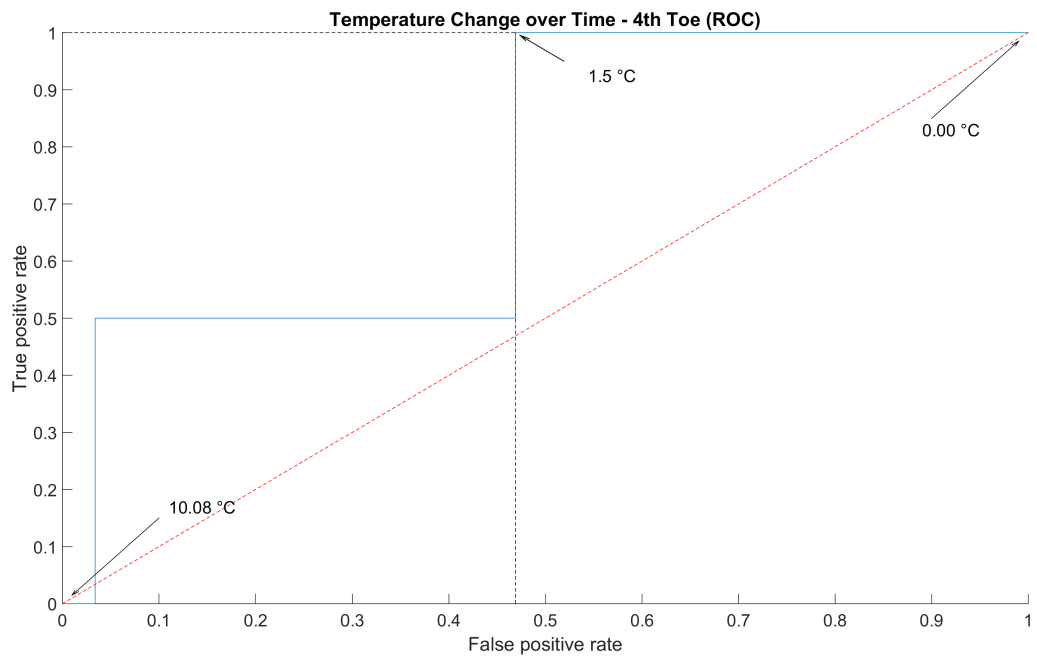


FIGURE B.26: Temperature change over time ROC - 4<sup>th</sup> MTH

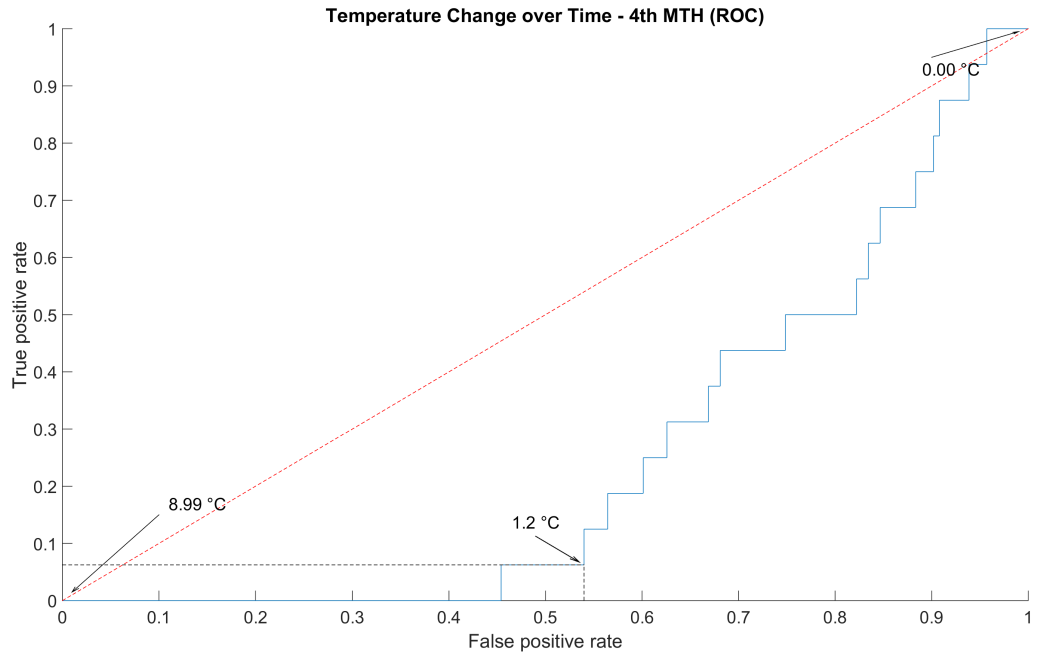


FIGURE B.27: ROI temperature vs Mean ROCs

FIGURE B.28: Temperature change over time ROC - 5<sup>th</sup> MTH

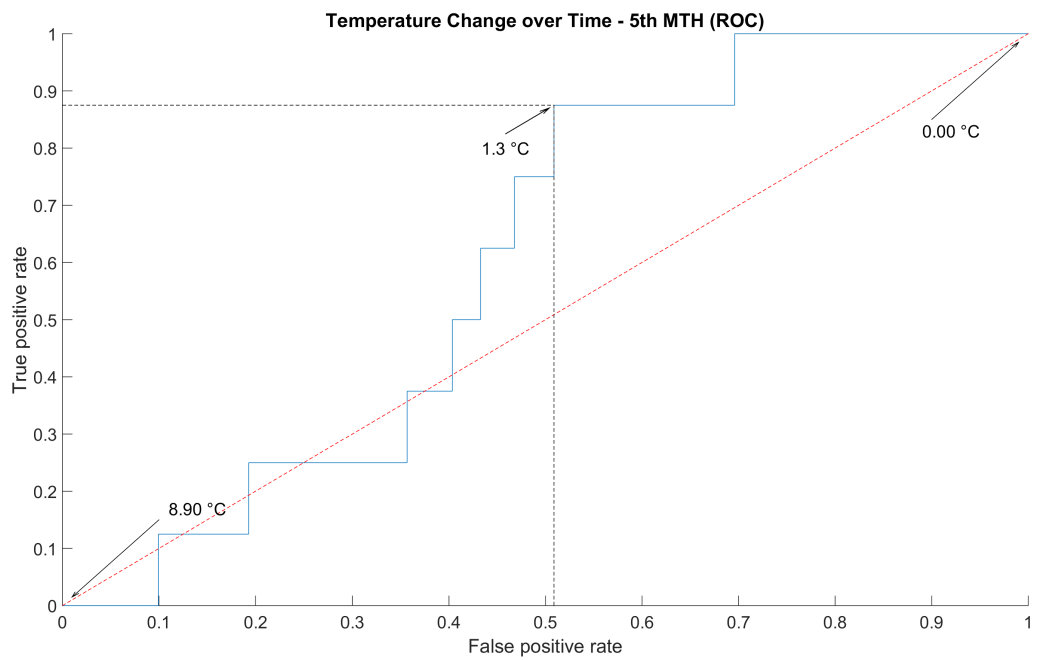


FIGURE B.29: Temperature change over time ROC - 5<sup>th</sup> MTH Base

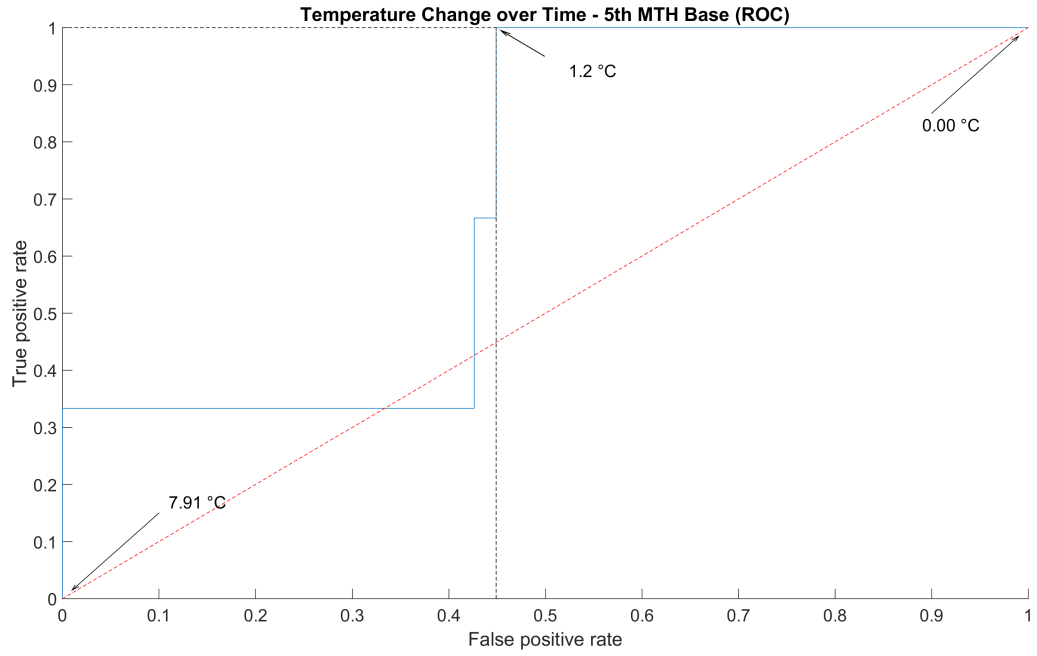


FIGURE B.30: Difference to baseline ROC - 1<sup>st</sup> Toe

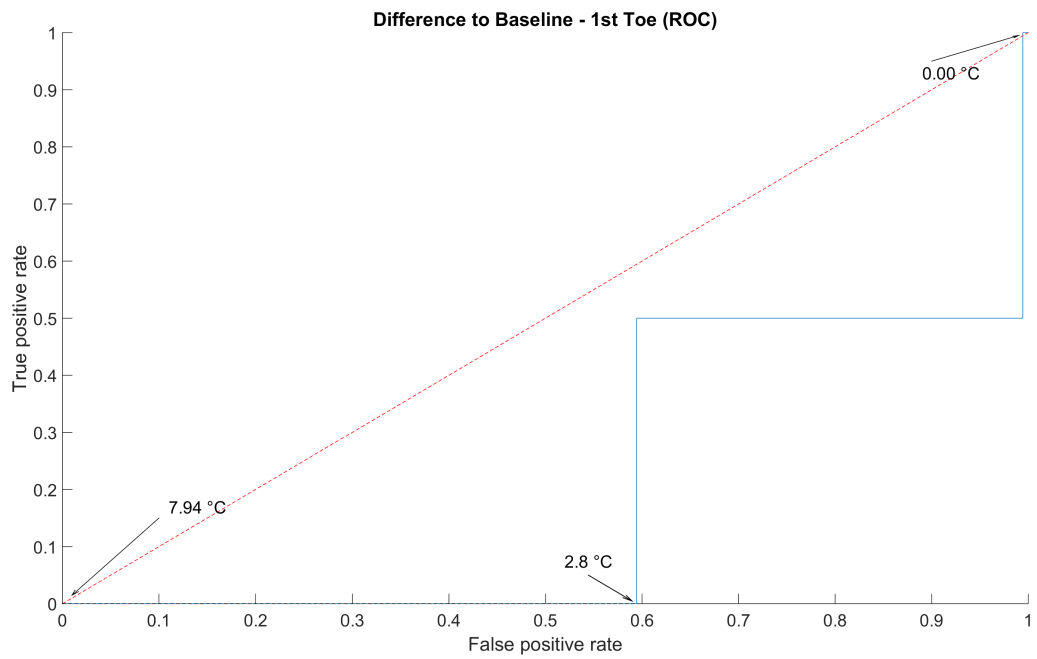


FIGURE B.31: Difference to baseline ROC - 2<sup>nd</sup> Toe

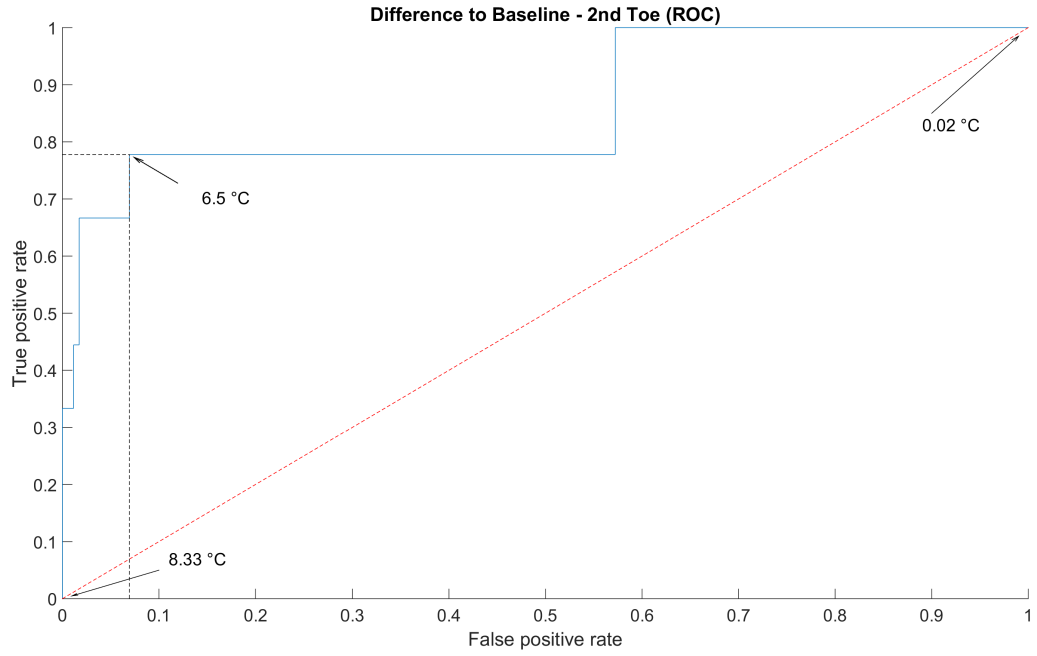


FIGURE B.32: Difference to baseline ROC - 3<sup>rd</sup> Toe

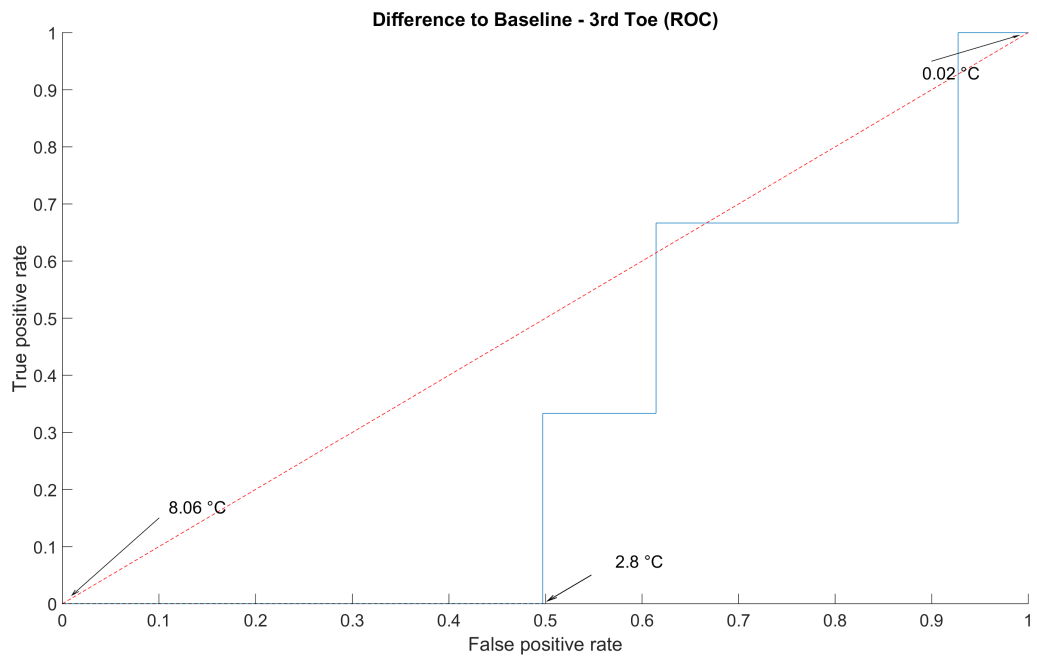


FIGURE B.33: Difference to baseline ROC - 4<sup>th</sup> Toe

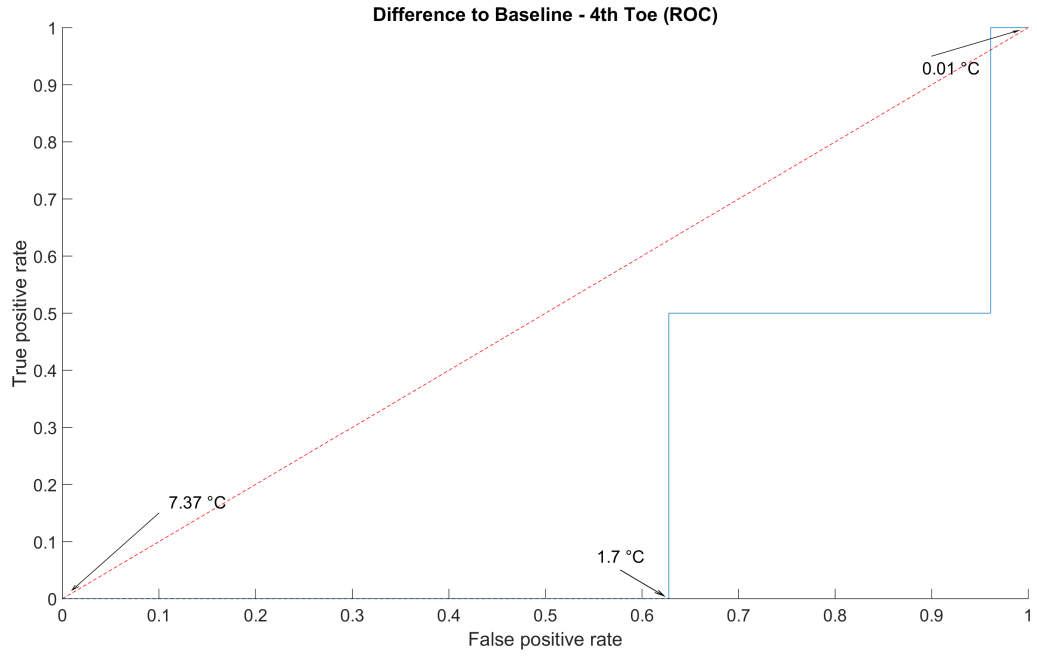


FIGURE B.34: Difference to baseline ROC - 4<sup>th</sup> MTH

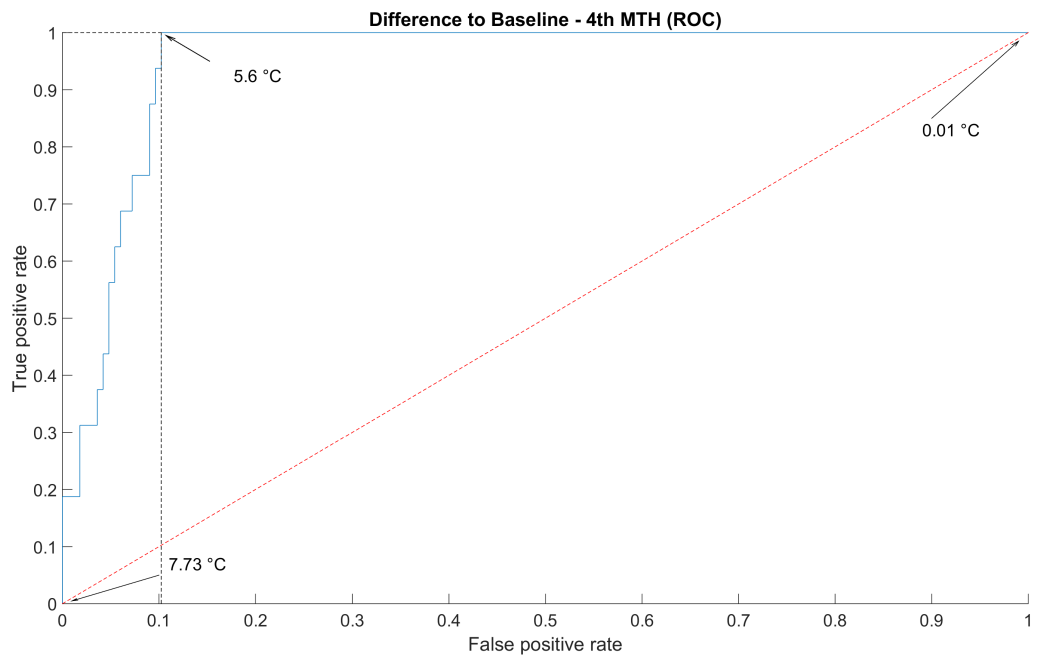


FIGURE B.35: Difference to baseline ROC - 5<sup>th</sup> MTH

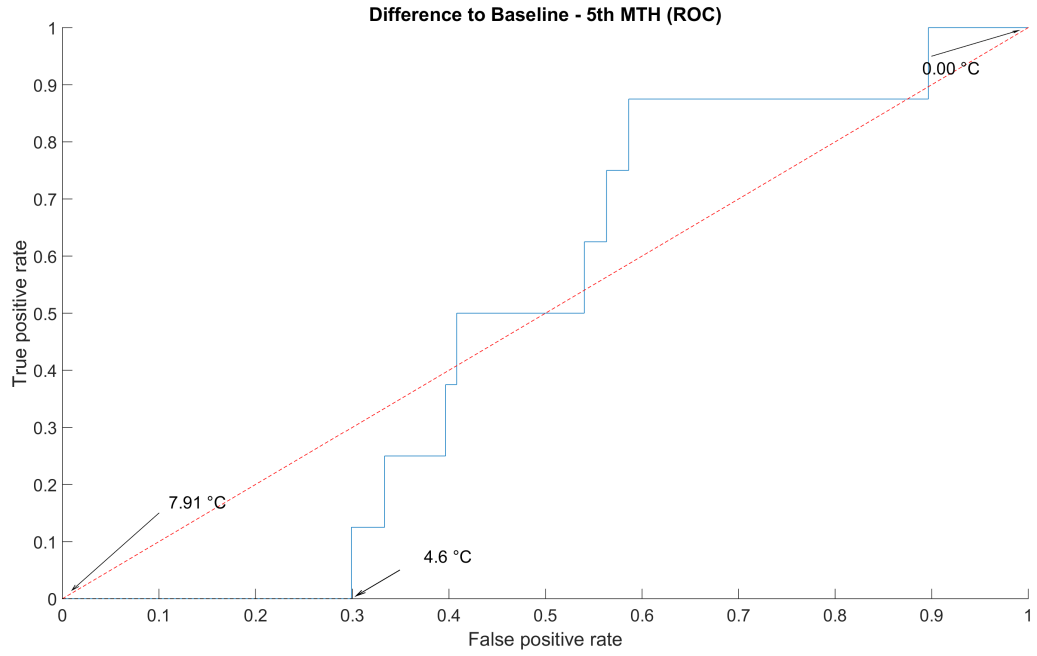
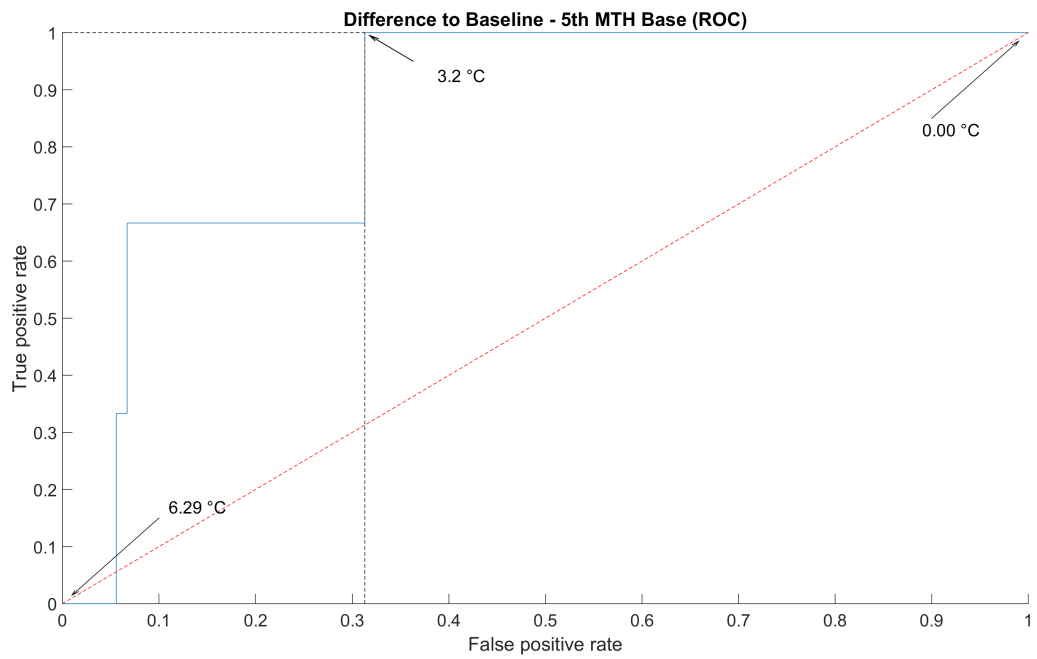


FIGURE B.36: Difference to baseline ROC - 5<sup>th</sup> MTH Base



## Appendix C

# Appendix - Applying Thresholds to ROIs

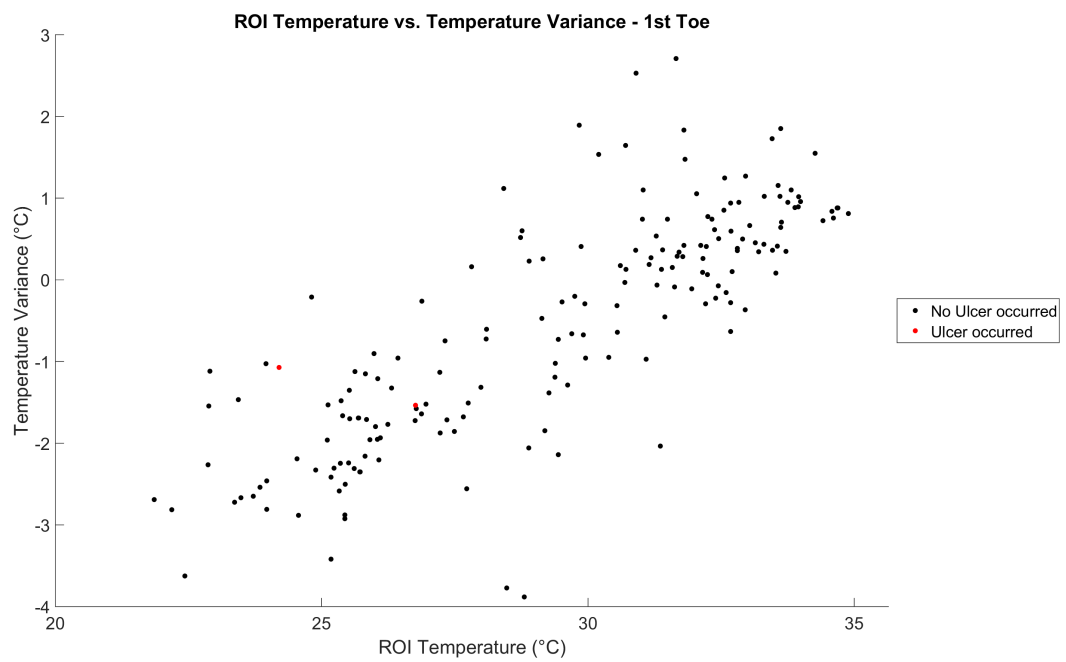


FIGURE C.1: ROI temperature vs temperature variance 1st toe plot



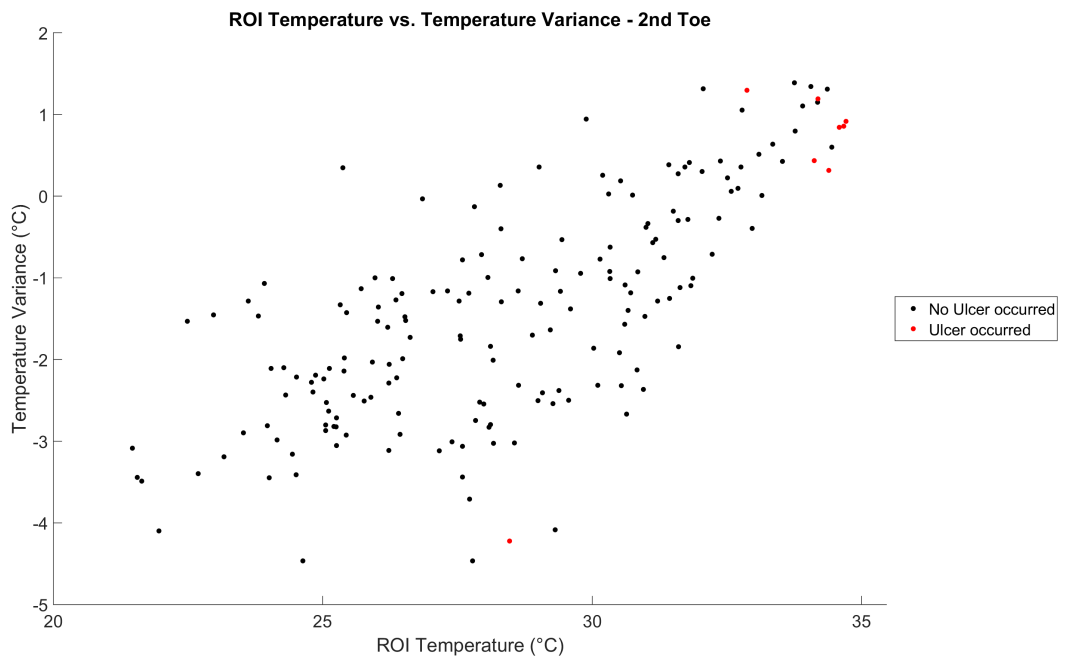


FIGURE C.2: ROI temperature vs temperature variance 2nd toe plot

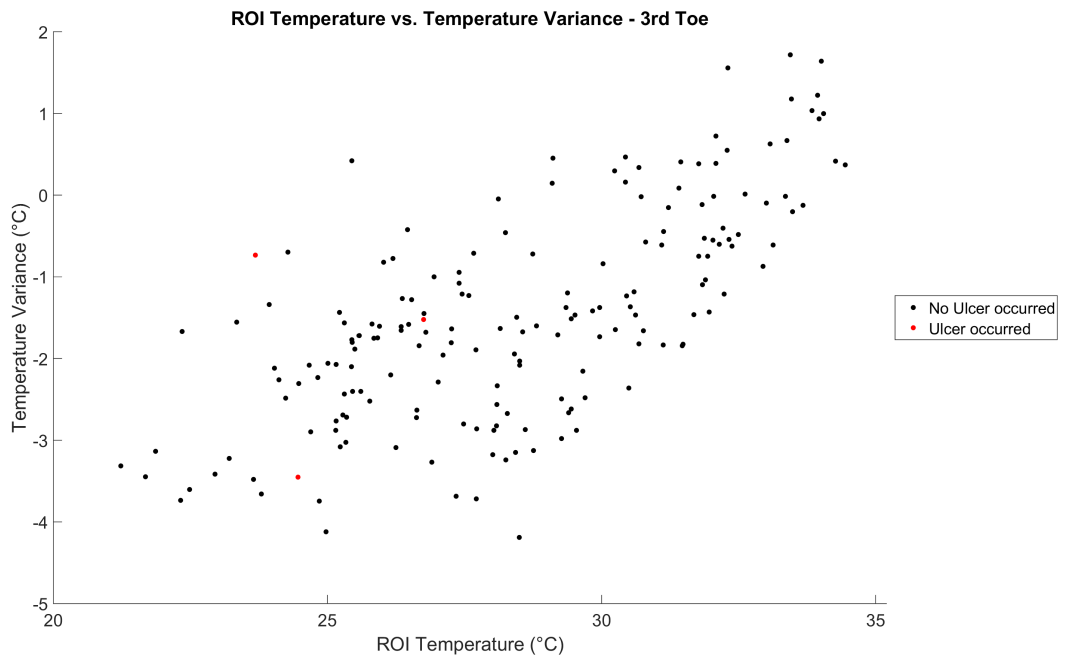


FIGURE C.3: ROI temperature vs temperature variance 3rd toe plot

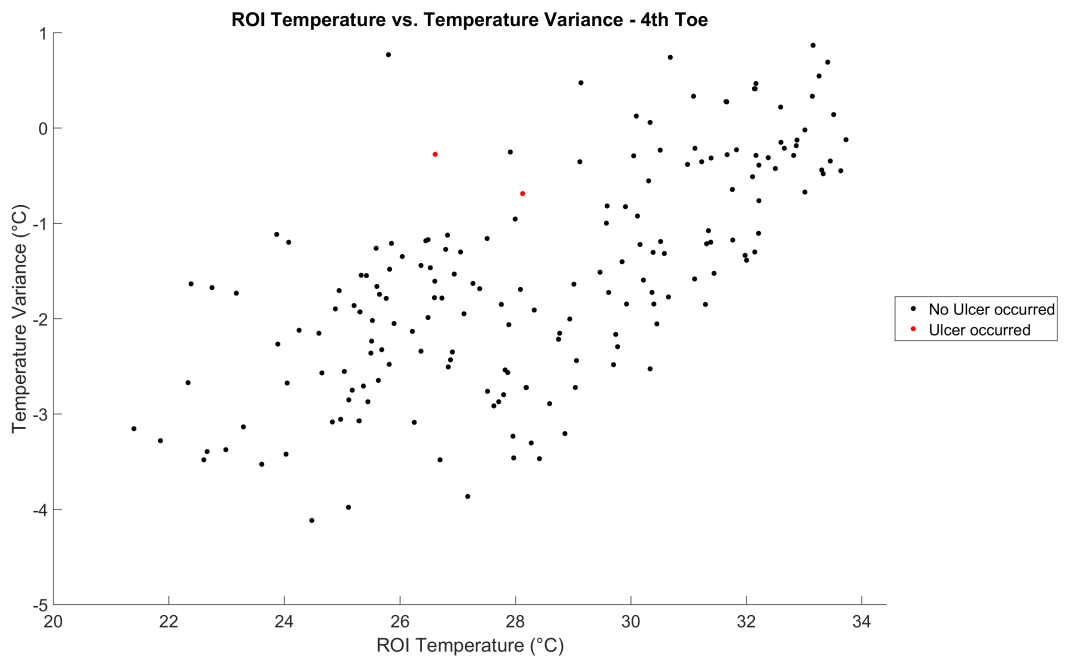


FIGURE C.4: ROI temperature vs temperature variance 4th toe plot

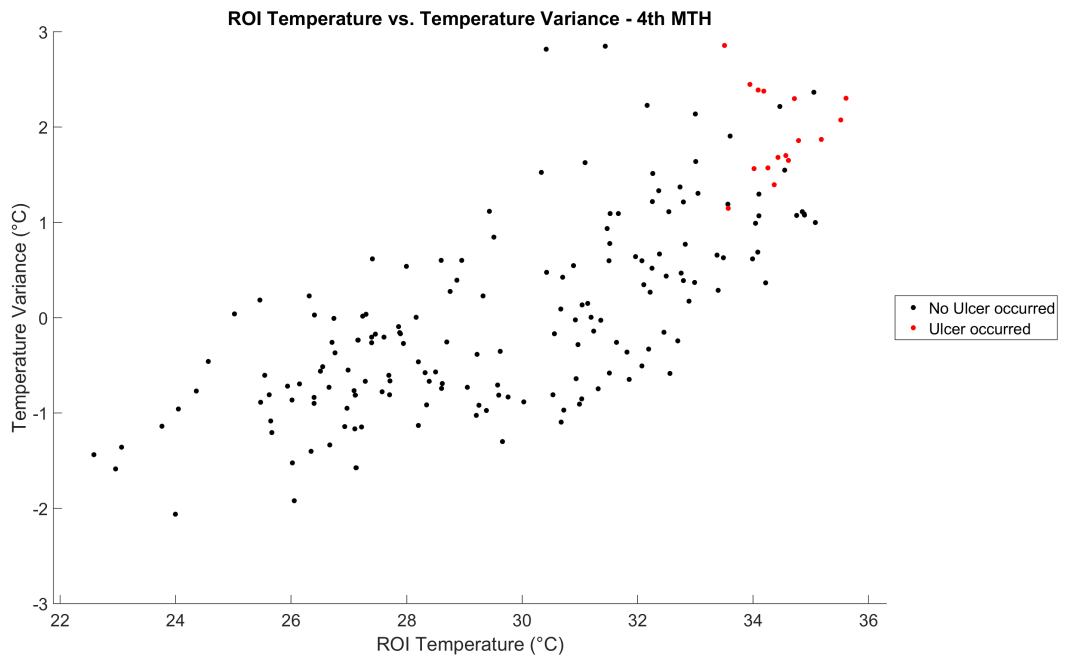


FIGURE C.5: ROI temperature vs temperature variance 4th MTH plot

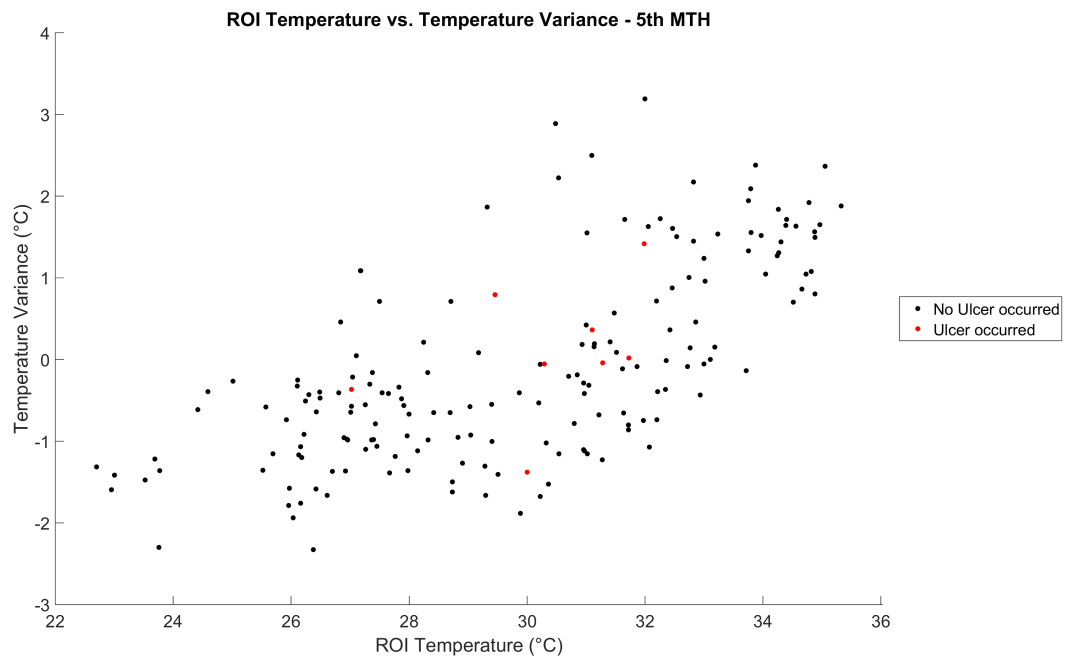


FIGURE C.6: ROI temperature vs temperature variance 5th MTH plot

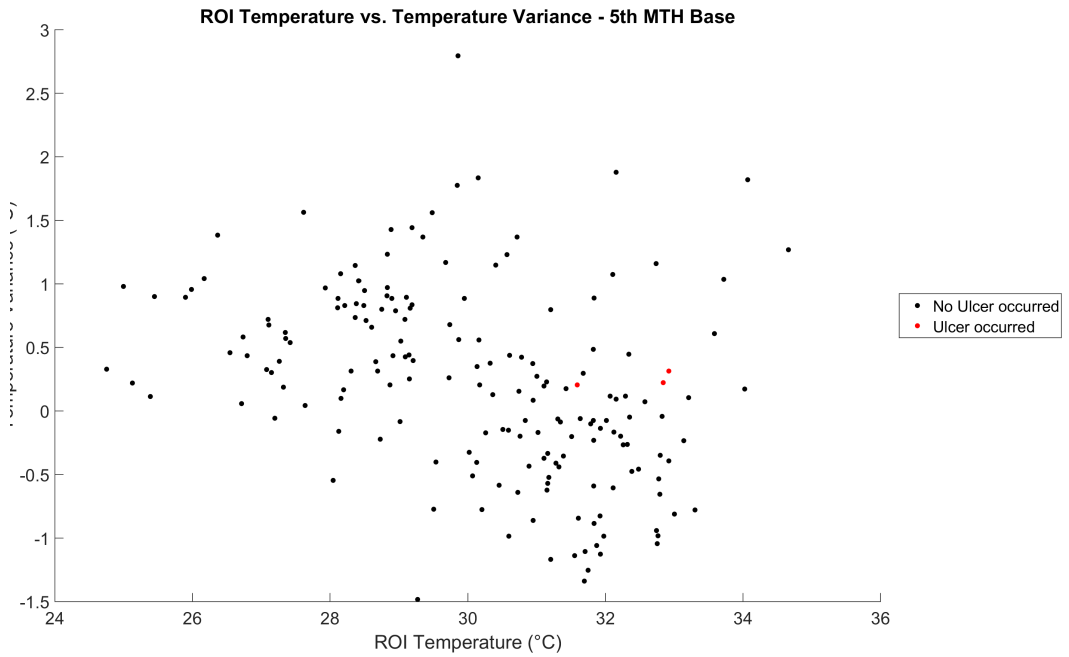


FIGURE C.7: ROI temperature vs temperature variance 5th MTH Base plot

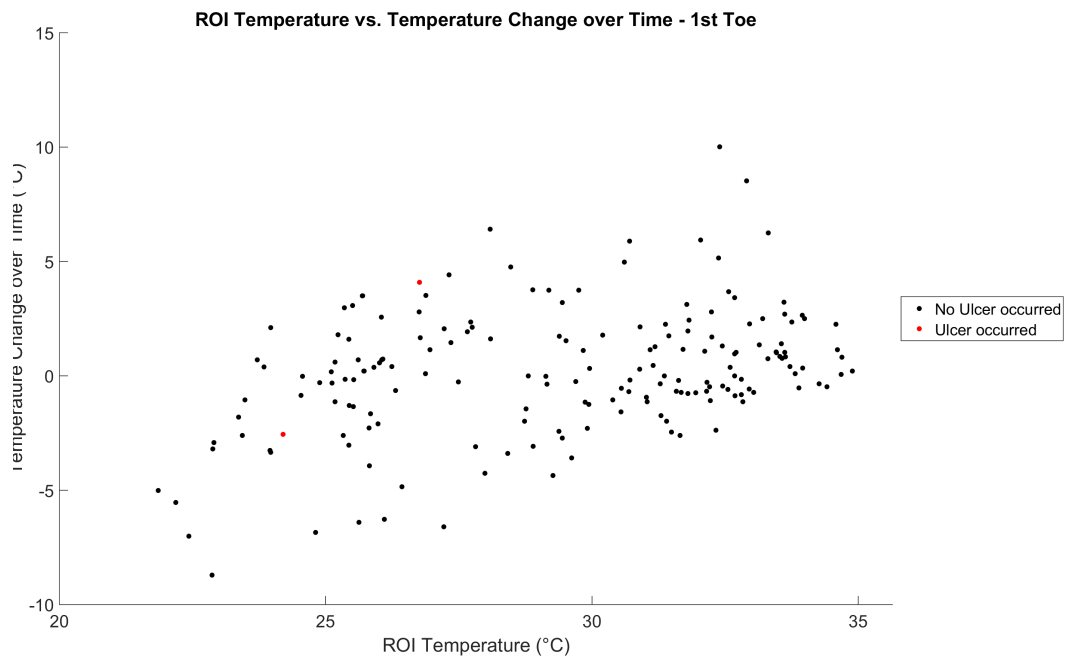


FIGURE C.8: ROI temperature vs temperature change over time 1st toe plot

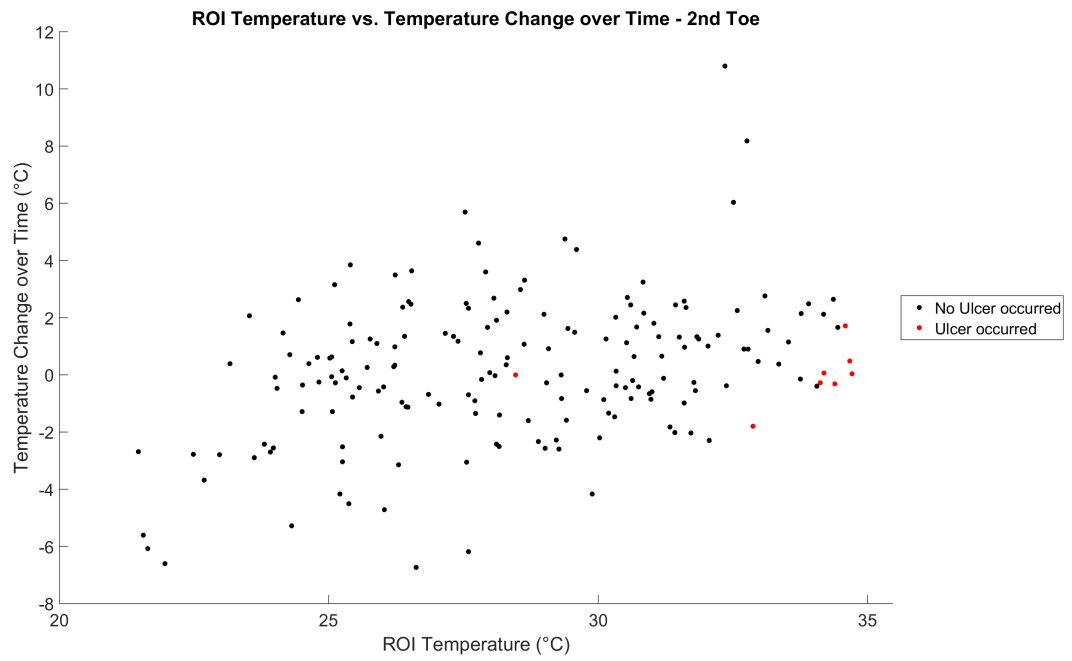


FIGURE C.9: ROI temperature vs temperature change over time 2nd toe plot

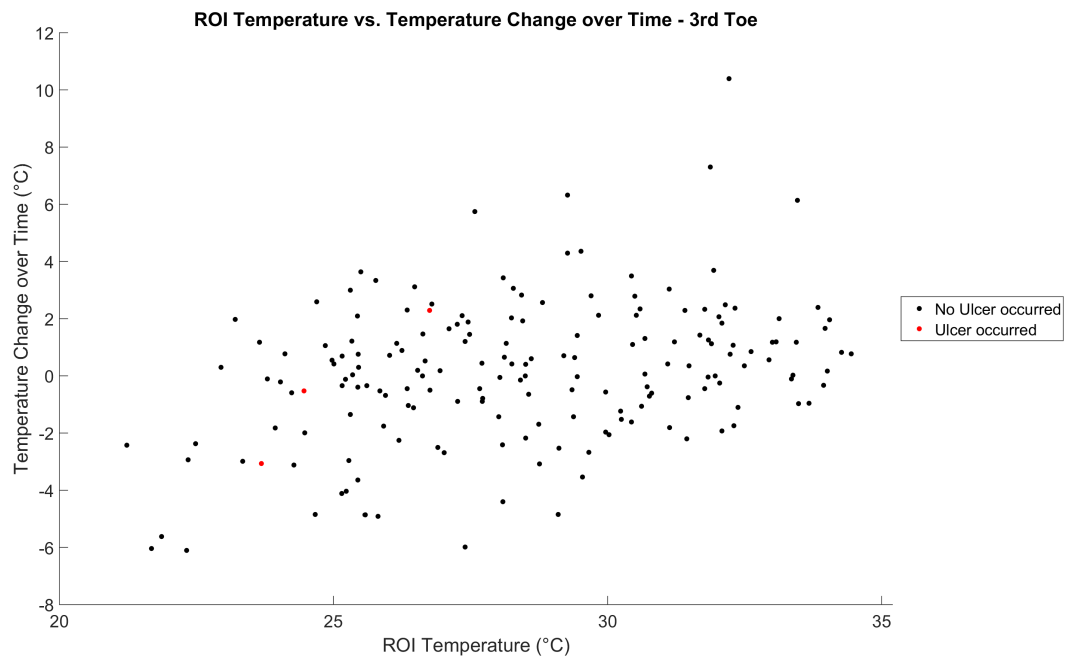


FIGURE C.10: ROI temperature vs temperature change over time 3rd toe plot

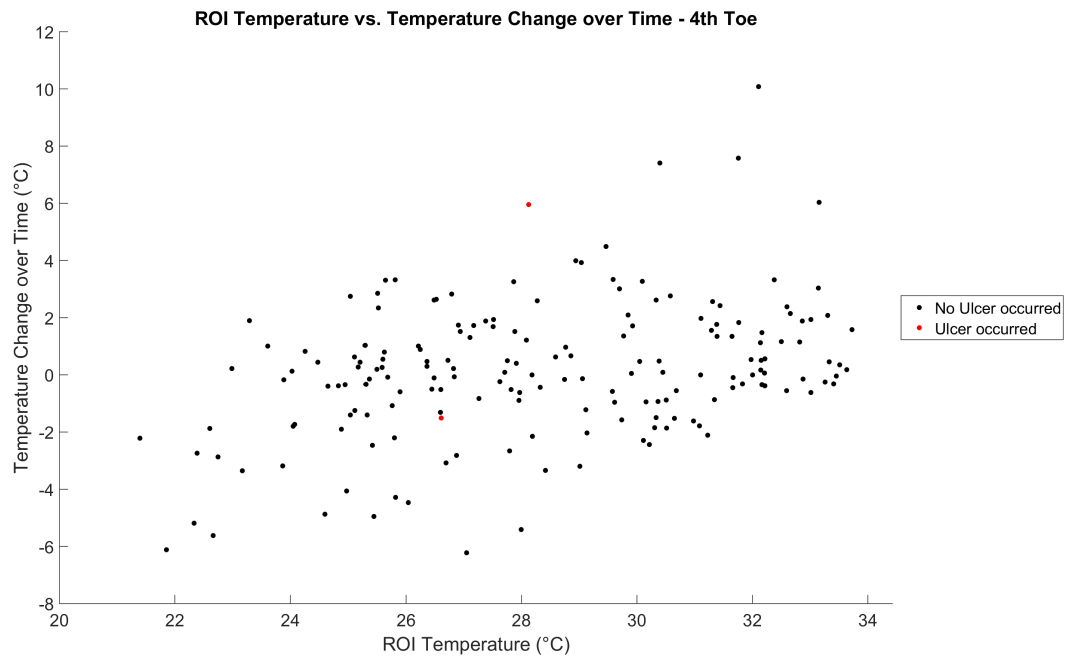


FIGURE C.11: ROI temperature vs temperature change over time 4th toe plot

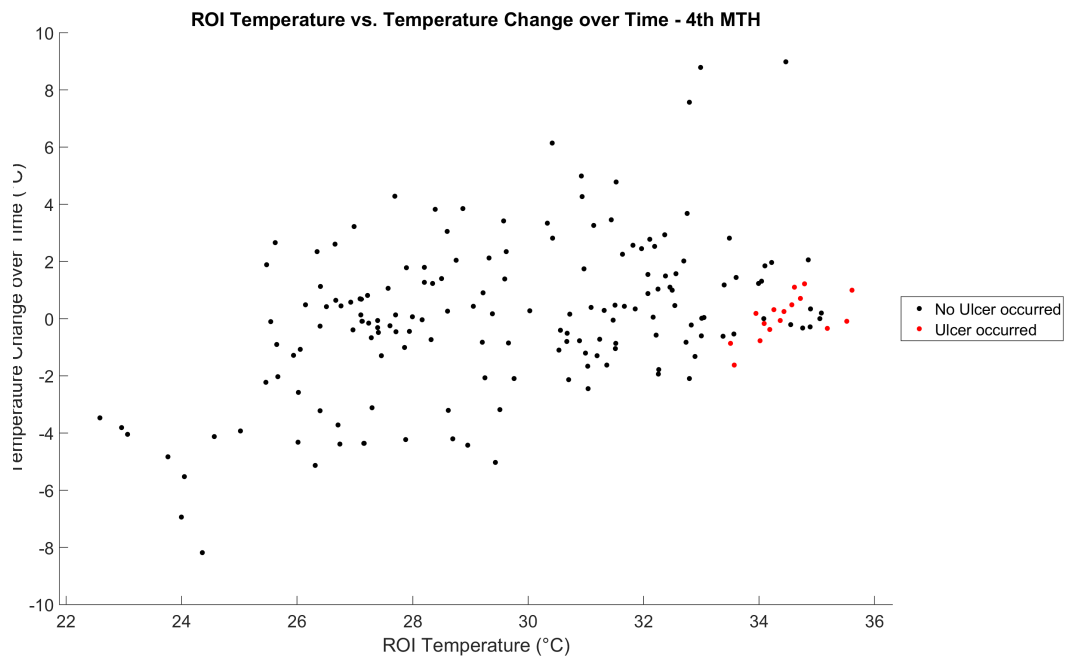


FIGURE C.12: ROI temperature vs temperature change over time 4th MTH plot

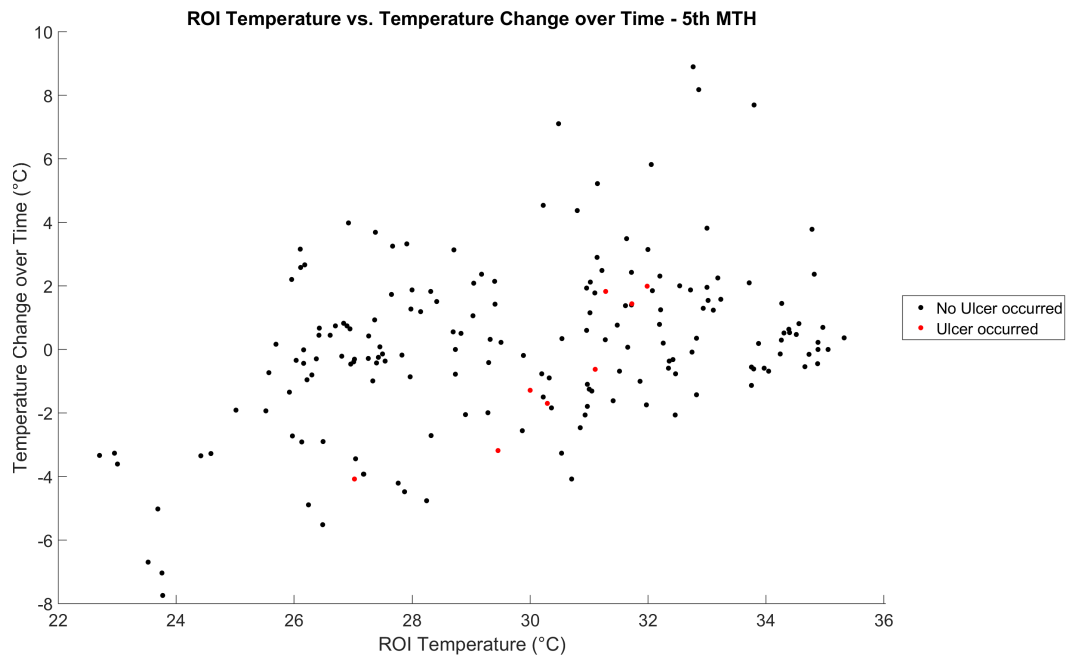


FIGURE C.13: ROI temperature vs temperature change over time 5th MTH plot

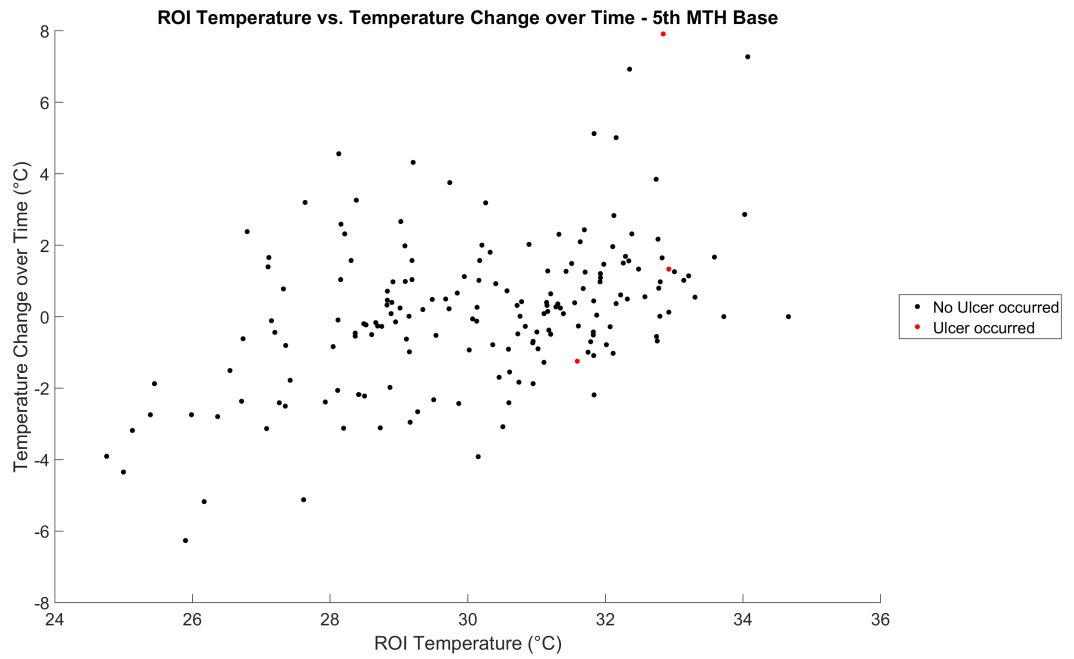


FIGURE C.14: ROI temperature vs temperature change over time 5th MTH Base plot

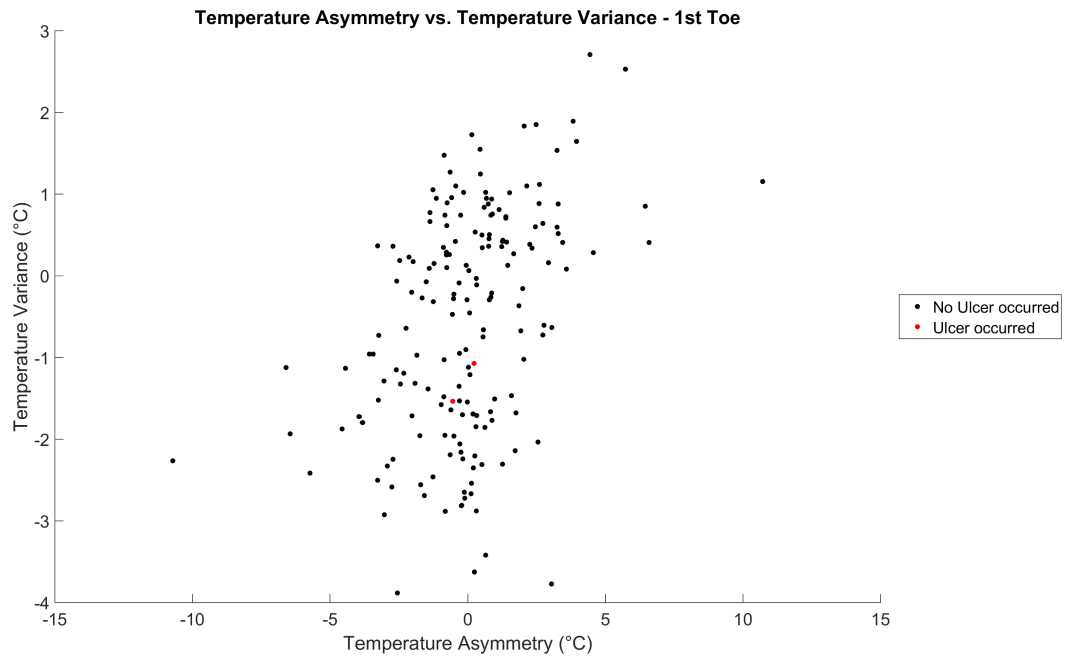


FIGURE C.15: temperature asymmetry vs temperature variance 1st toe plot

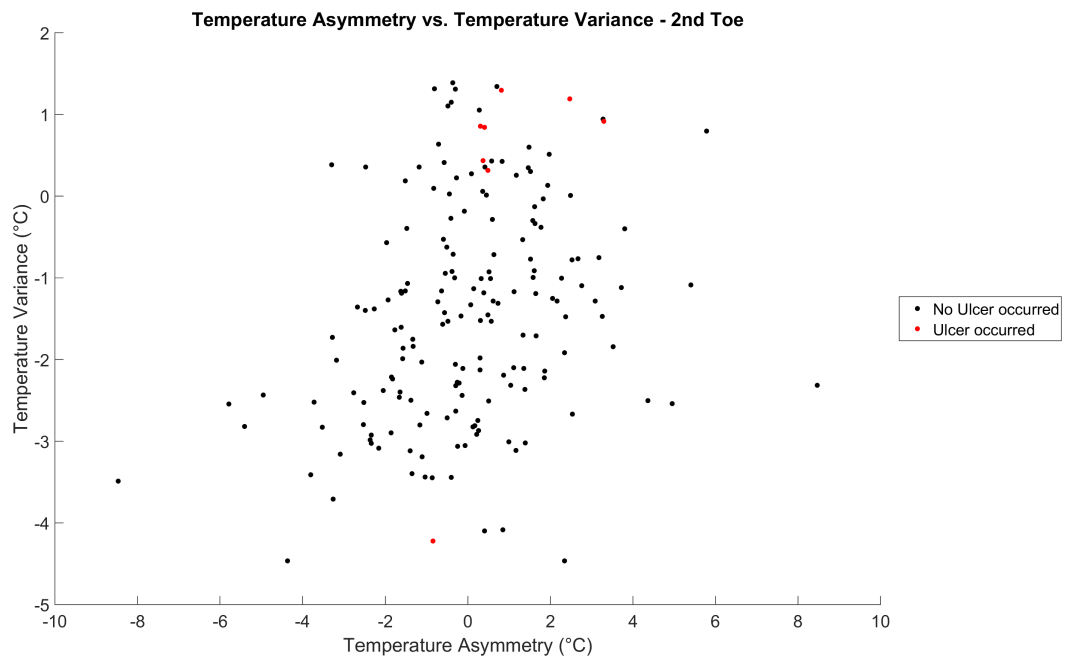


FIGURE C.16: temperature asymmetry vs temperature variance 2nd toe plot

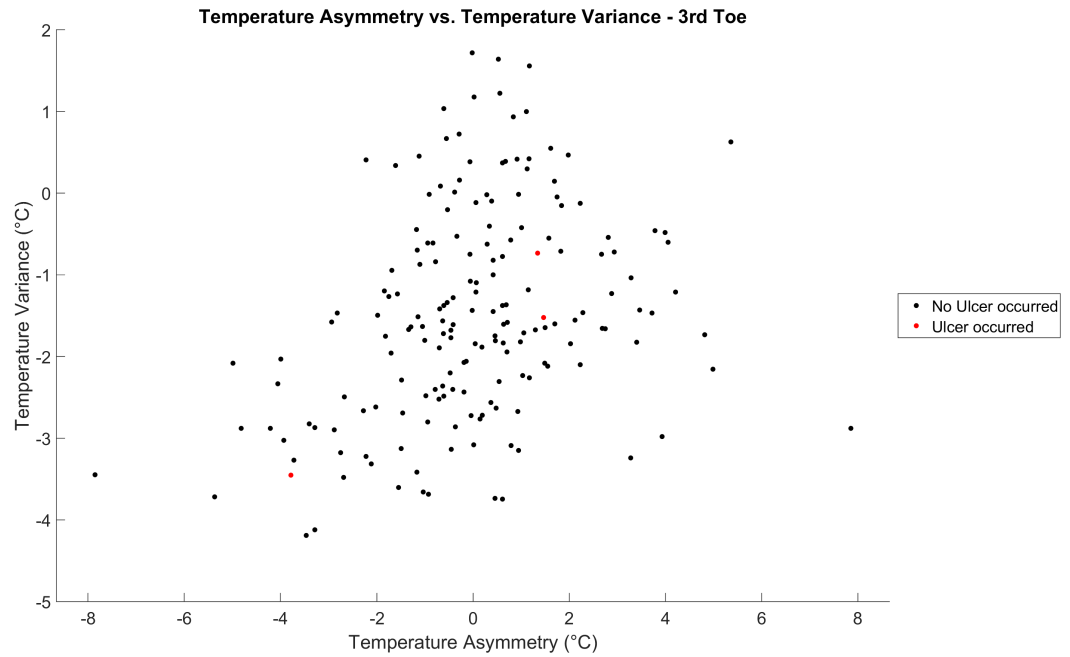


FIGURE C.17: temperature asymmetry vs temperature variance 3rd toe plot



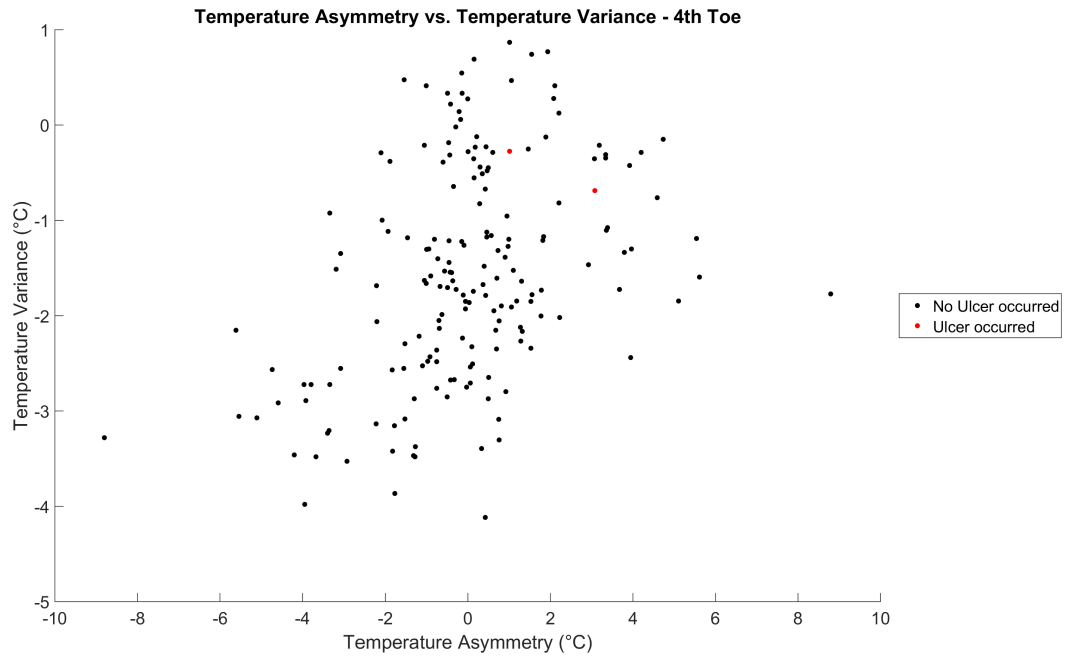


FIGURE C.18: temperature asymmetry vs temperature variance 4th toe plot

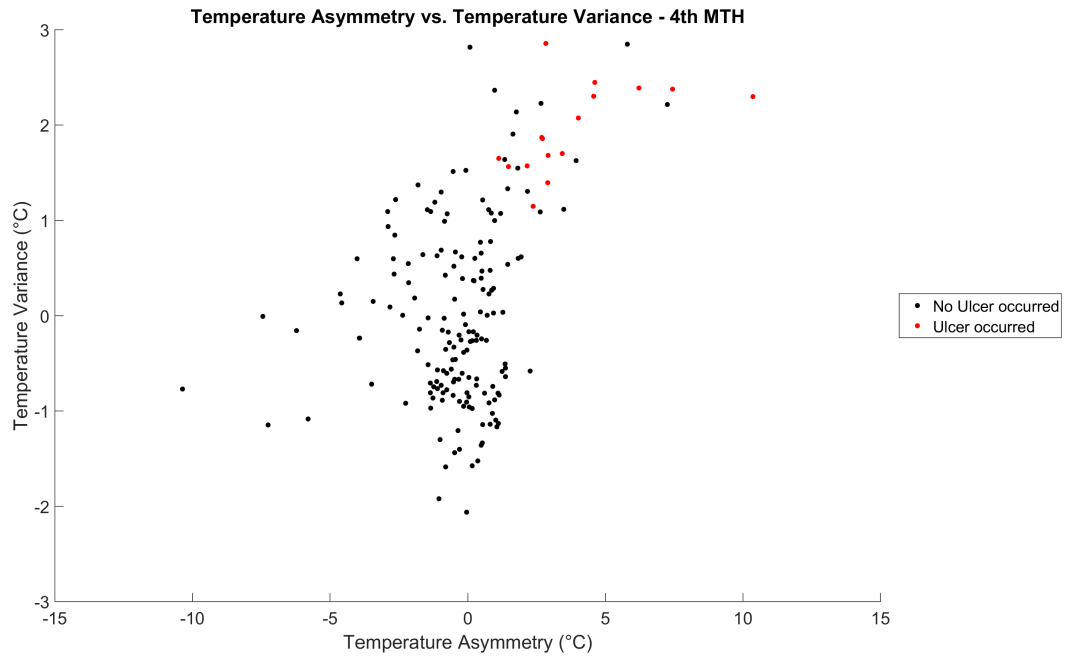


FIGURE C.19: temperature asymmetry vs temperature variance 4th MTH plot

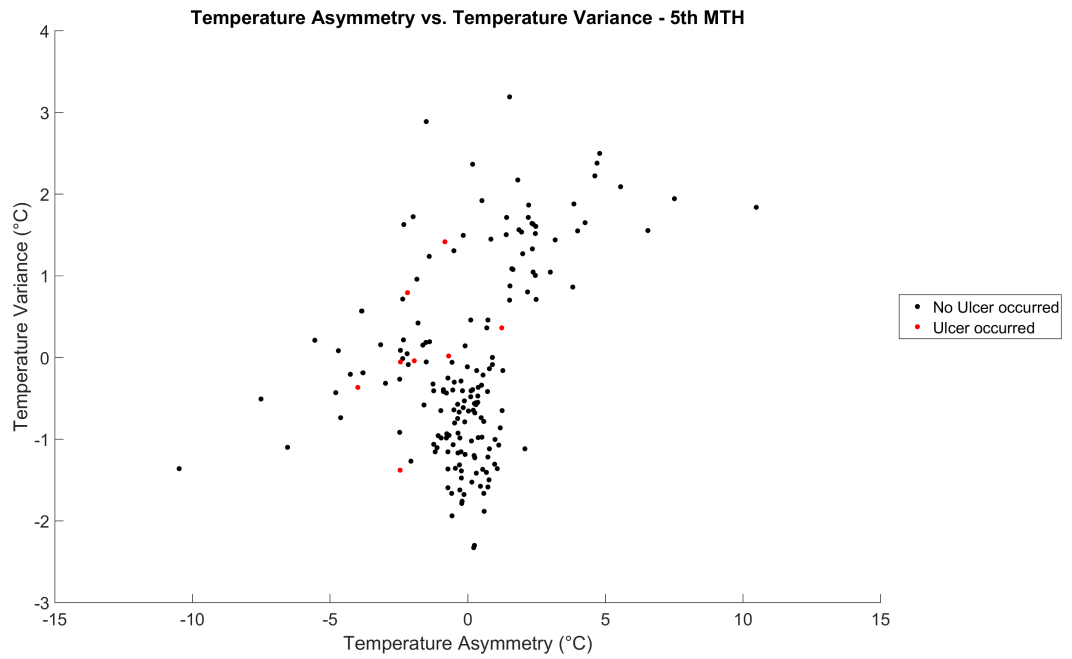


FIGURE C.20: temperature asymmetry vs temperature variance 5th MTH plot

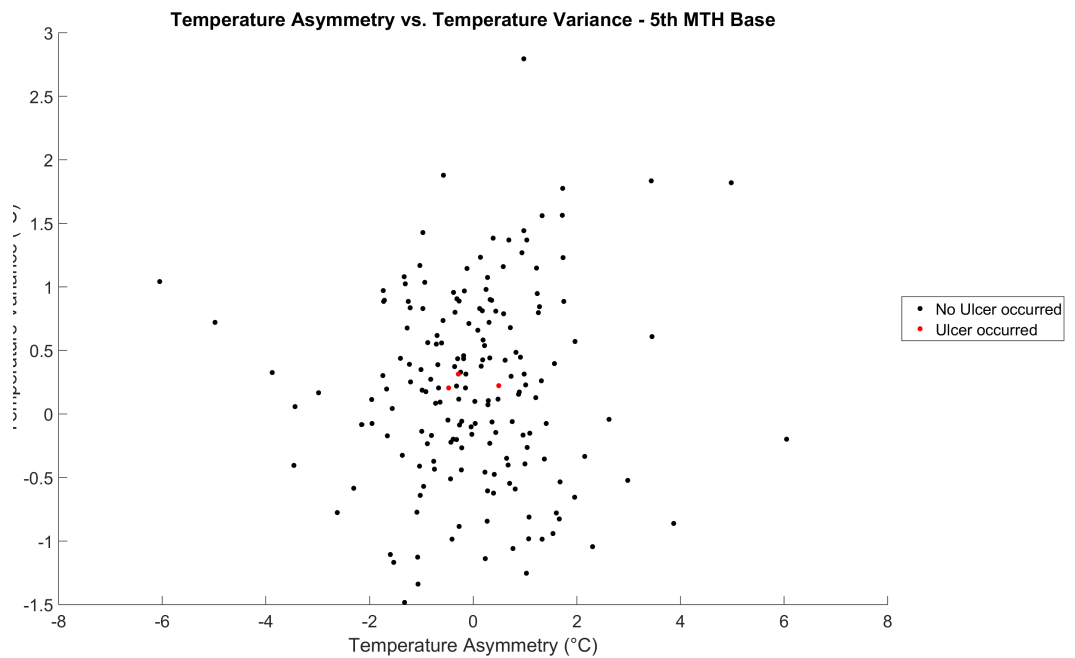


FIGURE C.21: temperature asymmetry vs temperature variance 5th MTH Base plot

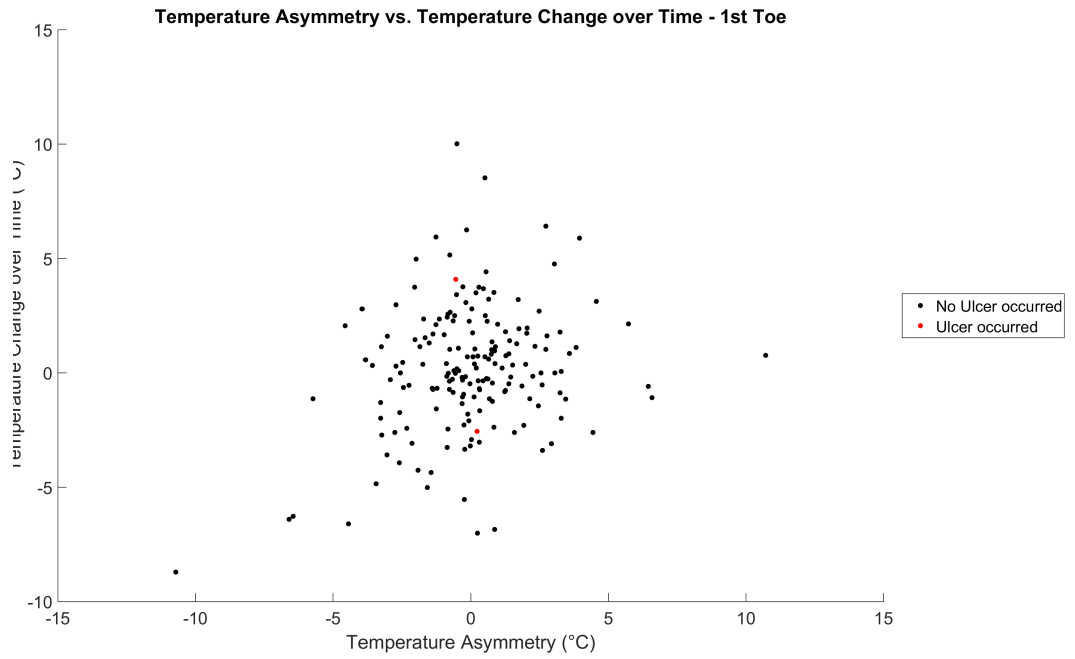


FIGURE C.22: temperature asymmetry vs temperature change over time 1st toe plot

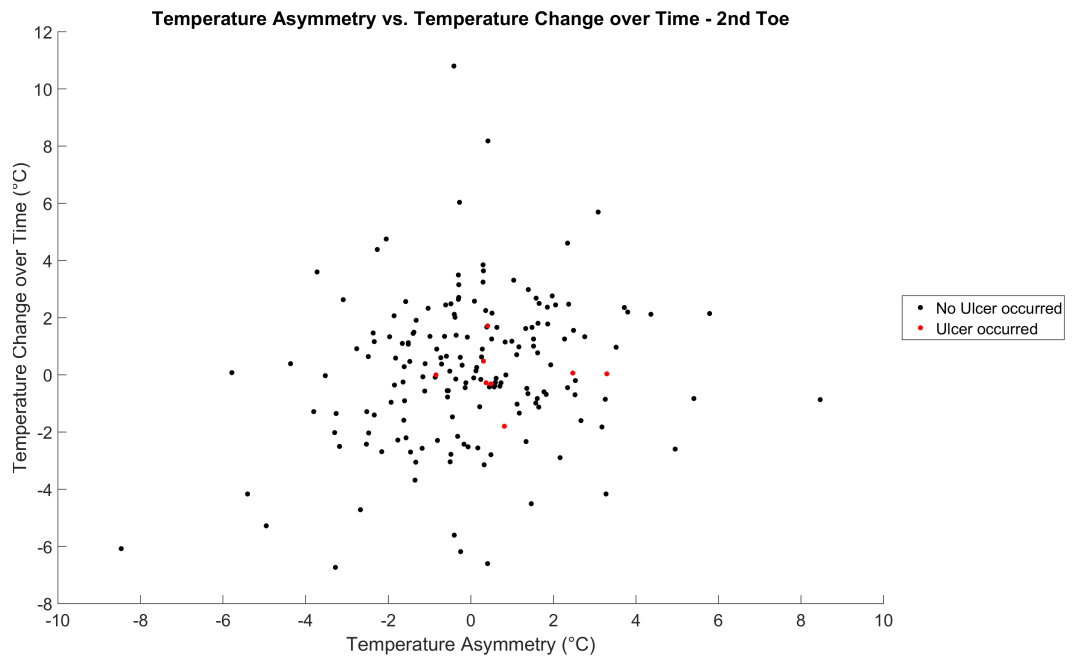


FIGURE C.23: temperature asymmetry vs temperature change over time 2nd toe plot

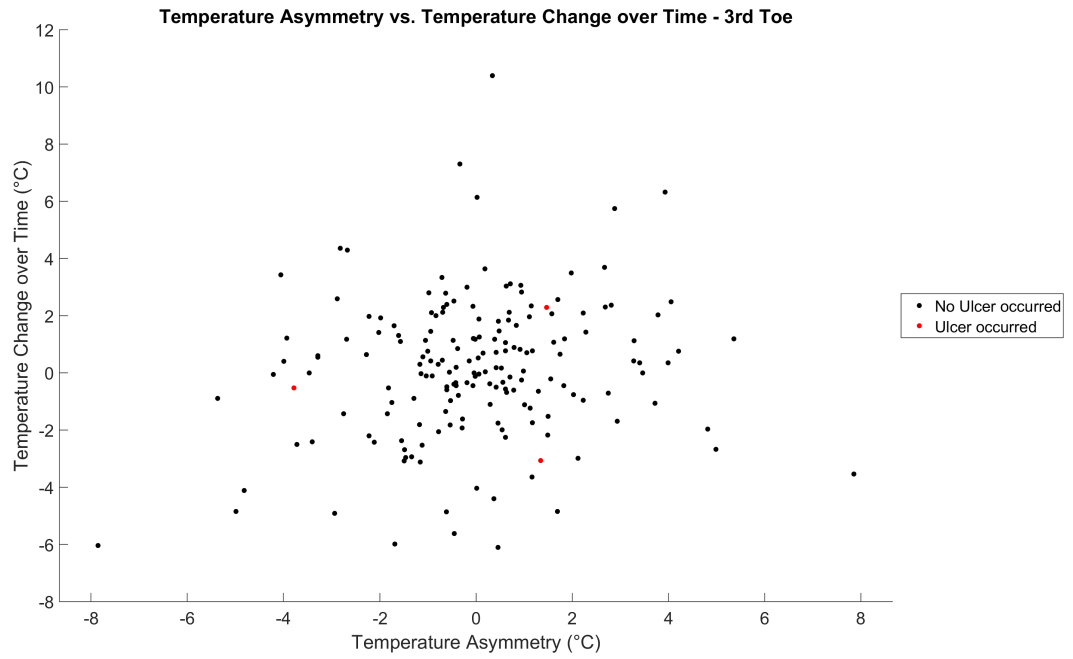


FIGURE C.24: temperature asymmetry vs temperature change over time 3rd toe plot

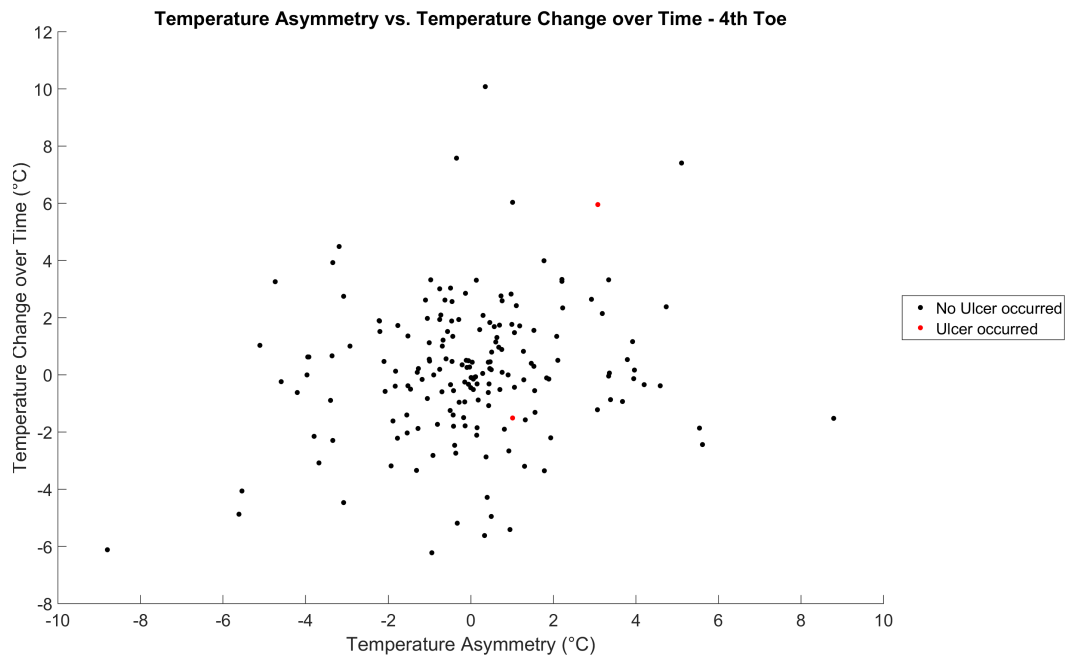


FIGURE C.25: temperature asymmetry vs temperature change over time 4th toe plot

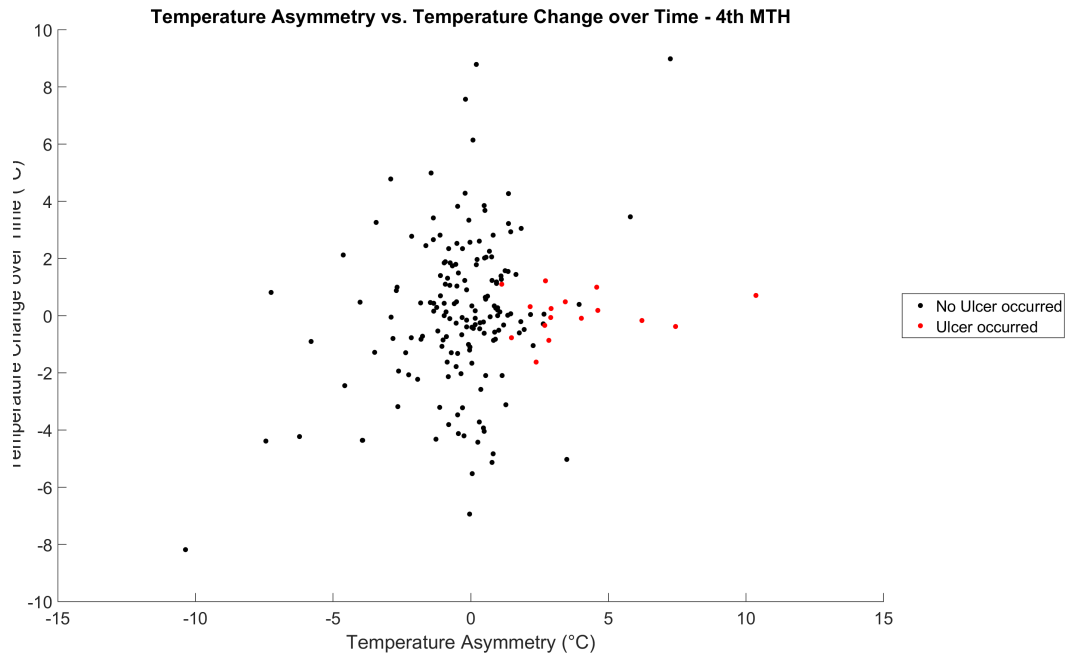


FIGURE C.26: temperature asymmetry vs temperature change over time 4th MTH plot

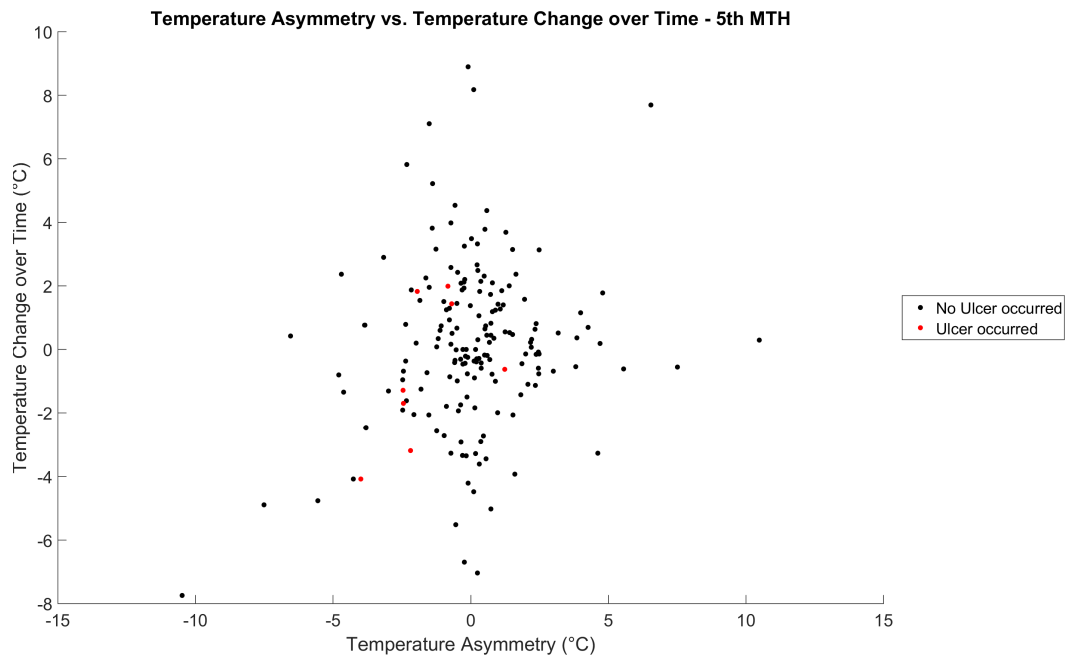


FIGURE C.27: temperature asymmetry vs temperature change over time 5th MTH plot

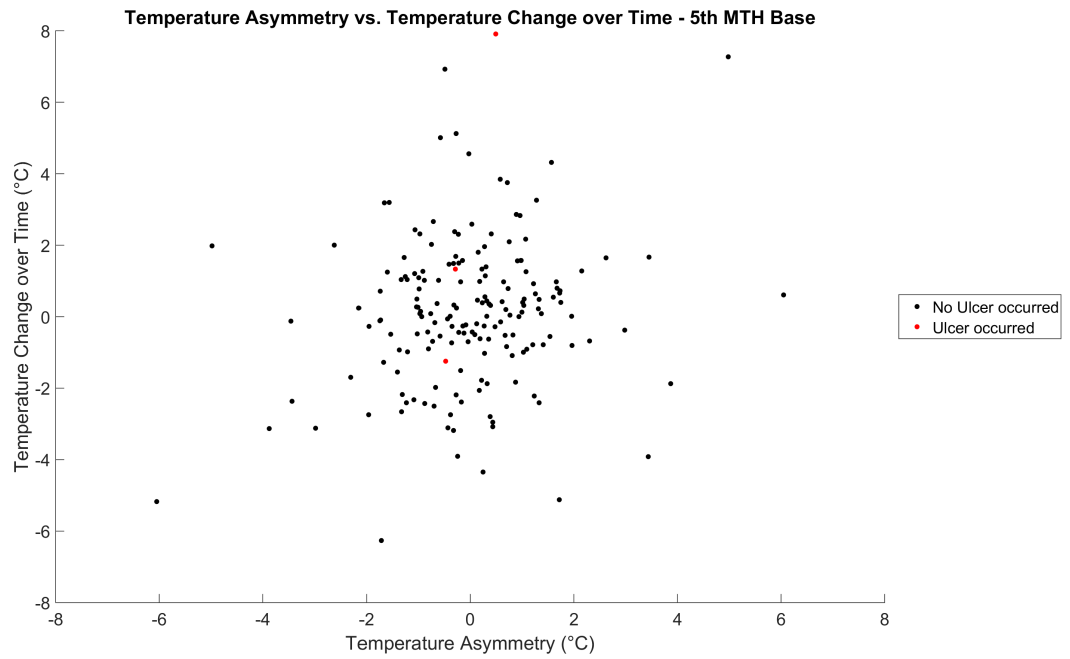


FIGURE C.28: temperature asymmetry vs temperature change over time 5th MTH Base plot

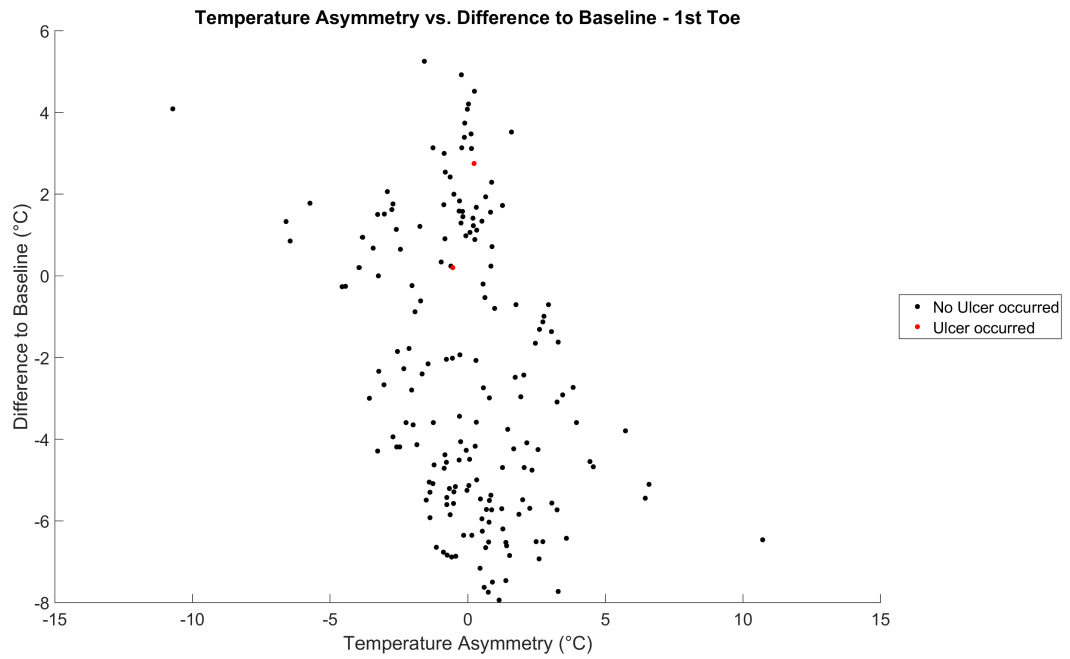


FIGURE C.29: temperature asymmetry vs difference to baseline 1st toe plot

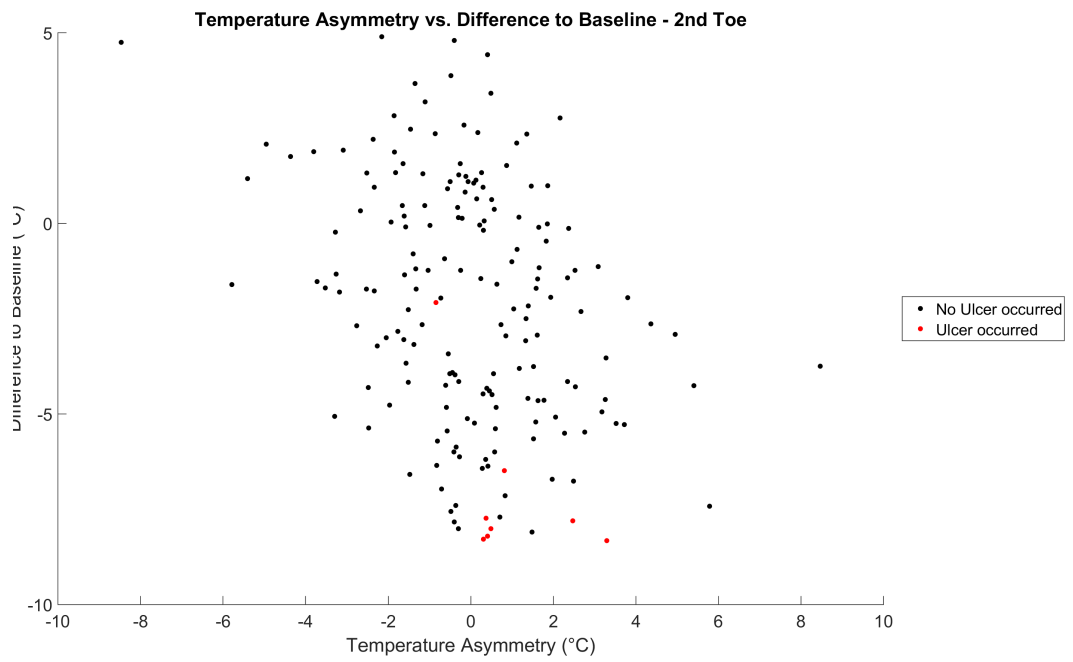


FIGURE C.30: temperature asymmetry vs difference to baseline 2nd toe plot

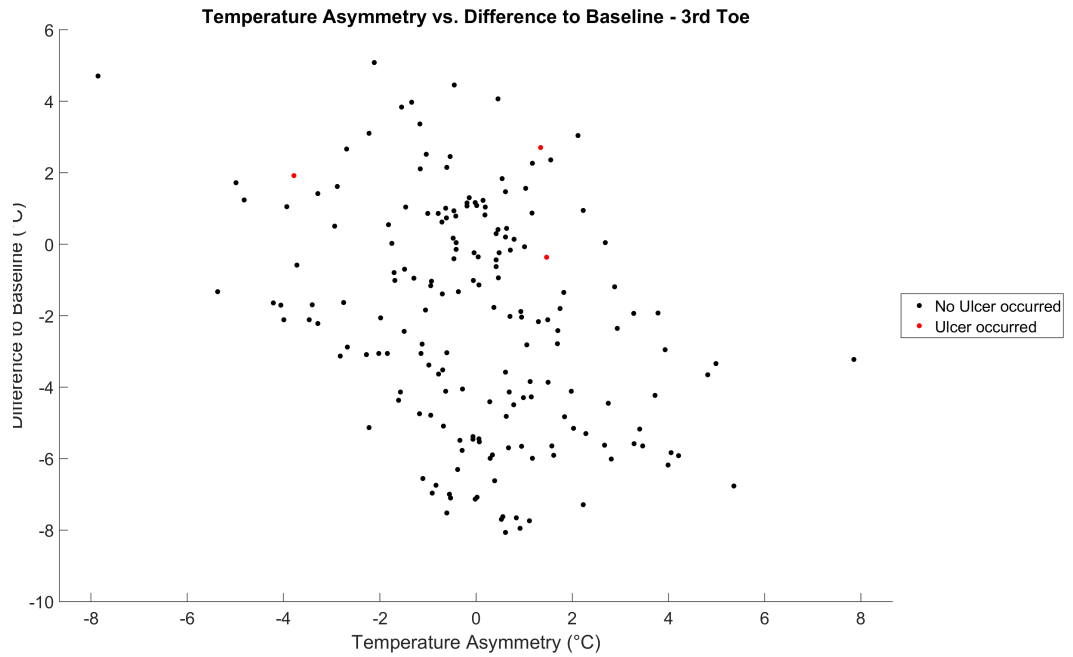


FIGURE C.31: temperature asymmetry vs difference to baseline 3rd toe plot

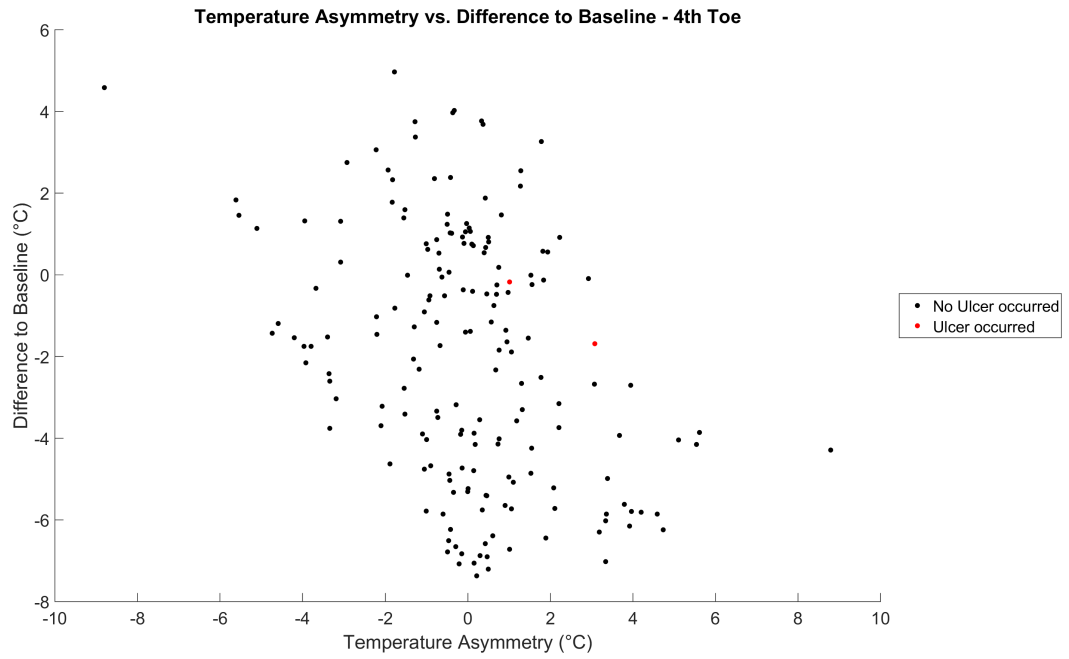


FIGURE C.32: temperature asymmetry vs difference to baseline 4th toe plot

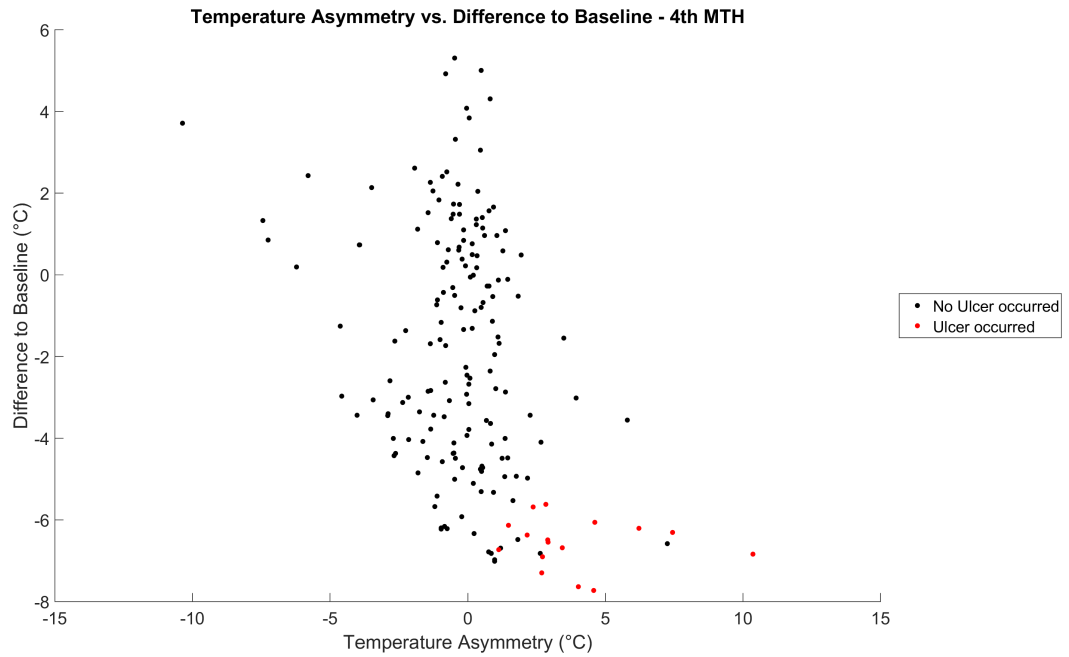


FIGURE C.33: temperature asymmetry vs difference to baseline 4th MTH plot



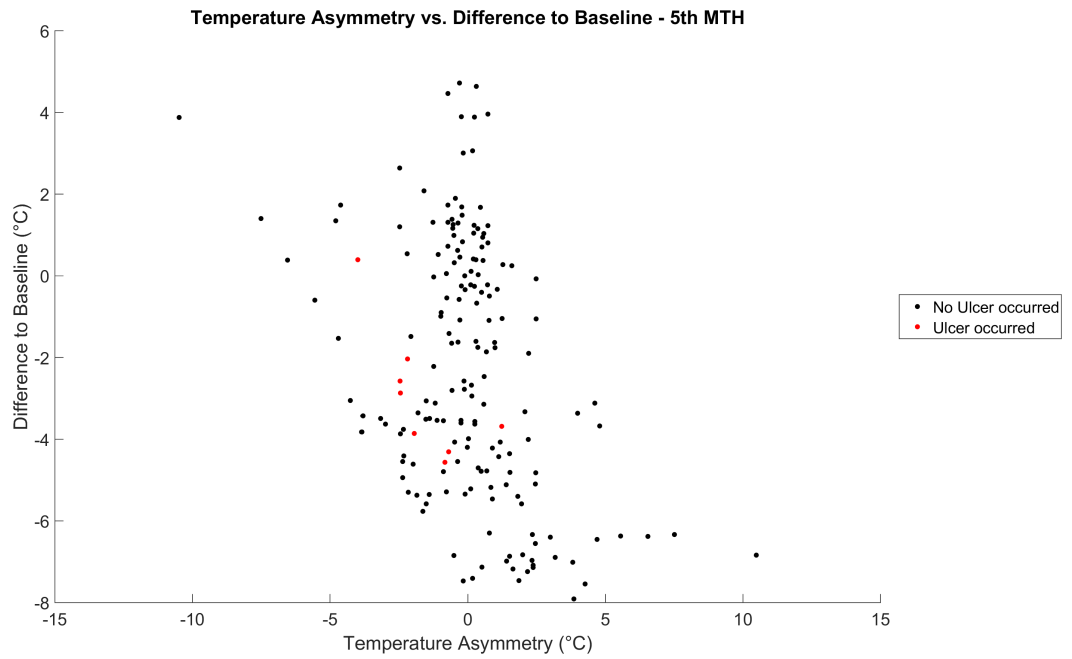


FIGURE C.34: temperature asymmetry vs difference to baseline 5th MTH plot

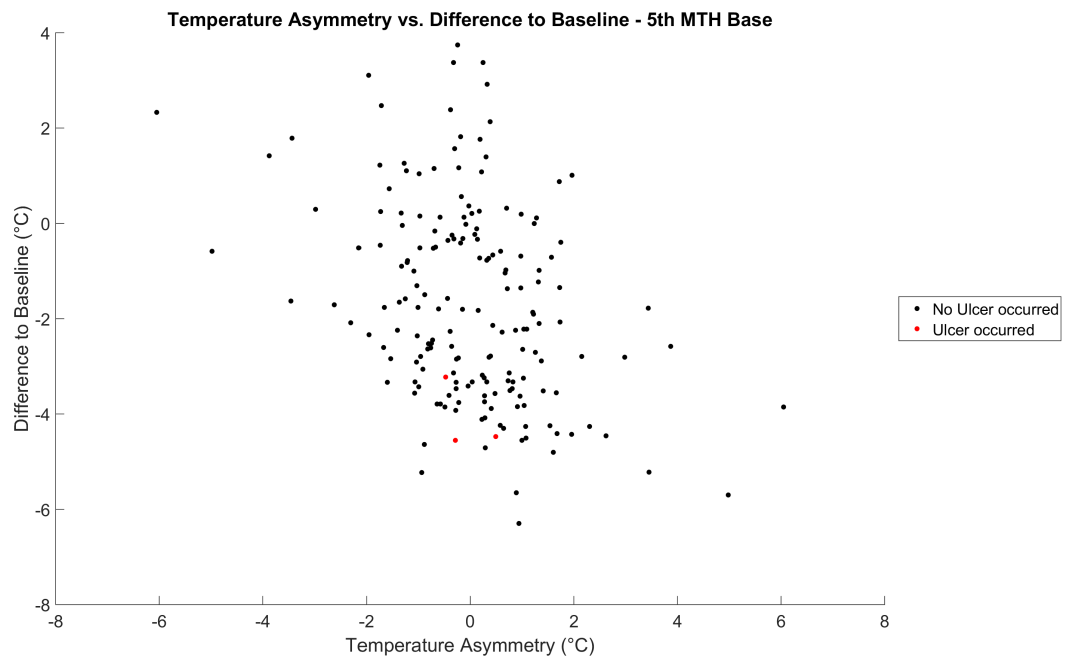


FIGURE C.35: temperature asymmetry vs difference to baseline 5th MTH Base plot

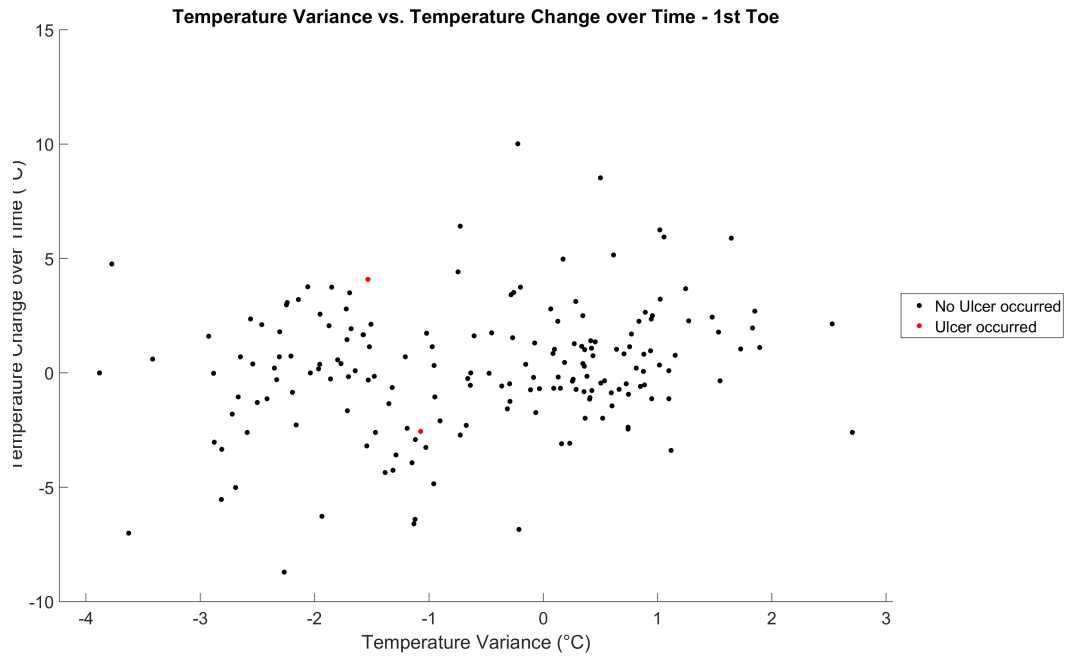


FIGURE C.36: temperature variance vs temperature change over time 1st toe plot

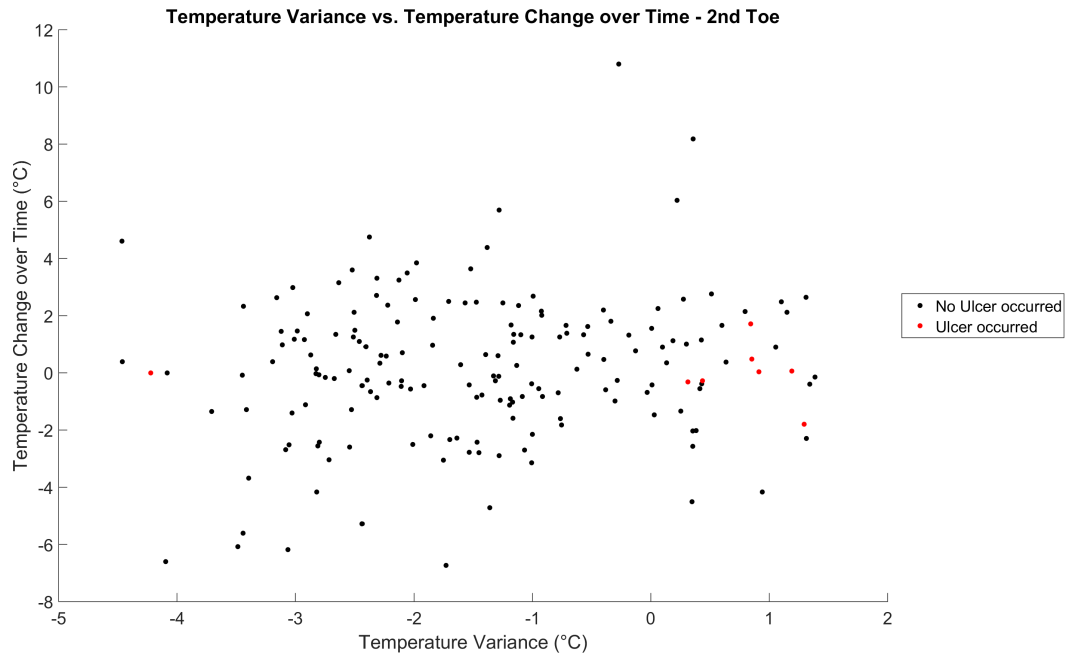


FIGURE C.37: temperature variance vs temperature change over time 2nd toe plot

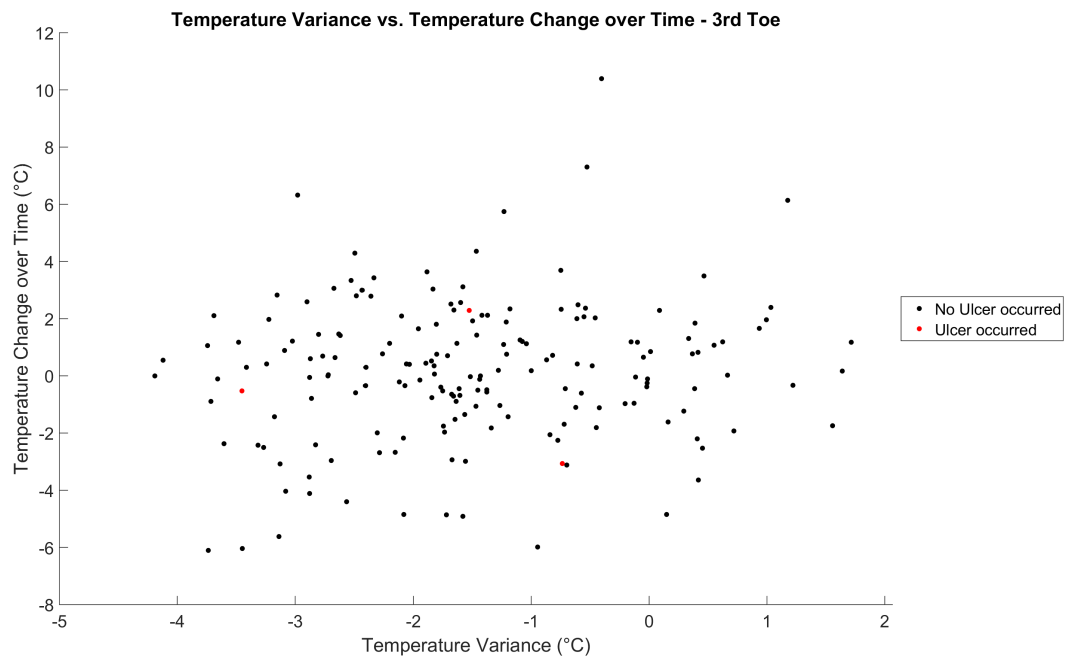


FIGURE C.38: temperature variance vs temperature change over time 3rd toe plot

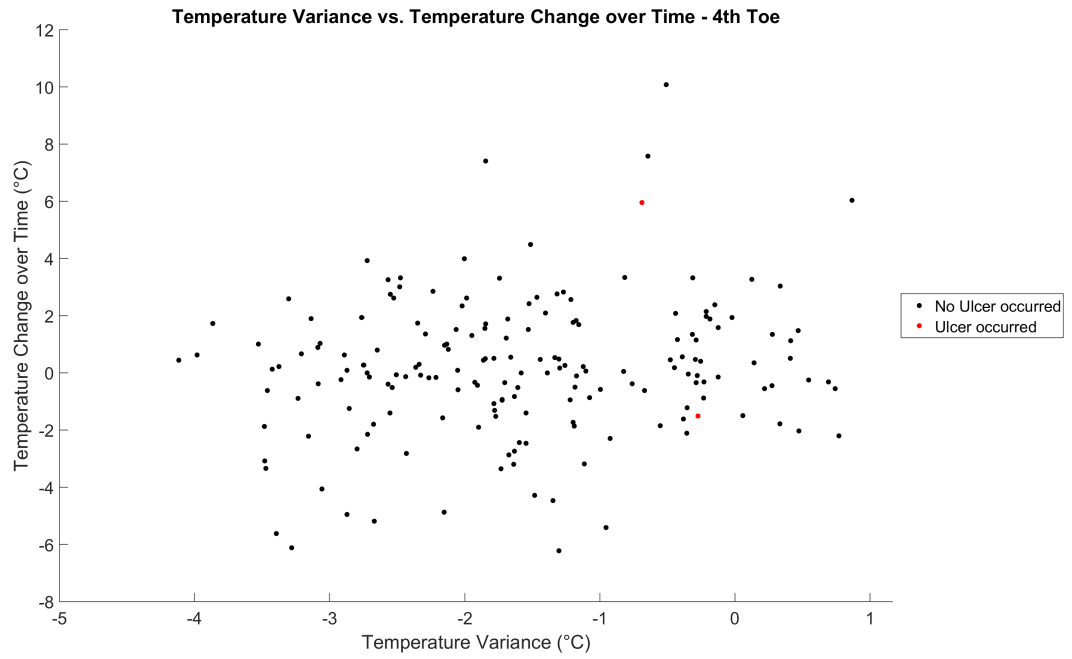


FIGURE C.39: temperature variance vs temperature change over time 4th toe plot

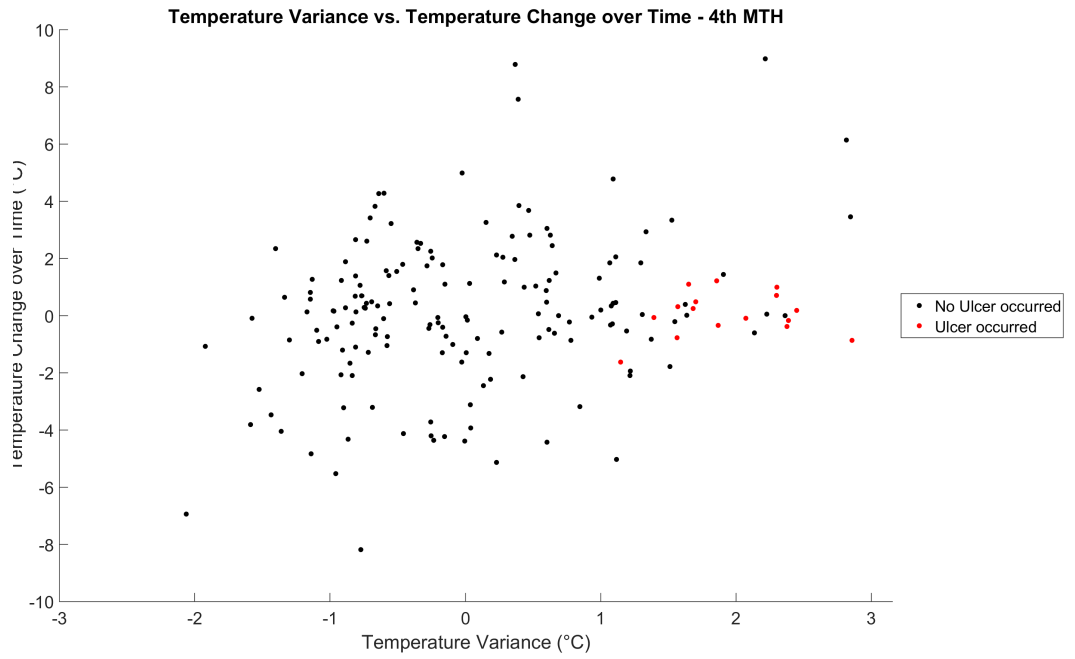


FIGURE C.40: temperature variance vs temperature change over time 4th MTH plot

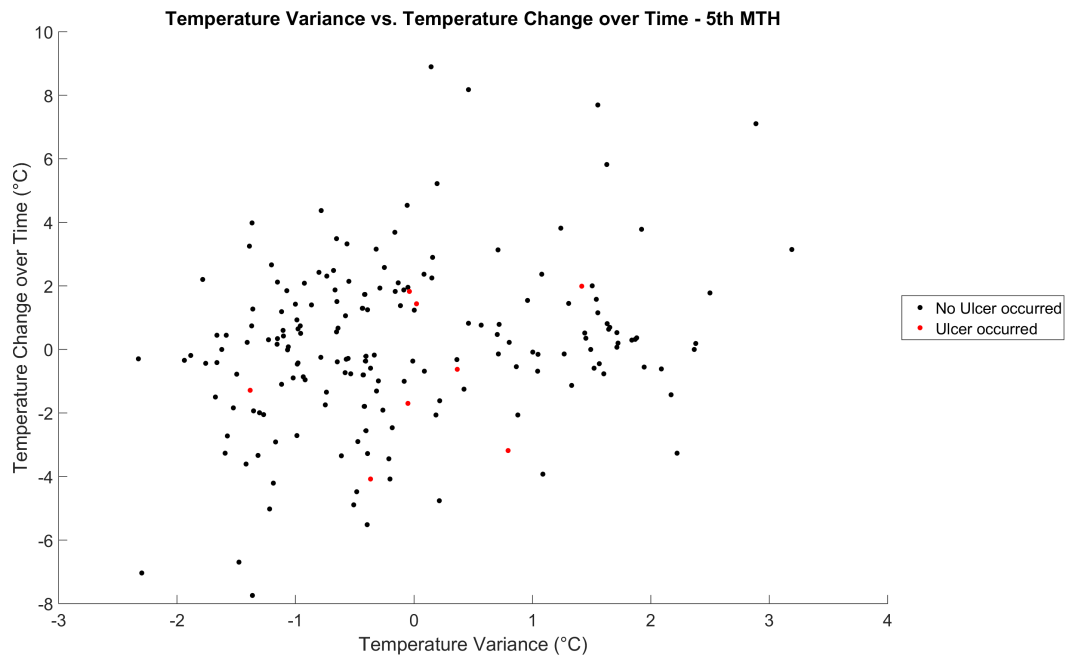


FIGURE C.41: temperature variance vs temperature change over time 5th MTH plot

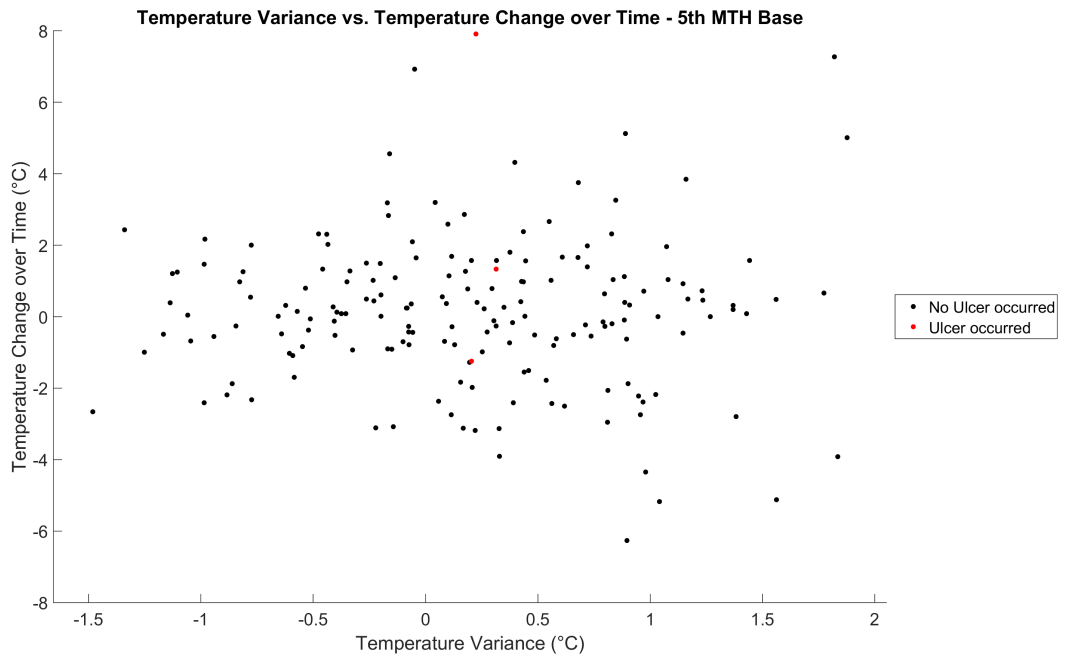


FIGURE C.42: temperature variance vs temperature change over time 5th MTH Base plot

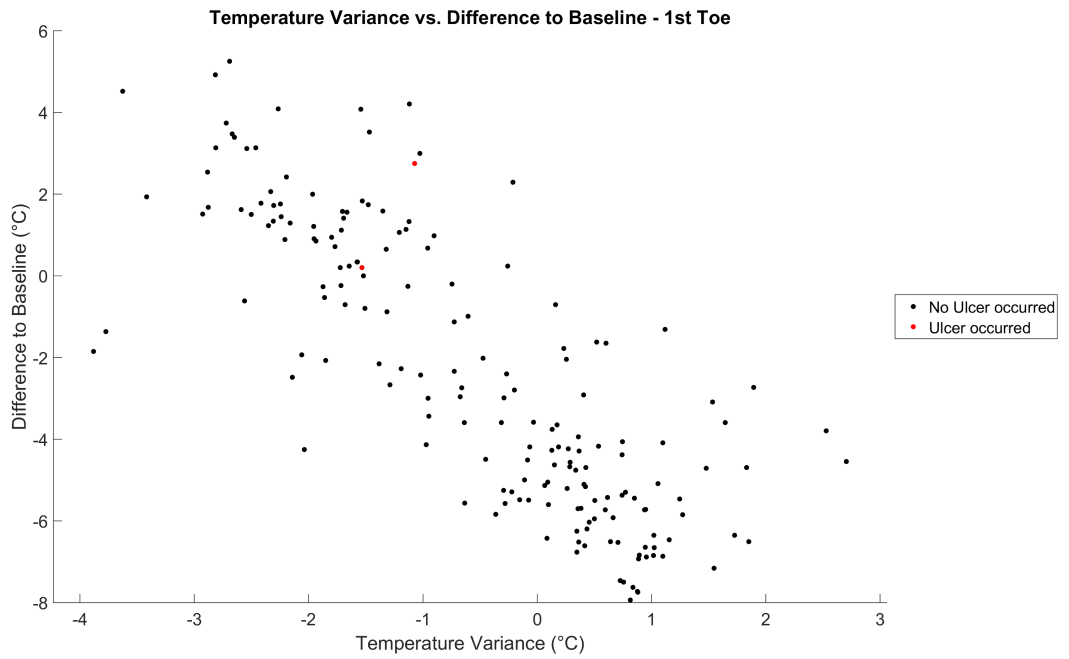


FIGURE C.43: temperature variance vs difference to baseline 1st toe plot

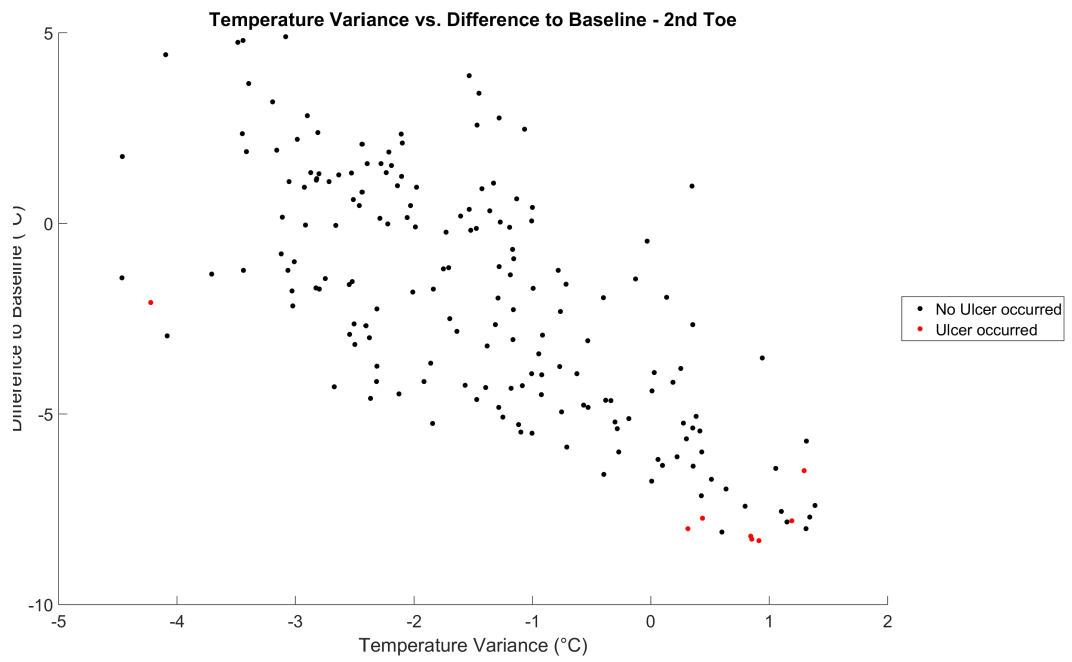


FIGURE C.44: temperature variance vs difference to baseline 2nd toe plot

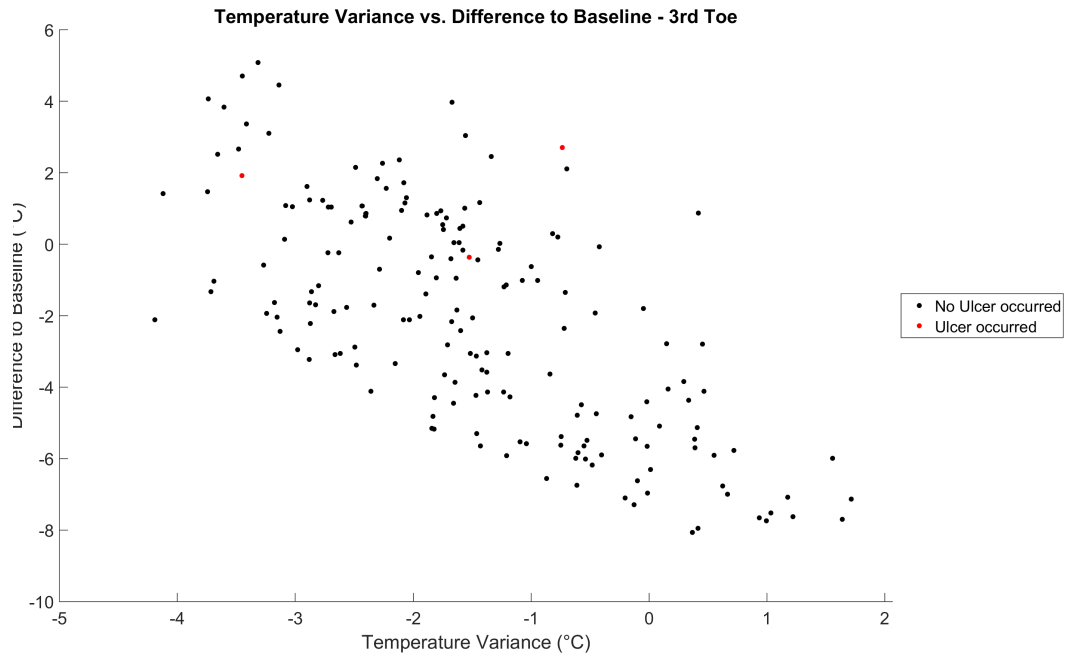


FIGURE C.45: temperature variance vs difference to baseline 3rd toe plot

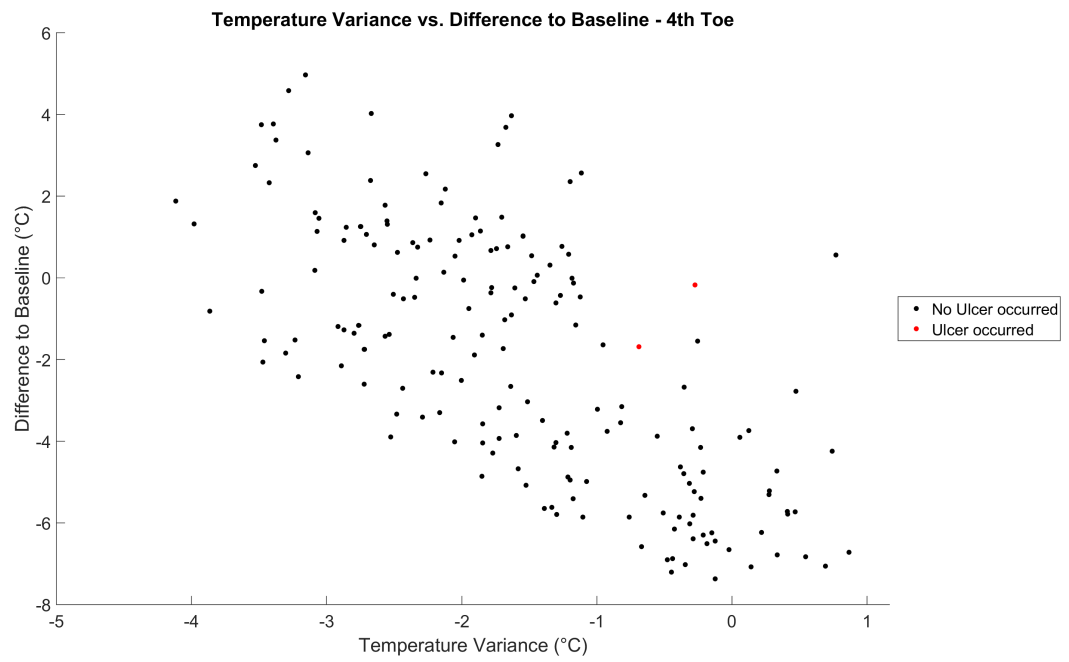


FIGURE C.46: temperature variance vs difference to baseline 4th toe plot

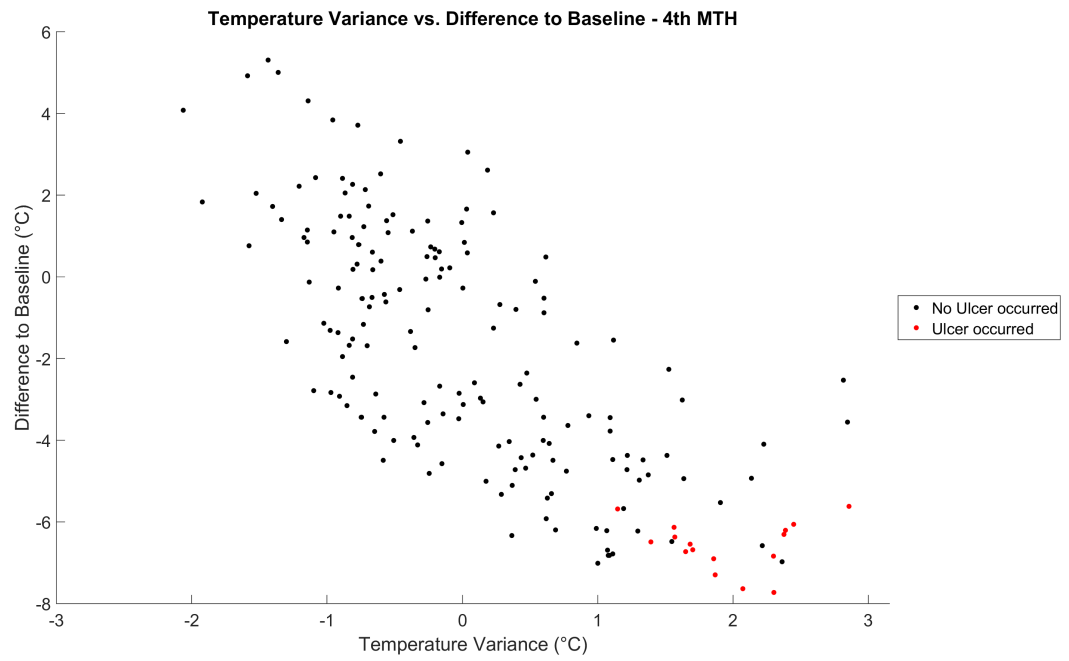


FIGURE C.47: temperature variance vs difference to baseline 4th MTH plot

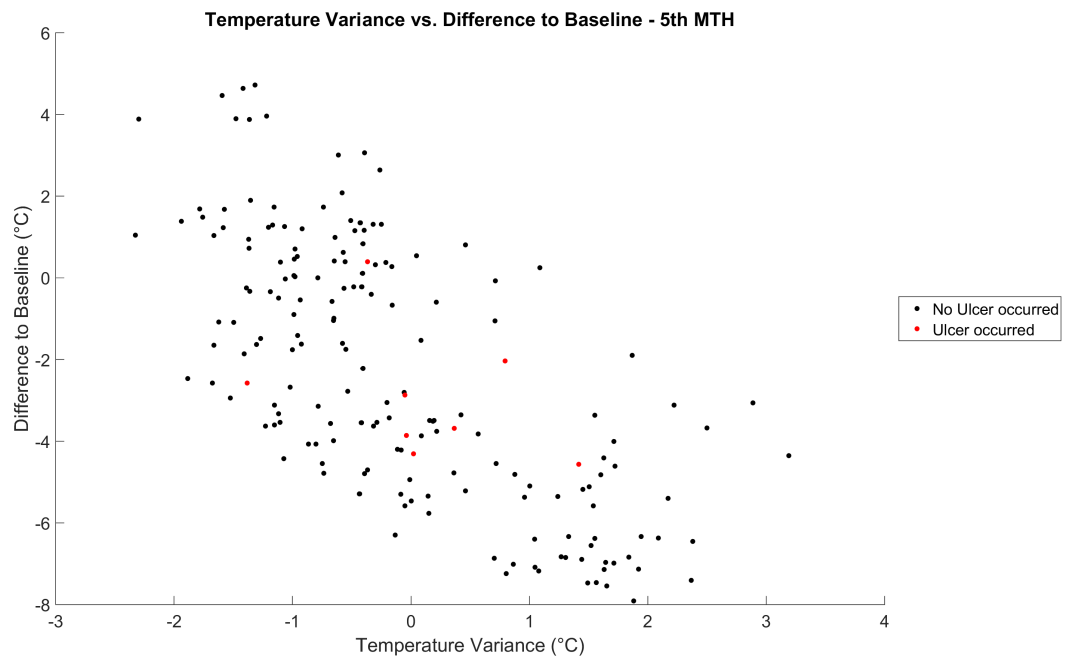


FIGURE C.48: temperature variance vs difference to baseline 5th MTH plot

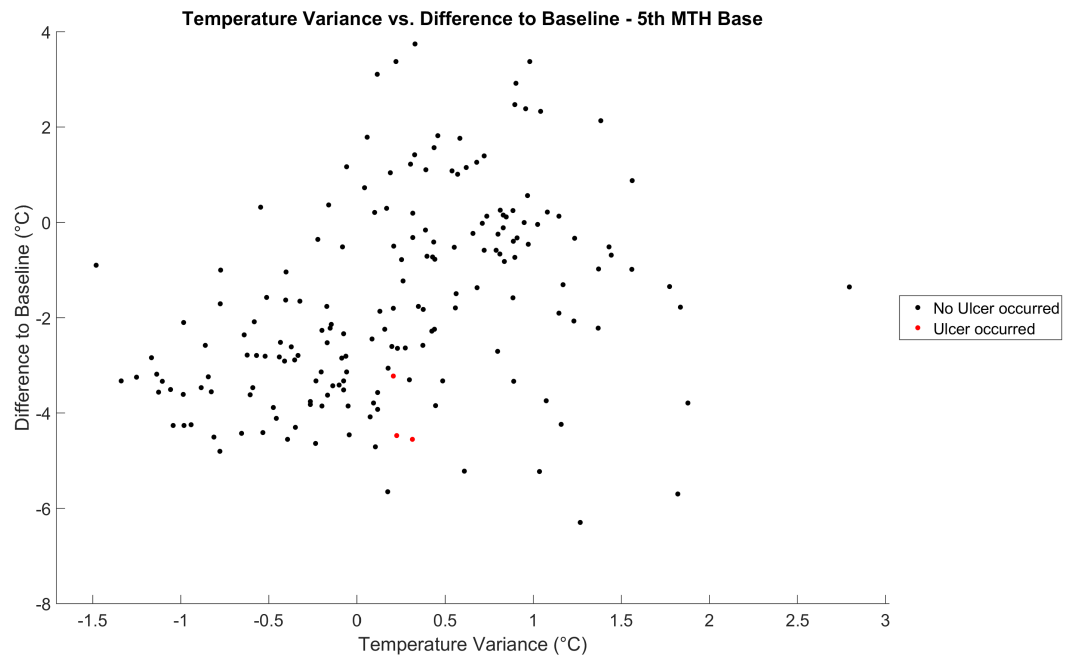


FIGURE C.49: temperature variance vs difference to baseline 5th MTH Base plot



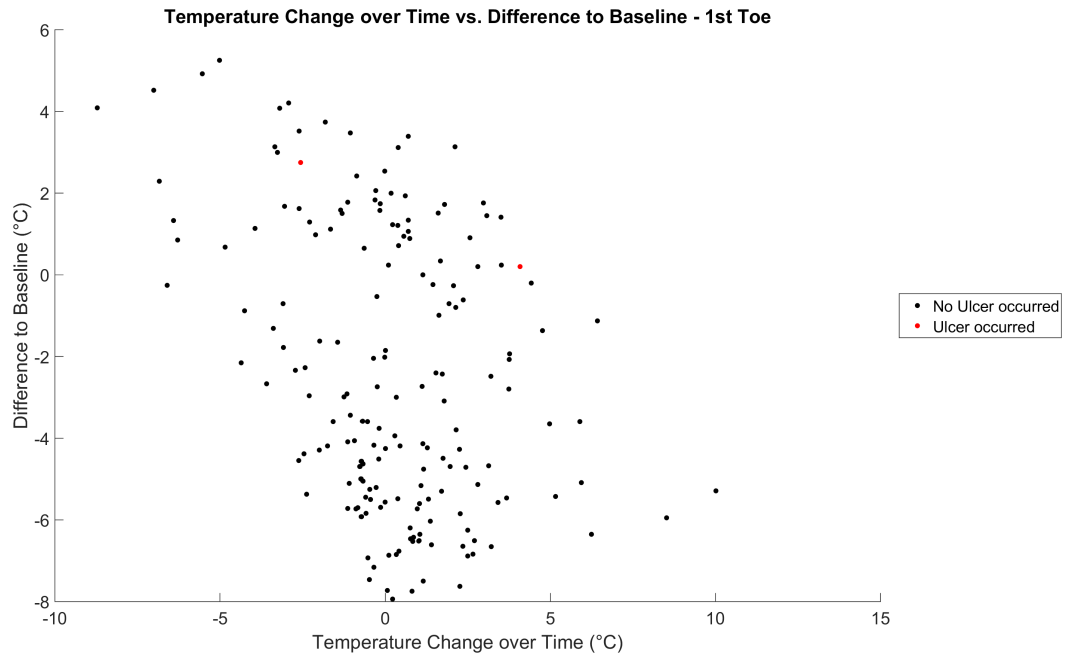


FIGURE C.50: temperature change over time vs difference to baseline 1st toe plot

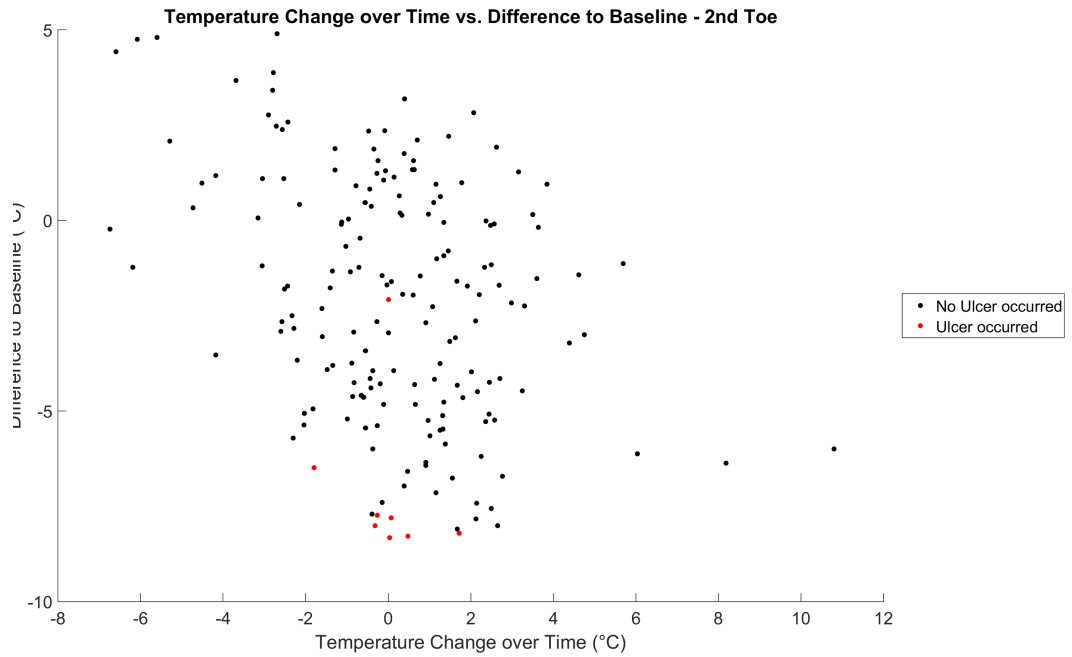


FIGURE C.51: temperature change over time vs difference to baseline 2nd toe plot

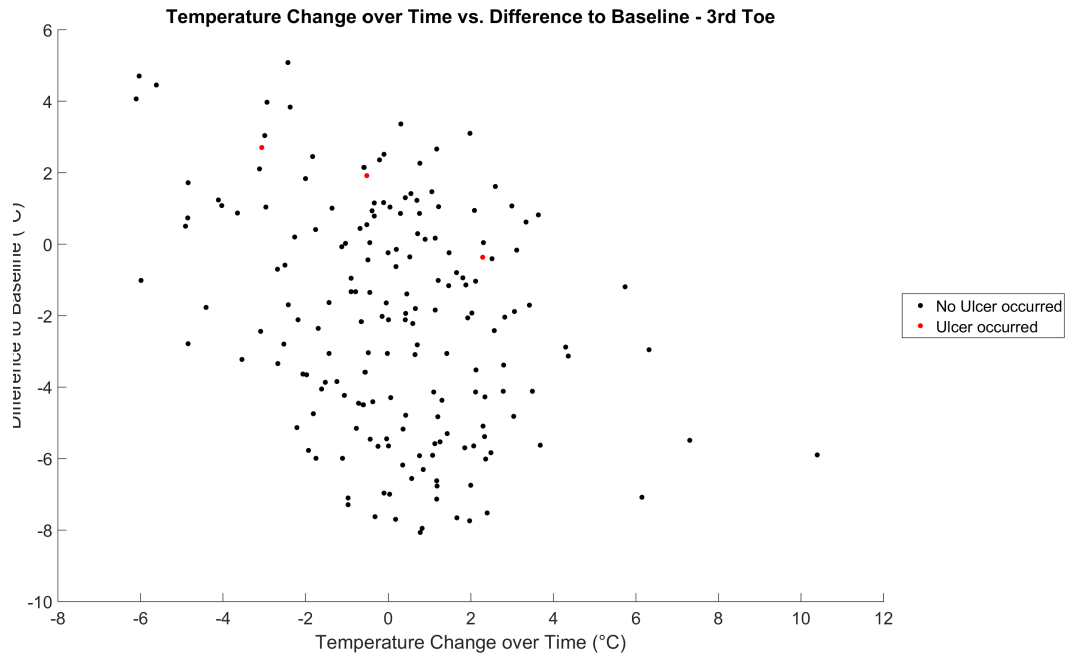


FIGURE C.52: temperature change over time vs difference to baseline 3rd toe plot

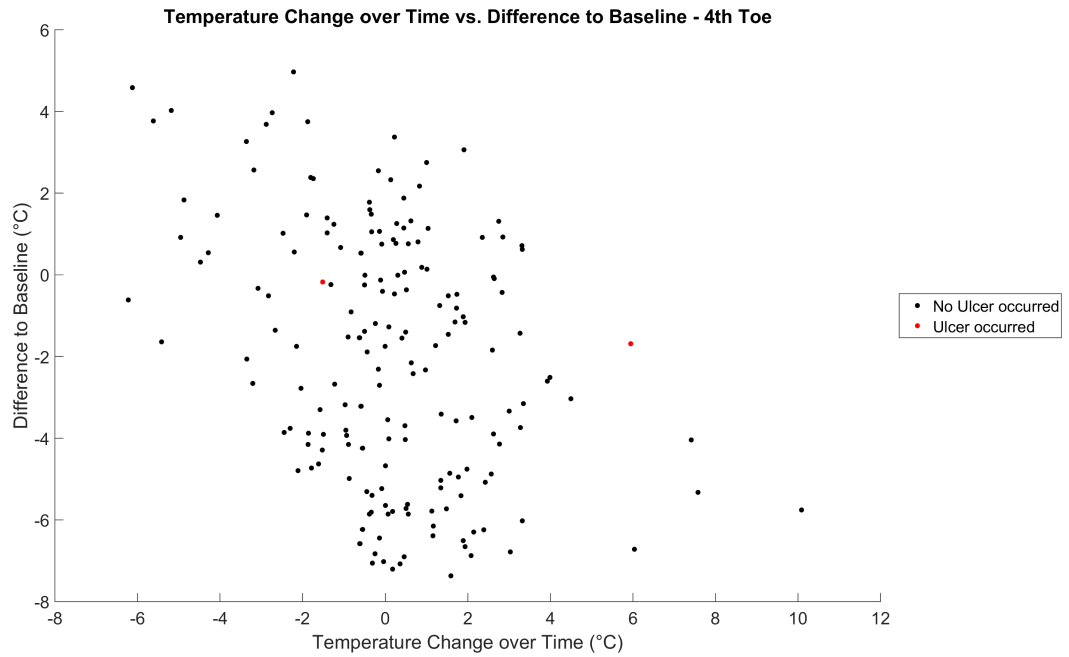


FIGURE C.53: temperature change over time vs difference to baseline 4th toe plot

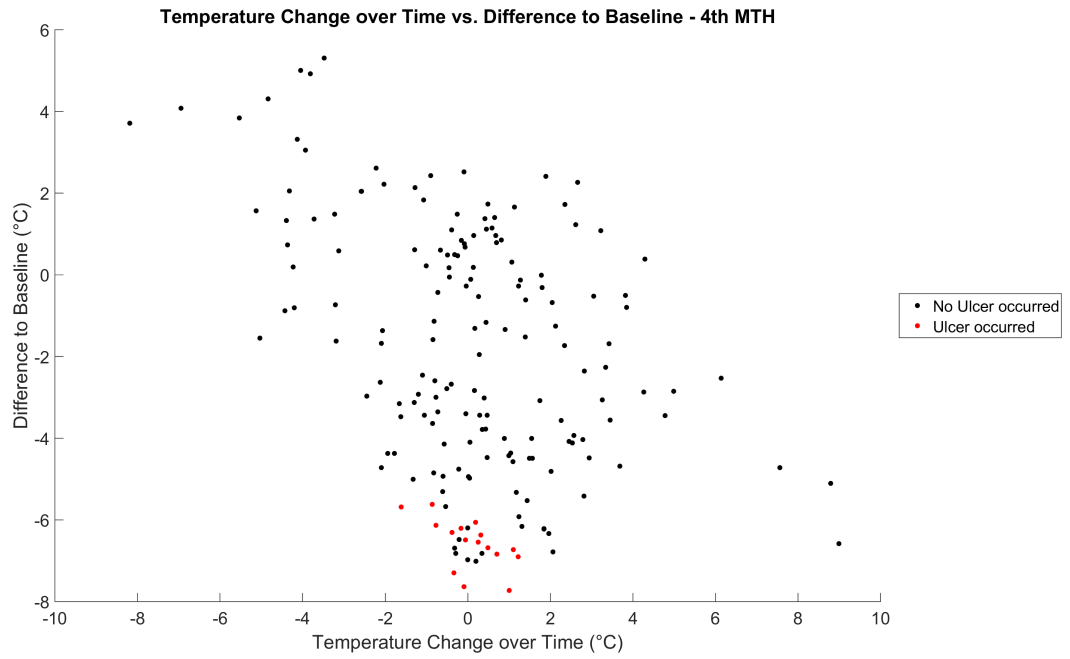


FIGURE C.54: temperature change over time vs difference to baseline 4th MTH plot

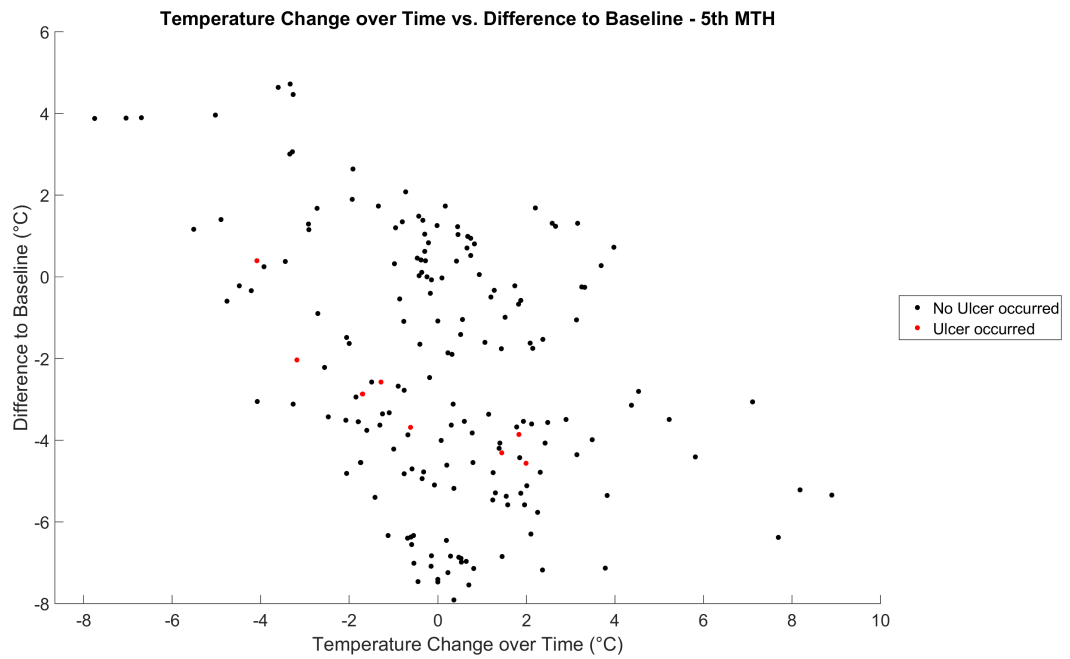


FIGURE C.55: temperature change over time vs difference to baseline 5th MTH plot

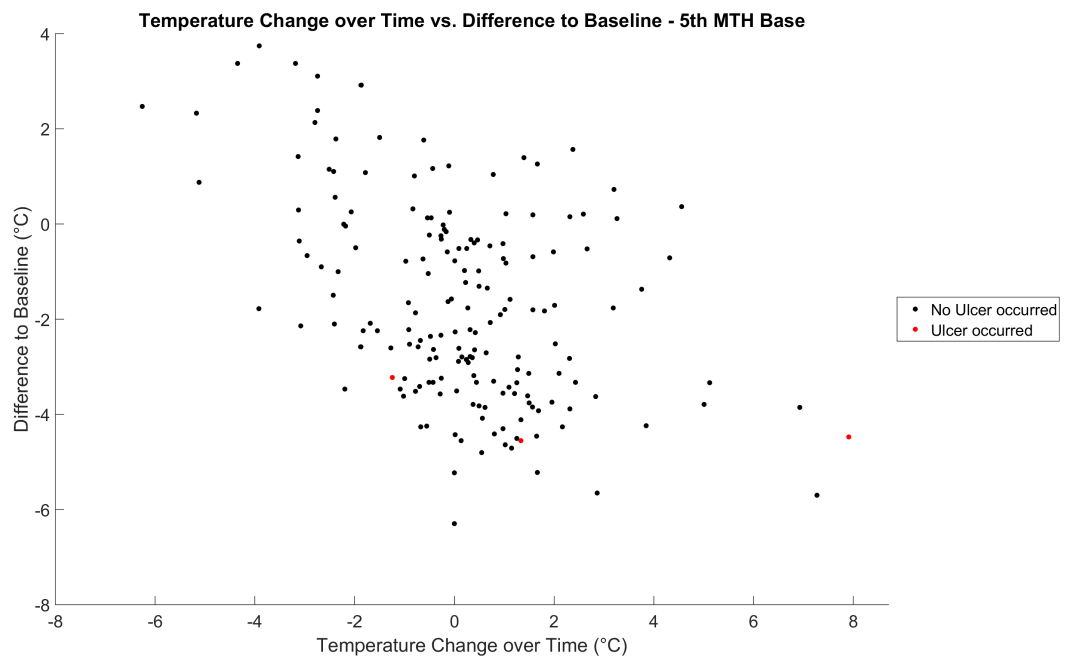


FIGURE C.56: temperature change over time vs difference to baseline 5th MTH Base plot

## Appendix D

# Appendix - Certificates of Contribution to Paper

# Certificate of Paper Contribution

## Title of Paper

"A medical thermal imaging system for the prevention of diabetic foot ulceration",  
Physiological Measurement, Volume 38, Number 3, published 3 February 2017

## Lead Author

Graham Machin, National Physics Laboratory *at*

## Other Authors

Aaron Whittam	National Physics Laboratory <i>at</i>
Suhail Ainarkar	Penine Acute Hospitals Trust
John Allen	Freeman Hospital Newcastle
John Bevans	Penine Acute Hospitals Trust
Mike Edmonds	Kings College Hospital London
Ben Kluwe	University of South Wales
Audrey Macdonald	Freeman Hospital Newcastle
Nina Petrova	Kings College Hospital London
Peter Plassmann	Photometrix Imaging Ltd.
Francis Ring	University of South Wales
Leon Rogers	National Physics Laboratory
Rob Simpson	National Physics Laboratory <i>at</i>

I hereby certify that Benjamin Kluwe, PhD Student at the University of South Wales, contributed the following aspects to the above mentioned paper:

1. The internal programming of the 'DFUPS' infra-red imaging device presented in the paper.
2. The programming of the Software used to analyse the images taken by the 'DFUPS' device.

6 Jul 17

Date

G. Machin

Signature of Lead Author

# Certificate of Paper Contribution

## Title of Paper

“Thermal symmetry of healthy feet: a precursor to a thermal study of diabetic feet prior to skin breakdown”, Physiological Measurement, Volume 38, Number 1, published 12 December 2016

## Lead Author

Audrey Macdonald, Freeman Hospital Newcastle

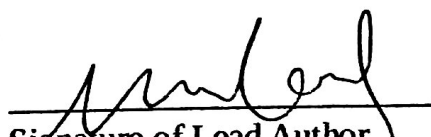
## Other Authors

Nina Petrova	Kings College Hospital London
Suhail Ainarkar	Penine Acute Hospitals Trust
John Allen	Freeman Hospital Newcastle
Peter Plassmann	Photometrix Imaging Ltd.
Aaron Whittam	National Physics Laboratory
John Bevans	Penine Acute Hospitals Trust
Francis Ring	University of South Wales
Ben Kluwe	University of South Wales
Rob Simpson	National Physics Laboratory
Leon Rogers	National Physics Laboratory
Graham Machin	National Physics Laboratory
Mike Edmonds	Kings College Hospital London

I hereby certify that Benjamin Kluwe, PhD Student at the University of South Wales, contributed the following aspects to the above mentioned paper:

1. The internal programming of the 'DFUPS' infra-red imaging device used to take the thermal images presented in the paper.
2. The programming of the Software used to analyse the images taken by the 'DFUPS' device.

6/7/2017  
Date

  
Signature of Lead Author

## Appendix E

# Appendix - Study Protocols



# **Protocol title: i4i NIHR An Innovative System for the Early Identification, Monitoring, Evaluation and Diagnosis of Diabetic Foot Ulcers**

## **1.1 Trial Identifiers**

REC Number –

## **1.2 Sponsor**

Name: King's College Hospital NHS Foundation Trust

Address: Denmark Hill, London SE5 9RS, UK

### **1.2.1 Sponsor Contact**

Dr Zoe Harris, Manager R&D

The Research Office

King's College Hospital NHS Foundation Trust

161 Denmark Hill

SE5 8EF

Telephone: 020 7188 3841

Email: [z.harris@nhs.net](mailto:z.harris@nhs.net)

### **1.2.2 Chief Investigator**

Name: Dr Michael Edmonds, Professor of Diabetic Foot Medicine

Address: Diabetic Foot Clinic, King's College Hospital, Denmark Hill, London, SE5 9RS

Telephone: 0203 299 3223

Fax: 0203 299 4536

Email: Michael.edmonds@nhs.net

### **1.2.3 Name and address of Co-Investigator(s), Statistician, Laboratories etc**

Name: Dr Nina Petrova,

Address: Diabetic Foot Clinic, King's College Hospital, Denmark Hill, London, SE5 9RS

Telephone: 0203 299 5124

Fax: 0203 299 4536

Email: [nina.petrova@nhs.net](mailto:nina.petrova@nhs.net)

Dr Nora Donaldson, Professor of Biostatistics

Address: Biostatistics Unit, KCL Dental Institute Denmark Hill Campus.

Dental Surgery Building. Office 209

Telephone: 020 32901654

Email: [Nora.Donaldson@kcl.ac.uk](mailto:Nora.Donaldson@kcl.ac.uk)

Name: Professor Graham Machin, Head, Temperature Standards, NPL Fellow

Address: National Physical Laboratory,

Temperature Group, Hampton Road

Teddington, Middlesex, United Kingdom

Post Code TW11 0LW

Phone number +44 0208 943 6742

Email [graham.machin@npl.co.uk](mailto:graham.machin@npl.co.uk)

Name: Dr Robert Simpson

Address: National Physical Laboratory,

Temperature Group, Hampton Road

Teddington, Middlesex, United Kingdom

Post Code TW11 0LW

Name: Dr Leon Rogers

Address: National Physical Laboratory,

Temperature Group, Hampton Road

Teddington, Middlesex, United Kingdom

Post Code TW11 0LW

Name: Aaron Whittam

Address: National Physical Laboratory,

Temperature Group, Hampton Road

Teddington, Middlesex, United Kingdom

Post Code TW11 0LW

Name: Dr John Bevans

Address:

Name: Dr John Allen

Address:

Name: Professor Francis Ring

Address:

Name: Dr Peter Plassmann

Address:

## 1.3 Background & Rationale

The global burden of diabetes is well recognised. At present, it is estimated that 382 million people have diabetes and by 2035 it is predicted that diabetes will affect 592 million people (<http://www.idf.org/diabetesatlas/introduction>). Diabetic neuropathy (nerve damage to the feet) is a common complication of diabetes. The lack of pain and the loss of protective sensation to the feet of people with diabetes puts them at risk of foot ulceration. These ulcers can become infected, seriously affect the patient's quality of life and increase the risk of amputation. Diabetic foot ulcer management requires significant resources. Early recognition of foot ulceration and timely management is critical to avoid adverse outcomes.

Current guidelines recommend the early identification of risk, based on foot screening and targeting of preventative interventions to 'high-risk' individuals. Prior to breakdown of the skin, at the start of an ulcer, an inflammatory state is developed which is characterised by a rise in local skin temperature<sup>i</sup>. The areas at risk may present with redness, thickness, warmth and swelling. Thermal imaging can be a valuable technology in the prevention and early identification of diabetic foot ulceration as it can detect areas at risk prior skin breakdown. Recently, the potential therapeutic benefit of temperature monitoring with single spot infra-red thermometry has been evaluated in a randomized controlled trial. A high-risk group of patients with previous history of neuropathic ulceration were randomised to either self-skin temperature monitoring and standard care or to standard care alone. There was a significant reduction in the ulcer reoccurrence rate in the active group compared with the control group (8% in the active group versus 30% in the control group,  $p < 0.05$ )<sup>ii</sup>. The patients in the control group were more than 4 times more likely to develop ulcers compared with patients in the active group during a 15 month follow up<sup>ii</sup>. Although its potential benefit, thermal imaging has not yet become a widely used method in clinical practice. At present, mainly single spot thermometers are used in clinical practice, which measure temperature only above the scanned area and do not provide information of the surrounding areas. Furthermore, an incipient lesion may also be characterised by a rise of skin foot temperature but is not obviously visible on clinical examination. Therefore, a thermal image of the feet will allow full examination and early detection of areas at risk.

It is now possible with recent advances in thermal imaging and image analysis to produce a low-cost clinical device that can generate temperature maps of the patient's feet. These maps can be used by clinicians to identify areas at risk of ulceration, presenting with a temperature rise.

Recently, a new non-invasive infrared thermal camera has been developed (diabetic foot ulcer prevention system (DFUPS)). Thermal imaging of a small sample of feet in healthy subjects has been carried out with this instrument under laboratory condition to assess the following specification requirements: temperature range/resolution, required spatial resolution and performance (stability/accuracy). Early data has shown that this instrument is robust, easy to use and can record repeatable measurements.

We propose to evaluate this instrument in a clinical setting by studying healthy volunteers.

## 1.4 Trial Objectives and Design

### 1.4.1 Trial Objectives

The main objectives are:

- To evaluate the usefulness of DFUPS in a clinical setting
- To iterate the design of the instrument.

In particular, the aim is to detect detailed temperature readings of the feet of healthy volunteers and to analyse temperature distribution by creating temperature maps. This novel instrument will be compared with "gold standard" single spot thermometry (Dermatemp 1001, Exergen). A detailed skin foot temperature measurement protocol will be developed which can be translated into clinical practice and used in the assessment of diabetic patients at risk of foot ulceration.

### **1.4.2 Trial design**

This is a multicentre study of healthy volunteers who will be recruited at 3 clinical sites.

1. Diabetic Foot Clinic, Kings College Hospital NHS Foundation Trust
2. Department of .... ; Freeman Hospital, Newcastle upon Tyne
3. Department of .....North Manchester General Hospital

The study will involve skin foot temperature measurements with the proposed prototype (DFUPS) and the current gold standard thermometry Dermatemp 1001 in a group of 100 healthy volunteers.

### **1.5 Selection of participants:**

Members of staff, relatives and friends will be invited to take part in the study. A letter/email of invitation will be sent. There will be also a poster in the clinic waiting area and eligible participants will be also invited.

The study volunteers will be invited to take part in the study and will be enrolled only after they have agreed to take part by making an informed consent and by signing a consent form.

#### **1.5.1 Inclusion criteria**

A subject will be eligible for study participation if he or she meets the following criteria:

1. Aged 18 years or older (We agreed to study predominantly subjects between 40-75 years old, however, I suggest to have age >18 for the protocol to avoid "screening failure" due to someone being younger than 40).
1. Has no history of diabetes
2. Has no previous history of foot ulceration
3. Has no previous history of foot surgery
4. Has palpable foot pulses on both feet (palpable posterior tibial artery or dorsal pedal artery or both)
5. Has no history of peripheral neuropathy
6. Has no history of peripheral arterial disease
7. Must be able to provide meaningful written informed consent for the study

#### **1.5.2 Inclusion criteria**

A subject will be excluded from the study if he or she meets the following exclusion criteria

1. Has active foot ulceration and infection
2. Has foot deformity which in the opinion of the Investigator, would interfere with interpreting the results of the study
3. Has any uncontrolled illness that, in the opinion of the Investigator, would interfere with interpreting the results of the study

#### **1.5.3 Selection of participants**

All participants will be recruited over a period of 6 months. A total of 100 participants will be recruited between the three clinical centres.

#### **1.5.4 Trial procedures**

All subjects will be seen at one visit by the study investigator. The following procedures will be performed at the research visit.

1. Obtain written informed consent
2. Assign a subject number
3. Review inclusion/ exclusion criteria
4. Record demographics (age and gender)

5. Brief medical history to rule out diabetes, past medical history of foot ulceration/ foot surgery, peripheral neuropathy; history of peripheral artery disease
6. Foot check to ensure that the feet are intact and the person has palpable foot pulses.
  - a. Check plantar, dorsal, lateral and medial part of the foot for any lesion;
  - b. check for lesions between the toes
  - c. palpate pulses at the posterior tibial artery or dorsal pedal artery; if one of the pulses is present then the person can be recruited in the study )
7. Perform skin foot temperature measurements

All subjects should be seen in a temperature controlled room (air-conditioned room set at 21 °C). Subjects will be asked to lie down in supine position on a treatment couch and will be asked to take off their shoes and socks. They will be asked to rest quietly for 10 minutes to allow equilibration of foot temperature.

Skin foot temperatures of the right and left foot will be measured.

- a) Temperature measurement with DFUPS (to follow)

Subjects will be instructed to place their feet in XXXXX position

Foot protocol measurement:

Sites: ( plantar site, dorsal site, media part of the foot; lateral part of the foot)

Position of camera;

Specifications (light in the room, heating source??? Etc.)

Image analysis:

Temperature assessment of regions of interest?

- b) Temperature measurement with Dermatemp 1001.

The Dermatemp 1001 thermometer is a non-contact thermometer which measures radiated heat. It should be set at the MAX mode and held perpendicular to the scanned area. The reading at the display show the maximum temperature of the scanned area (scanned area ≤ size of a 10 pence coin).

The following areas should be scanned and the readings should be recorded in degrees Centigrade. :

REGION OF INTEREST:	Right foot Degree (C)	Left foot Degree (C)	Temperature difference (ΔT)
<b>PLANTAR:</b>			
a. 1 <sup>st</sup> toe			
b. 2 <sup>nd</sup> toe			
c. 3 <sup>rd</sup> toe			
d. 4 <sup>th</sup> toe			
e. 5 <sup>th</sup> toe			
f. 1 <sup>st</sup> metatarsal head			
g. 2 <sup>nd</sup> metatarsal head			
h. 3 <sup>rd</sup> metatarsal head			
i. 4 <sup>th</sup> metatarsal head			
j. 5 <sup>th</sup> metatarsal head			
k. 5 <sup>th</sup> metatarsal base			
l. Heel			
<b>DORSAL</b>			
m. 1 <sup>st</sup> toe			
n. 2 <sup>nd</sup> toe			
o. 3 <sup>rd</sup> toe			
p. 4 <sup>th</sup> toe			
q. 5 <sup>th</sup> toe			
r. 1 <sup>st</sup> metatarsal/ phalangeal joint			

s.	2 <sup>nd</sup> metatarsal/ phalangeal joint			
t.	3 <sup>rd</sup> metatarsal/ phalangeal joint			
u.	4 <sup>th</sup> metatarsal/ phalangeal joint			
v.	5 <sup>th</sup> metatarsal/ phalangeal joint			
w.	5 <sup>th</sup> metatarsal/ phalangeal joint			
x.	1 <sup>st</sup> metatarsal/ tarsal joint			
y.	2 <sup>nd</sup> metatarsal/ tarsal joint			
z.	3 <sup>rd</sup> metatarsal/ tarsal joint			
aa.	4 <sup>th</sup> metatarsal/ tarsal joint			
bb.	5 <sup>th</sup> metatarsal/ tarsal joint			
<b>MEDIAL</b>				
cc.	1 <sup>st</sup> metatarsal/ phalangeal joint			
dd.	1 <sup>st</sup> metatarsal base			
ee.	Medial malleolus (over bony prominence)			
<b>LATERAL</b>				
ff.	5 <sup>th</sup> metatarsal/ phalangeal joint			
gg.	5 <sup>th</sup> metatarsal base			
hh.	Lateral malleolus (over bony prominence)			

The skin foot temperature measurement with the Dermatemp and with the DFUPS will be repeated three times as following:

1. DFUPS measurement
2. Dermatemp 1001
3. DFUPS measurement
4. Dermatemp 1001
5. DFUPS measurement
6. Dermatemp 1001

## 1.6 Data analysis

The average of three readings for both Dermatemp and DFUPS will be taken for the purpose of the analysis.

Temperature analysis will include comparisons between corresponding sites between the left and the right foot for each instrument and also comparison of temperatures recorded with both instruments at the same site.

Normal variability of foot temperature will be recorded with both instruments.

A temperature measurement protocol will be developed.

## 1.7 Expected outcome

The study will involve skin foot temperature measurements with the proposed prototype and the current gold standard thermometry. Although there is no potential benefit for the subjects, these measurements will be very important to determine normal ranges and normal variability of foot temperature. This study will be fundamental for the subsequent randomised controlled study which will be carried out in patients with a previous history of foot ulceration.

---

<sup>ii</sup> Boulton AJM; Diabetic foot – what can we learn from leprosy?

Legacy of Dr Paul W. Brand; Diabetes Metab Res Rev 2012; 28(Suppl 1): 3–7

<sup>ii</sup> Lavery LA, Higgins KR, Lanctot DR, et al. Preventing diabetic foot ulcer recurrence in high risk patients: use of temperature monitoring as a self-assessment tool. Diabetes Care 2007; 30: 14–20.

Site	Screening Number	Participant Study Number	An Innovative System for the Early Identification, Monitoring, Evaluation and Diagnosis of Diabetic Foot Ulcers

PARTICIPANT INFORMED CONSENT:	<input type="text"/> <input type="text"/> <input type="text"/> <input type="text"/> <input type="text"/> <input type="text"/> Date (dd/mm/yy)	DATE OF FIRST TRIAL-RELATED PROCEDURE	<input type="text"/> <input type="text"/> <input type="text"/> <input type="text"/> <input type="text"/> <input type="text"/> Date (dd/mm/yy)
-------------------------------	--	---------------------------------------	--

- Please ask the Participant to remove shoes and socks and to take a seat on the examination couch with legs extended and supported
- Please switch on the DFUPS device to allow it to reach steady state (remove the flap of the camera)
- Record TIME AT THE START:  :  (hh:mm);

ROOM TEMPERATURE .  °C ; ROOM HUMIDITY .  % rH

(Room temperature range - 22°C-24°C)

DEMOGRAPHIC DATA:			
Initials <input type="text"/> <input type="text"/> <input type="text"/>	Date of Birth: (dd/mm/yy) <input type="text"/> <input type="text"/> <input type="text"/> <input type="text"/> <input type="text"/> <input type="text"/> <input type="text"/> <input type="text"/> <input type="text"/> <input type="text"/>	Sex : <input type="checkbox"/> Male <input type="checkbox"/> Female	
Height: <input type="text"/> <input type="text"/> . <input type="text"/> <input type="text"/> m	Weight: <input type="text"/> <input type="text"/> . <input type="text"/> <input type="text"/> kg	BMI <input type="text"/> <input type="text"/> . <input type="text"/> <input type="text"/> kg/m <sup>2</sup>	

MEDICAL HISTORY (please insert <b>X</b> to indicate the appropriate answer)	Yes	No
1. Have you ever been found to have high blood glucose (e.g. in a health examination, during an illness, during pregnancy)?	<input type="checkbox"/>	<input type="checkbox"/>
2. Have you had a previous history of foot ulceration?	<input type="checkbox"/>	<input type="checkbox"/>
3. Have you ever had a foot surgery either for correction of a previous foot deformity or following a foot trauma)?	<input type="checkbox"/>	<input type="checkbox"/>
4. Screening for peripheral neuropathy (Diabetic neuropathy symptom score)		
A. Do you feel unsteady when you walk (unsteadiness in gait)?	<input type="checkbox"/>	<input type="checkbox"/>
B. Do you experience pain, burning or aching of the feet or legs?	<input type="checkbox"/>	<input type="checkbox"/>
C. Do you feel prickling sensation of the feet or legs?	<input type="checkbox"/>	<input type="checkbox"/>
D. Do you have numbness in the feet or legs?	<input type="checkbox"/>	<input type="checkbox"/>
5. Do you have discomfort in the calf muscle when walking that is relieved with rest?	<input type="checkbox"/>	<input type="checkbox"/>
6. Do you have any chronic illness which also affects your feet and legs?	<input type="checkbox"/>	<input type="checkbox"/>
7. Do you have an implantable electronic device	<input type="checkbox"/>	<input type="checkbox"/>

SCREENING FOOT INSPECTION AND EXAMINATION				
CHECK PLANTAR, DORSAL, LATERAL AND MEDIAL PART OF THE FOOT FOR ANY SKIN LESIONS				
CHECK FOR SKIN LESIONS BETWEEN THE TOES				
PALPATE PULSES AT THE POSTERIOR TIBIAL ARTERY AND DORSALIS PEDIS ARTERY (if one of the pulses on each foot is present then the person can be recruited in the study)				
	RIGHT FOOT		LEFT FOOT	
INTACT FOOT	YES <input type="checkbox"/>	NO <input type="checkbox"/>	YES <input type="checkbox"/>	NO <input type="checkbox"/>
POSTERIOR TIBIAL PULSE	YES <input type="checkbox"/>	NO <input type="checkbox"/>	YES <input type="checkbox"/>	NO <input type="checkbox"/>
DORSALIS PEDIS PULSE	YES <input type="checkbox"/>	NO <input type="checkbox"/>	YES <input type="checkbox"/>	NO <input type="checkbox"/>



Site	Screening Number	Participant Study Number	An Innovative System for the Early Identification, Monitoring, Evaluation and Diagnosis of Diabetic Foot Ulcers

<b>INCLUSION CRITERIA</b> The following criteria <b>MUST</b> be answered <b>YES</b> for participant to be included in the trial (except where NA is appropriate):		Yes	No
1.	Aged 18 or over	<input type="checkbox"/>	<input type="checkbox"/>
2.	Answered <b>NO</b> to all questions from medical history	<input type="checkbox"/>	<input type="checkbox"/>
3.	Has intact feet	<input type="checkbox"/>	<input type="checkbox"/>
4.	Has palpable foot pulses	<input type="checkbox"/>	<input type="checkbox"/>
5.	Able to fluently speak and understand English and be able to provide meaningful written informed consent for the study	<input type="checkbox"/>	<input type="checkbox"/>

<b>EXCLUSION CRITERIA</b> The following criteria <b>MUST</b> be answered <b>NO</b> for participant to be included in the trial (except where NA is appropriate):		Yes	No
1.	Has active foot ulceration and infection	<input type="checkbox"/>	<input type="checkbox"/>
2.	Has foot deformity which in the opinion of the Investigator, would interfere with interpreting the results of the study	<input type="checkbox"/>	<input type="checkbox"/>
3.	Has any uncontrolled illness that, in the opinion of the Investigator, would interfere with interpreting the results of the study	<input type="checkbox"/>	<input type="checkbox"/>
4.	Has an implantable electronic device	<input type="checkbox"/>	<input type="checkbox"/>

<b>REVIEW INCLUSION AND EXCLUSION CRITERIA</b>			
		Yes	No
1.	Does the participant satisfy the inclusion and exclusion criteria to date?	<input type="checkbox"/>	<input type="checkbox"/>
2.	Is the participant still willing to proceed in the trial?	<input type="checkbox"/>	<input type="checkbox"/>
IF <b>YES</b> to 1 and 2 proceed to skin foot temperature measurement protocol			

Please record the time at the start of the skin foot temperature measurement You should allow <b>10</b> minutes for the feet of the participant to equilibrate with the room temperature	<input type="text"/> <input type="text"/> : <input type="text"/> <input type="text"/> (hh : mm)
---	--

<b>PATIENT IDENTIFIER FOR DFUPS DEVICE</b>	<input type="text"/> <input type="text"/> <input type="text"/> / <input type="text"/> <input type="text"/> <input type="text"/> / <input type="text"/> <input type="text"/> <input type="text"/> Centre Initials      Participant study number      Participant initials
--	---

Site	Screening Number	Participant Study Number	An Innovative System for the Early Identification, Monitoring, Evaluation and Diagnosis of Diabetic Foot Ulcers

**1. TEMPERATURE MEASUREMENT WITH DFUPS DEVICE AT 10 MINUTES POST SOCKS OFF**  
Please insert (X) for each image you have captured

- A. **COMBINED PLANTAR VIEW:** RIGHT FOOT AND LEFT FOOT  (P1)  
 B. **COMBINED DORSAL VIEW:** RIGHT FOOT AND LEFT FOOT  (D1)  
 C. **MEDIAL VIEW:** RIGHT FOOT  (RM1) **LATERAL VIEW** RIGHT FOOT  (RL1)  
 D. **MEDIAL VIEW:** LEFT FOOT  (LM1); **LATERAL VIEW** LEFT FOOT  (LL1)

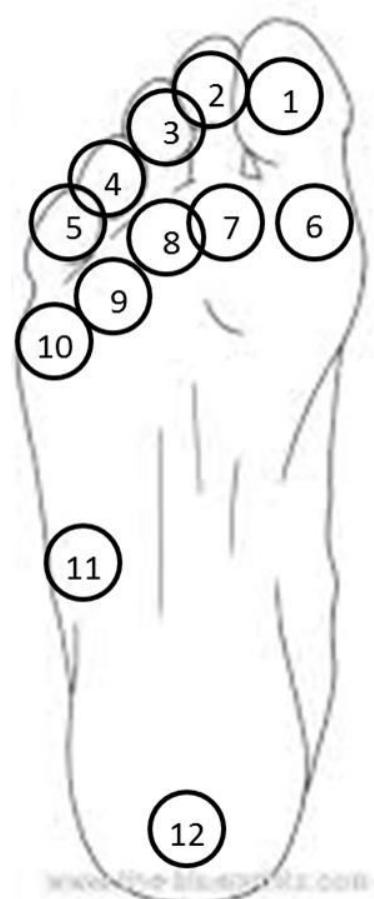
**2. TEMPERATURE MEASUREMENT WITH DFUPS DEVICE AND HAND-HELD THERMOMETER**

**PLANTAR SITE** PLEASE INSERT (X) FOR EACH IMAGE YOU HAVE CAPTURED

**TEMPERATURE MEASUREMENT WITH DFUPS DEVICE:**  
**COMBINED PLANTAR VIEW:** RIGHT FOOT AND LEFT FOOT  (P2)

**SKIN FOOT TEMPERATURE MEASUREMENT WITH HAND-HELD THERMOMETER**

MEASURE CORRESPONDING SITES INITIALLY ON THE RIGHT FOOT AND THEN ON THE LEFT FOOT. AT THE END OF THE SKIN FOOT TEMPERATURE MEASUREMENT CALCULATE THE TEMPERATURE DIFFERENCE ( $\Delta T$ )

PLANTAR SITE	REGION OF INTEREST:	RIGHT FOOT °(C)	LEFT FOOT °(C)	( $\Delta T$ )
	1. 1 <sup>ST</sup> TOE (APEX)			
	2. 2 <sup>ND</sup> TOE (APEX)			
	3. 3 <sup>RD</sup> TOE (APEX)			
	4. 4 <sup>TH</sup> TOE (APEX)			
	5. 5 <sup>TH</sup> TOE (APEX)			
	6. 1 <sup>ST</sup> METATARSAL HEAD			
	7. 2 <sup>ND</sup> METATARSAL HEAD			
	8. 3 <sup>RD</sup> METATARSAL HEAD			
	9. 4 <sup>TH</sup> METATARSAL HEAD			
	10. 5 <sup>TH</sup> METATARSAL HEAD			
	11. 5 <sup>TH</sup> METATARSAL BASE			
	12. HEEL			

Site	Screening Number			Participant Study Number			An Innovative System for the Early Identification, Monitoring, Evaluation and Diagnosis of Diabetic Foot Ulcers

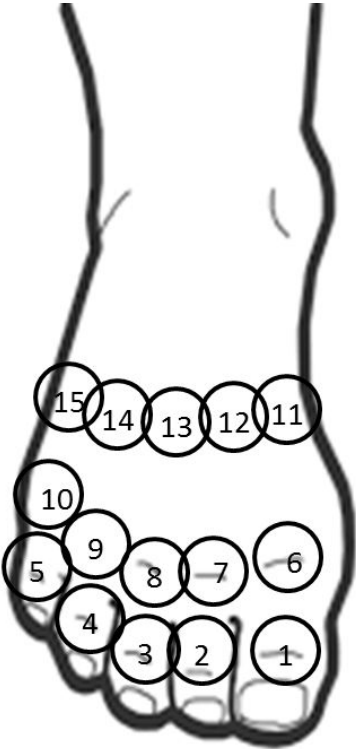
**DORSAL SITE** (PLEASE INSERT (X) FOR EACH IMAGE YOU HAVE CAPTURED)

**SKIN FOOT TEMPERATURE MEASUREMENT WITH DFUPS**

**COMBINED DORSAL VIEW: RIGHT FOOT AND LEFT FOOT** ; **(D2)**

**SKIN FOOT TEMPERATURE MEASUREMENT WITH HAND-HELD THERMOMETER**

MEASURE CORRESPONDING SITES INITIALLY ON THE RIGHT FOOT AND THEN ON THE LEFT FOOT. AT THE END OF THE SKIN FOOT TEMPERATURE MEASUREMENT CALCULATE THE TEMPERATURE DIFFERENCE ( $\Delta T$ )

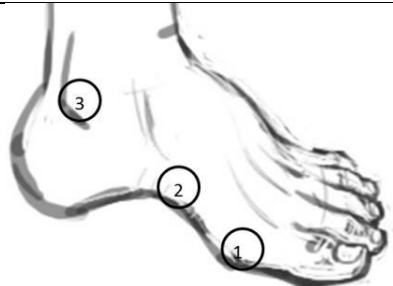
DORSAL SITE	REGION OF INTEREST:	RIGHT FOOT °(C)	LEFT FOOT °(C)	( $\Delta T$ )
	1. 1 <sup>ST</sup> TOE (proximal interphalangeal joint)			
	2. 2 <sup>ND</sup> TOE (proximal interphalangeal joint)			
	3. 3 <sup>RD</sup> TOE (proximal interphalangeal joint)			
	4. 4 <sup>TH</sup> TOE (proximal interphalangeal joint)			
	5. 5 <sup>TH</sup> TOE (proximal interphalangeal joint)			
	6. 1 <sup>ST</sup> METATARSO-PHALANGEAL JOINT			
	7. 2 <sup>ND</sup> METATARSO-PHALANGEAL JOINT			
	8. 3 <sup>RD</sup> METATARSO-PHALANGEAL JOINT			
	9. 4 <sup>TH</sup> METATARSO-PHALANGEAL JOINT			
	10. 5 <sup>TH</sup> METATARSO-PHALANGEAL JOINT			
	11. 1 <sup>ST</sup> METATARSO-TARSAL JOINT			
	12. 2 <sup>ND</sup> METATARSO-TARSAL JOINT			
	13. 3 <sup>RD</sup> METATARSO-TARSAL JOINT			
	14. 4 <sup>TH</sup> METATARSO-TARSAL JOINT			
	15. 5 <sup>TH</sup> METATARSO-TARSAL JOINT			

Site	Screening Number			Participant Study Number			An Innovative System for the Early Identification, Monitoring, Evaluation and Diagnosis of Diabetic Foot Ulcers

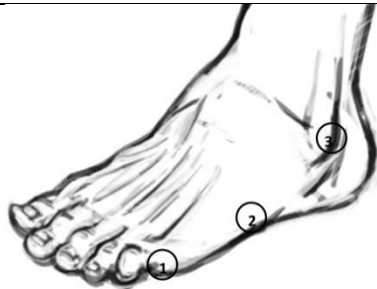
**RIGHT FOOT MEDIAL AND LATERAL SITE**  
**LEFT FOOT MEDIAL AND LATERAL SITE**  
(PLEASE INSERT (X) FOR EACH IMAGE YOU HAVE CAPTURED)

**SKIN FOOT TEMPERATURE MEASUREMENT WITH DFUPS**  
**MEDIAL VIEW: RIGHT FOOT**  **(RM2)** **LATERAL VIEW RIGHT FOOT**  **(RL2)**  
**MEDIAL VIEW: LEFT FOOT**  **(LM2)**; **LATERAL VIEW LEFT FOOT**  **(LL2)**

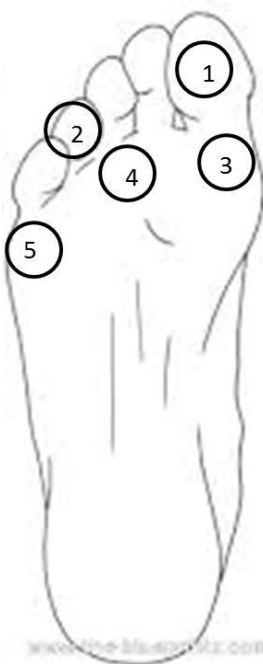
**SKIN FOOT TEMPERATURE MEASUREMENT WITH HAND-HELD THERMOMETER**  
MEASURE CORRESPONDING SITES INITIALLY ON THE RIGHT FOOT AND THEN ON THE LEFT FOOT. AT THE END OF THE SKIN FOOT TEMPERATURE MEASUREMENT CALCULATE THE TEMPERATURE DIFFERENCE ( $\Delta T$ )

<b>MEDIAL SITE</b>	<b>REGION OF INTEREST:</b>	<b>RIGHT FOOT °(C)</b>	<b>LEFT FOOT °(C)</b>	<b>(<math>\Delta T</math>)</b>
	1. 1 <sup>ST</sup> METATARSO-PHALANGEAL JOINT			
	2. 1 <sup>ST</sup> METATARSAL BASE			
	3. MEDIAL MALLEOLUS (OVER BONY PROMINENCE)			

**SKIN FOOT TEMPERATURE WITH HAND-HELD THERMOMETER**  
MEASURE CORRESPONDING SITES INITIALLY ON THE RIGHT FOOT AND THEN ON THE LEFT FOOT. AT THE END OF THE SKIN FOOT TEMPERATURE MEASUREMENT CALCULATE THE TEMPERATURE DIFFERENCE ( $\Delta T$ )

<b>LATERAL SITE</b>	<b>REGION OF INTEREST:</b>	<b>RIGHT FOOT °(C)</b>	<b>LEFT FOOT °(C)</b>	<b>(<math>\Delta T</math>)</b>
	1. 5 <sup>TH</sup> METATARSO-PHALANGEAL JOINT			
	2. 5 <sup>TH</sup> METATARSAL BASE			
	3. LATERAL MALLEOLUS (OVER BONY PROMINENCE)			

Site	Screening Number	Participant Study Number	An Innovative System for the Early Identification, Monitoring, Evaluation and Diagnosis of Diabetic Foot Ulcers

REPEATED TEMPERATURE MEASUREMENTS WITH DFUPS AND HAND-HELD THERMOMETER – (PLANTAR SITE ONL)					
PLANTAR SITE	DFUPS DEVICE: COMBINED <b>PLANTAR VIEW</b> RIGHT AND LEFT FOOT <input type="checkbox"/> ; <b>(P3)</b>				
PLANTAR SITE	SKIN FOOT TEMPERATURE WITH HAND-HELD THERMOMETER				
	<b>REGION OF INTEREST:</b>	<b>RIGHT FOOT °(C)</b>	<b>LEFT FOOT °(C)</b>	<b>(ΔT)</b>	
	1. 1 <sup>ST</sup> TOE (APEX)				
	2. 4 <sup>TH</sup> TOE (APEX)				
	3. 1 <sup>ST</sup> METATARSAL HEAD				
	4. 3 <sup>RD</sup> METATARSAL HEAD				
	5. 5 <sup>TH</sup> METATARSAL HEAD				
	DFUPS DEVICE: COMBINED <b>PLANTAR VIEW</b> RIGHT AND LEFT FOOT <input type="checkbox"/> ; <b>(P4)</b>				
	SKIN FOOT TEMPERATURE WITH HAND-HELD THERMOMETER				
	<b>REGION OF INTEREST:</b>	<b>RIGHT FOOT °(C)</b>	<b>LEFT FOOT °(C)</b>	<b>(ΔT)</b>	
	1. 1 <sup>ST</sup> TOE (APEX)				
	2. 4 <sup>TH</sup> TOE (APEX)				
	3. 1 <sup>ST</sup> METATARSAL HEAD				
	4. 3 <sup>RD</sup> METATARSAL HEAD				
	5. 5 <sup>TH</sup> METATARSAL HEAD				
	DFUPS DEVICE: COMBINED <b>PLANTAR VIEW</b> RIGHT AND LEFT FOOT <input type="checkbox"/> ; <b>(P5)</b>				
	SKIN FOOT TEMPERATURE WITH HAND-HELD THERMOMETER				
	<b>REGION OF INTEREST:</b>	<b>RIGHT FOOT °(C)</b>	<b>LEFT FOOT °(C)</b>	<b>(ΔT)</b>	
	1. 1 <sup>ST</sup> TOE (APEX)				
	2. 4 <sup>TH</sup> TOE (APEX)				
	3. 1 <sup>ST</sup> METATARSAL HEAD				
4. 3 <sup>RD</sup> METATARSAL HEAD					
5. 5 <sup>TH</sup> METATARSAL HEAD					

Site	Screening Number	Participant Study Number	An Innovative System for the Early Identification, Monitoring, Evaluation and Diagnosis of Diabetic Foot Ulcers

Record TIME AT THE END of temperature measurement:  :  (hh:mm);

<b>Visit Checklist:</b>		
CHECK PLANTAR, DORSAL, LATERAL AND MEDIAL PART OF THE RIGHT AND LEFT FOOT FOR ANY DEVICE-RELATED ADVERSE EVENTS		
	<b>Yes</b>	<b>No</b>
1.	<b>Have there been any DEVICE-RELATED Adverse Events (AE)?</b> (If yes, please record in Adverse Events Log)	<input type="checkbox"/>
		<input type="checkbox"/>

<b>DEVICE-RELATED Adverse Events EVENTS LOG</b>	
<b>AE No</b>	<b>Event Name</b> (Please define below)
—	
—	
—	
—	

**IN THE RARE CASE OF AN ADVERSE EVENT, PLEASE REFER THE PATIENT FOR AN ASSESSMENT BY THE MEDICAL TEAM AND TREAT ACCORDINGLY.**

**PLEASE REPORT ANY DEVICE-RELATED ADVERSE EVENTS TO THE CLINICAL SPONSOR OF THE STUDY**

**END OF STUDY PROTOCOL  
THANK THE PARTICIPANT; DON'T FORGET TO CHARGE THE BATTERY FOR DFUPS DEVICE;**

**Protocol title: Efficacy and safety of Diabetic Foot Ulcer Prevention System (DFUPS) - a single blind randomised clinical trial in diabetic foot patients at high risk of foot ulceration**

### **Trial Identifiers**

REC Number –

ClinicalTrials.gov Identifier (NCT number): NCT02579070

### **Sponsor**

Name: King's College Hospital NHS Foundation Trust

### **Sponsor Contact**

Research Office, King's College Hospital NHS Foundation Trust

161 Denmark Hill, LONDON, SE5 8EF

Tel: 020 3299 1980 / Fax: 020 3299 5155

e-mail: [kch-tr.research@nhs.net](mailto:kch-tr.research@nhs.net)

### **Chief Investigator**

Name: Dr Michael Edmonds, Professor of Diabetic Foot Medicine

Address: Diabetic Foot Clinic, King's College Hospital, Denmark Hill, London, SE5 9RS

Telephone: 0203 299 3223/ Fax: 0203 299 4536

Email: [michael.edmonds@nhs.net](mailto:michael.edmonds@nhs.net)

### **Name and address of Co-Investigator(s)**

Name: Dr Nina Petrova,

Address: Diabetic Foot Clinic, King's College Hospital, Denmark Hill, London, SE5 9RS

Telephone: 0203 299 5124 / Email: [nina.petrova@nhs.net](mailto:nina.petrova@nhs.net)

Dr Ana Nora Donaldson, Professor of Biostatistics

Address: Diabetic Foot Clinic, King's College Hospital, Denmark Hill, London, SE5 9RS

Email: [ana.donaldson@nhs.net](mailto:ana.donaldson@nhs.net)

Name: Dr John Bevans

Address: Community Podiatry Department,

Pennine Acute Hospitals Trust,

Harpurhey Health Centre, 1, Church Lane, Harpurhey, Manchester, Post Code: M9 4BE

Tel: 0161 861 2414/ Fax: 0161 205 5860

[john.bevans@pat.nhs.uk](mailto:john.bevans@pat.nhs.uk)

Name: Dr John Allen

Address: Microvascular Diagnostics,

Regional Medical Physics Department

Freeman Hospital; Newcastle upon Tyne, NE7 7DN

Telephone number: 0191 21 38199

[John.Allen@nuth.nhs.uk](mailto:John.Allen@nuth.nhs.uk)

Dr Nicola Leech

Address: Diabetes Centre

Centre for Aging and Vitality (CAV), Newcastle upon Tyne Hospitals Trust

Westgate Road,

Newcastle upon Tyne, NE4 6BE

[Nicola.leech@nuth.nhs.uk](mailto:Nicola.leech@nuth.nhs.uk)

0191 233 6161 (x23844)



## Table of Contents

1. Background & Rationale.....	4
2. Trial Device, Objectives and Design .....	5
A. Description of the Device: .....	5
B. Trial Objectives.....	5
C. Trial Design .....	6
D. Trial flowchart .....	7
3. Selection and Withdrawal of Participants .....	9
A. Inclusion Criteria .....	9
B. Exclusion Criteria .....	9
C. Selection of Participants: .....	9
D. Randomisation Procedure .....	10
E. Subject Withdrawal.....	10
F. Subject Compliance .....	10
G. Expected Duration of Trial .....	11
4. Trial Procedures .....	11
A. Trial procedures by visit .....	12
5. Assessment of Efficacy.....	14
A. Primary efficacy parameters .....	14
B. Secondary efficacy parameters .....	14
6. Procedures for Recording and Reporting Adverse Events.....	15
7. Statistics .....	15
A. Sample Size:.....	15
B. Randomisation .....	15
C. Data Analysis.....	15
8. Data Handling .....	16
9. Publication Policy .....	16
10. Funding Aspect .....	16
Reference list: .....	17

## 1. Background & Rationale

The global burden of diabetes is well recognised. At present, it is estimated that 382 million people have diabetes and by 2035 it is predicted that diabetes will affect 592 million people (<http://www.idf.org/diabetesatlas/introduction>). Almost 50% of the people with diabetes develop neuropathy (nerve damage to the feet). The latter is characterised by a lack of pain and protective sensation to the feet of people with diabetes and increases the risk of foot ulceration, infection and even amputation. The lifetime risk of a patient with diabetes to develop foot ulcer is between 15 and 25% (1). Foot ulceration seriously affects the patient's quality of life and is associated with increased mortality (2, 3, 4).

Foot ulceration is the commonest reason for people with diabetes to be admitted to hospital. It is currently estimated that about £10 billion is spent by the NHS on diabetes and diabetic foot disease accounts for a significant amount of these resources. Furthermore, up to 70% of patients with a history of foot ulcers experience recurrence within 1 year (5, 6, 7). Early recognition and management of foot ulceration is critical to avoid adverse outcomes, as it is now well accepted that "TIME IS TISSUE". Thus, prevention of foot ulcers is of paramount importance and its priority is well recognised by the International Working Group on the Diabetic Foot (IWGDF), (8).

Timely identification of patients is fundamental in the prevention of diabetic foot ulceration. Recently, infrared thermography has attracted a lot of attention as a possible useful modality for early detection of incipient tissue damage in high-risk patients (9). The importance of foot skin temperature monitoring to identify the early signs of inflammation has been emphasised in the 2015 guidelines of the IWGDF, as it may facilitate the early recognition of patients at risk (8).

There is now a variety of instruments evaluated in the examination of the diabetic foot (9, 10, 11), but neither of these has become widely available. At present, mainly single spot hand-held thermometers are used in clinical practice, which measure temperature only above the scanned area and do not provide information of the surrounding area (9). Furthermore, an incipient lesion may also be characterised by a rise of skin foot temperature but is not obviously visible on clinical examination. Therefore, a thermal image of the feet will allow full examination and early detection of areas at risk. Indeed, the potential of thermal map imaging (thermography) to assess diabetic foot disorders has been recently emphasised (12).

Recently, in collaboration with scientists from the National Physical Laboratory, Photometrix Imaging Ltd and the University of South Wales, we have developed a new non-invasive infrared thermal camera called Diabetic Foot Ulcer Prevention System (DFUPS). This camera captures at the same time a visual image and a thermal image. The performance of this imaging camera has been evaluated under laboratory conditions at the National Physical Laboratory.

In addition, we carried out a multi-centre clinical trial and assessed the usefulness of DFUPS device to measure the temperature distribution in the feet of healthy participants. We demonstrated the efficacy and safety of DFUPS device to detect temperature distribution (thermal map imaging) in normal feet. Taking thermal images with DFUPS is fast, non-invasive and reproducible. This technique allows spatial mapping of the foot in a single image. We developed a protocol to assess with DFUPS all sites of each foot (plantar, dorsal, medial and lateral). In addition to a temperature map of each foot, this technique allows the comparisons of corresponding areas of interest between feet. This principle is widely

accepted in the assessment of the diabetic foot to identify areas at risk of ulceration. The images captured with DFUPS allowed visual and thermal assessment of all sites of the feet and also between corresponding sites. Thus DFUPS device holds the potential to become a real asset in the diabetic foot clinic, fulfilling the requirements of “an ideal device being user friendly, reproducible and accurate” (9). We now plan to translate the skin foot temperature measurement protocol with DFUPS into clinical practice and use it in the assessment of diabetic patients at risk of foot ulceration. We plan to measure with DFUPS the temperature distribution in the feet of diabetic patients with past history of one or more foot ulcerations. In addition, we plan to follow up these patients with or without thermography to assess the ulcer recurrence rate.

We hypothesise that monitoring patients with DFUPS together with standard foot care will be more effective compared with standard foot care alone as it will identify incipient tissue damage in patients at high risk for diabetic foot ulceration thus reducing the incidence of foot complications. In particular, we hypothesise that the ulcer recurrence rate will be significantly lower in the active group (thermography plus standard foot care) compared with standard foot care alone.

If we demonstrate the efficacy and safety of DFUPS to reduce the incidence of foot ulceration in diabetic patients at high risk, we plan to carry out a further phase III efficacy trial to assess the usefulness of this instrument in ulcer prevention. The overall aim is to translate this technique to everyday routine clinical practice so that DFUPS is not only an instrument used at annual diabetes review but also an instrument available in every podiatry practice for routine monitoring of high risk patients. We believe that this technique, if available and accessible to clinical centres, could become a useful tool to prevent diabetic foot ulceration and significantly reduce ulcer reoccurrence.

## **2. Trial Device, Objectives and Design**

### **A. Description of the Device:**

The DFUPS device is a two-camera instrument for capturing images of feet. One of the cameras is a standard digital colour camera that works with visible light. The other camera is an infrared camera that registers the heat emissions from objects and converts these into an image from which temperature measurements can be made (thermogram). We will request an MHRA approval to use this device in the proposed clinical trial.

### **B. Trial Objectives**

1. Primary objectives
  - To assess the performance of DFUPS in detecting areas of impending tissue breakdown in high-risk patients with diabetes and past history of foot ulceration.
  - To assess the safety of thermal imaging using DFUPS in a clinical setting

Primary measures will be collected at baseline and then monthly with a final visit at month 12. The primary endpoint with respect to effectiveness of DFUPS in reducing the incidence of diabetic foot ulcers will be the proportion of patients in each group developing a foot ulcer of any type. Ulceration will be defined as the full thickness loss of epidermis and dermis or involvement of deeper structures below the malleoli.

The safety of DFUPS will be assessed and any device-related adverse events will be recorded.

## 2. Secondary objectives

- Time to ulceration
- Health related quality of life (EQ-5D-5L)
- Number of visits to the foot clinic (study visits and clinical visits)
- DFUPS usability feedback from patients and from health care professionals
- Post treatment evaluation at 12 months
  - ✓ Total number of ulcers per patient developed over the last 12 months
  - ✓ Total number of hospital admissions as a result of a foot ulceration over the last 12 months
  - ✓ Total duration of hospital admissions over the last 12 months
  - ✓ Number of amputations over the last 12 months
  - ✓ Number of deaths

## C. Trial Design

This is a multi-centre single blinded randomised clinical trial in people with diabetes. Patients should have either type 1 or type 2 diabetes and a past history of foot ulcer which has been healed for at least 3 months.

Patients will be recruited consecutively and asked whether they would like to take part in the study. They will be provided with verbal and written explanation of the study aims and details (Patient Information Sheet). Subjects will be given ample time to decide whether or not they wish to take part in the study. Patients will be enrolled in the study only after they have agreed to take part. Patients should express their willingness to take part in the study by signing a consent form.

Patients will be seen at an initial visit to assess their suitability to take part in the study. Initial investigations at this visit will consist of brief medical history, foot assessment (inspection, palpation of pulses and assessment of neuropathy), thermal image with DFUPS and review of the inclusion/ exclusion criteria.

Patients who fulfil the study criteria and are willing to take part in the study will be randomised at this visit and then monitored monthly in the clinic and assessed with DFUPS at each study visit. The device will be set up in the visual mode and visual images of all sites of both feet will be obtained at each visit. All patients will receive foot care as per local standards of care. Patients will be randomised in a 1:1 ratio into the following groups:

**Group A:** Intervention group: Visual and thermal imaging with DFUPS and standard foot care. The study investigator will have access to the thermal and visual images captured with DFUPS.

**Group B:** Placebo group: Visual and blinded thermal imaging with DFUPS and standard foot care. The study investigator will have access only to the visual images and will be blinded to the thermal images which will be captured at each visit but accessed only at the end of the study.

It is expected that thermal imaging with DFUPS in the active group will be able to detect a hot spot area (an early fore-runner of foot ulcer) which may not be readily detected by a routine podiatric assessment. We hypothesise that if these hot spots are detected early and monitored until they resolve, the intervention with thermal imaging will reduce the risk of ulcer recurrence in group A.

Patients will be allocated to treatment groups using randomisation numbers obtained from the study statistician at King's College Hospital NHS Foundation Trust.

All patients will receive podiatric treatment which includes callus debridement and pressure offloading (general therapeutic offloading with footwear/ insoles) as per local standards of care. Patients will be followed monthly for routine foot care. Between the follow up visits, the visit window will be  $\pm 7$  days.

In addition patients, allocated to group A, will be monitored monthly with thermal imaging using DFUPS. All sites of the foot will be assessed for the presence of hot spots. A hot spot will be defined as an area with a temperature difference between corresponding sites equal to or greater than  $2.2^{\circ}\text{C}$ , (7, 11). If a hot spot is detected, the patient will be informed and asked to reduce his/her daily activity and will be reassessed within 2 weeks with DFUPS (visual and thermal imaging). If the hot spot is still present, the area will be monitored/protected as per local standards of care and the patient will be followed up every 2 weeks until the hot spot resolves. Resolution of the hot spot will be defined as a temperature difference between corresponding sites less than  $2.2^{\circ}\text{C}$  (7, 11).

Patients will be followed monthly for routine foot care and imaging assessment with DFUPS. The following tests will be performed:

- Foot inspection to rule out foot ulceration at presentation and ulcer recurrence on follow up.
- Imaging assessment with DFUPS. The device captures at the same time a visual and a thermal image (thermogram). For the study, the device will be set up to display only the visual image. Plantar, dorsal, medial and lateral views of each foot will be taken. During the study, the investigator will have access to the visual images for all subjects (Group A and Group B) and to the thermal images only for subjects allocated to Group A.  
At each visit, the thermal images in group A will be assessed for the presence of hot spots. Although Group B will be also imaged with thermography, both the patient and the study investigator will be blinded to the captured thermal images at each visit. The study investigator will be able to access the thermal images only when the subject has completed the study
- Safety evaluation. At each study visit, we will record any device related adverse events.

#### **D. Trial flowchart**

Activity	INITIAL VISIT (screening / randomisation)	TREATMENT VISITS											FINAL STUDY VISIT (Last treatment visit and/ or post treatment evaluation)	
		2	3	4	5	6	7	8	9	10	11	12		
Visit Number	1													13
Month	0	1	2	3	4	5	6	7	8	9	10	11		12
Patient information and informed consent	X													
Medical history and demographics	X													
Foot inspection to rule out any lesion	X	X	X	X	X	X	X	X	X	X	X	X	X	X
Palpation of pulses to rule out peripheral arterial disease	X													
Neuropathy assessment	X													
Assessment with DFUPS (visual mode)	X	X	X	X	X	X	X	X	X	X	X	X	X	X
EQ-5D-5L	X			X				X			X			X
Assessment of thermal images*	Group A	Group A	Group A	Group A	Group A	Group A	Group A	Group A	Group A	Group A	Group A	Group A	Group A	Group A
Post-treatment evaluation														X

\*Group A only – assess thermal images and if according to the investigator there is an evidence of hot spot advise the patient accordingly and assess at an intermediate study visit at 2 weeks

### 3. Selection and Withdrawal of Participants

#### A. Inclusion Criteria

A subject will be eligible for study participation if he or she meets the following criteria:

- Aged 18 years or older
- Has either type 1 or type 2 diabetes
- Has intact feet as defined by the absence of a skin breakdown below the malleoli.
- Has neuropathy confirmed by impaired sensation to neurothesiometer (vibration perception threshold > 25 volts on one OR both feet)
- Has a past history of  $\geq 1$  foot ulceration (s) which has (have) resolved in the last 3 months
- Has palpable foot pulses on both feet (palpable posterior tibial artery pulse OR dorsalis pedis artery pulse OR both)
- Has no history of peripheral arterial disease
- Has footwear which in the opinion of the investigator is not likely to cause pressure damage
- Must be able to provide meaningful written informed consent for the study

#### B. Exclusion Criteria

A subject will be excluded from the study if he or she meets the following exclusion criteria

- Is aged <18
- Has foot deformity that in the opinion of the investigator would interfere with the interpreting of the results of the study.
- Has previous history of foot surgery which in the opinion of the study investigator could interfere with the interpreting the results of the study
- Has active foot ulceration and infection
- Has active Charcot osteoarthropathy
- Has established Charcot foot deformity that in the opinion of the study investigator would interfere with the interpreting of the results of the study.
- Has any uncontrolled illness that, in the opinion of the study investigator, would interfere with interpreting the results of the study
- Has an implantable electronic device

#### C. Selection of Participants:

People with diabetes will be recruited at 3 clinical sites:

- Diabetic Foot Clinic, Kings College Hospital NHS Foundation Trust, London
- Podiatry Department, Centre for Aging and Vitality; Newcastle upon Tyne Hospitals NHS Trust, Newcastle upon Tyne
- Community Podiatry Department and North Manchester General Hospital Diabetes Centre, Pennine Acute Hospitals Trust, Manchester.

Patients will be treated and followed up in the recruiting centre. We plan to randomise 100 patients between the 3 centres and follow them up until a recurrence of a foot ulcer or up to a period of 12 months (whichever comes first). The expected maximum number of visits/subject will be 13 visits over 12 months. These will include an initial visit (screening/randomisation) and 12 follow up monthly treatment visits (group A and B).

In addition, if the thermogram at the initial visit or at any one of the follow up treatment visits indicates a hot spot, the subjects randomised in group A will be advised to reduce their physical activity and will be seen at a 2-weekly intervals to assess the resolution of the hot spot. Thus in the rare event of a persistent hot spot during the whole study, the maximum number of visits for subjects randomised in group A will be 25 visits over 12 months. We anticipate that patients should attend at least 75% of the follow up treatment visits (Group A and Group B).

If a subject develops a foot ulcer at any one of the follow up monthly treatment visits, this will be their last treatment visit. These patients will be asked to attend a post treatment evaluation at 12 months. If the patient cannot attend the post treatment evaluation at 12 months for whatever reason, at the last treatment visit we will ask the patient's permission to contact him/her by phone at 12 months as part of a telephone assessment.

#### **D. Randomisation Procedure**

Patients will be randomised in a 1:1 ratio to assessment with visual and thermal imaging with DFUPS and standard foot care (Group A) or to assessment with visual imaging and blinded thermal imaging with DFUPS and standard foot care (Group B) using simple randomisation based on computer generated list. All subjects will be assessed with visual imaging with DFUPS. Thermal images will be only accessible during the study for subjects randomised in group A. Thermal images for subjects randomised in group B will be accessible by the study investigator only after the subject has completed the study. The study participants will be blinded to the group allocation.

#### **E. Subject Withdrawal**

Subjects will be withdrawn if:

- They develop an acute active Charcot foot
- They sustain a foot or ankle fracture
- They develop any condition which in the opinion of the investigator would interfere with interpreting the results of the study
- They are not compliant (it is expected that the study participants should attend at least 75% of the follow up treatment visits ( $\geq 9$  follow up treatment visits))

In addition subjects are free to withdraw at any time without giving a reason. Patients who develop adverse events which necessitate withdrawal from the study will be followed up in the recruiting Foot Clinic at each investigation site.

If a subjects withdraws from the study for any reason, we will use all the data collected up to withdrawal, provided the subject consents to this by signing the informed consent form.

If a subject is withdrawn from the trial as a result of a (serious) adverse event, the subject will be followed-up until the event resolves or stabilises.

#### **F. Subject Compliance**

The number of attended research visits will be recorded. Subject compliance will be determined monthly. We anticipate that each patient should attend at least 75% of the follow up treatment visits.



## G. Expected Duration of Trial

The study is planned for 18 months. Recruitment will take place over 4 months. We plan to randomise a total of 100 patients between 3 clinical centres and follow them up for a period of 12 months. Last patient last visit will define the end of the trial at each site.

## 4. Trial Procedures

At each centre, all trial procedures will be carried out by delegated and trained members of the research team.

Subjects will be initially seen at an initial visit for screening and randomisation (if eligible) and then will be monitored monthly for 12 months (12 follow up treatment visits). At the last treatment visit at 12 months we will also carry out a post-treatment evaluation. This will be the study final visit. If a patient develops and ulcer at any one of the follow up visits, this visit will be the last treatment visit for this patient (early termination) and at 12 months, this patient will be invited to attend the final study visit for a post-treatment evaluation.

Initially, the patients will be asked to take off their shoes and socks and then to sit on a treatment couch with legs extended and supported. They will be asked to rest quietly for 10 minutes to allow equilibration of their foot temperature with the room temperature (22-24°C). Room temperature and humidity will be measured at the beginning and at the end of each foot assessment using a calibrated room temperature sensor (HygroPalm, Rotronic).

The following tests will be performed:

### 1. Imaging with DFUPS.

All sites of the right and left foot (plantar, dorsal, medial and lateral) will be imaged with DFUPS. The camera will be set up on the visual mode according to instrument requirements detailed in the instructions for use of medical device. A baseline imaging sequence (10 minutes post sock-off) will be captured. The imaging sequence will be repeated after 10 minutes (20 minutes post socks-off). If the patient has hard skin (callus); the imaging sequence will be repeated 10 minutes post callus removal.

Thermal images will be assessed only in subjects randomised in Group A. If the thermal image shows a hot spot on both sequences (baseline and repeated imaging sequence), which in the opinion of the investigator is indicative of incipient tissue damage, the patient will be advised to reduce their daily physical activity and assessed in 2 weeks.

### 2. Self-administered EQ-5D-5L questionnaire

Patients' quality of life will be assessed using EuroQol questionnaire. We plan to use EQ-5D-5L. Applicable to a wide range of health conditions and treatments, this questionnaire provides a simple descriptive profile and a single index value for health status. It will be administered at the initial visit and then at 3 monthly intervals. If at any of the follow up treatment visits the patient presents with a new ulcer (ulcer recurrence), EQ-5D-5L will be administered at this visit (early withdrawal visit) and then at the final study visit at 12 months. The rate of change in the mean difference of EQ-5D-5L scores from baseline and up to the final visit will be assessed.

3. Patient satisfaction/ experience questionnaire.

Patients will be asked to complete a short experience questionnaire about DFUPS at screening.

4. Number of foot clinic appointments since their previous study visit will be recorded.

Patients will be asked for any foot clinic appointments that they may have had since their previous study visit.

5. Post treatment evaluation at 12 months

This will be carried out at the final study visit (defined either as the last treatment visit if the patient has not developed an ulcer or as a post treatment evaluation if the patient has developed an ulcer at any one of the treatment follow up visits). For the latter, the post treatment evaluation will be carried out either in the clinic or as part of a telephone assessment and/or assessment of electronic patient records. We will record data on:

- a. total number of ulcers that the patient has developed since randomisation
- b. total number of hospital admissions required for treating diabetic foot ulcer over the last 12 months
- c. total duration of hospital admissions over the last 12 months
- d. number of amputations required for the treatment of diabetic foot ulcer over the last 12 months
- e. number of deaths

## A. Trial procedures by visit

### *Initial visit (Screening/ Randomisation Visit)*

The following procedures will be performed.

- A. Screening:
  1. Obtain written informed consent
  2. Assign a subject number
  3. Record medical history and demographics
  4. Foot check to ensure that the feet are intact and the patient has palpable foot pulses.
    - a. Check plantar, dorsal, lateral and medial part of each foot for any lesion;
    - b. Check for lesions between the toes
    - c. Palpate pulses at the posterior tibial artery and dorsalis pedis artery; if one of the pulses is present then the patient can be recruited in the study
    - d. Determine presence of neuropathy, confirmed by impaired sensation to neurothesiometer (vibration perception threshold  $\geq 25$  volts on one or both feet) Vibration perception threshold in volts will be measured at the apex of the hallux and will be determined as an average of three readings as previously described (13); Vibration perception threshold  $> 50$  V will be taken as 50 V for the purpose of the analysis.
  5. Assess current footwear and encourage the patient to wear properly fitted shoes

6. Image both feet with DFUPS. The camera will be set up on the visual mode; all sites of both feet will be imaged (plantar, dorsal, medial and lateral sites).
  7. Assess for any device related adverse events
  8. Administer DFUPS satisfaction/experience questionnaire
  9. Review inclusion/ exclusion criteria
    - a. If the patient fulfils the study entry criteria and is still willing to take part in the study, please proceed to randomisation
    - b. There will be no further study visits for subjects who do not fulfil the inclusion/ exclusion criteria.
- B. Randomisation - all patients who fulfil study entry criteria will be randomised at this initial visit. The following procedures will be performed:
1. Assign a randomisation number if the patient is eligible to take part in the study.
  2. Repeat imaging with DFUPS. The camera will be set up on the visual mode; all sites of both feet will be assessed (plantar, dorsal, medial and lateral sites).
  3. Administer EQ-5D- 5L
  4. Check group allocation
  5. If the subject is randomised to group A, assess thermal images of both feet for any hot spots and advise accordingly.
  6. Assess for any device-related adverse events

#### *Treatment visits (visit 2 (month 1); visit 3 (month 2) etc.*

The following procedures will be performed at each follow up monthly treatment visit.

1. Carry out routine podiatric assessment and treatment (foot inspection for any skin breakdown, callus removal and general foot assessment)
2. Administer EQ-5D- 5L at 3-monthly intervals (months 3, 6, 9 and 12); (visit 4,7,10 and 13).
3. Capture images with DFUPS
4. Assess for any device-related adverse events
5. If the subject is randomised to group A, assess thermal images of both feet for any hot spots and advise accordingly.

#### *Post treatment evaluation*

The post treatment evaluation will take place at month 12. This will be carried out during the last treatment visit for subjects from Groups A and B who have not developed an ulcer. Patients who have developed an ulcer from Groups A or B at any one of the follow up visits (early termination visit) will be invited for an assessment to the clinic at 12 months. If the patient is not willing to attend this appointment we will ask their permission to carry out a telephone assessment and to review the electronic patient's records.

At this post treatment evaluation we will record data on:

- ✓ Total number of ulcers per patient developed over the last 12 months
- ✓ Total number of hospital admissions as a result of a foot ulceration over the last 12 months

- ✓ Total duration of hospital admissions over the last 12 months
- ✓ Number of amputations over the last 12 months
- ✓ Number of deaths

### *Early termination visit*

Early termination visit may take place at any time if the patient decides to withdraw; or the patient develops an ulcer/ ulcers below the malleoli on either foot.

If the patient develops an ulcer at any one of the treatment visits, this will be their last treatment visit. These patients will be invited to attend a final study visit at 12 months or if unwilling to attend the clinic, the patients will be asked to take part in a post-treatment evaluation by telephone. We will also ask for their permission to access their electronic patients' records.

## **5. Assessment of Efficacy**

### **A. Primary efficacy parameters**

The primary objective is to determine whether thermography with DFUPS together with standard foot care can reduce the incidence of ulcer recurrence in diabetic patients at high risk of foot ulceration. We aim to determine whether there is a difference between the proportions of patients in each group developing a foot ulcer of any type.

We will compare the groups with regards to:

Device Efficacy, assessed as percentage of patients with recurrent foot ulcer

Device Safety, assessed as device-related adverse events

### **B. Secondary efficacy parameters**

The secondary objectives will be to determine whether there is a difference between the two groups with regard to:

- Time to ulceration
- Rate of change of score in quality of life from baseline and up to the final visit using the EQ-5D-5L
- Total number of visits to the foot clinic (study visits and clinical visits)

In addition at 12 months, we will carry out a post treatment evaluation and we will assess any differences between the groups with regards to:

- Total number of ulcers developed over the last 12 months

- Total number of hospital admissions as a result of foot ulceration over the last 12 months
- Total duration of hospital admissions over the last 12 months
- Number of amputations
- Number of deaths

## **6. Procedures for Recording and Reporting Adverse Events**

At each visit subjects will be assessed for any device related adverse events which will be reported in timely manner to Medicines and Healthcare products Regulatory Agency (MHRA).

## **7. Statistics**

### **A. Sample Size:**

We will recruit an effective sample size of 100 patients to be randomised to the two groups (Placebo is the standard care group and Intervention is the thermography monitored group). Recurrence of ulceration within one year has been found to be 70% in the placebo group and between 30% and 45% in the intervention group (7). An effective sample size of 50 patients in each group will provide 80% power, at the 5% significance level, to detect groups differences of: an odds ratio of 0.29 (70% vs 40% in terms of the percentage of recurrences), an intervention vs placebo hazard ratio of 0.5 (in terms of recurrence and survival times) and an effect of size 0.58 in terms of the difference in the change in the quality of life score from baseline.

We aim to recruit 112 patients in total among the 3 centres (average 37 patients per centre) to allow 10% drop-out rate.

### **B. Randomisation**

Randomisation will be carried out in the Diabetic Foot Clinic at King's College Hospital by the study statistician using simple randomisation based on computer generated list.

### **C. Data Analysis**

This is a randomised controlled trial. The primary outcomes for treatment efficacy are: a binary indicator for ulcer recurrence after 1 year follow up and the time to ulcer recurrence. The secondary outcome for efficacy is the change in quality of life from baseline as measured by the EQ-5D-5L instrument. Primary measures will be collected at baseline and every 3 months thereafter (months 0, 3, 6, 9 and 12), with a final visit at month 12 and safety will be monitored in terms of the rate of adverse events as defined in the protocol. Interim analyses (stopping rules) on the primary and secondary outcomes will not be performed.

We will use logistic regression to model the likelihood of ulcer recurrence within one year and a Cox's regression to model the time-to-ulcer-recurrence patterns in the control and experimental groups. Linear regression will be used to model the changes in quality of life scores from baseline.

### **8. Data Handling**

Personal data will be stored on password protected NHS hospital computers and each principal investigator will act as custodian for the trial data at each site. Paper files will be kept in locked safety cabinets at each participating centre.

All patients' data will be anonymised. Only anonymised data will be sent across sites and used for the analysis.

### **9. Publication Policy**

It is intended that the results of the study will be reported and disseminated at international conferences and in peer-reviewed scientific journals.

### **10. Funding Aspect**

Funding to conduct the trial is provided by the National Institute of Health Research (NIHR). The grant holder is the National Physical Laboratory. King's College Hospital NHS Foundation Trust is the clinical sponsor of this study.

## Reference list:

- 1 Boulton AJM, Vileikyte L, Ragnarson-Tennvall G, Apelqvist J. The global burden of diabetic foot disease *The Lancet*; Volume 366, Issue 9498, 12–18 November 2005, Pages 1719–1724
- 2 Winkley K, Stahl D, Chalder T, Edmonds ME, Ismail K. Quality of life in people with their first diabetic foot ulcer: a prospective cohort study. *J Am Podiatr Med Assoc.* 2009 Sep-Oct;99(5):406-14.
- 3 Winkley K, Sallis H, Kariyawasam D, Leelarathna LH, Chalder T, Edmonds ME, Stahl D, Ismail K. Five-year follow-up of a cohort of people with their first diabetic foot ulcer: the persistent effect of depression on mortality. *Diabetologia.* 2012 Feb;55(2):303-10.
- 4 Brownrigg JR, Davey J, Holt PJ, Davis WA, Thompson MM, Ray KK, Hinchliffe RJ. The association of ulceration of the foot with cardiovascular and all-cause mortality in patients with diabetes: a meta-analysis. *Diabetologia.* 2012 Nov;55(11):2906-12.
- 5 Pound N, Chipchase S, Treece K, Game F, Jeffcoate W. Ulcer-free survival following management of foot ulcers in diabetes. *Diabet Med* 2005 Oct;22(10):1306-1309.
- 6 Bus SA, Waaijman R, Arts M, de Haart M, Busch-Westbroek T, van Baal J, et al. Effect of custom-made footwear on foot ulcer recurrence in diabetes: a multicenter randomized controlled trial. *Diabetes Care* 2013 Dec; 36:4109-4116.
- 7 Armstrong DG, Holtz-Neiderer K, Wendel C, Mohler MJ, Kimbriel HR, Lavery LA. Skin temperature monitoring reduces the risk for diabetic foot ulceration in high-risk patients. *Am J Med.* 2007 Dec;120(12):1042-6.
- 8 IWGDF Guidance on the prevention of foot ulcers in at-risk patients with diabetes.
- 9 Pafili K, Papanas N. Thermography in the follow up of the diabetic foot: best to weigh the enemy more mighty than he seems *Expert Rev. Med. Devices* 12(2), 131–133 (2015).
- 10 Roback K. An overview of temperature monitoring devices for early detection of diabetic foot disorders. *Expert Rev Med Devices.* 2010 Sep;7(5):711-8.
- 11 Van Netten et al. Values for Skin Temperature Assessment to Detect Diabetes-Related Foot Complications; *Diabetes Technology & Therapeutics* Volume 16, Number 11, 2014
- 12 Mendes R1, Sousa N2, Almeida A3, Vilaça-Alves J2, Reis VM2, Neves EB4. Thermography: a technique for assessing the risk of developing diabetic foot disorders. *Postgrad Med J.* 2015 Sep; 91(1079):538.
- 13 Petrova NL, Foster AV, Edmonds ME. Calcaneal bone mineral density in patients with Charcot neuropathic osteoarthropathy: differences between Type 1 and Type 2 diabetes. *Diabet Med.* 2005 Jun;22(6):756-61.

# Appendix F

## Appendix - Website

**Instructions**

**Aim:**

Move the points on the image to correspond to the foot/feet in the image. **The ordering of the points is important.**

If there are two feet in the image and only one outline, then you should place the points to outline only the foot that has the big toe on the same side as the outline template.

Some images may already be finished in which case you need to verify that the points have been placed correctly by editing misplaced points and finally pressing "Finished, get a new image" at the bottom of the page.

**Point Allocation:**

**On Plantar (Sole of the Foot) Images**

ANATOMICAL SPOT	AMOUNT OF POINTS	FIRST FOOT POINTS	SECOND FOOT POINTS IF PRESENT
Heel	4	1, 2, 3, 4	30, 31, 32, 33
Sides	2	20, 21, and 5, 6	57, 58, and 34, 35
Between Toes and Sides	1	7, 27	36, 59
Between Toes	1	11, 15, 19, 23	40, 44, 48, 52
First (Big) Toe	3	8, 9, 10	37, 38, 39
Second Toe	3	12, 13, 14	41, 42, 43
Third Toe	3	16, 17, 18	45, 46, 47
Fourth Toe	3	20, 21, 22	49, 50, 51
Fifth Toe	3	24, 25, 26	53, 54, 55

**On Lateral (View from the side) Images**

ANATOMICAL SPOT	AMOUNT OF POINTS	FIRST FOOT POINTS
Infront of Toes	1	12, 21, 4
Dorsal (Top)	2	5, 6
Ankle	4	7, 8, 9, 10
Heel	3	11, 12, 13
Sole	2	14, 15

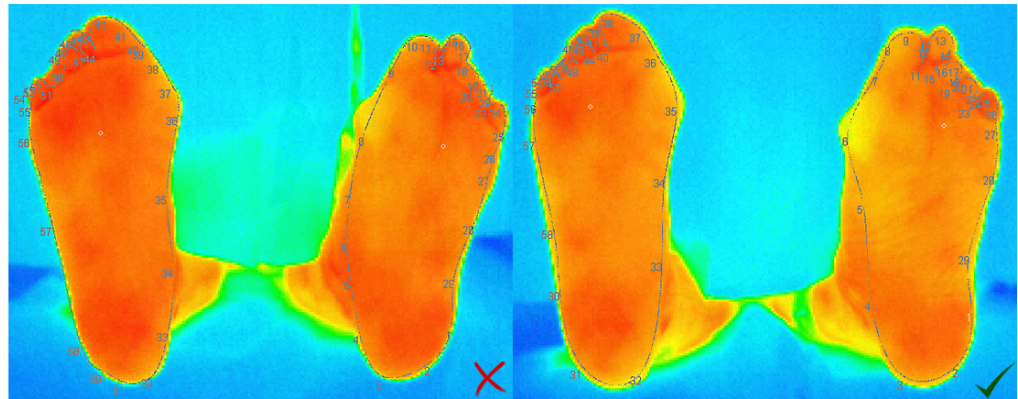
If the image is not sufficient to create an outline of the foot/feet, then finish by pressing "Cannot be Outlined" at the bottom of the page.

FIGURE F.1: Website instructions (part 1)



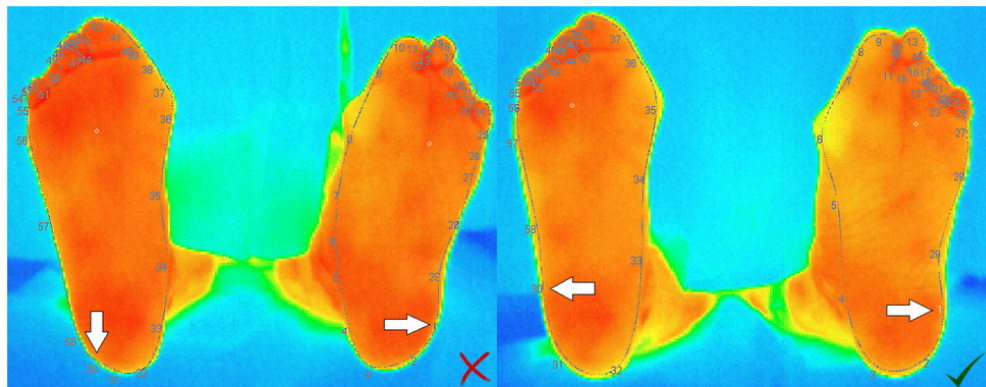
Examples

Plantar Images

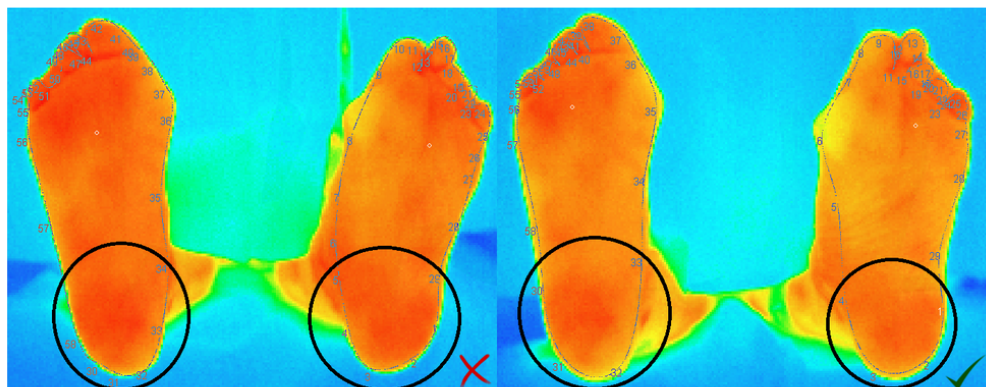


An example of **how not to** and **how to** Outline Plantar Images with two feet.

FIGURE F.2: Website instructions (part 2)



The two starting points of each outline (points numbered 1 and 30).



Four Points on each heel (numbers 1, 2, 3, 4 and 30, 31, 32, 33).

FIGURE F.3: Website instructions (part 3)

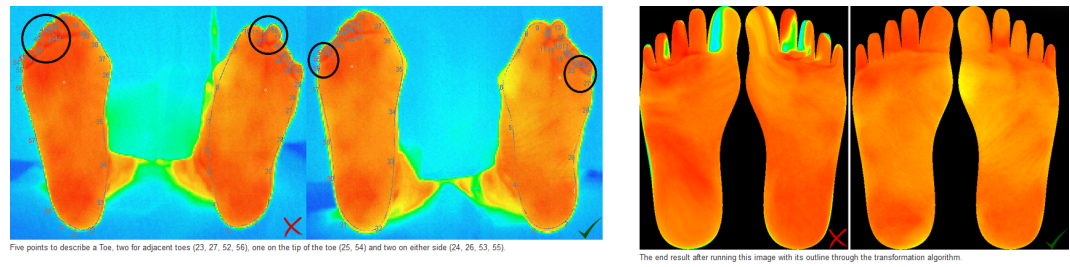


FIGURE F.4: Website instructions (part 4)

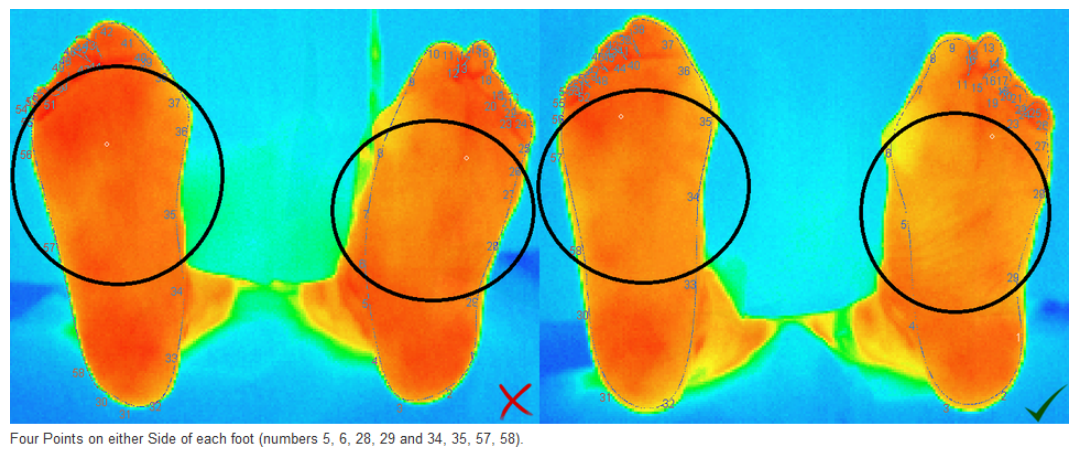


FIGURE F.5: Website instructions (part 5)

logged in as: 10046887@students.southwales.ac.uk  
Currently editing: 921c1b8856943091bc143e8f4e99aba7

Editing Mode  
 Mouse mode  
 Touch Pad mode

Points in-between Control Points  
 1 Outline Size 20  
 1 Control Point Size 5  
 Show Control Point Numbers  
 Control Point Size 10  
 Make Control Points stand out more  
 By 1 10

Transformation  
 Translate  Rotate  Scale

Selection Colour  
 Pins is anywhere on the colour map to pick a selection colour or type in a RGB (Red, Green, Blue) colour manually.

 RGB 0,0,0

First foot:

Second foot:

IMAGE TYPE	AMOUNT	*	PAYOUT	=	TOTAL
New One-Foot Plantar Image	6	*	£0.35	=	£2.1
New Two-Foot Plantar Image	3	*	£0.71	=	£2.13
Verified One-Foot Plantar Image	0	*	£0.05	=	£0
Verified Two-Foot Plantar Image	0	*	£0.09	=	£0
Cannot Solve Plantar Image (as Editor)	0	*	£0.14	=	£0
Cannot Solve Plantar Image (as Verifier)	0	*	£0.03	=	£0
New Lateral Image	0	*	£0.11	=	£0
Verified Lateral Image	0	*	£0.05	=	£0
Cannot Solve Lateral Image (as Editor)	0	*	£0.04	=	£0
Cannot Solve Lateral Image (as Verifier)	0	*	£0.03	=	£0
New Medial Image	0	*	£0.11	=	£0
Verified Medial Image	0	*	£0.05	=	£0
Cannot Solve Medial Image (as Editor)	0	*	£0.04	=	£0
Cannot Solve Medial Image (as Verifier)	0	*	£0.03	=	£0
Total (Using Payout Data from the 12.2.2017, 17:21:00)					£4.23

FIGURE F.6: Toolbox and working area

# Bibliography

- [1] Diabetes.co.uk. *Statistics*. 2016. URL: [https://diabetes-resources-production.s3-eu-west-1.amazonaws.com/diabetes-storage/migration/pdf/DiabetesUK\\_Facts\\_Stats\\_Oct16.pdf](https://diabetes-resources-production.s3-eu-west-1.amazonaws.com/diabetes-storage/migration/pdf/DiabetesUK_Facts_Stats_Oct16.pdf) (visited on 10/31/2017).
- [2] Singh N, Armstrong DG, and Lipsky BA. “Preventing foot ulcers in patients with diabetes”. In: *JAMA* 293.2 (2005), pp. 217–228. DOI: 10.1001/jama.293.2.217. eprint: /data/Journals/JAMA/4959/JCR40054.pdf. URL: <http://dx.doi.org/10.1001/jama.293.2.217>.
- [3] Gayle E Reiber, Benjamin A Lipsky, and Gary W Gibbons. “The burden of diabetic foot ulcers”. In: *The American Journal of Surgery* 176.2, Supplement 1 (1998), 5S–10S. ISSN: 0002-9610. DOI: [http://dx.doi.org/10.1016/S0002-9610\(98\)00181-0](http://dx.doi.org/10.1016/S0002-9610(98)00181-0). URL: <http://www.sciencedirect.com/science/article/pii/S0002961098001810>.
- [4] William J Jeffcoate and Keith G Harding. “Diabetic foot ulcers”. In: *The Lancet* 361.9368 (2003), pp. 1545–1551. ISSN: 0140-6736. DOI: [http://dx.doi.org/10.1016/S0140-6736\(03\)13169-8](http://dx.doi.org/10.1016/S0140-6736(03)13169-8). URL: <http://www.sciencedirect.com/science/article/pii/S0140673603131698>.
- [5] Jeffrey M Robbins et al. “Mortality rates and diabetic foot ulcers: is it time to communicate mortality risk to patients with diabetic foot ulceration?” In: *Journal of the American Podiatric Medical Association* 98.6 (2008), pp. 489–493.
- [6] National Institute for Health and Care Excellence. *Diabetic foot problems: prevention and management 1 - Recommendations Guidance and guidelines NICE*. 2015. URL: <https://www.nice.org.uk/guidance/ng19/chapter/1-recommendations#assessing-the-risk-of-developing-a-diabetic-foot-problem-2> (visited on 10/15/2015).

- [7] Takashi Nagase et al. "Variations of plantar thermographic patterns in normal controls and non-ulcer diabetic patients: Novel classification using angiosome concept". In: *Journal of Plastic, Reconstructive & Aesthetic Surgery* 64.7 (2011), pp. 860–866. ISSN: 1748-6815. DOI: <http://dx.doi.org/10.1016/j.bjps.2010.12.003>. URL: <http://www.sciencedirect.com/science/article/pii/S1748681510007333>.
- [8] Jaap J. van Netten et al. "Diagnostic Values for Skin Temperature Assessment to Detect Diabetes - Related Foot Complications". In: *Diabetes Technology & Therapeutics* 16.11 (Aug. 2014), pp. 714–721. ISSN: 1520-9156. DOI: 10.1089/dia.2014.0052. URL: <http://dx.doi.org/10.1089/dia.2014.0052> (visited on 08/21/2015).
- [9] David G Armstrong et al. "Skin temperature monitoring reduces the risk for diabetic foot ulceration in high-risk patients". In: *The American journal of medicine* 120.12 (2007), pp. 1042–1046.
- [10] Lawrence A Lavery et al. "Preventing Diabetic Foot Ulcer Recurrence in High-Risk Patients Use of temperature monitoring as a self-assessment tool". In: *Diabetes care* 30.1 (2007), pp. 14–20.
- [11] Jaap J. van Netten et al. "Infrared Thermal Imaging for Automated Detection of Diabetic Foot Complications". In: *Journal of Diabetes Science and Technology* 7.5 (2013), pp. 1122–1129. DOI: 10.1177/193229681300700504. eprint: <http://dst.sagepub.com/content/7/5/1122.full.pdf+html>. URL: <http://dst.sagepub.com/content/7/5/1122.abstract>.
- [12] Robert G Frykberg et al. "Feasibility and Efficacy of a Smart Mat Technology to Predict Development of Diabetic Plantar Ulcers". In: *Diabetes Care* (2017), p. dc162294.
- [13] Nigel A.S. Taylor et al. "Hands and feet: physiological insulators, radiators and evaporators". English. In: *European Journal of Applied Physiology* 114.10 (2014), pp. 2037–2060. ISSN: 1439-6319. DOI: 10.1007/s00421-014-2940-8. URL: <http://dx.doi.org/10.1007/s00421-014-2940-8>.
- [14] JA Cosh and EFJ Ring. "Thermography and rheumatology". In: *Rheumatology* 10.7 (1970), pp. 342–348.
- [15] M. Diakides, J.D. Bronzino, and D.R. Peterson. *Medical Infrared Imaging: Principles and Practices*. CRC Press, 2012. ISBN: 9781439872505. URL: <https://books.google.de/books?id=FzLOBQAAQBAJ>.
- [16] all spec.com. *Thermal Imaging Cameras*. 2015. URL: <http://www.all-spec.com/compare/TST-28/> (visited on 09/29/2015).

- 
- [17] FLIR. *FLIR Lepton*. 2015. URL: [http://www.flir.com/uploadedFiles/CVS\\_Americas/Cores\\_and\\_Components\\_NEW/Resources/flir-lepton-datasheet.pdf](http://www.flir.com/uploadedFiles/CVS_Americas/Cores_and_Components_NEW/Resources/flir-lepton-datasheet.pdf) (visited on 10/01/2015).
- [18] Micro Epsilon. *Miniature infrared camera in high resolution*. 2015. URL: [http://www.micro-epsilon.com/temperature-sensors/thermoIMAGER/thermoIMAGER\\_400/index.html](http://www.micro-epsilon.com/temperature-sensors/thermoIMAGER/thermoIMAGER_400/index.html) (visited on 10/01/2015).
- [19] Hardkernel. *Odroid-U3*. 2015. URL: [http://www.hardkernel.com/main/products/prdt\\_info.php?g\\_code=g138745696275](http://www.hardkernel.com/main/products/prdt_info.php?g_code=g138745696275) (visited on 09/30/2015).
- [20] SolidRun. *HummingBoard Specifications*. 2017. URL: <http://solid-run.com/freescale-imx6-family/hummingboard/hummingboard-specifications/> (visited on 11/06/2017).
- [21] Raspberry Pi Foundation. *Buy a Raspberry Pi*. 2017. URL: <https://www.raspberrypi.org/products/> (visited on 11/06/2017).
- [22] Sinovoip and Foxconn. *Banana Pi Products*. 2017. URL: <http://www.banana-pi.org/product.html> (visited on 11/06/2017).
- [23] R Vardasca et al. “A template based method for normalizing thermal images of the human body”. In: *The 12th International Conference on Quantitative infrared Thermography, at Bordeaux, France*. 2014.
- [24] Thaddeus Beier and Shawn Neely. “Feature-based image metamorphosis”. In: *ACM SIGGRAPH Computer Graphics*. Vol. 26. 2. ACM. 1992, pp. 35–42.
- [25] Peter Kaufmann et al. “Finite element image warping”. In: *Computer Graphics Forum*. Vol. 32. 2pt1. Wiley Online Library. 2013, pp. 31–39.
- [26] Michael S Floater. “Mean value coordinates”. In: *Computer aided geometric design* 20.1 (2003), pp. 19–27.
- [27] Alec Jacobson et al. “Bounded biharmonic weights for real-time deformation.” In: *ACM Trans. Graph.* 30.4 (2011), p. 78.
- [28] Juyong Zhang et al. “Local barycentric coordinates”. In: *ACM Transactions on Graphics (TOG)* 33.6 (2014), p. 188.
- [29] IJ Schoenberg. “Spline functions, convex curves and mechanical quadrature”. In: *Bulletin of the American Mathematical Society* 64.6 (1958), pp. 352–357.
- [30] Inc. Wolfram Research. *Cubic Spline*. 2017. URL: <http://mathworld.wolfram.com/BezierCurve.html> (visited on 11/06/2017).
- [31] Inc. Wolfram Research. *Cubic Spline*. 2017. URL: <http://mathworld.wolfram.com/B-Spline.html> (visited on 11/06/2017).

- 
- [32] Inc. Wolfram Research. *Cubic Spline*. 2017. URL: <http://mathworld.wolfram.com/CubicSpline.html> (visited on 11/06/2017).
- [33] The QT Company Ltd. 2018. URL: <http://doc.qt.io/qt-5/>.
- [34] Itseez. *Open Source Computer Vision Library*. <https://github.com/itseez/opencv>. 2018.
- [35] *Information technology – Digital compression and coding of continuous-tone still images: JPEG File Interchange Format (JFIF)*. 2011. URL: <http://www.itu.int/rec/T-REC-T.871-201105-I/en>.
- [36] *Bounded Biharmonic Weights for Real-Time Deformation*. 2011. URL: <http://igl.ethz.ch/projects/bbw/>.
- [37] *JavaCC The Java Parser Generator*. URL: <https://javacc.org/>.
- [38] K Busch and E Chantelau. “Effectiveness of a new brand of stock ‘diabetic’ shoes to protect against diabetic foot ulcer relapse. A prospective cohort study”. In: *Diabetic medicine* 20.8 (2003), pp. 665–669.
- [39] Luigi Uccioli et al. “Manufactured shoes in the prevention of diabetic foot ulcers”. In: *Diabetes care* 18.10 (1995), pp. 1376–1378.
- [40] *File:ROC space-2.png*. 2009. URL: [https://en.wikipedia.org/wiki/File:ROC\\_space-2.png](https://en.wikipedia.org/wiki/File:ROC_space-2.png).
- [41] Thomas Fletcher et al. “Comparison of non-contact infrared skin thermometers”. In: *Journal of medical engineering & technology* (2018), pp. 1–7.
- [42] Surya Prakash, Pei Yean Lee, and Antonio Robles-Kelly. “Stereo techniques for 3D mapping of object surface temperatures”. In: *Quantitative Infrared Thermography Journal* 4.1 (2007), pp. 63–84.
- [43] G Chernov, V Chernov, and M Barboza Flores. “3D dynamic thermography system for biomedical applications”. In: *Application of Infrared to Biomedical Sciences*. Springer, 2017, pp. 517–545.
- [44] D Rzeszutarski and B Więcek. “Single thermal and visual camera system for 3D image fusion”. In: ().
- [45] Benjamin Kluwe et al. “Segmentation of Infrared Images Using Stereophotogrammetry”. In: *European Congress on Computational Methods in Applied Sciences and Engineering*. Springer. 2017, pp. 1025–1034.